NTNU – Trondheim
Norwegian University of
Science and Technology

Modeling of heat exchange with the ground and analyses of energy use for a frost proof leisure building with active solar heating

Ida Karin Auråen

Master of Science in Mechanical Engineering
Submission date: June 2013
Supervisor: Per Olaf Tjelflaat, EPT
Co-supervisor: Rasmus Høseggen, EPT

Norwegian University of Science and Technology
Department of Energy and Process Engineering

Preface

This Master's thesis was prepared in the spring of 2013 at the Norwegian University of Science and Technology in Trondheim. The thesis was written at the Department of Energy and Process Engineering in my 10th semester as a part of the Master Programme in Mechanical Engineering.

With the title *Modeling of heat exchange with the ground and analyses of energy use for a frost proof leisure building with active solar heating* is this thesis a continuation of the project thesis prepared in the fall of 2012 together with fellow student Ragnhild Haukland Løge.

I would like to thank my supervisor Per Olaf Tjelflaat for good guidance and advice during this work, and co supervisor Rasmus Z. Høseggen for good advice regarding ESP-r. I would also like to thank Ragnhild Haukland Løge for good teamwork in the preparation of the project thesis which is the basis of this report and Ørjan Ringstad Kristiansen for personal support along the way.

Trondheim, June 7, 2013

Ida Karin Auråen

Summary

Requirements regarding efficient energy use and reduction in CO_2 emissions are becoming increasingly strict. The building sector accounts for a large part of CO_2 emissions and the potential for reductions within this sector should be considerable.

This thesis is a continuation of the author's project thesis. The main focus is to improve the earlier model emphasizing the modeling of the interactions between the leisure home building and the ground. The goal is to develop a prototype of a leisure home where sanitary installations are kept frost proof throughout the year without the use of primary energy sources or electricity, minimizing net CO_2 emissions. The building envelope is constructed of poorly insulated log walls. The sanitary installations are placed in a thermally insulated internal zone, and an active solar heating system is developed to transfer heat into the ground in this internal zone. The intention is to store the heat, transferred to the internal zone during sunny periods, in a thermal mass under the cabin. This would then passively arise during cold periods, maintaining frost proof conditions. The leisure home is planned to be located in the southern mountain regions of Norway.

Different simulation tools were considered for modeling the leisure home and its energy system. The dynamic simulation tool ESP-r was chosen, and an improved model from the project thesis was developed. Different methods and theories concerning how the solar heating system and the ground could be modeled have been studied. The interactions between the building and the ground were modeled by implementing a new basement zone for the leisure home, and defining a BASESIMP configuration as boundary conditions for the surfaces adjacent to the ground. BASESIMP performs quasi 3-dimensional calculations for the heat transfer between the building and the ground. Since the heat storage is not taken into account in the BASESIMP configuration, the storage is represented in the ground construction; the basement floor of the inner zone. The solar heating system is represented in a control loop. The control loop injects electric heat into the basement floor for a given period each day. The electric data is based on solar radiation data, and the time intervals for when heat is injected into the floor are determined from when solar radiation is available in the day.

Climate data from Östersund, Sweden has been used as an approximation as there was no available climate file for the southern mountain regions of Norway. Different system parameters have been changed to investigate the influence they have on the temperature

conditions in the internal zones throughout the year. The internal zones maintain much more stable temperatures throughout the year than the outer zones. This shows that isolating the frost proof zones in the leisure home, represent a major advantage in the design process.

The ground construction in the basement floor of the inner zone has been modeled as a thermal mass with high density and high specific heat capacity. This dense thermal mass is modeled to account for the whole area under the cabin. A south facing solar collector with an area of 4 m^2 and an inclination of 70 $^\circ$ indicates that the temperature in the internal zones stays above 4.2 $^\circ C$ throughout the year, subject to the given ground conditions and without collecting heat during May until August. The delivered energy to the ground construction in the basement floor of the inner zone for a year under the given conditions and with a collector efficiency of 45 % turned out to be 878 kWh.

Heat transfer from the ground into the internal zone turned out to have a significant heat contribution in cold periods. Results also showed a noticeable potential for seasonal storage of the energy extracted from the solar heating system.

For further studies, the interactions between the heat storage and the surrounding ground should be studied in a 3-dimensional conduction program. Insulation regarding snow should also be implemented in a future model to study the effect of extra insulation on the ground surface.

Sammendrag

Kravene til energieffektivisering av bygninger og redusering av CO_2-utslipp blir stadig strengere. Bygningssektoren står for en stor del av det årlige CO_2-utslippet og potensialet er stort for å redusere utslipp i denne sektoren.

Masteroppgaven er en fortsettelse av forfatterens prosjektoppgave. Fokuset for masteroppgaven er å forbedre tidligere modell, med vekt på modelleringen av interaksjonene mellom hytta og grunnen. Målet er å utvikle en prototyp av en fritidsbolig hvor sanitær installasjonene kan holdes frostfrie gjennom hele året. Dette uten å måtte ta i bruk oppvarming ved hjelp av elektrisitet eller annen primærenergi som gir netto CO_2-utslipp. Fritidsboligen er dårlig isolert med laftede yttervegger. Sanitærinstallasjonene er tenkt plassert i en godt isolert indre sone. Videre har en modell av et aktivt solvarmeanlegg blitt utviklet for å overføre varme til grunnen i kjelleren i den indre sonen. Intensjonen er at varme som blir overført til grunnen i den indre sonen i solrike perioder skal lagres i den termiske massen under hytta. I kalde perioder kan denne varmen utnyttes passivt ved at varmen stiger opp fra grunnen inn til den indre sonen og frostfrie forhold opprettholdes. Hyttens plassering er tenkt i fjellandskapet i Sør-Norge.

Ulike simuleringsprogram har blitt vurdert for modellering av hytta og dets energisystem. Det dynamiske simuleringsverktøyet ESP-r ble valgt for denne studien, og en forbedret modell fra prosjektoppgaven er utviklet. Ulike modelleringsmetoder og -teorier har blitt studert. Interaksjonene mellom bygningen og grunnen ble modellert ved å implementere en ny kjellersone i hyttemodellen, og definere en BASESIMP-konfigurasjon som grensebetingelse for flatene som grenser til grunnen. BASESIMP foretar 3-dimensjonale beregninger for varmetransporten mellom bygningen og grunnen. Siden varmelagring ikke blir tatt hensyn til i BASESIMP-konfigurasjonen, er varmelageret representert i grunnkonstruksjonen i kjellergulvet i den indre sonen. Solsystemet er reprentert ved hjelp av en kontrol sløyfe basert på solinnstrålingsdata. Kontrol sløyfen injiserer varme til kjellergulvet i den indre sonen for et gitt tidsintervall hver dag.

Klimadata fra Östersund i Sverige er brukt som en tilnærming i simuleringsprosessen. Dette fordi det ikke eksisterer klimadata for fjellområder i Sør-Norge for implementering i ESP-r. Ulike systemparametere har blitt justert for å studere hvordan de virker inn på temperaturforholdene i de indre sonene i løpet av et år. De indre sonene opprettholder en mye mer stabil temperatur gjennom året enn de ytre sonene. Dette viser at det i

designprosessen er fordelaktig å plassere sanitærinstallasjonene i godt isolerte indre soner.

Grunnen i kjellergulvet i den indre sonen er modellert med en termisk masse med høy tetthet og høy varmekapasitet. Den termiske massen er modellert på denne måten for å representere den termiske massen i grunnen under *hele* fritidsboligen, ikke bare under den indre sonen. En sydvendt solfanger med et areal på 4 m^2 plassert med en helning på 70 ° indikerer at temperaturene i de indre sonene holdes over 4.2 $°C$ gjennom hele året. Det hentes ikke ut solvarme for perioden mai til august og solfangerens virkningsgrad er satt til 45 %. Levert solenergi til grunnkonstruksjonen i den indre kjellersonen for et år ved de gitte forutsetningene er 878 kWh.

Varmeoverføringen fra grunnen inn til den indre kjellersonen utgjorde et vesentlig varmetilskudd i kalde perioder. Resultatene viste et stort potensiale for sesonglagring av varme hentet fra solfangeranlegget.

For videre arbeid bør interaksjonene mellom varmelageret og den omgivende grunnen studeres i mer detalj i et program som behandler 3-dimensjonal konduksjon. Snø vil isolere overflaten til grunnen, og bør også implementeres i modellen for å studere denne isoleringseffekten.

Contents

Lists

List of Figures

List of Tables

List of Equations

Chapter 1

Introduction

The number of leisure homes in Norway has increased dramatically in recent years, along with a growing demand for increased comfort. Traditionally, the electricity use in Norwegian leisure homes has represented a relatively small part of the total electricity use in Norway. Conventional leisure homes have usually been primitive, simple timber houses with a short heating season. Modern leisure homes are normally equipped with sanitary installations and electricity. This trend has resulted in increased energy and power demand, and further increased greenhouse gas emissions. A major factor contributing to the increased energy and power demand is that leisure homes are often left partly heated throughout the year to prevent frost damage in sanitary installations. The potential to reduce this excess load should be considerable, as the majority of the Norwegian leisure homes are only being used for short periods of the year.

This report studies the potential to utilize solar energy to cover the heating demand in periods when leisure homes are left unused. This thesis is a continuation of the author's project thesis where different system solutions for keeping the leisure home frost proof were studied. A part of the project thesis was to learn and study the dynamic simulation tool ESP-r. The main goal of this report is to present a potential way to keep a leisure home in the southern mountain regions of Norway frost proof throughout the year with minimal use of primary energy sources. Norway is currently in a situation where it is partly dependent on imported power and energy. In some cases this energy comes from highly polluting coal-fired plants. The model from the project thesis is to be improved and a main focus of this report is to improve the modeling of the interactions between the building and the ground.

The first part of the report consists of a literature study explaining the background for the thesis. This part includes a discussion about the development and new trends of leisure homes, potential solar heating system solutions and the possibility of storing heat in the ground. Further, different simulation tools are studied, and modeling theories and methods are presented. All the simulations and calculations are based on climate data from Östersund, Sweden.

The issue of maintaining frost proof sanitary installations in a leisure home while minimizing the use of primary energy sources has been assessed in several previous projects and master theses. Different simplified system solutions have been analysed in previous reports for the leisure home, and this thesis will continue addressing possible system solutions.

It is assumed that the reader has basic knowledge regarding building engineering, heat and mass transfer and relevant technical terminology.

Chapter 2

Background

2.1 Energy and leisure homes

As of May 2013 there are 445 918 existing leisure homes in Norway, whereof 413 318 are listed as cabins and summerhouses and 32 600 as permanent residences and farms used as leisure homes (Statistisk sentralbyrå, 2013a). The distribution of leisure homes in the different Norwegian counties can be seen in Figure 2.1.

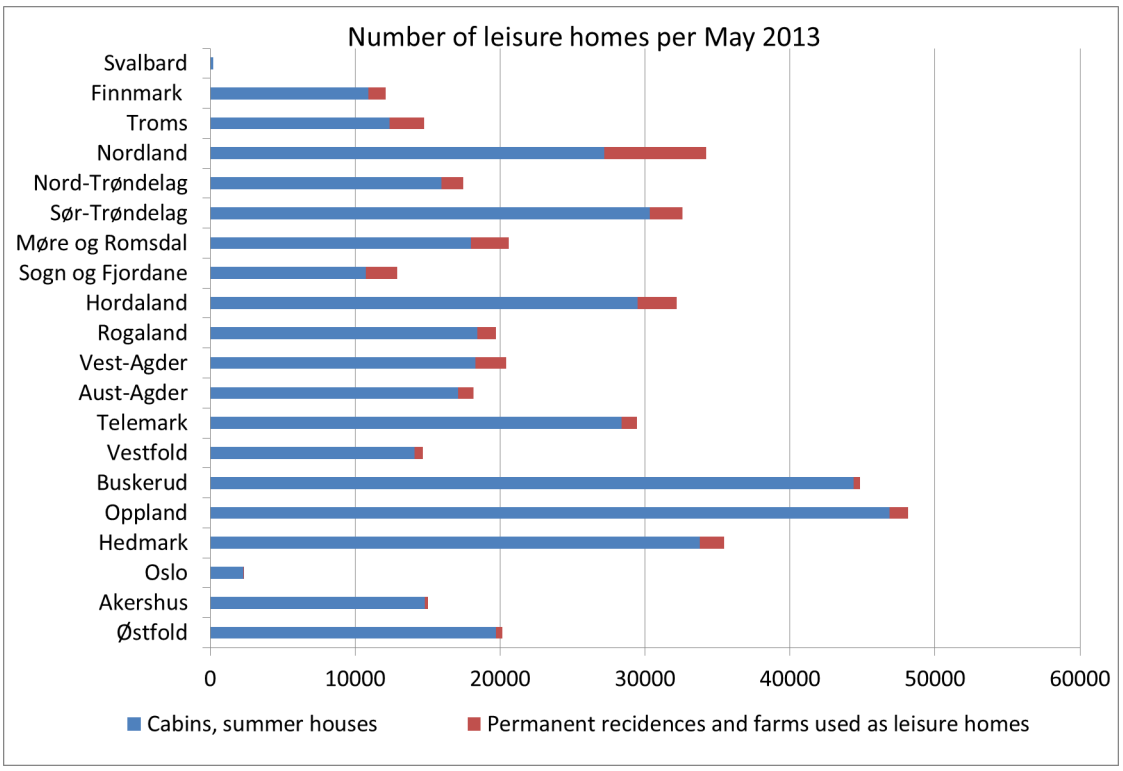

Figure 2.1: Number of leisure homes in the different Norwegian counties

The three counties with the most leisure homes today are Oppland, Buskerud and Hedmark respectively. *Permanent residences and farms used as leisure homes* constitute about 7 % of the total. Figure 2 shows the relationship between the number of leisure homes and the electricity consumption in leisure homes from 2001 to 2010.

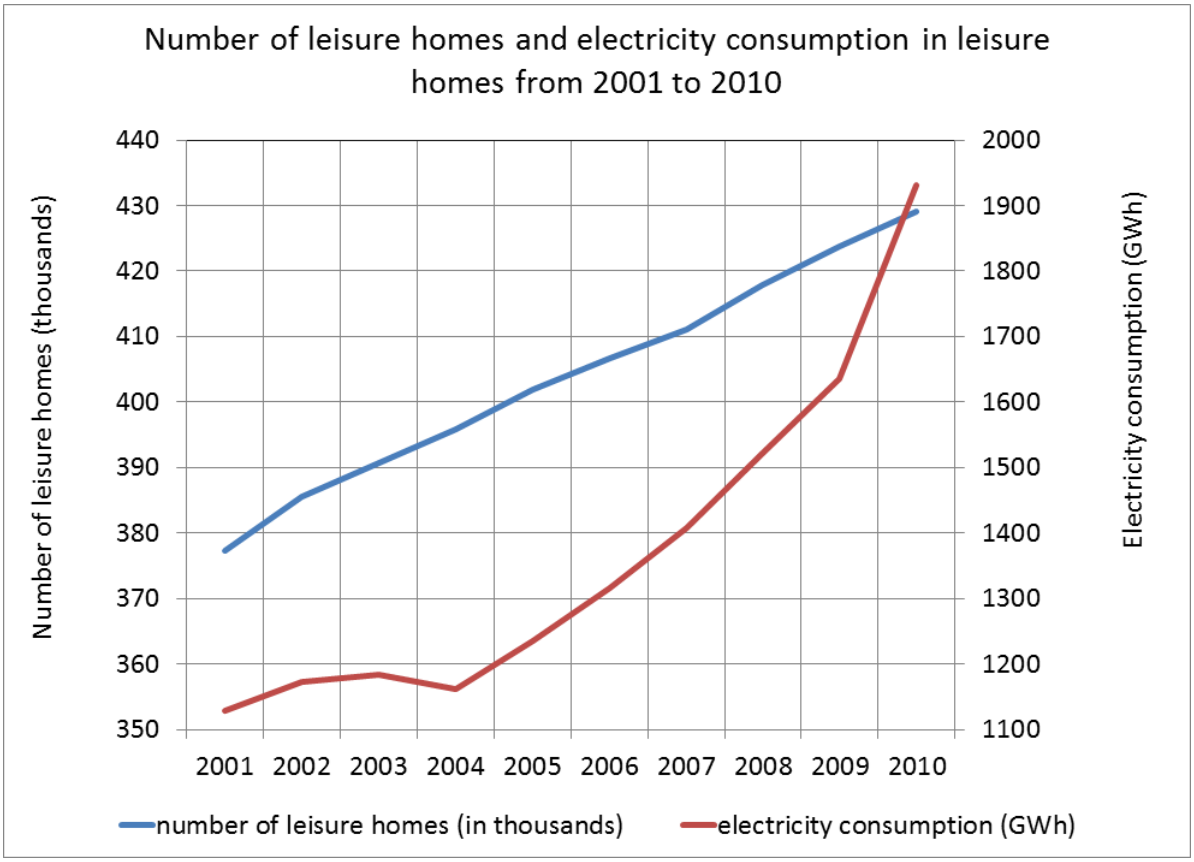

Figure 2.2: Number of leisure homes and electricity consumption in leisure homes

Figure 2.2 shows that as the growth in number of leisure homes are close to constant, the electricity consumption has a steeper increase. From 1993 to 2010 the electricity consumption in leisure homes increased by almost 64 % from 696 GWh to 1 931 GWh. The average use area in Norwegian leisure homes, being a major factor for the growing energy use, increased from 62.2 m^2 to 87.1 m^2 during the period 1983 to 2011 (Statistisk sentralbyrå, 2013a).

Unless preventive measures are being implemented, such an increase will automatically lead to a growth in the energy consumption. The number of leisure homes in Norway is increasing rapidly. The energy consumption in Norwegian leisure homes is increasing and today constitutes a larger part of the energy budget for a household, even though it is still a relatively small part. The net electricity consumption in leisure homes in 2010 was 1.9 TWh. From 1993 to 2006 the net electricity consumption in Norwegian leisure homes increased by 85 % from 0.7 TWh to 1.3 TWh. During the same period, the number of leisure homes increased by approximately 15 %, reaching a total of 380 000 by January 2006 (Statistisk sentralbyrå, 2013a). This shows that the increased energy consumption is

not only a consequence of the development of new leisure homes, but must be attributed several factors. One of them is that the increased average use area has contributed to a stronger growth in the electricity consumption.

Figure 2.3 and Figure 2.4 shows statistics for number of leisure homes that is built and the use area from 1983 to 2011 (Statistisk sentralbyrå, 2013b).

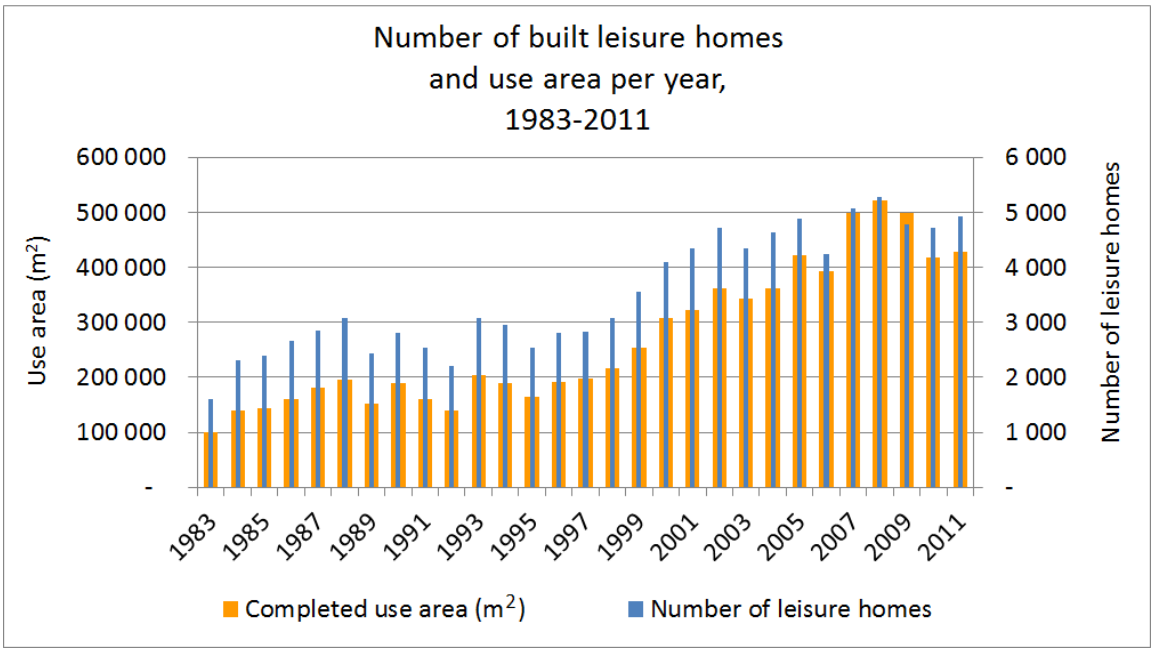

Figure 2.3: Number of built leisure homes and use area per year, 1983 to 2011

Figure 2.4 shows the same statistic summarized.

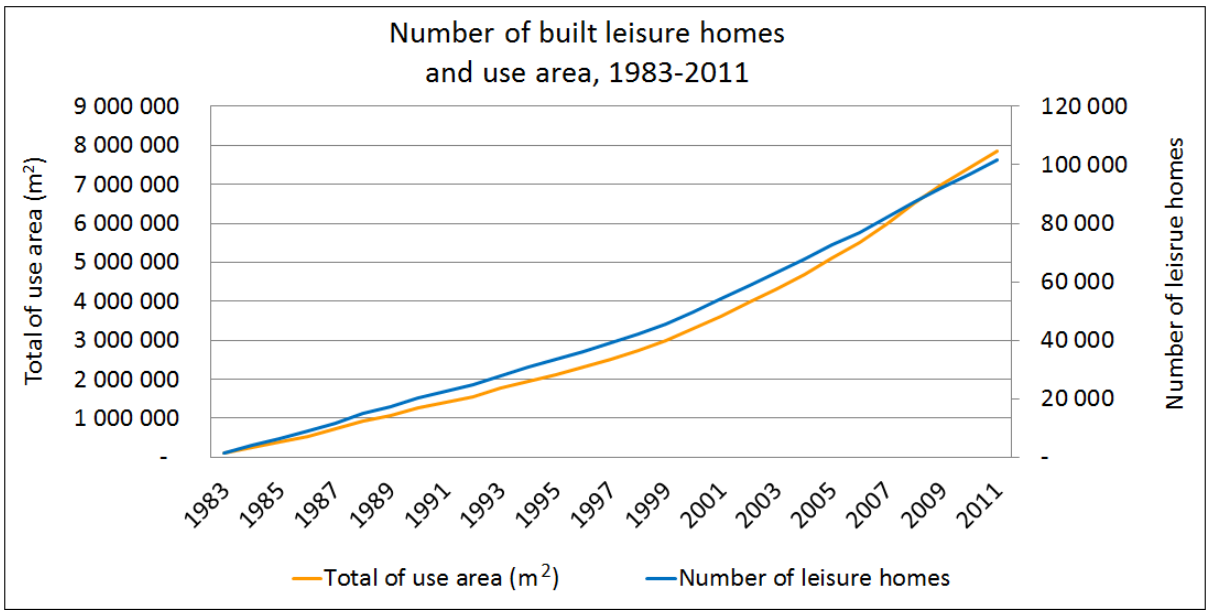

Figure 2.4: Number of built leisure homes and use area, 1983 to 2011

An important note is that Figure 2.4 does not show the total of leisure buildings for each year. This statistic started in 1983, so at the starting point there are zero leisure homes in the country. This figure shows how many leisure buildings that were built and the use area for this period.

Both Figure 2.3 and Figure 2.4 show that the use area has a steeper increase than the number of built leisure homes, hence the average use area has increased since 1983. As the use area increases, there are more room for sanitary installations and the importance of keeping the leisure home above freezing point during winter increases. Also more electrical equipment has been installed. SINTEF recommends a minimum temperature of 10 $°C$ in leisure homes to avoid frost damages. Insurance companies annually spend approximately 100 million NOK on frost damages (SINTEF, 2011). This emphasises the importance of finding alternative ways to deliver excess heat needed for frost protection. Another major factor that contributes to the increase in electricity consumption is that several conventional leisure homes have been upgraded with installed power.

2.2 Requirements

Traditionally, the development of leisure homes has been carried out without considering energy efficiency. This is in conflict with the requirements set for permanent houses today. Even though the energy use in leisure homes represents a relatively small part of the total energy use, this consumption can be seen as a luxury and not a necessity. According to the new Norwegian Building Regulation TEK10 §14 – 4 leisure homes with a use area larger than 150 m^2 have the same requirements as permanent houses. Table 2.1 show the minimum requirements for U-values and air density in buildings. Requirements for leisure homes with a use area smaller than 150 m^2 and for leisure homes with log walls are slightly different. They are presented in Table 2.2 (Lovdata, 2010). For leisure homes with a use area smaller than 50 m^2 there are no requirements for energy efficiency.

U-value external wall $[W/m^2K]$	≤ 0.22
U-value roof $[W/m^2K]$	≤ 0.18
U-value floor and to the exterior $[W/m^2K]$	≤ 0.18
U-value window $[W/m^2K]$	≤ 1.6
Air infiltration, air changes per hour at 50 Pa pressure difference	≤ 3.0

Table 2.1: Requirements for use area larger than 150 m^2

	Building with log walls	Leisure homes with a use area smaller than 150 m^2 with log walls
Dimension external wall	$\geq$ 8 " logs	$\geq$ 6 " logs
U-value roof $[W/m^2K]$	≤ 0.13	≤ 0.18
U-value floor and to the exterior $[W/m^2K]$	≤ 0.15	≤ 0.18
U-value window $[W/m^2K]$	≤ 1.4	≤ 1.6

Table 2.2: Requirements for leisure homes with a use area smaller than 150 m^2 and with log walls

Historical building regulation requirements are presented in Table 2.3 (dsb, 2010),(Lovdata, 2010).

Building Regulation	Roof	Floor	Exterior wall	Window
1969	0.23	0.30	0.45*	*included in exterior wall value
1987	0.20	0.20	0.30	2.40
1997 (TEK97)	0.15	0.15	0.22	1.60
2007 (TEK07)	0.13	0.15	0.18	1.20
2010 (TEK10)	0.13	0.15	0.18	1.20
2010 (NS3700 Passive- and low energy houses)	0.13	0.15	0.15	0.80

Table 2.3: Historical U-value requirements

Chapter 3

The leisure home model

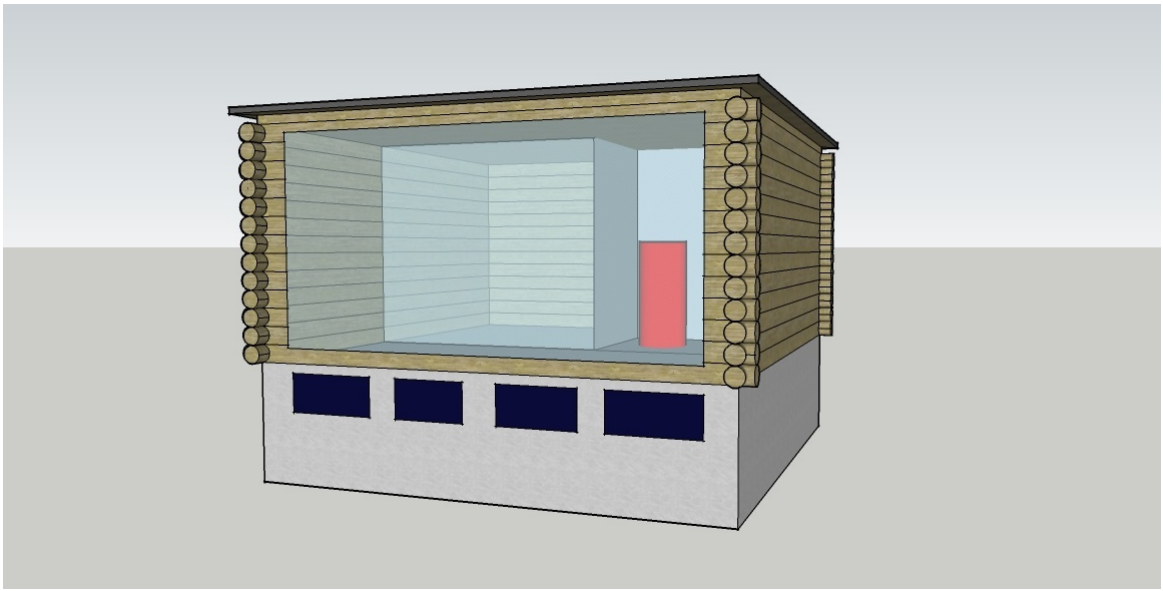

Figure 3.1: Leisure home building

Figure 3.1 shows the leisure home building that is to be modeled.

This report examines possible solutions to keep the sanitary installations in a leisure home in the southern mountain regions of Norway frost proof throughout the winter without the use of electricity. The idea is to use a solar heating system to cover the heating demand. Solar collectors will transfer heat into the basement floor in an internal zone. The idea is that the heat injected into the basement floor will disperse to the thermal mass underneath the building. The heat from the solar collectors will be stored in the thermal mass under the building and be used during winter when there is little or no solar radiation available.

3.1 The model used in previous studies

The model geometry and construction of the leisure home model used in the simulations were after discussion with the supervisor chosen to be the same as used in previous studies. A floor slab and a partition wall divide the cabin into four zones. In addition, an internal zone is placed both in the first floor and in the basement creating a total of six zones. A window is placed on the south wall in 1st floor, and it covers 80 % of the wall. This geometry is continued from the project thesis and it has also been used by Are Siljan Børset (Børset, 2009) and Anne Kristine Amle (Amble, 2008) among others.

Figure 3.2 shows a floor plan of the leisure home illustrating the division of the zones in one floor and the dimensions.

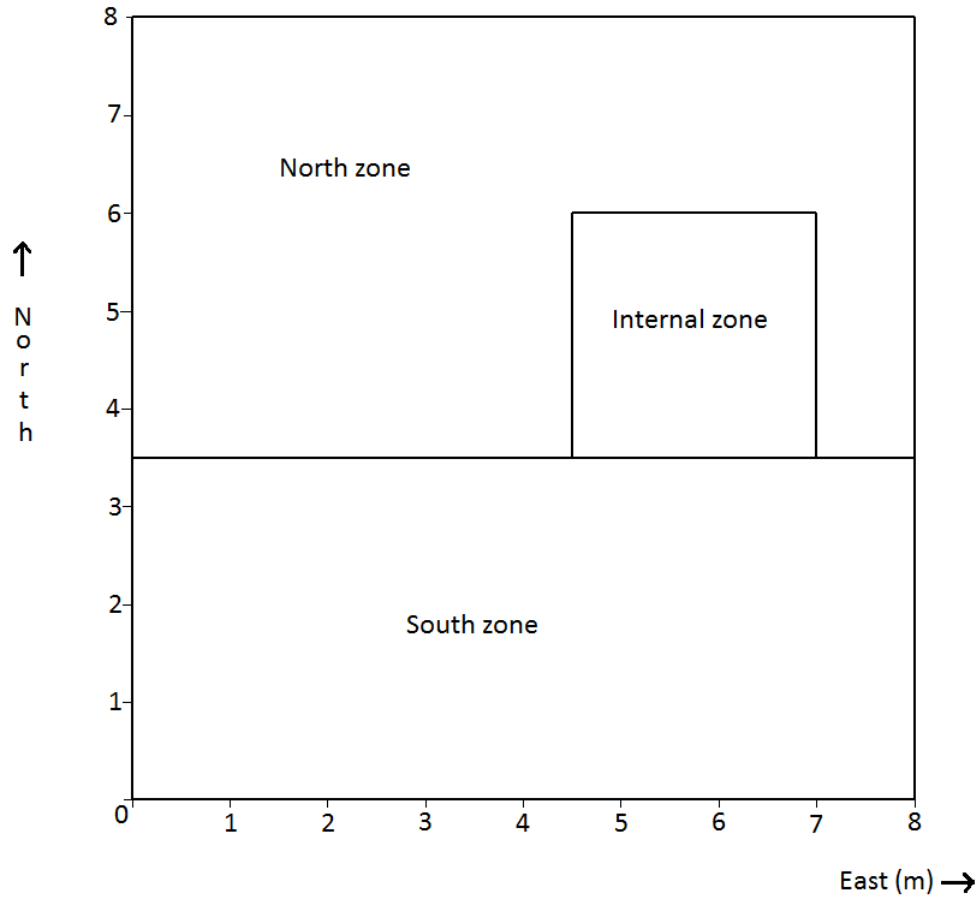

Figure 3.2: Leisure home floor plan

Figure 3.3 shows a cross section of the leisure home with dimensions.

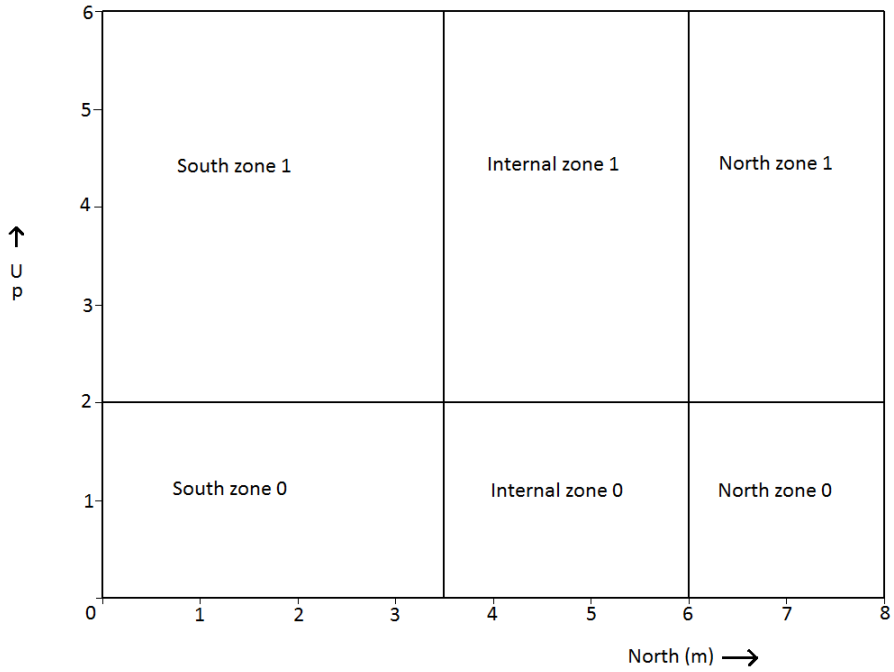

Figure 3.3: Leisure home cross section

Figure 3.4 shows a 3D view of the model in ESP-r from the project thesis.

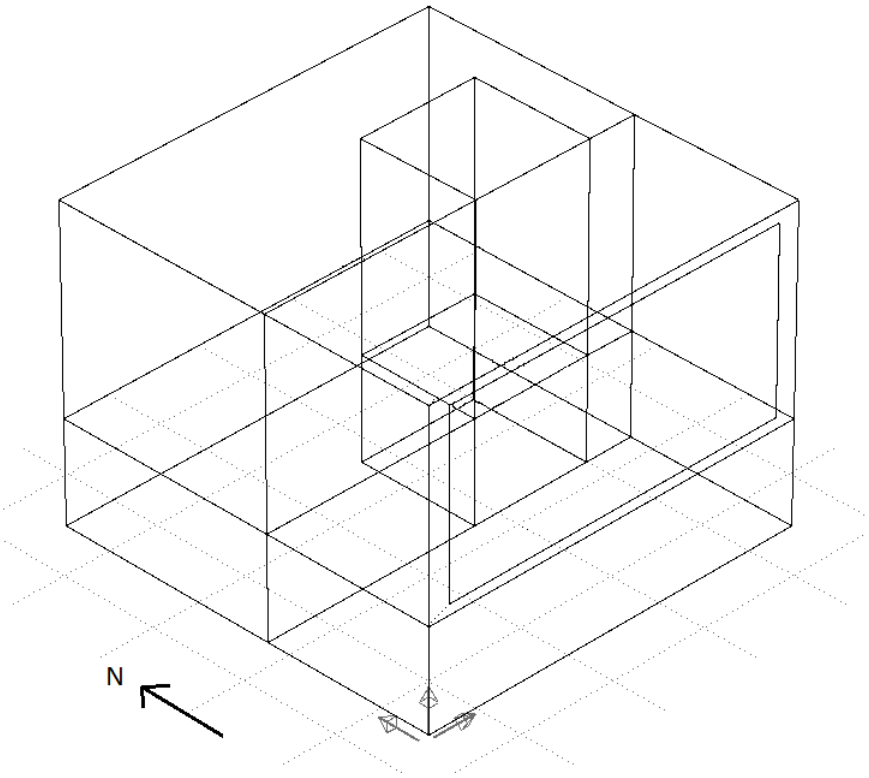

Figure 3.4: Leisure home model from previous studies

The construction details for the leisure home are presented in Table 3.1.

Construction	**Material**	**Thickness** $[mm]$	**U-value** $[W/m^2K]$
External wall first floor	Fir	150	0.806
Internal zone wall	Polyurethane foam	250	0.117
	Heavy mix concrete	100	
South-facing window	Plate glass	6	1.458
	Air	16	
	Plate glass	6	
Partition wall between north and south zone	Plate glass	6	2.811
	Air	12	
	Plate glass	6	
Floor slab	Heavy mix concrete	150	3.608
Internal zone basement floor*	Heavy mix concrete	500	0.379
	Massive concrete	3000	
External wall basement	Heavy mix concrete	200	0.128
	Glasswool	300	
Basement floor	Flooring	100	0.106
	EPS	250	
	Heavy mix concrete	250	
Roof	Snow	300	0.052
	Fir	160	
	Polyurethane foam	350	

Table 3.1: The defined building constructions from project thesis. * The structure of the internal basement floor of the inner zone will be changed

As seen from Table 3.1 the internal basement floor is 3.5 m thick and constructed by massive concrete. This massive floor was an approximation for the ground underneath the building used in the project thesis. The modeling and simulation of the ground is one of the main focuses of this report and will be discussed later.

All the constructions apart from the internal basement floor will be used further in the simulations.

It is noteworthy that the building elements are constructed only with their main parts, without elements like wind and vapour barrier. This will probably not have any large effects on the results of the simulations, and are therefore neglected to simplify the model.

3.2 Climate data

Statistics from climate databases can give information about ambient temperatures which can be used to estimate the heating demand. An issue in the design process is whether to design the system for the average heating demand over a year, the heating demand in a typical winter month, or for the extreme winter month. In this report the main issue is to keep the sanitary installations frost proof over the winter, so for this case the design point should be the extreme winter month with very low ambient temperatures that may not occur every year, but possibly every 5-10th year.

The location of the modeled leisure home is in the southern mountain regions of Norway. In ESP-r there is no climate file available for this area and an approximation was done using the climate file from Östersund, Sweden in the project thesis. Because of comparison reasons Östersund climate will be used in this study also.

Figure 3.5 shows a map of the southern parts of Norway and Sweden. Östersund is located at point A.

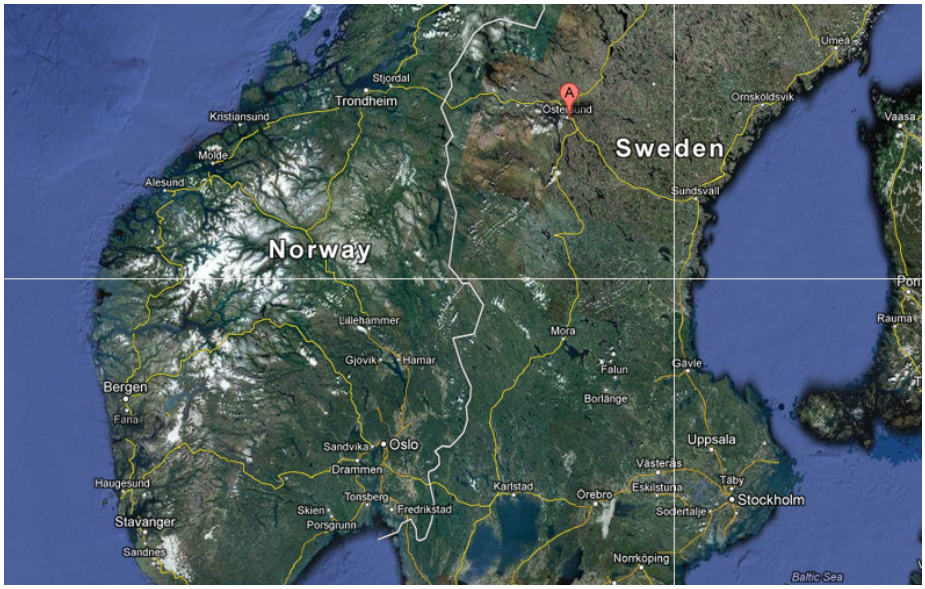

Figure 3.5: Map of Norway and Sweden (Google, 2013)

Östersund, Sweden is located at a latitude of 63.18° north and longitude of 14.67° east at an elevation of 312 meters above sea level. Solar radiation data and ambient temperature over the year can be found in the Appendix 14.

3.3 Possible solutions

For the leisure home studied in this report are the sanitary installations placed in well-insulated internal zones. The goal is to keep the inner zones above the freezing point. An active solar heating system is implemented in the model to heat up the internal zones. Different possibilities for heat storage have been considered.

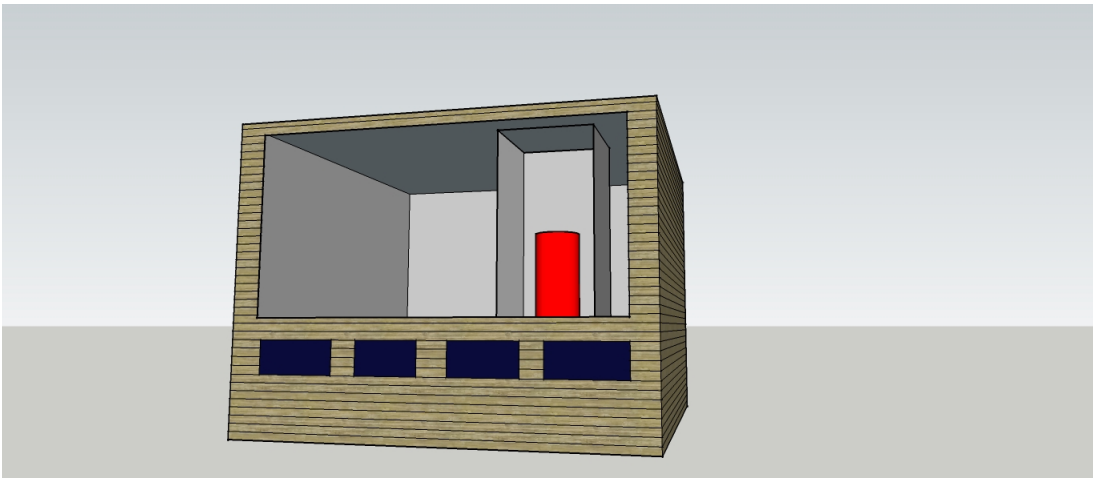

Figure 3.6: Leisure home with solar collectors and a heat storage tank in the upper internal zone

One approach is to transfer the heat from the solar collector to the tank, emitting heat to the surrounding room. The amount of heat transferred to the tank will vary a lot depending on the season and how much solar radiation that is available. The solar collectors should be installed with a relatively steep incline to absorb sufficient amount of heat in the winter months.

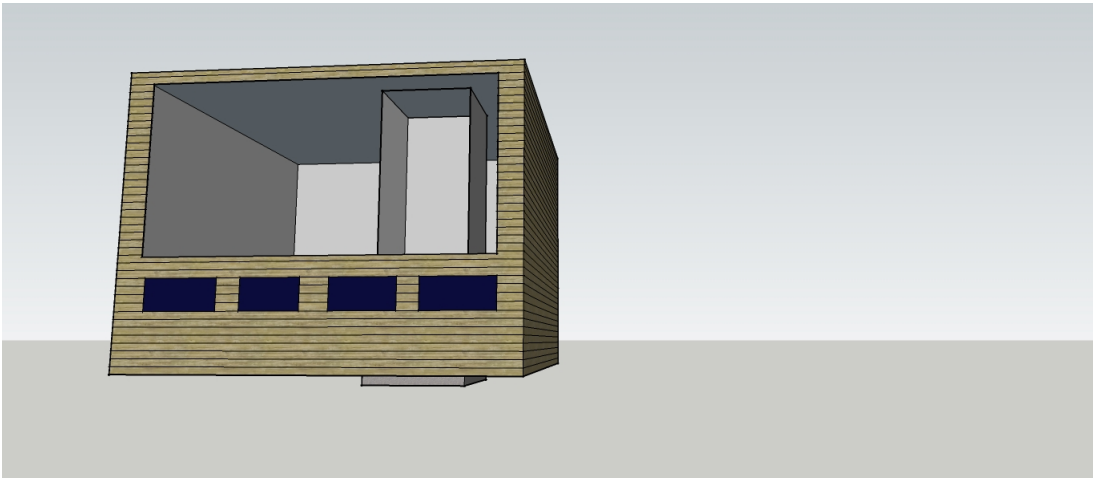

Figure 3.7: Leisure home with solar collectors and heat exchange with the ground

Another approach is to transfer heat from the solar collectors into the ground. A simple system consisting of solar collectors, a distribution system and a pump can be used to transfer heat to the ground under the internal zones. During the winter, passive heat transfer will occur from the ground and into internal basement floor. An advantage of using the ground as a heat storage compared to a water tank is that the heat is stored for a longer period of time as the heat capacity in the ground is larger than the heat capacity in water. This reduces the dependency of sunlight during the winter, compared to the case with a water tank, where the water has to be heated continuously. The solar collectors should be installed at an incline were most heat is collected over the year.

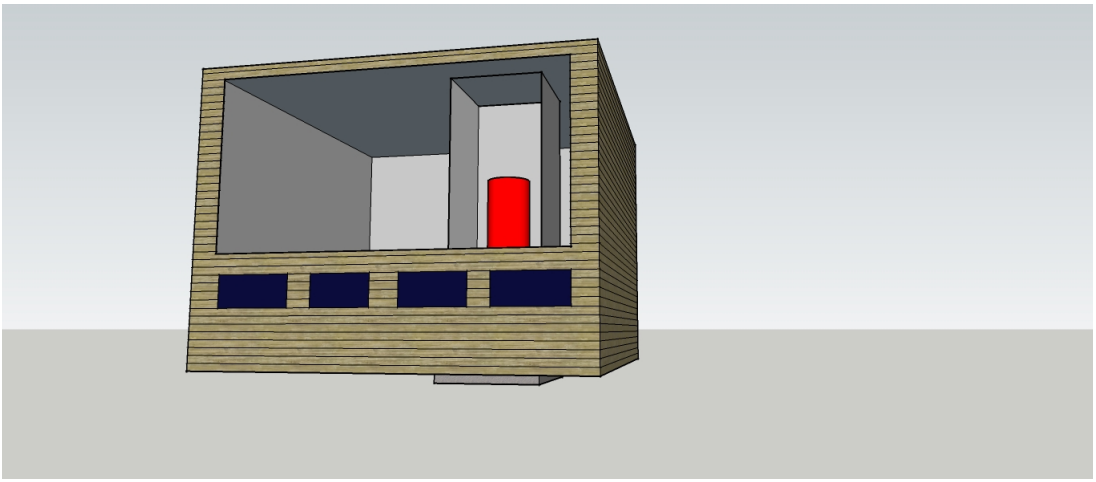

Figure 3.8: Leisure home with solar collectors, a heat storage tank in the internal zone and heat exchange with the ground

A third way to store heat in order to keep the internal zones above the freezing point is a combination of the two approaches above. Depending on when the cabin is being used, heat from the solar collectors could be transferred to either a hot water tank or into the ground.

3.4 Some results from the project thesis

The purpose of the project thesis was to gain knowledge about the dynamic simulation tool ESP-r, and to use ESP-r to analyse the energy use in a leisure home with an active solar heating system and seasonal heat storage. The goal was to maintain frost proof conditions for the sanitary installations placed in an internal zone throughout the year without the use of electricity or primary energy sources.

The ground under the entire cabin was modeled as a massive concrete pillar placed under the internal zone in the basement. The idea was that this large thermal mass would represent the entire ground under the cabin. The thermal properties were adjusted to investigate the influence of the available amount of thermal mass. The predefined parameters for concrete in ESP-r were adjusted, creating a new concrete material. The

product of the density and the specific heat capacity was multiplied by different factors to investigate the sensitivity of thermal mass under the cabin. Heat was transferred into the floor of the bottom inner zone, and stored in this pillar under the cabin. This is a rather rough approximation and the idea is illustrated in Figure 3.9.

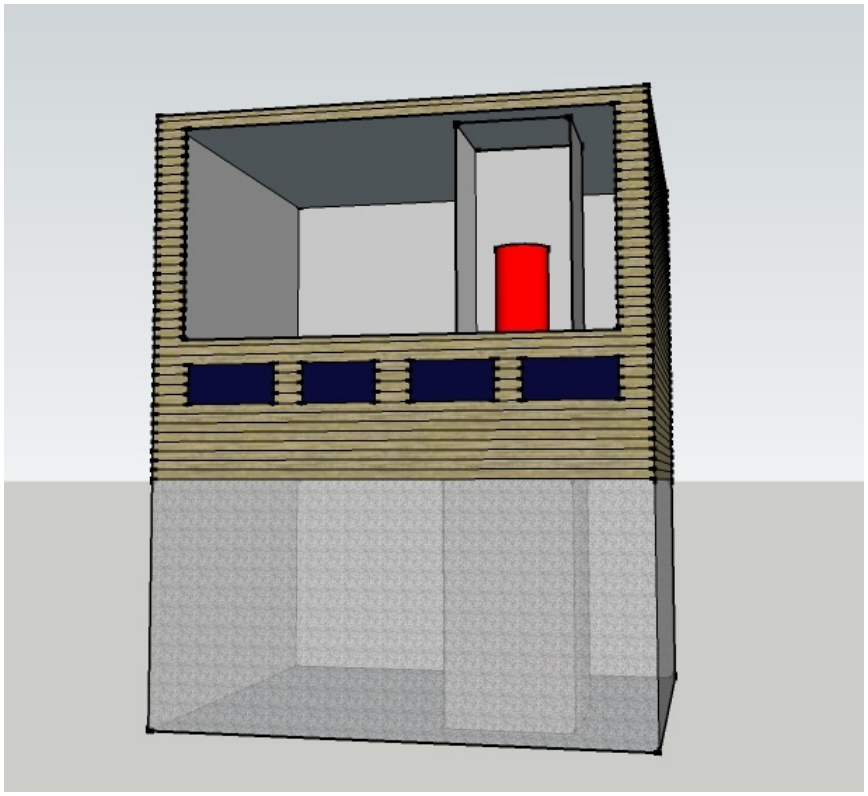

Figure 3.9: Demonstration of thermal mass

Solar radiation data was collected for different inclines and a control loop for the inner zone in the basement was developed. This control loop injected heat into the concrete pillar for a given period each day. This works more like an electric heating system and not as a hydronic heating system which is what would have been used if a solar heating system was created.

An incline of 45 ° was chosen, and azimuth south to collect as much solar radiation as possible. A collector efficiency of 45 % and a collector area of 4 m^2 were chosen based on discussion with the supervisor.

Heat was injected at 0.5 m depth and the ground was modeled with different thermal properties. Simulations were also performed using a collector area of 6 m^2 and different depths of heat injection.

Table 3.2 shows the results for Case 4 were the density and the specific heat capacity was multiplied by a factor of 10.

	Minimum temperature	Maximum temperature
Inner zone ground floor	8 °C	42 °C
Inner zone first floor	5 °C	38.5 °C
Time of peak value	Week 5	Week 32

Table 3.2: Peak temperatures for Case 4

With a collector area of 4 m^2 and an efficiency of 45 % the total delivered energy over the year turned out to be 1908 kWh. For the case were the density and the specific heat capacity was multiplied by 10 accounting for the total volume under the cabin, and heat injection at 0.5 m, the minimum temperature occurred in the first floor of the inner zone at a temperature of approximately 5 $°C$.

This temperature does not meet the requirements from SINTEF requiring a minimum temperature of 10 $°C$ in leisure homes. However the safety margin of 5 $°C$ is probably sufficient to obtain frost proof conditions for sanitary installations in the well-insulated internal zones.

The most central results from the simulations in the project thesis are attached in Appendix 14.

3.5 Improvement and further development of the leisure home model

Further improvements of the model from the project thesis is considered in the following section.

3.5.1 The leisure home model

The geometry of the modeled building is quite simple. The building is modeled as a large box, with only one large window and no doors. The building elements are made only with their main parts. These are simplifications that probably would not have any large impact on the results of the simulations and the leisure home model will therefore not be further developed in this study.

Infiltration was not implemented in the model in the project thesis. In reality there will be air flow between adjacent rooms, and between the inside and outside of the building. This will neither be implemented for the further study as this is not the main focus of this report.

Buildings that are constructed in colder climates today are built with ground insulation under the floor slab. In most cases ground insulation is placed around the perimeter of the floor slab, like a skirt.

To minimize heat loss from the building and the heat storage under the building, ground insulation should be implemented in the model around the perimeter of the floor slab. Insulation on the northern and southern basement floor is already a part of the constructed floor in the model and should be kept this way.

Figure 3.10 shows the principle of ground insulation around the perimeter and how this will prevent heat loss to the surrounding air.

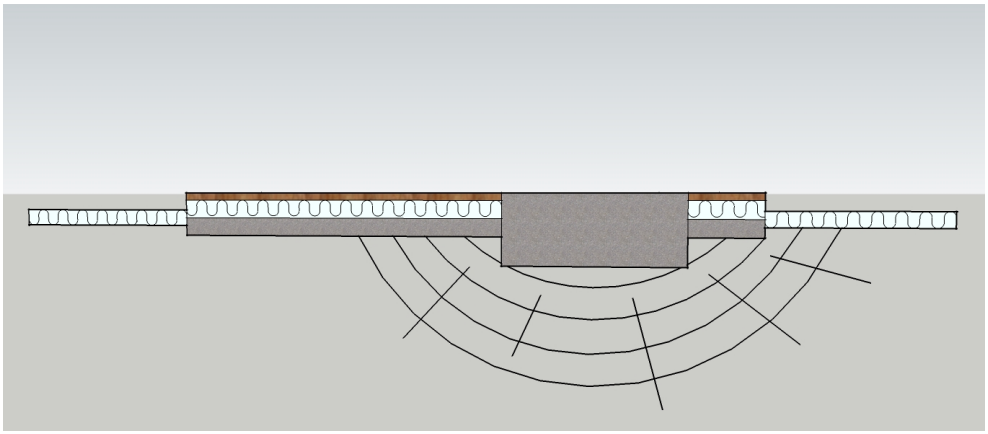

Figure 3.10: Ground insulation around the perimeter of the floor slab

3.5.2 The modeling of heat transfer between the building and the ground

The heat transfer through the concrete pillar that represented the entire ground in the project thesis was modeled 1-dimensionally. The boundary condition on the lower side of the pillar was a monthly ground temperature profile at 4 m depth. A main focus for this study will be to improve the modeling of the heat transfer between the building and the ground. Ideally 3D-modeling of the ground should be implemented together with appropriate boundary conditions.

Different simulation tools should be studied further to see if there are any other tools that are more suitable for this kind of simulation.

It has been decided in consultation with the supervisor that the main focus of this study will be to improve the modeling between the ground and the leisure home building.

3.5.3 Solar heating system

In the project thesis a control loop based on solar radiation data was used to represent a solar heating system.

Solar radiation data was studied and the amount of solar energy that was available, multiplied with an efficiency and a collector area, was injected into the floor by the control loop.

If a solar heating system with a hydronic floor was implemented it would not be able to extract the same amount of energy that is available from the sun. Especially in the summer would the error be large. A longer period with a lot of solar energy available would result in a heated floor. When the floor is already heated the heat transfer fluid will not be able to deliver all the heat that it is carrying and neither extract all the energy that is available from the collector, because the temperature difference between the floor and the collector will be too small.

A solar heating system consisting of solar collectors, pump and hydronic floor should be implemented to improve the model. This will give a more realistic view of how much heat that can be extracted from the solar system and stored in the basement floor.

Figure 3.11 illustrates the solar heating system. When the floor heats up, the excess heat will disperse into the surrounding soil, working as a thermal storage.

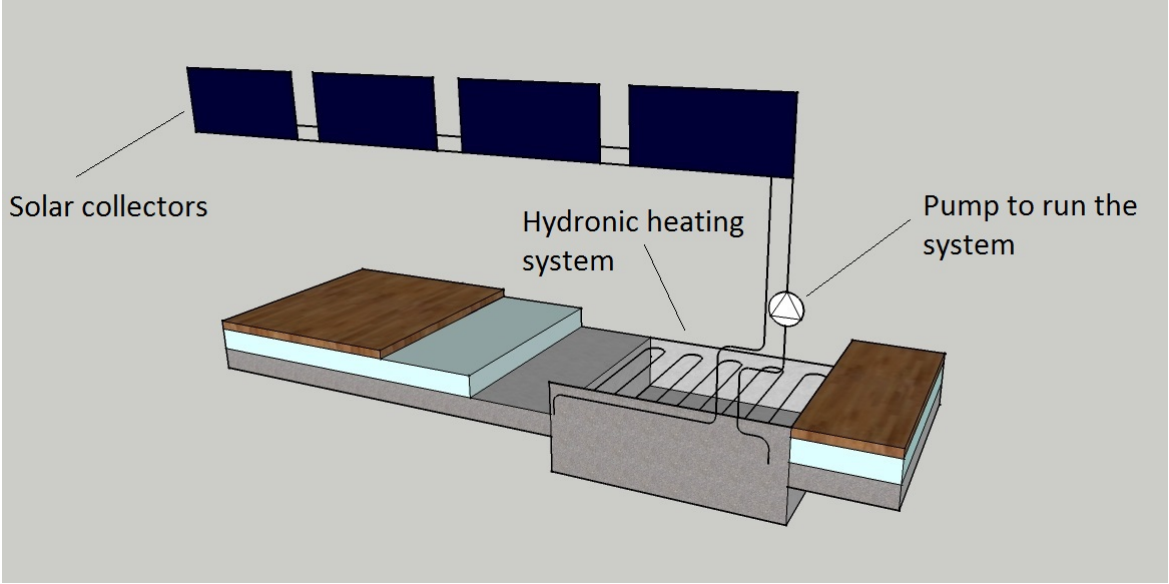

Figure 3.11: Solar collectors with hydronic heating system implemented in the basement floor of the inner zone

However, it is the ground modeling that is the main focus of this report.

Chapter 4

Solar Energy

A solar heating system can be used to keep the internal zones frost proof. The system can also be used for space heating and to produce domestic hot water in leisure homes. In this chapter will important definitions regarding solar radiation and available resources be presented along with a description of different solar heating systems and components.

4.1 Solar radiation and availability

The sun is a natural, environmentally friendly and free energy source. Solar energy is available all over the earth, in great amounts, and is relatively uniformly distributed. Each year the earth receives 15 000 times more energy than what is used (Andresen, 2008). With a constant increasing awareness regarding energy use and greenhouse gas emissions, solar energy is considered to be one of the potential ways to escape the current predicament regarding fossil fuels. Although solar energy has great potential, the technology cannot yet generate the amount of power offered by fossil fuels. However the technology is an internationally growing industry.

Solar irradiance is defined as the rate at which radiant energy is incident on a surface per unit of surface. Outside the earth's atmosphere, the solar irradiance is approximately constant equal to 1367 W/m^2 with a variation of $\pm$ 3 %. This variation is due to the changing distance between the earth and the sun. On average, approximately 30 % of the solar radiation is reflected before it reaches the surface of the earth (SINTEF, 2007). The solar radiation is scattered by the atmosphere, spreading light and mitigating certain wavelengths. The mitigation varies according to the atmospheric content of gases. The amount of solar radiation that can be utilized for energy use therefore depends on the following conditions:

- Geographical location: the sun is lower on the northern and the southern hemisphere compared to close to the equator. Far from the equator, solar rays have to pass through more air to reach the ground, increasing the scattering.
- Time of the year: the sun is higher in the summer than in the winter, except from in tropic areas.

- Local conditions: local cloud formation and shadows from nearby nature and buildings will decrease the incoming radiation upon a surface influenced by these factors.

Figure 4.1 shows the path of the sun at different times of the year at central European latitude (London, Berlin).

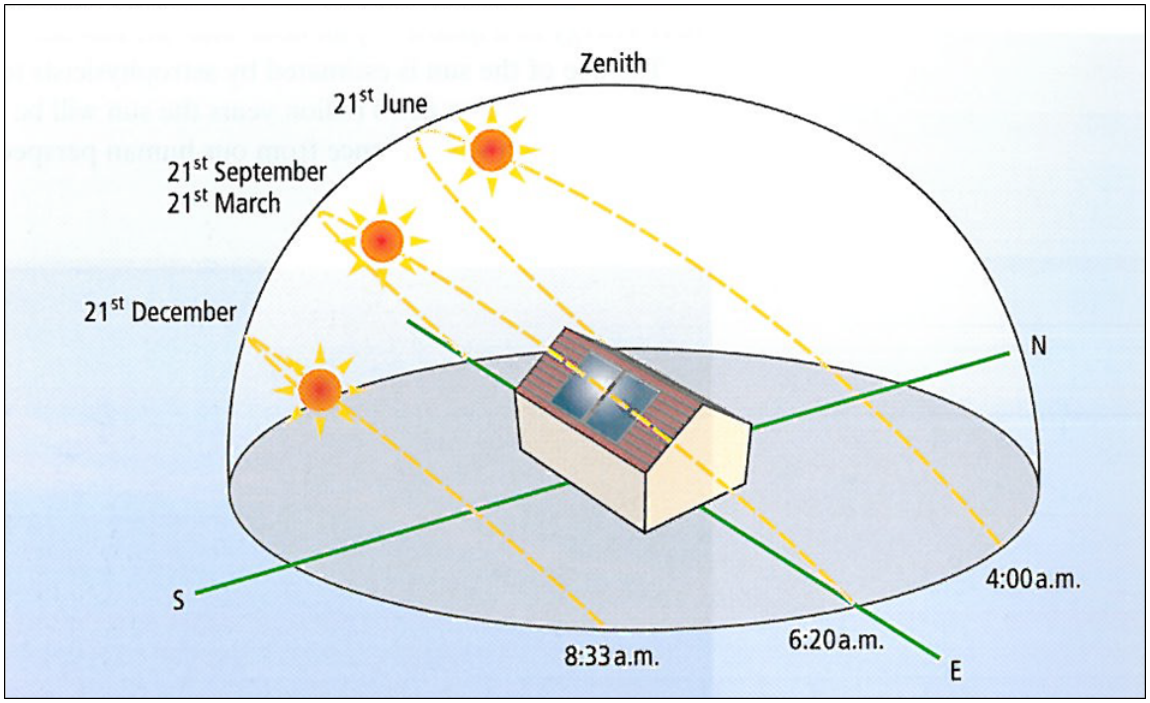

Figure 4.1: The sun's path at different times of the year at central European latitude, London/Berlin (*Planning an Installing Solar Thermal Systems: A guide for installers, architects and engineers*, 2005)

The solar energy reaching the surface of the earth consists of two components: direct and diffuse radiation. Direct solar radiation is received directly from the sun, while diffuse radiation is scattered from the sky and from the surroundings in all directions. Additional radiation received from the surroundings depends on the local albedo, defined as the ratio of reflected radiation from the surface to incident radiation upon it. Figure 4.2 shows the principal of direct, diffuse and reflected radiation.

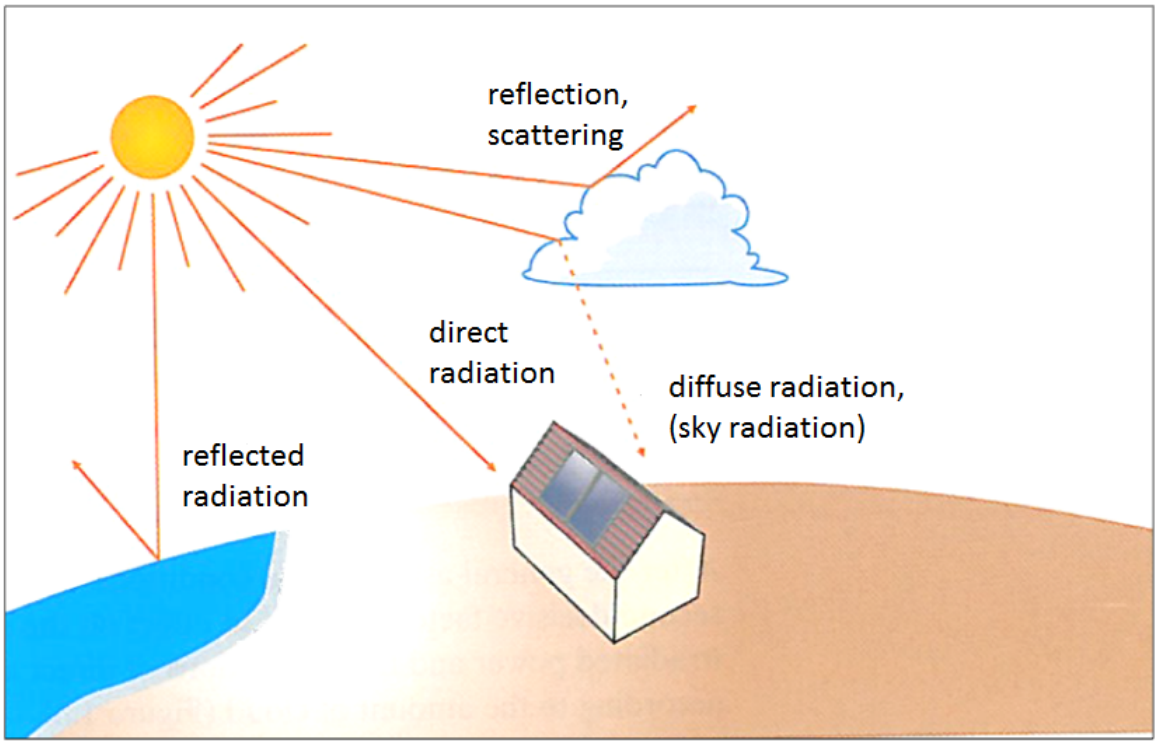

Figure 4.2: Global solar irradiance and its components (*Planning an Installing Solar Thermal Systems: A guide for installers, architects and engineers*, 2005)

Figure 4.3 shows the annual solar radiation on an optimally angled plate (SINTEF, 2007).

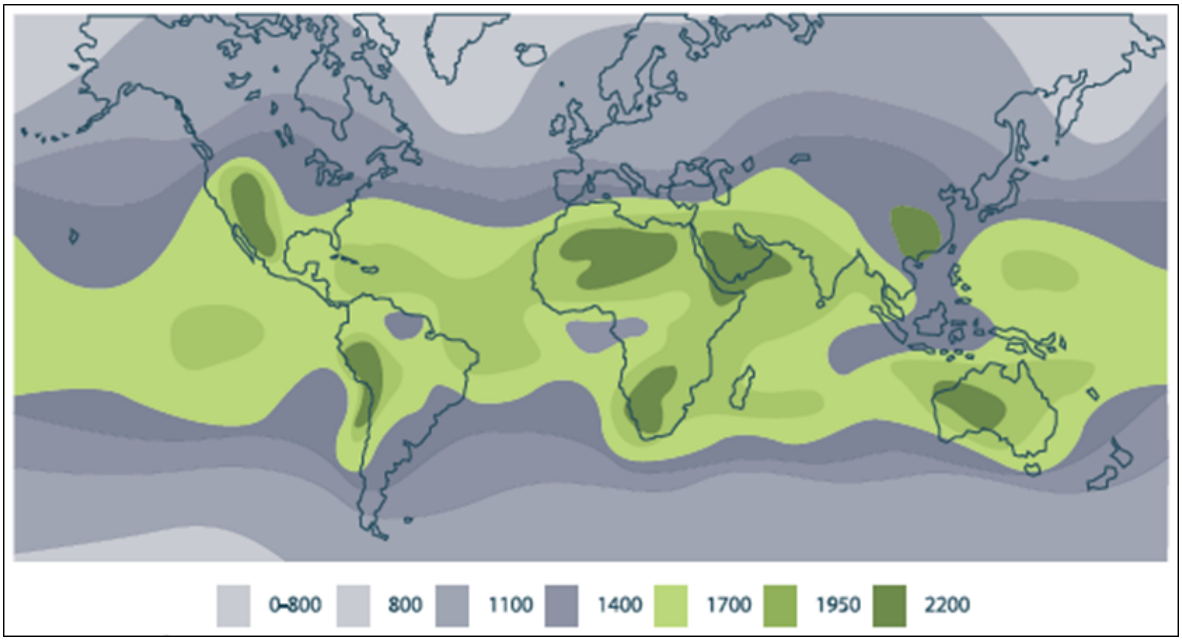

Figure 4.3: Annual solar radiation on an optimally angled plate, average kWh/m^2year (SINTEF, 2007)

There are three main principles for utilizing energy from the sun: Passive solar systems, active solar systems and photovoltaic cells. Passive solar systems and active solar systems exploit thermal energy from the sun, while photovoltaic cells convert solar energy to electricity. Emphasis will be placed on active solar systems.

4.2 Solar radiation in Norway

Despite Norway's location on the northern hemisphere, the availability of solar energy here has great potential. More than 1 500 times the energy used in a year is radiated over the country (Andresen, 2008).

Figure 4.4 shows daily solar irradiance against a horizontal plate in January and July in Norway. The figure shows that the solar irradiance is highest in the south of Norway during the summer.

Figure 4.4: Daily solar irradiance incident on a horizontal plate in January and July respectively (SINTEF, 2007)

The energy gained from the solar irradiance can be greater than the values shown in Figure 4.4. This can be obtained by placing solar collectors at an optimal angle towards the sun. This would increase direct solar radiation incident on the solar collectors, as the sun is low on the horizon in Norway.

4.3 Components of a solar heating system

The main components of a solar heating system are solar collectors, a heat-storage, heat exchangers, a distribution system, and a control system. A heat-storage is necessary to store heat in periods when there is little or no solar irradiance incident, such as during the night or in cloudy periods. The distribution system consists of pipes and pumps transferring the heat from the solar collector to the storage tank and to the consumption site. Usually a solar heating system cannot account for the total energy supply and an auxiliary energy supply is needed. Figure 4.5 shows a principal sketch of a solar water heating system for a house. The auxiliary energy supply, a heating boiler in this case is connected to the upper part of the storage tank.

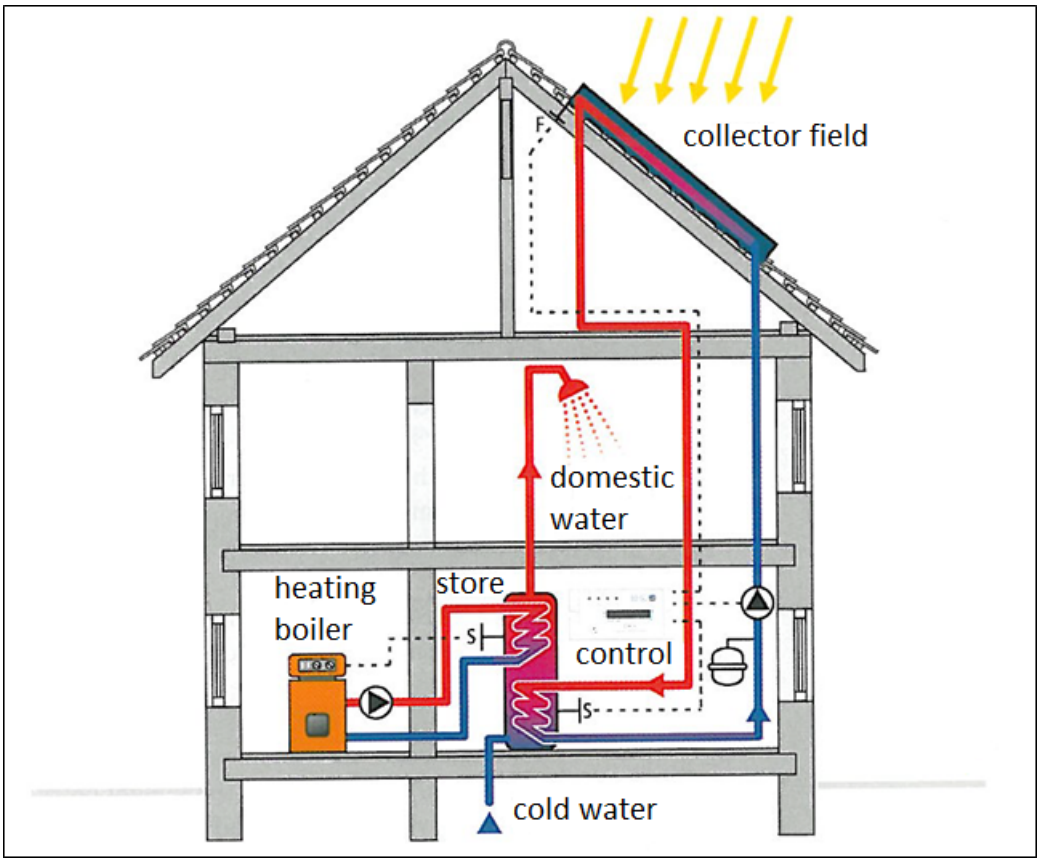

Figure 4.5: Standard solar water heating system with heating boiler for additional heating (*Planning an Installing Solar Thermal Systems: A guide for installers, architects and engineers*, 2005)

4.3.1 Solar collectors

A solar collector is the heart of a solar heating system. This is where the solar irradiance is absorbed and converted to thermal energy. There are a number of different types of solar collectors, such as flat plate collectors, evacuated tube collectors, parabolic collectors and trough-shaped collectors. The different collectors have different strengths and weaknesses, and the choice of collector is often based on climatic conditions. Traditionally the flat plate collector is the most widely used in Norway. Eventually the evacuated tube collector has become a larger part of the market as well. The flat plate collectors and the evacuated tube collectors are the ones that are likely to be used on leisure homes and these will be further discussed.

Most solar collectors consist of an absorber, a translucent coating layer often referred to as glazing and insulation. Flat plate collector systems and evacuated tube collector systems use a heat transfer fluid that flows through the collector. The sun shines through the glazing and hits the absorber, heating the fluid inside the tubes.

The absorber is the key component in the solar collector. This is where the solar irradiance is converted to thermal energy. The absorber is usually a thin metal plate with a black colour or a selective surface. A selective surface absorbs a large part of visible light, around 98 %, in the same way as a black painted surface does, but it emits less infrared radiation (Andresen, 2008). This means that by using a selective surface, the heat loss from the solar collector is reduced, resulting in a more efficient solar collector. The task of a solar collector is to achieve the highest possible thermal yield. The absorber is therefore provided with a high light-absorption capacity and the lowest possible thermal emissivity.

Glazing is used to protect the collector from weather conditions, and to utilize the greenhouse effect that occurs. Glazing is especially useful for collectors used in cold and windy areas. The layer acts as a "heat trap" by taking up short wave solar radiation while preventing long wave heat radiation from escaping. Usually the glazing layer is made of glass or plastic. Using a glazing layer with a low emitting coating or with transparent insulation materials can further reduce the heat loss. Measures taken to reduce the heat loss from the solar collector will however often result in a reduction of the transmission properties in the glazing, and it is therefore necessary to consider what the optimal combination is for each individual case.

To increase the performance of the solar collector, it is essential to insulate the collector. This will reduce the thermal conduction and the heat losses to the surroundings. A common insulation material for solar collectors is mineral fibre, as maximum temperatures of 150-200 °C are possible (*Planning an Installing Solar Thermal Systems: A guide for installers, architects and engineers*, 2005). To avoid precipitation onto the glass pane and damaging of the light-transmitting capacity, it is important to choose an insulation material that will not vaporize at the given temperatures.

Flate plate collectors

Figure 4.6 shows a cross section through a traditional flat plate fluid based solar collector. Flat plate solar collectors are made with an insulated robust frame, a glazing attached to the front of the collector and a solid back. An absorber plate lies just beneath the glazing and metal tubes are positioned under the absorber. A heat transferring fluid flows through the metal tubes and further through the heat exchanger and the storage tank. Flat plate collectors are not the most efficient solar collectors because they suffer more heat loss than other types of collectors. However, flat plate collectors can use heat mediums resistant to freezing temperatures and are thus suited for a wider range of climates. These collectors have an operating range from well below -20 $^{\circ}C$ to around 80 $^{\circ}C$ (*Solar Water Heating*, 2006).

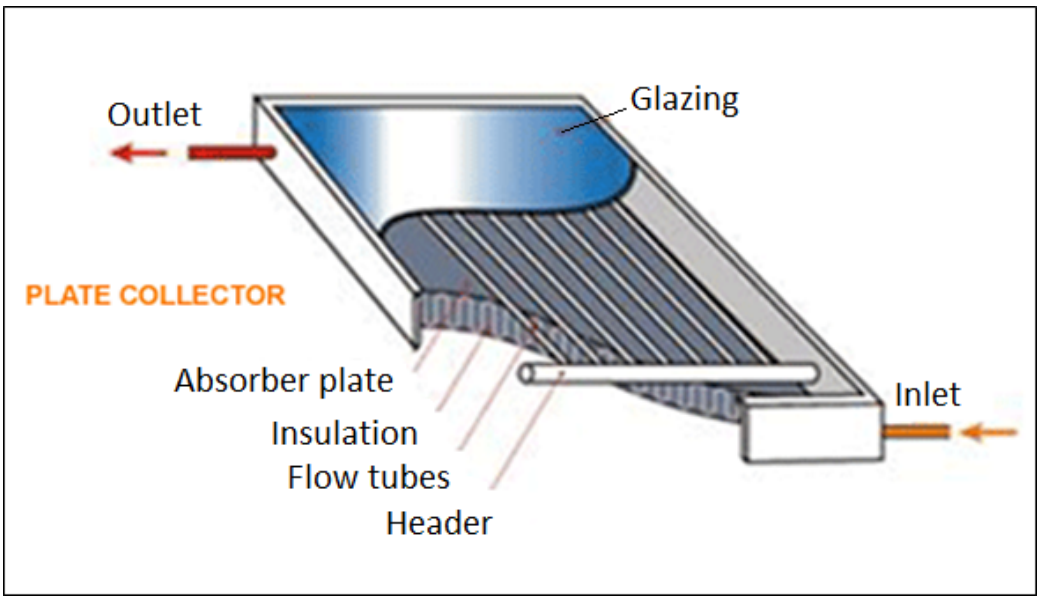

Figure 4.6: Cross section through a traditional fluid based flat plate collector (Adam Solar Resources, 2012)

Evacuated tube collectors

Unlike flat plate collectors, evacuated tube collectors vary widely in their construction and operation. In evacuated tube solar collectors absorbers are placed inside hollow glass tubes. All the air is removed from the tubes creating a vacuum. The absence of air in the tubes creates excellent insulation, allowing higher temperatures to be achieved in the absorber plate, making these the most efficient collectors.

There are several different types of evacuated tube collectors. Two examples are heat-pipe collectors and direct throughput collectors. A heat-pipe collector consists of a copper tube with a vacuum and a small amount of fluid. The vacuum enables the fluid to evaporate at low temperatures, around 30 $^{\circ}C$ (Andresen, 2008). The steam rises towards the heat exchanger at the top of the collector, where it condenses, and in this way the heat is

transferred from the solar collector to the solar circuit. The heat-pipe collector needs to be placed at a certain angle to function. Figure 4.7 shows a heat-pipe evacuated tube collector.

Another type of evacuated tube collectors is the throughput collector. Here, the heat medium flows through metal tubes inside the vacuum tubes, and the heat is transferred in the same way as for a flat plate collector. An evacuated tube collector can work well in cloudy conditions and in low temperatures.

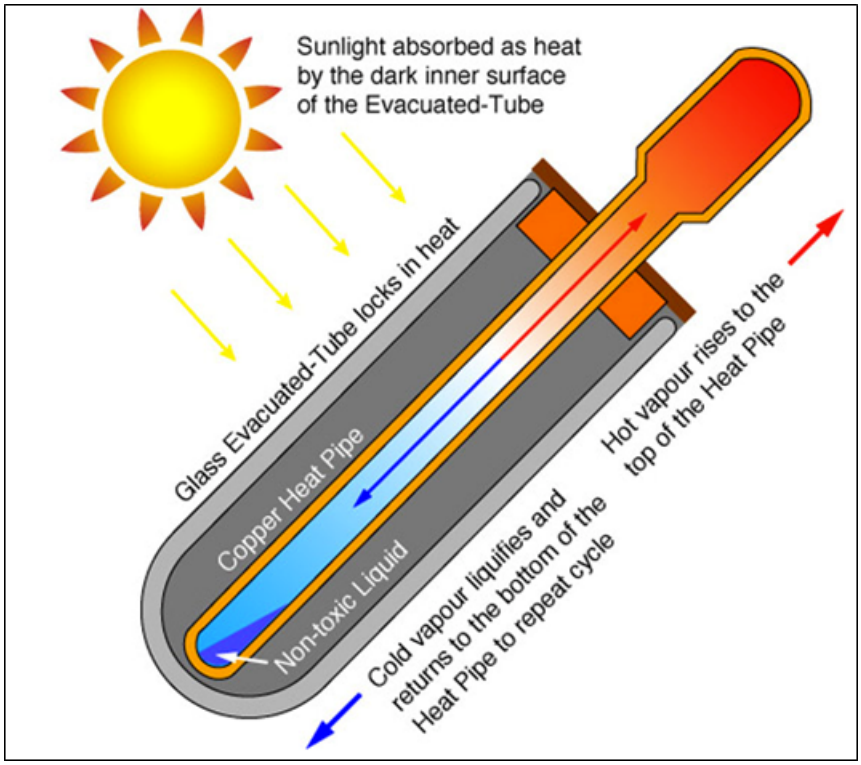

Figure 4.7: Heat-pipe evacuated tube collector (Adam Solar Resources, 2012)

Comparing flat plate and evacuated tube collectors

Advantages and disadvantages of glazed flat plate collectors and evacuated tube collectors are presented in Table 4.1 and Table 4.2 respectively (*Planning an Installing Solar Thermal Systems: A guide for installers, architects and engineers*, 2005).

Glazed flat plate collector	
Advantages	Disadvantages
• Cheaper than vacuum collectors • Offers multiple mounting options (on-roof, integrated into roof, façade mounting and free installation) • Good price/performance ratio • Possibility for do-it-yourself assembly	• Lower efficiency than vacuum collectors, because its k-value is higher • For flat roof mounting, a supporting system is necessary • Not suitable for generating higher temperatures, as required for example for steam generation • Requires more roof space than vacuum collectors

Table 4.1: Advantages and disadvantages of glazed flat plate collectors

Evacuated Tube Collector	
Advantages	Disadvantages
• Achieves a high efficiency even with large temperature differences between absorber and surroundings • Achieves high efficiency with low radiation • Supports space heating applications more effectively than glazed flat-plate collectors do • Can be easily transported to any installation site because of its low weight • In the form of direct through-flow tubes it can be mounted horizontally on a flat roof, hence providing less wind load and lower installation costs.	• More expensive than glazed flat-plate collectors • Cannot be used for in-roof installation • Cannot be used for horizontal installation for heat pipe systems (inclination must be at least 25 °)

Table 4.2: Advantages and disadvantages of evacuated tube collectors

4.3.2 Hot water heat storage

Because of the changing path of the sun, there is only a limited time in which we can exploit solar energy. Therefore all solar water heating systems will need a storage tank where the heated water from the solar system is stored.

There are several different types of heat storages or accumulator tanks suitable for solar water systems. Storage tanks without built-in heat exchangers are the most common kind found in solar water heating systems. The tank has to be insulated and has to have suitable connections to fit to the water supply, the heat exchanger and a drain. Tanks with built-in heat exchangers are specialized tanks primarily used for solar water heating technology. There are two typical configurations. The heat exchanger can either be removable and placed inside the tank, or be wrapped around the outside of the tank, between the tank and the tank insulation. A system with an internal heat exchanger is usually less efficient over time than a system using an external heat exchanger. Figure 4.8 shows a storage tank with an auxiliary heat exchanger.

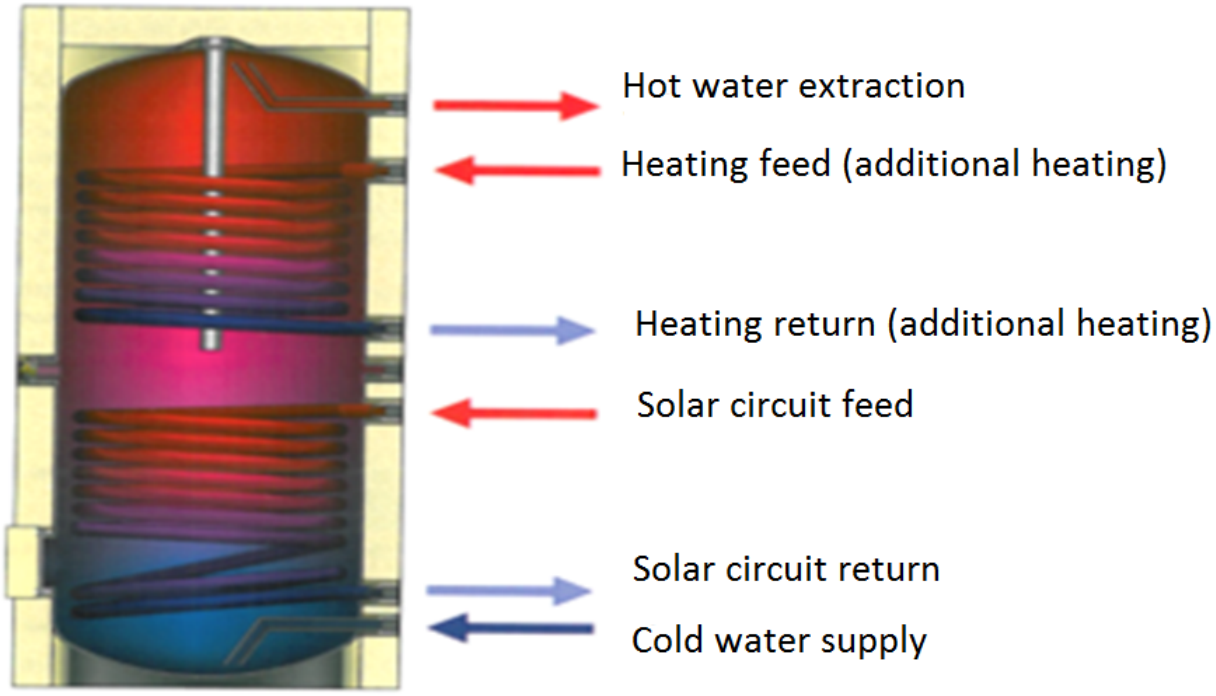

Figure 4.8: Hot water storage tank with auxiliary heat exchanger (*Planning an Installing Solar Thermal Systems: A guide for installers, architects and engineers*, 2005)

Two important parameters to be considered when choosing a heat storage tank are temperature layering and thermal insulation in the tank.

Temperature layering

To achieve optimal function of a solar water system, temperature layering is important. In a layered tank, the warm water stays at the top and cold water at the bottom, and the mixing is minimal. A high tank gives better temperature layering. The solar collector efficiency increases with a lower inlet temperature. The hot water at the top of the tank is used for domestic hot water. If an auxiliary energy source is needed this should be connected to the upper part of the tank. An alternative to a high tank is to connect several smaller tanks in series. This could be an easier installation to build and to maintain.

Insulation of the storage tank

Good heat insulation is essential for an efficient solar storage tank. In total, the heat loss rate should be less than 2 W/K. The insulation consists of CFC- and PVC-free materials with a thermal conductivity, $\lambda < 0.035\ W/mK$. As for a collector, a k-value (W/m^2) can also be defined for a storage as the ratio of the thermal conductivity to insulation thickness ($k = \frac{\lambda}{D}$ where D is the diameter of the tank). The product of the $k - value$ and the surface area of the storage tank, A, gives the heat loss rate, kA (W/K) of the tank (*Planning an Installing Solar Thermal Systems: A guide for installers, architects and engineers*, 2005).

4.3.3 Heat exchangers

Liquid-to-liquid heat exchangers are used in solar water heating systems to transfer the heat from the solar fluid into the domestic water. These can either be single-walled or double-walled. Single-walled heat exchangers have a single membrane between the two fluids and are the most efficient heat exchangers. Double-walled heat exchangers are also used in solar water heating system where domestic hot water is needed. They require an extra layer of protection to the consumption water to avoid leakage. However there is no need for double-walled heat exchangers unless a toxic solar fluid is being used, which is usually not the case.

4.3.4 Distribution systems

Normally either copper tubes or steel tubes are used in the solar heating circuit. The distribution system must withstand the pressure and the temperature gradient it is subject to, and be well insulated. According to European standard; EN 12976 the minimum heat insulation should be approximately 20-30 mm depending on the tube diameter (*Planning an Installing Solar Thermal Systems: A guide for installers, architects and engineers*, 2005).

The distribution system contains a number of components such as circulation pump, thermometer, manometer, expansion tank, safety valves, particle filter and valves for

filling and discharging the heat medium. These components are often integrated in one operational unit.

An antifreeze medium can be added to the working fluid to provide sufficient temperature difference. The thermal properties will change when antifreeze is added. If the viscosity increases, a greater pump is needed, and the operating costs will increase. Fluids that can be used as heat transfer mediums include water, salt solutions, glycol solutions and alcohol.

4.3.5 Pump

A pump is needed to operate the system. The pump requires electricity. If the leisure home is not connected to the grid, photovoltaic panels could be installed to produce electricity for this purpose. Another solution could be to use a portable generator.

4.4 Solar collector efficiency

In general, the efficiency of a solar collector can be described by (*Planning an Installing Solar Thermal Systems: A guide for installers, architects and engineers*, 2005):

$$\eta = \frac{\dot{Q}_A}{G} \tag{4.1}$$

where $\dot{Q}_A$ is the available thermal power (W/m^2) and G is the irradiance incident on the glass pane (W/m^2). The available power is calculated from the available irradiance at the absorber, converted into thermal energy, minus the losses due to convection, conduction and radiation:

$$\dot{Q}_A = G_A - \dot{Q}_L \tag{4.2}$$

where G_A is the available irradiance (W/m^2), and $\dot{Q}_L$ represents the thermal losses (W/m^2). The available irradiance G_A is defined as the product of the irradiance incident on the glass pane, the degree of transmission of the glass τ and the degree of absorption of the absorber α:

$$G_A = G \cdot \tau \cdot \alpha \tag{4.3}$$

The thermal losses depend on the temperature difference between the absorber and the air, $\Delta\theta$. This relationship can as a first approximation be considered linear and can be described by the heat loss coefficient k (W/m^2K):

$$\dot{Q}_L = k \cdot \Delta\theta \tag{4.4}$$

With the equations mentioned above, the collector efficiency can be written as:

$$\eta = \frac{G \cdot \tau \cdot \alpha - k \cdot \Delta\theta}{G} = \frac{G \cdot \eta_0 - k \cdot \Delta\theta}{G} \tag{4.5}$$

where η_0 describes the optical efficiency.

At higher absorber temperatures the thermal losses no longer increase linearly with the temperature difference. This is because of increasing thermal radiation. The equation for the second order approximation for higher absorber temperatures can be written as:

$$\eta = \eta_0 - \frac{k_1 \cdot \Delta\theta}{G} - \frac{k_2 \cdot \Delta\theta}{G} \tag{4.6}$$

where k_1 is the linear heat loss coefficient (W/m^2K) and k_2 is the quadratic heat loss coefficient (W/m^2K).

Figure 4.9 shows typical efficiency curves and areas of application with the same global solar irradiance for the following collector types: swimming pool absorber, glazed flat-plate collector, and evacuated tube collector. The efficiency is given as a function of the temperature difference between collector- and surrounding temperature.

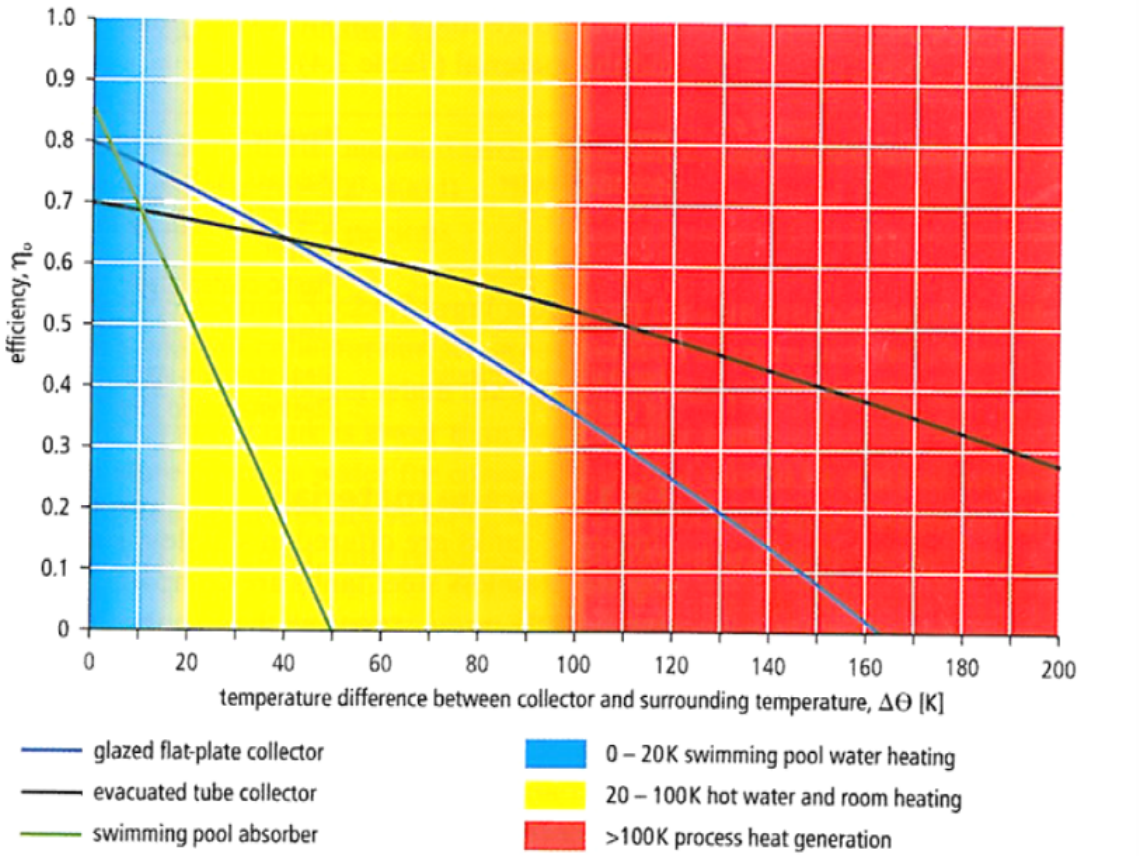

Figure 4.9: Efficiency characteristic curves for different types of collectors and their areas of application, at irradiation 1000 W/m^2K (*Planning an Installing Solar Thermal Systems: A guide for installers, architects and engineers*, 2005)

Figure 4.9 shows that as the temperature difference between the collector and the surroundings increases, the evacuated tube collector is eventually the most efficient collector. This means that in cold climates the evacuated tube collector is preferable. The average annual efficiency of a system with evacuated tube collectors is between 45 % and 50 % (*Planning an Installing Solar Thermal Systems: A guide for installers, architects and engineers*, 2005).

4.5 Active solar heating systems

In an active solar heating system solar energy is used to heat a fluid, either liquid or air. Liquid systems are commonly used when the system contains a storage tank. An active system requires a pump to circulate the fluid throughout the system. The solar heat is transferred directly to the interior space or to a storage system for later use. An active solar heating system needs some sort of control mechanism to assure that the fluid only circulates through the collector when the useful energy gain for the system is positive. Usually an active solar system cannot account for the total energy load and an auxiliary

or back-up system is used to provide the additional heat. This is because the solar gain is not always larger than the heat loss, and the storage system is too small to account for the load difference. Typical auxiliary energy supplies can be an electric resistance in the storage system, a heat pump or a boiler.

An important factor to consider for domestic hot water is to avoid bacteria such as legionella. This bacteria has its optimal growing condition between 30 $°C$ and 40 $°C$. The cold water temperature must therefore not exceed 25 $°C$ and the hot water should maintain a temperature of at least 60 $°C$. To assure that the hot water temperature does not fall below its limit, all solar water heaters must have an auxiliary heater always on and set to at least 60 $°C$.

4.5.1 Direct circulation system

In a direct circulation system the hot water from the solar collector is directly transferred to the storage tank without use of a heat exchanger. Figure 4.10 shows a direct circulation system for hot water heating, including the components.

In a direct system there is usually an extra hot water tank in addition to the storage tank as it is undesirable to mix the consumption water with the water from the collector circuit. The extra hot water tank can be integrated in the storage tank. The water must be drained from the solar collector circuit when the ambient temperature falls below freezing point.

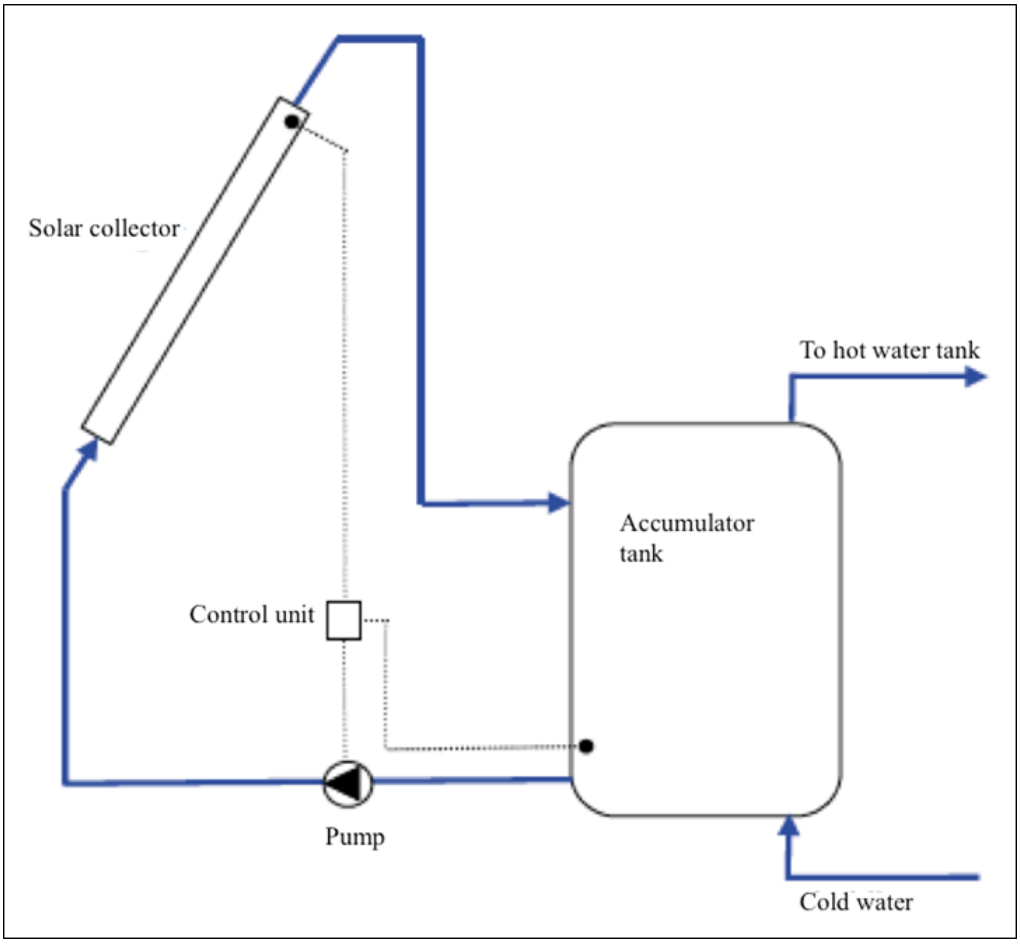

Figure 4.10: Direct system for hot water heating (Andresen, 2008)

Drain-down systems

A variant of the direct circulation system is a drain-down system. In this system the fluid in the storage tank is pumped from the tank to the collector array where it is heated. The controller will switch the pump off if freezing conditions occur or if the useful energy gain for the system is negative. The water in the collectors and in the outdoor piping system can be drained. The solar collectors and exterior piping must be carefully sloped in order for the fluid to drain when circulation stops.

4.5.2 Indirect circulation system

In an indirect system the heat from the solar collector is transferred to the storage tank via a heat exchanger. In this way a heat medium resistant to freezing temperatures can be used in the solar collector circuit. Figure 4.11 shows an indirect circulation system for hot water heating, including the components.

The heat exchanger transferring heat from the solar collector circuit to the storage tank can either be placed inside or outside the tank. Heat exchange can also occur via a

mantle around the tank. The pump is controlled by a thermostat and is switched on when the temperature at the top of the solar collector is higher than the temperature in the bottom of the storage tank. A back-to-back valve is used to prevent the circulation from reversing during the night with subsequent heat loss from the solar collector.

To decrease the risk of water being stored for longer periods, providing good growing conditions for legionella, the heat exchanger could be placed on the user side of the tank. The solar collector and the hot water tank would then be a closed system.

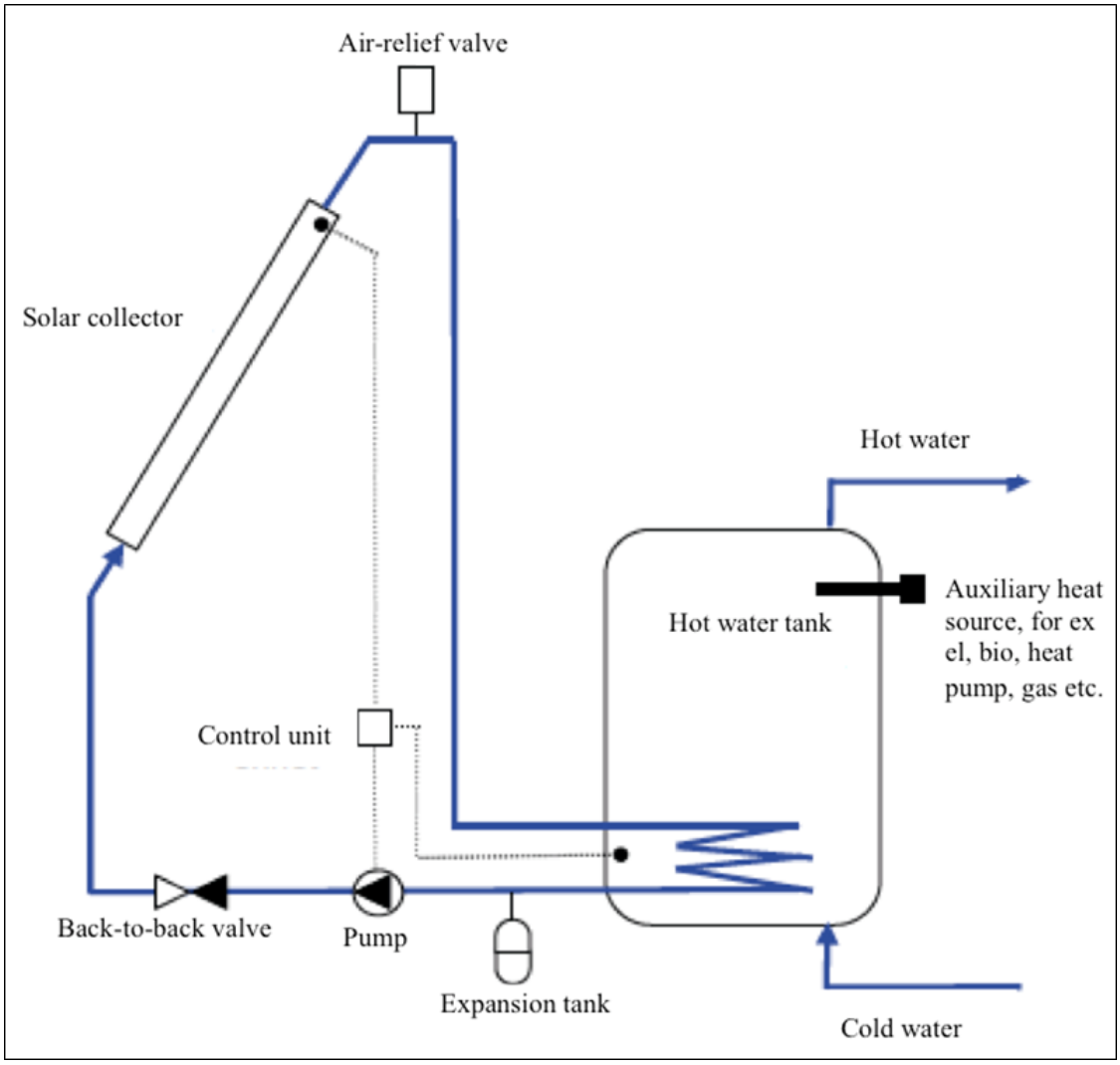

Figure 4.11: Indirect system for hot water heating (Andresen, 2008)

Drain-back systems

Drain-back systems are generally a solution used in indirect systems. In the same way as the drain-down system the circulation pump is switched off if freezing conditions occur or if the useful energy gain is negative. In a drain-back system however, the fluid in the collector and the exterior piping is not connected to a floor drain. Instead, the fluid in

the collector and exterior piping is drained by gravity to a drain-back tank. In drain-back systems, water can be used as the heat transfer fluid since the system has freeze protection. In a typical indirect circulation system the heat transfer fluid is usually a mixture of water and an antifreeze medium.

4.6 Passive solar heating system

Passive solar water heaters circulate a heat-transfer fluid through the system without the use of a pump. Passive systems require no external energy to operate. These systems are simple, reliable and easy to maintain.

Passive solar heating system can also be referred to solar radiation passing through a window hitting a wall or the floor which is constructed with concrete or another thermal material. This phenomena is discussed in Section 5.7 in Chapter 5.

Chapter 5

Heat transfer between a building and the ground

In the following chapter different storage media will be presented and theory about heat transfer in the ground. Thermal mass in the building envelope and different heat exchange systems will be discussed. Two different approaches for determining the temperatures and heat rates in the ground will also be presented.

5.1 Heat storage in the ground

Usually, not all the heat extracted from a source is needed immediately. It is therefore desirable to store the excess heat extracted. Renewable energy sources such as the sun and wind have huge potential for extracting heat and power. A challenge with these energy sources is that the largest potential for energy often occurs when the demand is low. The heat demand in Norway is at its peak during the months of January and February, while the availability of solar radiation is highest during the summer.

Heat stored in the ground originates from solar and geothermal energy. Below 10 m depth into the ground, the temperature can be considered somewhat stable. In the upper 10 m the temperature in the ground varies a lot. This temperature depends on seasonal variations, ambient temperatures, and other properties such as water content in the ground, porosity and minerals.

5.2 Two-dimensional, steady-state conduction

There are several approaches to determine temperatures and heat rates. They range from exact solutions for idealized conditions to approximate methods for varying complexity and accuracy.

Fourier's law:

$$\boldsymbol{q}'' = -k\nabla T = -k\left(\boldsymbol{i}\frac{\partial T}{\partial x} + \boldsymbol{j}\frac{\partial T}{\partial y} + \boldsymbol{k}\frac{\partial T}{\partial z}\right) \tag{5.1}$$

$$q_n'' = -k\frac{\partial T}{\partial n} \tag{5.2}$$

According to this, the local heat flux in the solid is a vector that is everywhere perpendicular to the isotherms. The heat low lines are often referred to as adiabats, because no heat can be conducted across a heat flow line (*Fundamentals of Heat and Mass Transfer*, 2007).

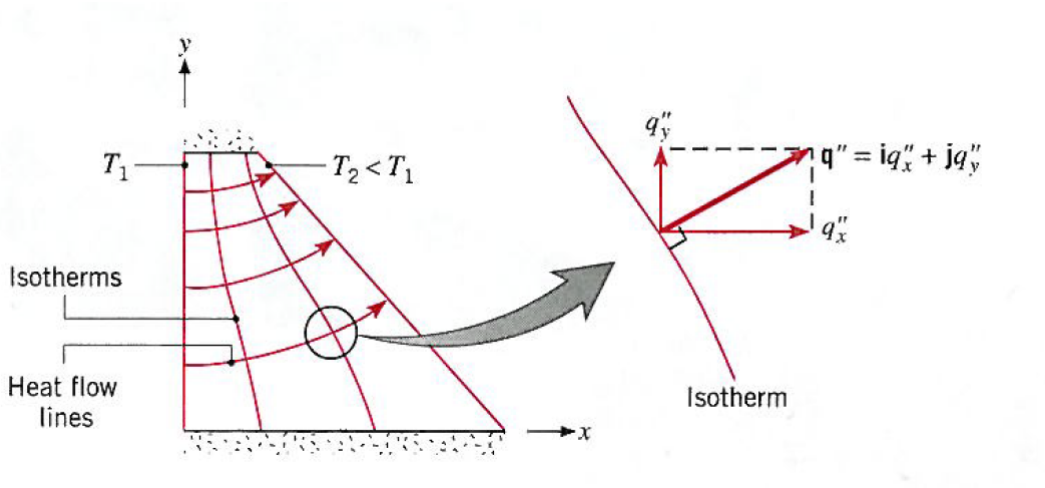

Figure 5.1: 2-dimensional conduction (*Fundamentals of Heat and Mass Transfer*, 2007)

In conduction analysis, there exists two major objectives to determine the temperature distribution in the medium and to determine the heat flux components in x-direction and y-direction.

For 2-dimensional, steady-state conditions with no generation and constant thermal conductivity, the temperature distribution can be determined by:

$$\frac{\partial^2 T}{\partial x^2} + \frac{\partial^2 T}{\partial y^2} = 0 \tag{5.3}$$

Equation 5.3 is solved by the use of analytical, graphical and numerical (finite-difference, finite-element, or boundary element) approaches.

The analytical methods provide exact mathematical solutions. The dependent variable T is determined as a continuous function of the independent variables (x, y). The temperature can be computed at any point of interest in the medium.

An analytical technique is the method of separation of variables. Conduction shape factors and dimensionless conduction heat rates that are compilations of existing solutions for typical geometries.

The next section will describe two solutions of the geometries that is approximate the same geometry as the heat storage facility for the leisure home model.

5.2.1 The conduction shape factor and the dimensionless conduction heat rate

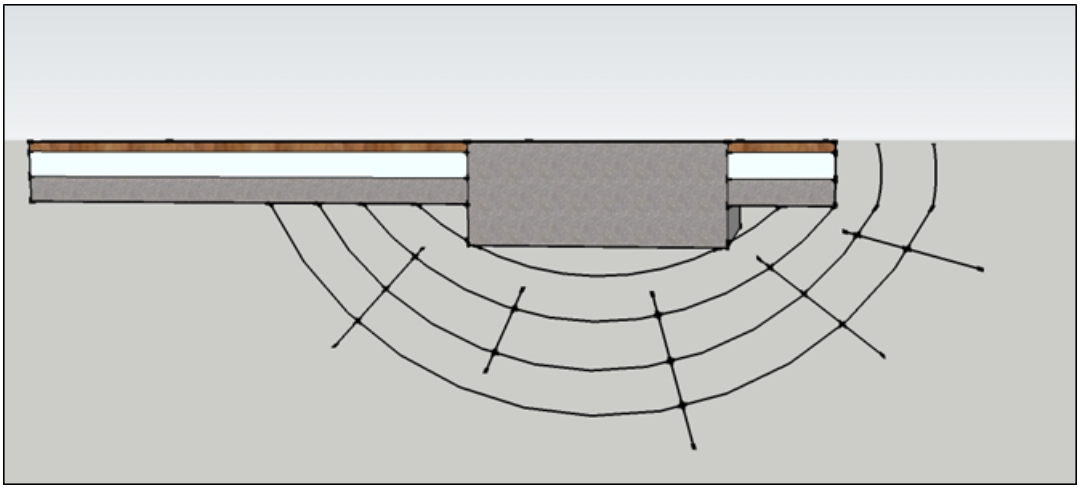

Figure 5.2: Heat loss to the surroundings

Figure 5.2 shows the heat storage facility for the leisure home model. The heat storage facility has a rectangular geometry. It is 2.5 m wide, 2.5 m long and 1.5 m thick.

Nomenclature:

A_s: Surface area (m^2)
L_C: Characteristic length (m)
q^*_{ss}: Dimensionless conduction heat rate (–)
q: Heat transfer rate (W)

The thermal mass under the cabin will experience heat loss to the surrounding soil. Assuming the concrete block is a solid held at an isothermal temperature T_1 placed in

an infinite medium with a uniform temperature T_2, a calculation of the conduction heat rate can be done.

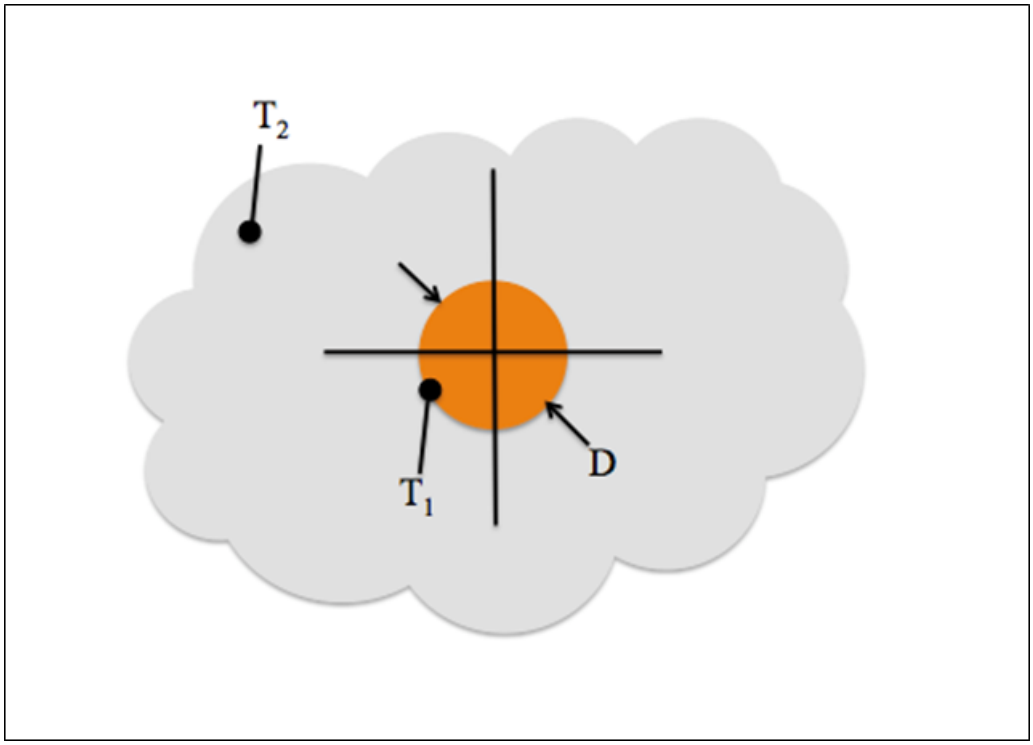

Figure 5.3: Case 1, Isothermal sphere of diameter D and temperature T_1 in an infinite medium of temperature T_2. This figure is drawn based on the figure in the book of Fundamentals of Heat and Mass Transfer (*Fundamentals of Heat and Mass Transfer*, 2007)

Surface area for Case 1:

$$A_s = \pi \cdot D^2 \tag{5.4}$$

Case 2 represents a cuboid shape with an isothermal temperature T_1 placed in an infinite medium with a uniform temperature T_2.

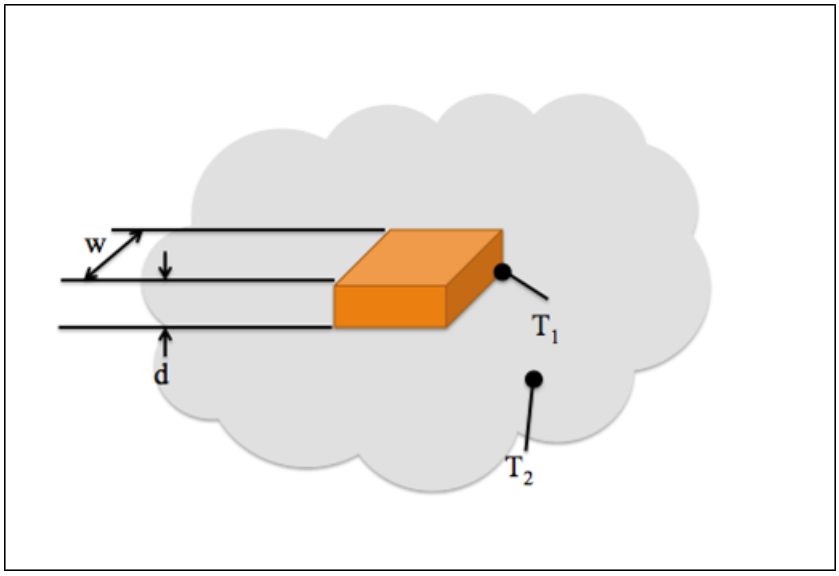

Figure 5.4: Case 2, Cuboid shape of height d with a square footprint of width w and temperature T_1 in an infinite medium of temperature T_2. This figure is drawn based on the figure in the book of Fundamentals of Heat and Mass Transfer (*Fundamentals of Heat and Mass Transfer*, 2007)

Surface area for Case 2:

$$A_s = 2 \cdot w^2 + 4 \cdot w \cdot d \tag{5.5}$$

For a solid in an infinite medium it is useful to define the characteristic length:

$$L_C \equiv \left(\frac{A_s}{4 \cdot \pi} \right)^{\frac{1}{2}} \tag{5.6}$$

The heat transfer rate is calculated from the equation below:

$$q = \frac{q^*_{ss} \cdot k \cdot A_s \cdot (T_1 - T_2)}{L_C} \tag{5.7}$$

Where q^*_{ss} is the dimensionless conduction heat rate and k is the thermal conductivity (W/mK). Values of q^*_{ss} have been obtained analytically and numerically and are similar for a wide range of geometrical configurations (*Fundamentals of Heat and Mass Transfer*, 2007). For a sphere, q^*_{ss} is a constant value of 1, while for a cuboid shape the value must be derived through interpolation. Calculations are shown in the tables below.

q^*_{ss} for Case 2	
$\frac{d}{w}$	q^*_{ss}
0.1	0.943
1.0	0.956
2.0	0.961
10	1.111

Table 5.1: Values used for interpolation of q^*_{ss} for Case 2

	Case 1	Case 2
A_s (m^2)	19.63	22.50
q^*_{ss}	1.00	0.95
L_C (m)	1.25	1.34
T_1 (K) solid	323.15	323.15
T_2 (K) medium	293.15	293.15
q (W)infinite medium	244.92	248.35
q (W) semi- infinite medium	122.46	124.17

Table 5.2: Obtained values for Case 1 and Case 2

Calculations have been carried out for both cases. For case 2, the value for q^*_{ss}, the dimensionless conduction heat rate, is obtained by interpolation from Table 5.1. The geometry of the heat storage facility was approximated to a sphere with diameter 2.5 m. The k-value for the infinite medium is assumed to be 0.52 W/mK for a soil at 300 K (*Fundamentals of Heat and Mass Transfer*, 2007).

In the calculations above are the temperatures assumed to be 50 °C for the solid and 20 °C for the surrounding medium. It is assumed that the solid has been subjected to heat injection for a longer period of time and has reached a stable temperature of 50 °C.

This approach assumes steady state conditions and uniform temperatures for the solid that is held at isothermal temperature T_1 and for the infinite medium at T_2.

The ground under the leisure home can be approximated to a semi-infinite medium, assuming the floor in the outer zones is super insulated. Therefore the heat transfer rate should be divided by two. The idea is shown in Figure 5.2.

This is a simplification of a real situation. For the leisure home with a thermal storage the temperature will vary all the time in both the solid and in the medium.

5.2.2 Finite-Difference method

When 2-dimensional problems involve geometries or boundary conditions that are not *typical* and there are not documented any exact solutions from analytical methods, a numerical technique can be used. Numerical methods are for example finite-difference, finite-element or boundary-element method. These numerical methods can readily be extended to 3-dimensional problems.

The numerical methods enable determination of temperature only at *discrete points*, not at any point as for the analytical methods.

The medium of interest is subdivided into a number of small regions as shown in Figure 5.5:

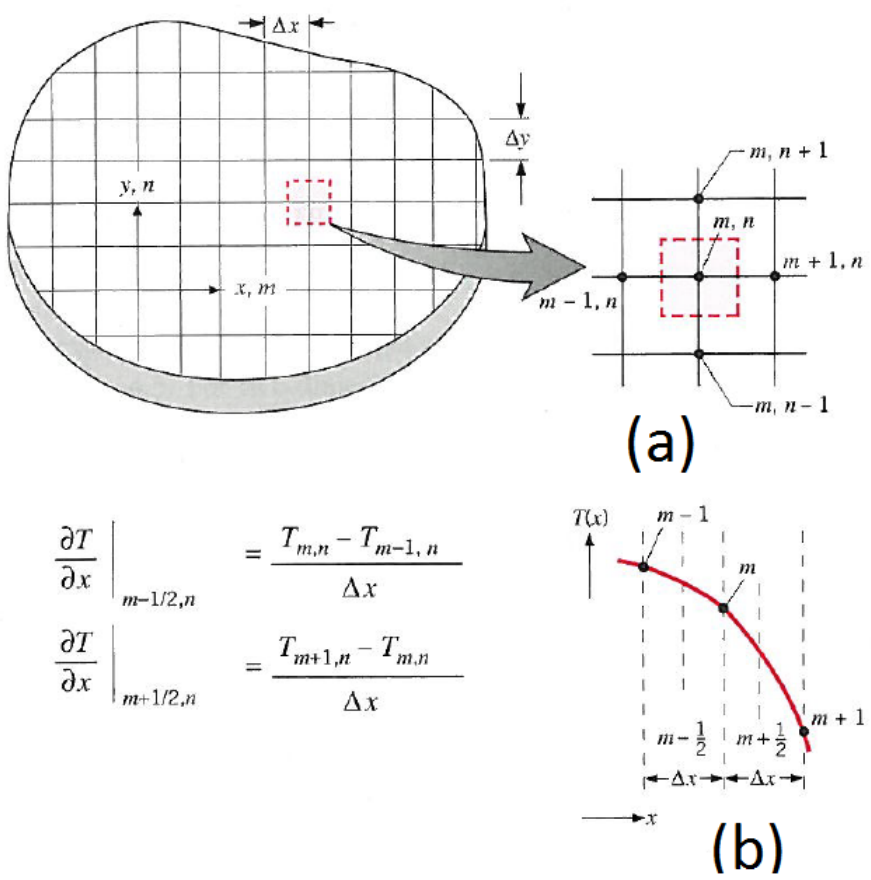

Figure 5.5: 2-dimensional conduction. (a) Nodal network. (b) Finite-difference approximation. (*Fundamentals of Heat and Mass Transfer*, 2007)

The reference point is termed a *nodalpoint*, or a *node*. The x and y locations are denoted m and n, respectively. The node shown in fig Figure 5.5a represents an average temperature of red square. The level of accuracy is dependent of the number of designated nodal points.

Finite-difference form of the heat equation

Using a network for which $\Delta x = \Delta y$:

$$T_{m,n+1} + T_{m,n-1} + T_{m+1,n} + T_{m-1,n} - 4T_{m,n} = 0 \tag{5.8}$$

The heat equation, which is an exact differential equation, is reduced to an approximate algebraic equation for the m, n node. Equation 5.8 requires that the temperature of an interior node is equal to the average of the temperatures to the neighbouring nodes. This approximate, finite-difference form of the heat equation may be applied to any interior node where $\Delta x = \Delta y$ to its neighbouring nodes (*Fundamentals of Heat and Mass Transfer*, 2007).

The energy balance method

An alternative approach to develop the finite-difference equations is to use the energy balance method. For this method, the finite-difference equation for a node is obtained by applying conservation of energy to a control volume about the nodal region.

For steady-state conditions:

$$\dot{E}_{in} + \dot{E}_g = 0 \tag{5.9}$$

The actual heat flow direction is often unknown. To obtain a finite-difference method it is assumed that all the heat flow is into the node. This is shown in Figure 5.6:

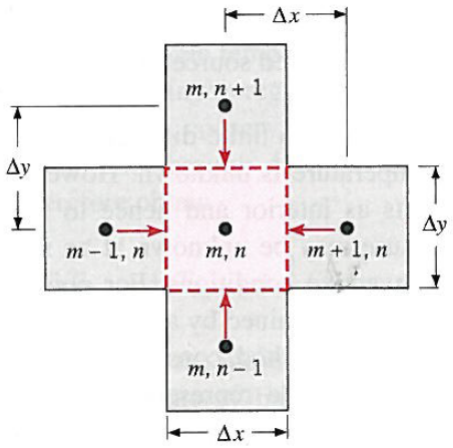

Figure 5.6: Conduction to an interior node from its adjoining nodes (*Fundamentals of Heat and Mass Transfer*, 2007)

This assumption is not possible in reality, but it is convenient to make this assumption and express the rate equation in the same manner. This way a correct form of the finite-

difference equation is obtained. The energy exchange for the 2-dimensional condition is influenced by conduction between textitm,n and its four adjoining nodes, as well as by generation.

$$\sum_{i=1}^{4} q_{(i)\to(m,n)} + \dot{q}(\Delta x \cdot \Delta y \cdot 1) = 0 \tag{5.10}$$

Once an appropriate finite-difference equation has been written for each node in the nodal network, the temperature difference may be determined. The finite-difference equations can be solved either by the matrix inversion method or by Gauss-Seidel iterations.

Finite-difference and Finite-element methods are often basis of building and energy simulation tools.

5.3 Longterm thermal storage media

Heating is mostly required in the winter months, while solar energy is mostly available in the summer months. Since the collecting potential is higher in the summer, seasonal storage of the heat would be of great value during the heating season. There are several ways to store heat, depending on the climatic and soil conditions.

Options of longterm thermal storage media are:

- Large insulated water tanks
- Small uninsulated water tanks surrounded by earth
- Uninsulated space filled with rocks
- Dry earth
- Wet earth
- Wetted earth surrounded by dry earth
- Deep aquifer
- Near surface aquifer
- High-pressure layer topped by a thermal layer
- Eutectic salts, phase change materials

(Givoni, 1977)

In this report the focus will be on thermal medium and earth storage.

5.3.1 Uninsulated space filled with rocks

The top of the earth is removed and filled with a bed of rocks. The embankments on the sides of the storage area will work as lateral insulation. The top would be covered with insulation and by an impermeable layer. An alternative is to dig out trenches and fill them with rocks. That would reduce the required volume of rocks and then be less expensive. Heated air from solar collectors is blown into the bottom of the storage area heating the rocks by convection. During the heating season hot air from the top of the storage space is blown into the building. This system is only applicable in arid regions.

5.3.2 Dry ground

A thermal storage in dry ground will not experience so much heat loss to the surrounding environment because of its low thermal conductivity. This reduces the heat rate into and out of the storage mass. The heat is usually transported by convection down to the storage mass as the low thermal conductance reduces the rate of heat in the vertical direction. The heat can be transported either by water flow or by air flow. This option for longterm thermal storage media is limited to desert and arid zones.

5.3.3 Wet ground

Wet ground has a higher heat capacity and thermal conductivity than dry ground and thus higher rate of heat transfer within the storage mass. There are two distinguishable paths of heat flow within a storage mass of wet ground and between the storage and its surroundings. One path is heat flow by water diffusion from hotter areas to cooler areas within the mass (evaporation-condensation mode of heat transfer). The second path is heat flow by direct conduction through the ground. Heat flow downwards in the storage mass can be recovered in the winter. On the other hand, lateral heat flow in the summer can represent a significant heat loss to the surrounding environment. To prevent this from happening, the impermeable cover over the storage mass should be extended. This approach for seasonal storage is suitable in humid regions.

5.3.4 Aquifer

An aquifer is an underground layer of water-bearing permeable rock or unconsolidated materials, such as sand or clay. This geological formation contains groundwater that can be used for long-term storage of heat. Solar energy can be injected into the storage mass in the summer and extracted from the aquifer in the winter using a well. If the depth of the aquifer is not adequately to prevent upwards heat loss, an impermeable insulation layer should cover the store area to provide more efficient heat storage.

5.3.5 Storage media for the leisure home

When a heat storage facility is to be built, the climate and ground conditions have a great impact for how well the heat storage works. Some storage media is more suitable in arid regions than in humid regions. Regardless of the climate and ground conditions it is important to be aware of how the heat behaves under the ground surface for different conditions.

For the leisure home studied in this report, the location is the southern mountain regions of Norway. There is quite a lot of rocky ground in Norway, so the leisure home should be modeled with granite or something similar for the heat storage facility. There is a database available from Geological studies of Norway at (*www.ngu.no*), where information about ground conditions can be collected for a selection of wells around the country. This might be worth to check out if information about the site is missing and a heat storage facility is to be planned.

5.4 Dry-out effects

Clay, silt and sand are all more or less unconsolidated soil types. The heat capacity and the thermal conductivity for these kinds of soil are strongly dependent on the water content especially at higher temperatures ($>60\ ^{\circ}C$) (Knoblich, Rammer, & Martin, n.d.) (*Bodenkunde*, 1983). Because of vapour diffusion along the temperature gradient, water losses can occur and lead to dry-out. In worst case cracking around the heat exchanger tubes can take place leading to a significant reduction to the heat transfer rate. Noticeable temperature gradients are produced when high grade thermal energy ($70\ ^{\circ}C$ - $90\ ^{\circ}C$) is injected into the ground. Simultaneously, moisture flow occurs in the vicinity of the heat exchangers. The heat transfer of the high grade thermal energy occurs both by conduction over a complex system of solid particles and by convection due to liquid moisture, air and vapour movement (Reuss, Beck, & Müller, 1997).

5.5 Thermal interaction between underground heat storage and the surrounding soil

Energy transport in soil may occur by one or more of these means:

- Conduction
- Convection
- Phase change of moisture in the ground

It can be quite difficult to make precise calculations of heat flow in the ground around a heat storage facility. Several assumptions are usually made, because of lack of information about the site.

Idealized calculations can be carried out assuming the ground to be a homogeneous and isotropic thermal conductor. The heat storage region is assumed to have a hemispherical geometry, with the flat face upwards. The heat flow and temperature patterns are assumed to only be dependent in radial direction. The radius of the hemisphere is measured from the centre of the upwards face. Steady-state conditions and constant storage temperature is also assumed.

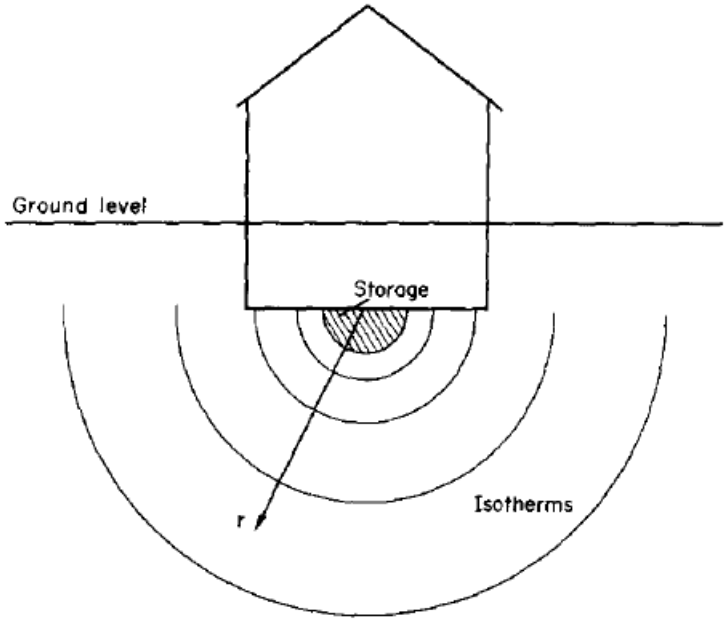

Figure 5.7: Assumed storage geometry and temperature profiles (Shelton, 1974)

The equation below describes spherically symmetric heat conduction in a homogeneous medium:

$$\frac{\partial^2 T}{\partial r^2} + \left(\frac{2}{r}\right)\frac{\partial T}{\partial r} = \left(\frac{\rho C}{k}\right)\frac{\partial T}{\partial t} \tag{5.11}$$

For steady state conditions, the temperature is described by:

$$T = \frac{C_1}{r} + C_2 \tag{5.12}$$

With the following boundary conditions:

$$\begin{aligned} T &= T_0 \quad \text{at} \quad r = r_0 \\ T &= T_\infty \quad \text{at} \quad r = \infty \end{aligned} \tag{5.13}$$

The constants are determined by:

$$\begin{aligned} C_1 &= (T_0 - T_\infty) \cdot r_0 \\ C_2 &= T_\infty \end{aligned} \tag{5.14}$$

T_0 is the temperature at the edge of the storage region, while T_∞ is the natural temperature of the ground at depths where seasonal variations are small.

The steady-state heat flow from the heat storage to the surrounding ground is given by the following equation:

$$\begin{aligned} q &= -k \cdot 2 \cdot \pi \cdot r^2 \cdot \left(\frac{\partial T}{\partial r} \right)_{r=r_0} \\ &= 2 \cdot \pi \cdot r_0 \cdot k \cdot (T_0 - T_\infty) \end{aligned} \tag{5.15}$$

The heat flow is proportional to the perimeter of the storage region, not its surface area. The heat flux through the hemisphere at r_0 is given by:

$$J = \frac{q}{2 \cdot \pi \cdot {r_0}^2} = k \cdot \frac{T_0 - T_\infty}{r_0} = U\,(T_0 - T_\infty) \tag{5.16}$$

$U = \frac{k}{r_0}$ represents the effective *U-factor*.

The heat loss to the surrounding soil compared to the heat stored in the storage volume is of interest to determine the fraction of heat loss that is dependent of storage volume. This is a measure of the characteristic time that the stored heat uses to leak out to the surroundings.

$$\frac{\text{Heat-loss rate to soil}}{\text{Heat storage capacity}} \propto \frac{r}{r^3} = \frac{1}{r^2} \tag{5.17}$$

The equation above shows that as the size of the facility increases the relative heat losses decreases.

The heat loss to the surrounding soil from the heat storage volume varies depending on what the initial temperature of the soil was before injecting heat into the storage volume, and for how long heat has been injected. When the storage volume and the adjacent ground have been heated for a while, the heat loss is decreasing. Hence the greatest heat loss occurs when the system is first used and the ground has not experienced any previous heating. The greatest gain occurs when the surrounding ground and the storage volume is at equilibrium and then the storage volume temperature decreases.

Jay Shelton have done some calculations with the steady-state equations above, both for a small and a large system, representing a one- and ten-family solar-assisted space heating system. He assumes that each day is either completely overcast with no solar heat collection or sunny with equal solar heat collection rates for eight hours. 220 kW of solar-heat is collected per sunny day for the small system. The simulations period is 30 days, and during this period, no heat is extracted from the storage region. There are 12 sunny days with heat injection to the ground for 8 hours per day, and 18 days with overcast sky, with no heat injection. He did simulations with two different initial conditions, one where the system has not previously been in operation, with a *cold start*, and one where the storage area has been heated for a while, so the ambient ground is hotter, a *hot start*. The cold start has an initial ground temperature of 10 $°C$, while the hot start has an initial ground temperature of 77 $°C$.

With a cold start 21 % of the collected heat was lost to the surrounding soil. With a hot start on the other hand, the storage volume gains heat from the ground in an amount equal to 10 % of the collected solar heat (Shelton, 1974)

More about how these simulations and calculations were done can be studied further in his report *Underground storage of heat in solar heating systems* (Shelton, 1974).

5.6 Soil temperature

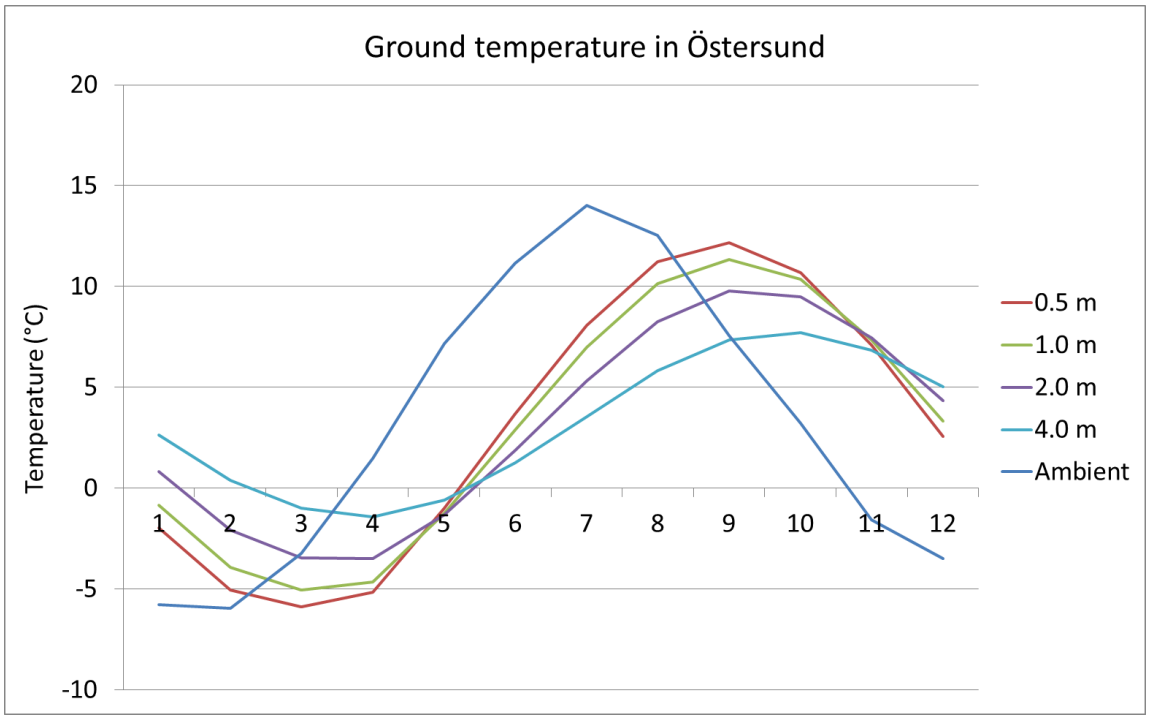

Figure 5.8: Estimated ground temperatures in Östersund plotted over the year together with average ambient temperature collected from the climate file in ESP-r

The soil temperature varies with the season. The peak values have a 2-3 months delay from the ambient temperature. This is seen in Figure 5.8 which shows the temperature distribution over the year in Östersund. The average ambient temperature for each month is plotted in the figure above to demonstrate the delay.

Figure 5.8 shows estimated ground temperatures in the climate file in ESP-r without any snow on the ground.

Buildings on grade will also affect the temperature distribution in the ground. Chuangchid and Krarti have studied heat loss from a heated concrete slab on grade (Chuangchid & Krarti, 2001). The indoor temperature is set to 20 $°C$ while the ground temperature at 4 m depth is set to approximately 11 $°C$ for conditions in Colorado for both summer and winter.

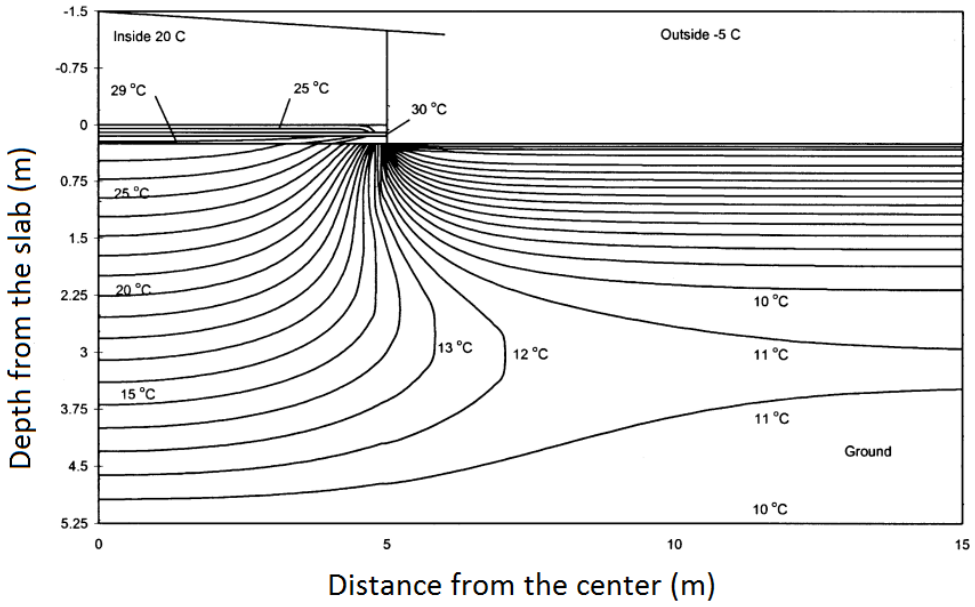

Figure 5.9: Temperature profile for uninsulated slab-on-grade the 15th of January, Colorado climate (Chuangchid & Krarti, 2001)

5.7 Active and passive systems

The two most favourable methods for seasonal storage from a technical and economical point of view is storage in an aquifer or in unsaturated ground. This applies to storage of thermal energy at higher temperatures (40 °C - 90 °C) (Reuss et al., 1997).

There are two ways to extract heat from longterm storage mass:

1. By using a heat pump, extracting heat from a low temperature ground storage (0 $°C$ - 40 $°C$).
2. Directly from a high temperature ground storage (40 $°C$ - 80 $°C$).

5.7.1 Geothermal heat pump

Thermal energy from the ground can be extracted in different ways. Today the most frequently used method to utilize this heat is via a geothermal heat pump where coils can be buried at different depths and with different geometries. There are four types of geothermal heat pumps. The different systems can be seen in Figure 5.10.

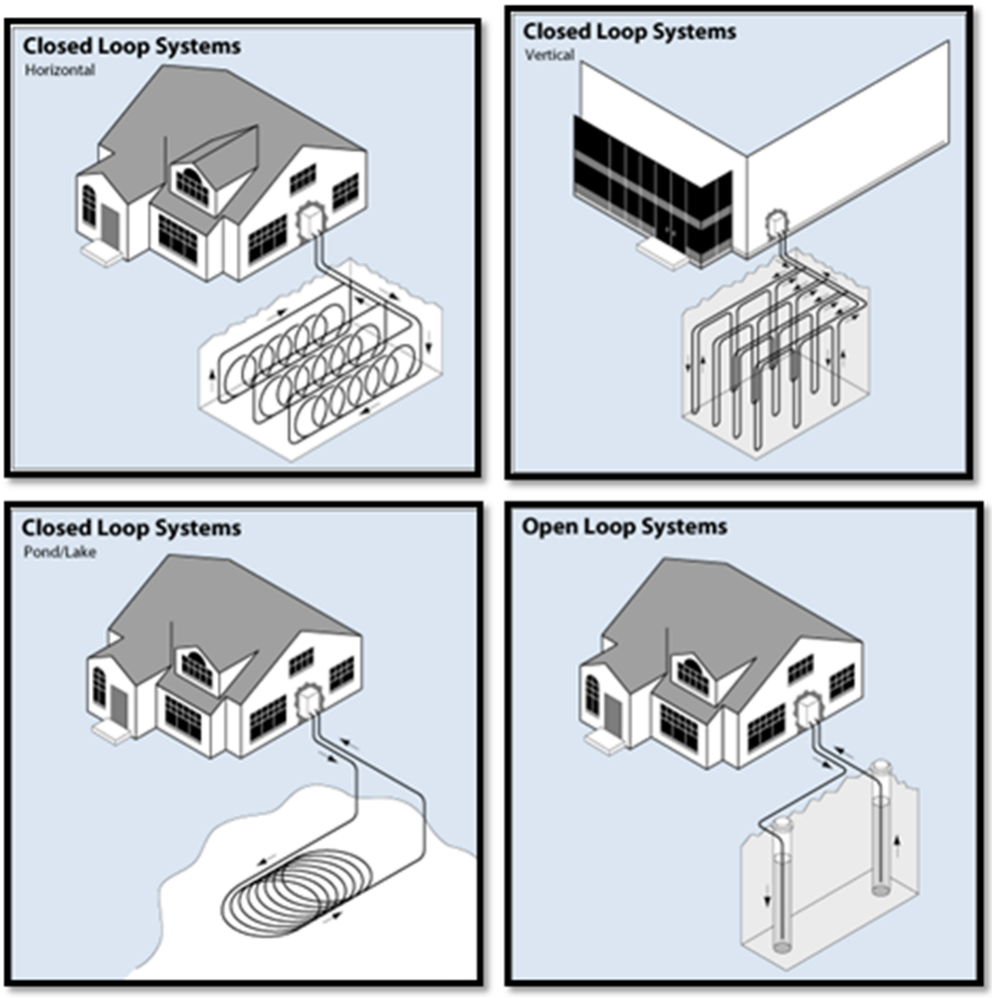

Figure 5.10: Geothermal heat pump systems (U.S. Department of Energy, 2012)

Closed loop systems are usually built up of plastic tubes with an antifreeze medium circulating inside the tubes. Copper tubes can also be used. The coil collects heat from the ground and the heat is transferred via the circulating medium to a heat exchanger inside the house.

Although the horizontal closed loop system requires a large installation area, it is probably the most cost effective of these systems. The slinky coil for this system needs to be buried at 1-2 m depth. The system allows more pipes in a shorter trench.

The vertical system is typical for schools and larger commercial buildings. The coils are brought down to a depth of 30-100 m.

A pond or lake system has coils buried at a minimum depth of 2.5 m and is a suitable instalment if there is a large enough water source available that meets the requirements of volume, quality and depth.

The open-loop system might be suitable if the installation location has a large enough clean water source. Water from a well or surface water can be used as a heat medium. The water is transferred to the heat exchanger inside the building before flowing back into the ground into another well.

For a leisure home with a short use period, these systems will most likely not be beneficial to install as installation costs are high and the payback time would probably be longer than the expected lifetime of the system.

5.7.2 Passive system

Passive heat exchange systems are systems that do not require electricity to operate. Solar energy passing through a window directly on to a concrete floor or wall is an example of a passive heat exchange system. The thermal mass will store the heat from the sun during the day and emit heat over the night. In such design, the window should be south-facing to utilize as much solar heat as possible. The energy can be stored in different building materials with high heat capacity, such as tile floors, concrete slabs and brick walls. The solar energy is distributed back to the living space through natural convection and radiation.

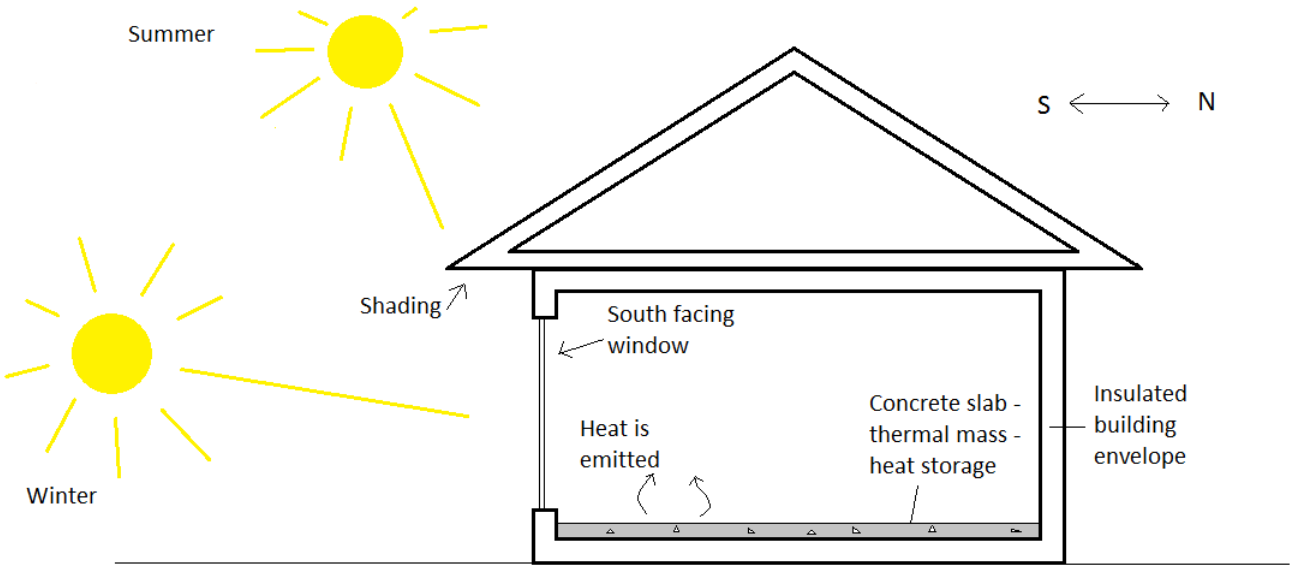

Figure 5.11: Principle of a passive solar heating system

Figure 5.11 shows the principle of a passive solar heating system. The extension of the roof creates shading which allows only the low sun in the winter to enter. During the summertime it is usually not necessary with excess heating, therefore shading should be applied.

If the thermal mass that will work as a heat storage is not in range of the solar radiation, solar collectors with an active distribution system could be used. If the building is not connected to the grid, a photovoltaic panel together with a battery could be installed as an alternative source of electricity.

Figure 3.11 in Chapter 3 shows an active solar heating system with solar collectors and a thermal storage built into the floor of the building. The room that needs to be heated has a massive concrete floor, while the surrounding floor is built up by concrete, insulation and flooring of wood. The solar collectors will collect heat as long as the sun is shining. The heat is transferred via pipes into the concrete block. The distribution system contains of pipes, a heat transferring fluid and a pump. The idea is that heat will passively arise from the ground into the internal basement floor during the winter working as a passive heat exchange system.

5.8 Thermal mass and how it affects building performance

The terms thermal mass and thermal inertia describe the absorption and storage of significant amounts of heat in building constructions. Heating or cooling of concrete is a slow process. A thermal massive construction delays and reduces heat transfer, resulting in reduced total heat loss or heat gain through the building envelope. Reduced heat transfer through concrete indicates that some of the heat is stored in the element. This is not necessarily considered a heat loss, because this stored heat can later be released back into the building. Therefore temperatures inside thermally massive buildings are less influenced by daily temperature cycles.

Concrete will generally have a higher heat capacity than other materials. The physical location of insulation relative to mass will significantly affect thermal performance. For maximum benefit from thermal mass, the mass should be in direct contact with the interior air. The building design and use can impact the thermal mass because different buildings use energy in different ways.

In this study, thermal mass is used to store heat gained through the solar collector and to maintain the boundary condition for the interior temperature where the goal is to avoid frost damages on the sanitary installations. Heat absorbed during the summer is preferably released in colder periods. Therefore the thermal mass storage effectiveness depends on the heat-storage capacity of the mass and the rate of heat flow through the mass. Thermal conductivity should be high enough to allow the heat to penetrate into the storage material but not so high that the storage time is shortened. To maximize the amount of solar energy that can be stored, the absorptivity should be high. Emissivity characteristics should be high in thermal storages to efficiently reradiate stored energy

back into the building envelope. The specific heat capacity should be high to maximize the amount of energy that can be stored in a material. Concrete fulfils these requirements for effective thermal storage.

Figure 5.12 shows that the temperature of a heavy construction is less influenced by temperature variations than a light construction.

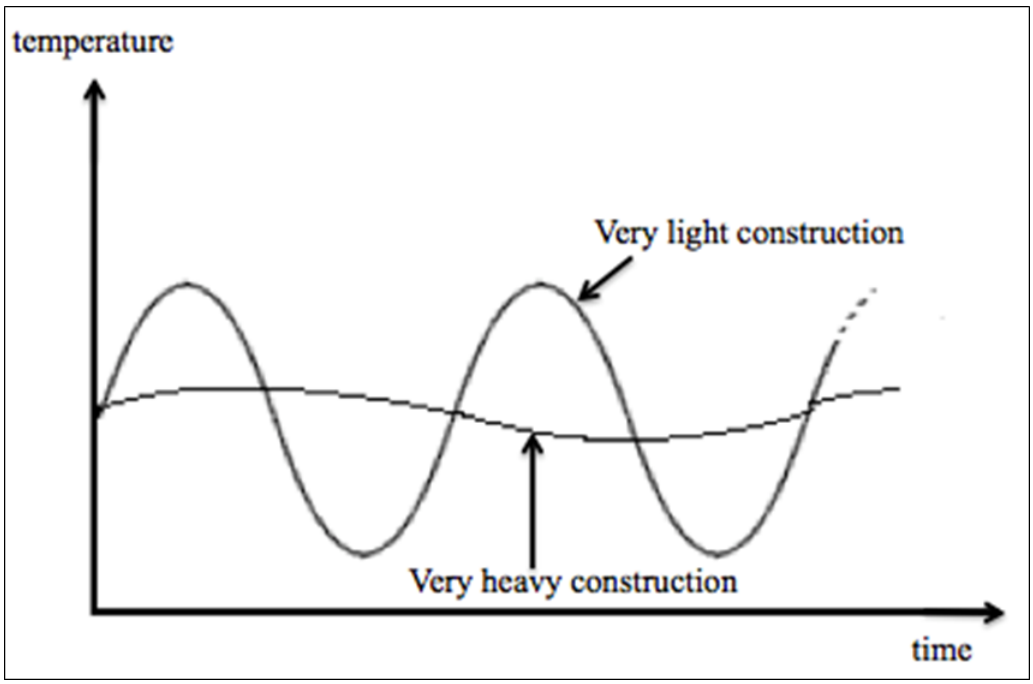

Figure 5.12: Thermal inertia

A thermal mass with an infinite thickness, which at the starting point has a uniform temperature of T_0, is exposed to a surface temperature T_s at a time t=0. The heat flux q (W/m^2) at the surface is a function of time, t (Novakovic, Hanssen, Thue, Wangsteen, & Gjerstad, 2007):

$$q(0,t) = (T_s - T_0)\sqrt{\frac{\lambda c\rho}{\pi t}} = (T_s - T_0)\frac{b}{\sqrt{\pi t}} \tag{5.18}$$

Where c (J/kgK) is the specific heat capacity, ρ (kg/m^3) is the density and b is the thermal effusivity $(J/m^2Ks^{0.5})$ defined as the ability to store heat:

$$b = \sqrt{\lambda c\rho} \tag{5.19}$$

where λ is the thermal conductivity (W/mK). Accumulated heat e (J/m^2) in the thermal

mass after a time t is:

$$e(t) = 2\left(T_s - T_0\right) b\sqrt{\frac{t}{\pi}} \tag{5.20}$$

A thermal mass exposed to temperature differences will achieve harmonic temperature variations in the surface. The surface temperature θ_s (K) is described by:

$$\theta_s(t) = \theta_0 \sin\frac{2\pi t}{t_0} \tag{5.21}$$

where θ_0 is the amplitude and t_0 is the time of the period, a year or a month for example.

The temperature at a depth x of the thermal mass can be calculated by:

$$\theta(x,t) = \theta_0 e^{-\frac{x}{\delta}} \sin\left(\frac{2\pi t}{t_0} - \frac{x}{\delta}\right) \tag{5.22}$$

where

$$\delta = \sqrt{\frac{\lambda t_0}{\pi\rho c}} = \sqrt{\frac{a t_0}{\pi}} \tag{5.23}$$

The parameter δ (m) is called the depth of fusion. That is, the depth at which the amplitude for the temperature variations is reduced with a factor of e in a homogenous material with an infinite thickness that is exposed to a sinusoidal temperature variation on the surface.

Where a is the thermal diffusivity:

$$a = \frac{\lambda}{c\rho} \tag{5.24}$$

Chapter 6

Simulation tools

Different simulation tools can be used to model the heat exchange between a solar heating system, the ground and the leisure building. It is important to note that a simulation never will represent a real case to full extent. A simulation is an approximation of a real case and the degree of accuracy depends on the quality of the program used.

There are a numerous simulation tools out there. Some tools focuses on the building and HVAC systems, other on 3D conduction and thermal bridging. For the purpose of this study, a simulation tool that models a simplified building that is thermally connected to the ground and has solar system available, would be suitable.

Examples of simulation tools that might be suitable for this study is EnergyPlus, CYMAP, VOLTRA, TRNSYS, HOT3000, HEAT3, ESP-r and IDA ICE to mention some of them. Three of them are described in more detail below. Since the focus of this report is the simulation of the ground under the leisure home, this is described in further extent.

6.1 ESP-r

ESP-r (Environmental System Performance Research) is an integrated energy-modeling tool for the simulation of thermal, visual and acoustic performance of buildings, and the energy use and gaseous emissions associated with environmental control systems. In undertaking its assessments, the system is equipped to model heat, air, moisture and electrical power flows at user determined resolution. ESP-r is developed by Energy Systems Research Unit (ESRU) at the University of Strathclyde in Glasgow. The program is free with an Open Source-license. ESP-r includes databases for materials, constructions and climate data. The databases can be adjusted and user defined. The climate files have to be in the right configuration and can be downloaded from the homepage of U.S Department of Energy, and contain average hourly values for dry bulb- and dew point temperature, wind speed and direction, solar irradiance (both direct and diffuse), relative humidity and precipitation. Use patterns for people, lighting, equipment and ventilation can be defined so that internal heat gains are accounted for (University of Strathclyde, Energy Systems Research Unit, 2013).

The possibilities with ESP-r are large and because of the open-source policy, new components that can be used in simulations are frequently added to the program. The strength of ESP-r is its ability to simulate many innovative or leading technologies in addition to standard simulation features. A weakness of the program is that specialist features require sufficient knowledge on each particular subject. Also, ESP-r lacks the extensive databases associated with commercial tools. ESP-r is a very advanced simulation tool, and is a challenging program to learn without a mentor (University of Strathclyde, Energy Systems Research Unit, 2013).

There is a mailing list where one can ask questions that go out to all mail-registered users of ESP-r. This communication channel can be quite useful when you are working on your own.

More details about the program and the ESP-r mailing list can be found on the website *http://www.esru.strath.ac.uk/Programs/ESP-r.htm*.

6.1.1 Ground modeling in ESP-r

ESP-r has different possibilities for ground modeling (ESRU & users, 2006-2013):

- The ground could be included in the definition of the slab construction. Number of layers can be added to the floor accounting for the nearby ground.
- One of the BASESIMP configurations can be used. This calculates the heat transfer rate from the building to the surrounding ground.
- Nakhi's 3D conduction method.

In the project thesis, the ground was implemented in the slab construction. Since the constructions are modeled 1-dimensionally, so is the ground. A main goal for this study is to improve the ground model, so the BASESIMP configurations or Nakhi's method should be studied further.

At the webpage of ESRU there is an archive of emails from users. Doctor Jon Hand has replied to a question about 3D ground modeling where he mentioned the three approaches above. He also wrote this about Nakhi's method:

> *Fair warning should be given that there might be Dragons lurking in that particular bit of code.* Jon Hand

BASESIMP is a regression-based algorithm which expresses both above-grade and below-grade time dependent heat losses (Beausoleil-Morrison & Mitalas, 1997). The data is generated by BASECALC which is a finite-element-based foundation heat-loss program. Using BASESIMP quasi-3D solutions are obtained.

ESP-r provides start-up periods for up to 100 days. For a system with heat storage in the ground it will take several years before the ground reaches a stable condition again after being heated.

6.1.2 Solar heating system in ESP-r

It is possible for the user to build up a custom solar heating system. There are several databases available with different types of solar collectors, pumps, heat storage facilities etc. Then the components need to be linked and given boundary conditions and other inputs. Another approach is to create a control loop and convert solar radiation data to electric heating input.

6.2 IDA ICE

IDA Indoor Climate and Energy (IDA ICE) is a dynamic multi-zone simulation tool for the study of energy consumption in buildings, indoor air quality, and thermal comfort.

The program is able to model buildings with several rooms and windows, shading, internal heating loads, heat storage in the building envelope, ventilation rates, floor- heating and cooling. There is a range of HVAC systems that can be modeled. Calculations and data of for example moisture content, temperatures, pressures, energies, effects and solar radiation, can be collected.

The program is developed in Sweden by a company called EQUA Simulation AB. It has been developed since the mid-eighties, and the first software product was commercially available in 1998 (EQUA, 2013c). IDA ICE has a multi-level user interface; Wizard, Standard and Advanced. This allows beginners to easily build up their models and simulate simple cases without to many inputs, and the advanced users to do more complex models with higher flexibility. The program is delivered in two editions, the Standard version and the Advanced version (EQUA, 2013a).

The program has a rather expensive license and can be purchased from EQUA Simulation AB. To reach users worldwide, IDA ICE can be adapted to local languages and requirements such as climate data, material data, standards and so on (EQUA, 2013c).

6.2.1 Ground modelling in IDA ICE

Among the plant and HVAC systems that can be modeled is *geothermal heat pump*. A weakness with the calculation of heat transfer out of the boreholes is that it does not take into account that there might be several boreholes. So if there are 10 boreholes, the program will calculate for 1 borehole and multiply that with 10. In reality it would be less heat available for the 10th borehole than for the 1st.

It does not exist any possibilities for inserting ground insulation around the building. However there are ways to insert insulation on the floor slab, or it could be defined as a layer in the construction of the ground.

There are two ground models in IDA ICE 4.5, ICE3-model and ISO13370-model. Both models require that the user creates a construction of the ground. Thermal properties can be edited. This ground construction is linked to the floor slab construction. Heat

transfer is calculated 1-dimensionally through all constructions in the program, i.e. also the ground construction.

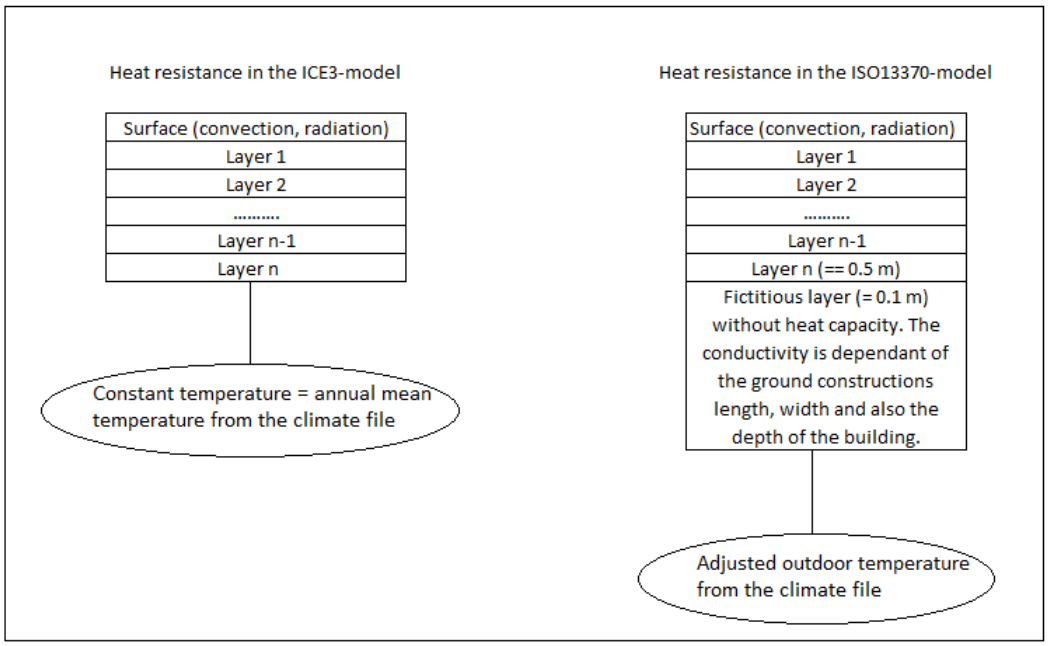

Figure 6.1: Ground models in IDA ICE. This figure is drawn based on the figure in the Course material Manual of IDA ICE 4 (EQUA, 2013b)

Figure 6.1 shows how IDA ICE can calculate the heat transfer to the ground. The ICE3-model has a constant temperature as boundary condition. The ISO13370-model has a temperature that varies continuous with the outdoor temperature. A weakness with the new ISO13370-model is that it does not take into account the phase lag between the outdoor temperature and the ground temperature. So the coldest day of the year will also have the coldest ground temperature. In reality there would be a 3 months delay due to the thermal mass in the ground. An improvement from the old model is that the users are able to define the depth of the floor slab.

IDA ICE provides start-up periods for up to several years. This means that one are able to do a simulation in year 5, relatively long time after the systems have been installed.

6.2.2 Solar heating system in IDA ICE

Among the plant components that are available in IDA ICE there is also solar collectors. The user defines collector area, incline and the azimuth.

6.3 TRNSYS

TRNSYS stands for transient system simulation tool. The software is widely used for the study of buildings, HVAC systems and renewable energy technologies. TRNSYS was originally developed by the Solar Energy Laboratory at the University of Wisconsin and the software has been commercially available in 35 years. The software has several applications such as: building simulation, solar thermal processes, ground coupled heat transfer, high temperature solar applications, power plants, hydrogen fuel cell systems, geothermal heat pump systems, wind and photovoltaic systems and others (Thermal Energy System Specialists, LLC, 2013b).

TRNSYS consists of two main parts; an engine called the kernel and an extensive library of components written by TESS (Thermal Energy System Specialists). The kernel reads and processes the input file and iteratively solves the systems. It plots the variables, determines convergence and provides utilities that can determine thermophysical properties, interpolate external data files, invert matrices, and several other things (Thermal Energy System Specialists, LLC, 2013b). The second part is an extensive TESS library of components. Each component models the performance of one part of the system.

Components that are available in the TESS component library is (Thermal Energy System Specialists, LLC, 2013a):

- Application components
- Controller components
- Electrical components
- Geothermal heat pump components
- Ground coupling components
- HVAC equipment components
- Hydronics components
- Loads and structures components
- Optimizations components
- Solar collector components
- Storage tank components
- Utility components
- Cogeneration (CHP) components
- High temperature solar components

The software has a quite expensive licence. TRNSYS can be purchased from TESS (Thermal Energy System Specialists) and a price list is found at at their webpage (Thermal Energy System Specialists, LLC, 2013b).

6.3.1 Ground modelling in TRNSYS

The TESS Library provides ground coupling components and different methods for calculating heat transfer through slab on grade, through basements and the ground. The following types are available in the ground coupling component library ("TESS Components Libraries, General Descriptions", 2013):

Type 653: Simple floor heating
This system operates under the assumption that the slab can be treated as a single lump of isothermal mass. The energy transfer between the fluid and the slab is modeled using a heat exchanger approach.

Type 714: ASHRAE method for calculating slab heat transfer
A simplified method for calculating the energy transfer through a rectangular slab on grade with various insulation schemes. The method is proposed by ASHRAE in 2001.

Type 715: ASHRAE method for calculating basement heat transfer
ASHRAE also purposed a method for calculating the energy transfer through rectangular basements with various insulation schemes.

Type 943: Vertical rectangular storage tank wrapper
This model provides a fully 3-D conduction soil wrapper for the fluid-filled tank which this component interacts with. There is another version available where there is a structure above the tank. Near and far field considerations are taken into account.

Type 957: Vertical rectangular storage tank wrapper under insulated surface
This type models the heat transfer to the soil for a buried, rectangular storage tank.

Type 993: Radiant slab on grade
This method models a series of fluid-filled, parallel, horizontal pipes buried in a radiant floor slab.

Type 1244: Multizone basement model
Heat transfer from horizontal or vertical surfaces to the surrounding soil is modeled. Moisture effects are not taken into account. The heat transfer is assumed to be conductive only. The heat transfer calculation into or out of the surface is based on a 3-dimensional finite difference model of the soil. The resulting inter-dependent differential equation is solved by a simple iterative method. This slab model is intended to be used together with Type 56 which is a detailed TRNSYS thermal multizone model that requires a large number of inputs. If a simplified building model is to be modeled on top of this basement, Type 702 should be used instead.

Type 1255: Slab on grade – monolithic pour
This type models a slab without footings. It is intended to work with building models that provides things like convection coefficients and zone temperatures to the ground coupling model.

Type 1256: Slab and basement model
The heat transfer from a multi-zone building, slab, basement or crawlspace communicated thermally with the ground. It is not intended to be used with Type 56. This routine

requires user inputs in manners of external data files which map the 3-dimensional air, soil, floor, wall, insulation and footer materials.

6.3.2 Solar heating system in TRNSYS

There are several different solar collectors available in the TESS library, both evacuated tube collectors and flat plate collectors, glazed and unglazed. Some of the types can rotate around several axes. There are a numerous of methods for modeling the collectors ("TESS Components Libraries, General Descriptions", 2013).

6.4 Selection of simulation tool

IDA ICE provides more start-up days than ESP-r. The start-up days are important in a ground modeling simulation since the thermal mass in the ground uses a significant amount of time to be heated. 100 days is the maximum time in ESP-r, and ideally it should be 1-3 years. However, IDA ICE does not provide the same opportunities for ground modeling as ESP-r since it only calculates the heat transfer 1-dimensionally.

In TRNSYS all the parts in a model is created separately, and later linked together. It seems like TRNSYS may provide good possibilities for a ground model. The question is how well the interactions between the building, the solar heating system and the ground are modeled.

Another program like HEAT3, which is a 3-dimensional transient and steady-state heat transfer program (BLOCON, 2011), is probably good when the ground or other 3D conduction problems are studied separately.

ESP-r is chosen as the simulation tool for this study. This was decided in consultation with the supervisor. It seems like this software provides the best opportunities for 3-dimensional ground modeling, even though it has a low limit for start-up days. The interactions between the building and the ground seem to be modeled well. The BASES-IMP configurations are to be studied further.

Chapter 7

Modeling methods and theories

In the following chapter will different modeling theories and methods in ESP-r be presented. The modeling of the ground and heat storage, the solar heating system, areas of heat injection and ground insulation are discussed.

7.1 The ground

According to information found at the ESRU homepage are there several different ways to represent the interactions between a building and the ground (ESRU & users, 2006-2013). The different approaches and methods will be presented and discussed in the following section.

7.1.1 The slab construction

The ground can be included in the definition of the slab construction, adding additional layers accounting for nearby ground. The properties of the materials which constitute the construction can be edited. The heat transfer is calculated 1-dimensionally through all constructions in the model. The boundary conditions can be set to different temperature profiles, user defined, or predefined by the climate file. The predefined temperature profiles do take the phase lag into account, which the ISO13370-model in IDA ICE not does.

7.1.2 BASESIMP

Another way to calculate heat transfer between the building and the ground is to use one of the basement correlations included in the BASESIMP method. This method is implemented by Natural Resources Canada.

BASESIMP (simplified basement model) is a regression-based algorithm, developed to improve the modeling of foundation heat-loss in whole-building energy programs. This algo-

rithm expresses both above-grade and below-grade time dependent heat losses (Beausoleil-Morrison & Mitalas, 1997). BASECALC is a finite-element-based foundation heat-loss program that is used to generate data for BASESIMP. There are done over 100 000 parametric finite-element based simulations using BASECALC to develop this BASESIMP algorithm (Beausoleil-Morrison et al., 2007). The BASECALC technique was developed at National Research Council in Canada, based on Mitalas method. Mitalas performed finite-element analyses of a large number of basements and analyzed the results to produce a series of basement heat-loss factors. BASECALC uses Mitalas basement heat loss factors and allows modeling of different basement geometries, exact insulation configurations and site conditions. By performing three 2D finite element simulations and using corner correction factors quasi 3D solutions are obtained.

Corner correction method

The nature of basement heat losses is illustrated in Figure 7.1 and Figure 7.2.

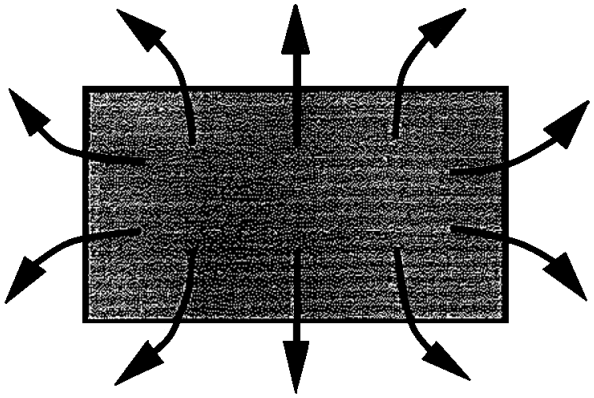

Figure 7.1: Plan view of basement with heat flow lines (Beausoleil-Morrison et al., 1995)

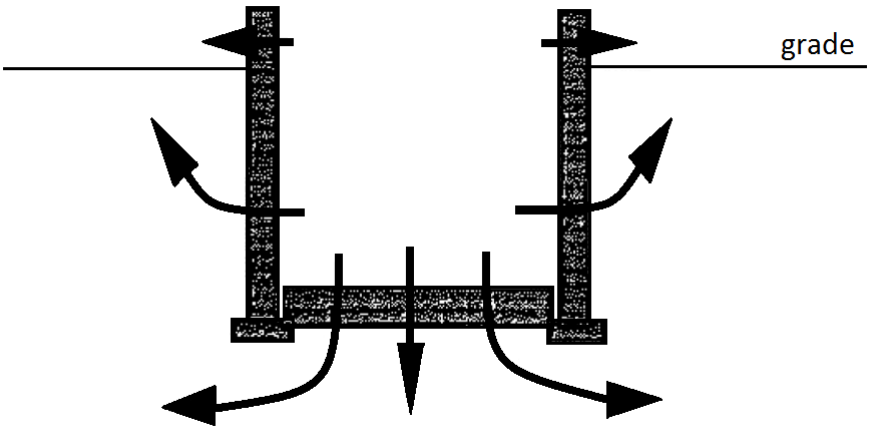

Figure 7.2: Cross-section of basement with heat flow lines (Beausoleil-Morrison et al., 1995)

The three-dimensionality is strongest near the corners. It decreases with increasing distance from the corners.

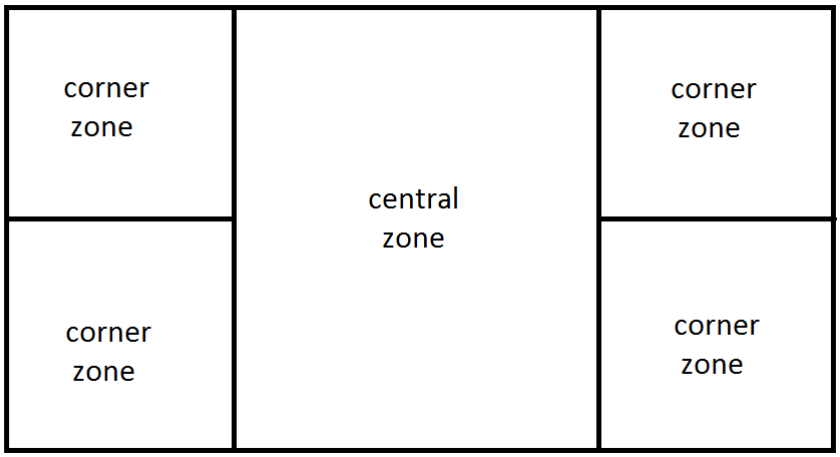

Figure 7.3: Plan view showing heat-flow zones. This figure is drawn based on the figure in report *Estimating Three-Dimensional Below-Grade Heat Losses from Houses Using Two-Dimensional Calculations* (Beausoleil-Morrison et al., 1995)

The heat flow lines is approximately 2-dimensional in the central zone, while it is strongly 3-dimensional in the corner zones. The corner factor is defined as as the ratio of the heat loss from the corner zones to the heat loss from the central zone, each normalized to its zone's perimeter (Beausoleil-Morrison et al., 1995):

$$F_C = \frac{\left\{ \frac{q_{\text{corner zones}}}{P_{\text{corner zones}}} \right\}}{\left\{ \frac{q_{\text{central zones}}}{P_{\text{central zones}}} \right\}} \tag{7.1}$$

The corner factor is dependant of the site and the basements characteristics. Numerous calculations have been made for different corner zones and central zones to develop correlations relating corner factors to different thermal and geometric basement characteristics. These correlations are implemented in BASECALC.

BASECALC performs 2-dimensional calculations on the central zone. Then the corner correction method is applied by calculating the corner factors with the correlations. Finally the results from the central zone are adjusted to account for the corner zones using the following equation:

$$\begin{aligned} q_{total} &= q_{\text{central zone}} + q_{\text{corner zones}} \\ &= q_{\text{central zone}} \cdot \left\{ 1 + F_C \cdot \frac{P_{\text{corner zones}}}{P_{\text{central zone}}} \right\} \end{aligned} \tag{7.2}$$

More information about the corner correction method can be found in the report *Estimating Three-Dimensional Below-Grade Heat Losses from Houses Using Two-Dimensional Calculations* written by Beausoleil-Morrison, Mitalas and Chin (Beausoleil-Morrison et al., 1995).

Heat loss calculations

A finite element run calculates the above-grade heat losses (Q_{ag}), while a steady-state run determines the below grade average heat losses ($Q_{bg,avg}$). To evaluate the below-grade variable heat losses ($Q_{bg,variable}$), a transient 3-year run is performed (Beausoleil-Morrison et al., 2007).

The finite element solutions have the form $S_{2dFE-AG}$, $S_{dFE-BG,avg}$ and $S_{dFE-BG,var}$ where:

- $S_{2dFE-AG}$ = calculated above grade heat loss factor ($W/m°C$)
- $S_{dFE-BG,avg}$ = calculated below grade average heat loss factor ($W/m°C$)
- $S_{dFE-BG,var}$ = calculated below grade variable heat loss factor ($W/m°C$)

By using the corner correction method are these solutions converted into 3-dimensional parametric heat loss factors:

$$S_{agr} = S_{2dFE-AG} \cdot [2(L+W)] \tag{7.3}$$

$$S_{bg,avg} = S_{dFE-BG,avg} \cdot [2(L-W) + 4W \cdot F_{c,avg}] \tag{7.4}$$

$$S_{bg,var} = S_{dFE-BG,var} \cdot [2(L - W) + 4W \cdot F_{c,var}] \tag{7.5}$$

Where:

- L = length of the basement (m)
- W = width of the basement (m)
- F_c = corner correction factor evaluated from the correlations of the corner correction method
- S_{ag} = calculated above grade heat loss factor $(W/°C)$
- $S_{bg,avg}$ = calculated below grade average heat loss factor $(W/°C)$
- $S_{bg,var}$ = calculated below grade variable heat loss factor $(W/°C)$

These factors are then converted into fluxes for any weather conditions. This is done by using:

$$Q_{ag,i} = S_{ag} \cdot (T_{basement} - T_{a,i}) \tag{7.6}$$

$$Q_{bg,avg} = S_{bg,avg} \cdot (T_{basement} - T_{g,avg}) \tag{7.7}$$

$$Q_{bg,var,I} = S_{bg,var} T_{g,amp} \cos\left(\frac{2\pi}{365 \quad middleday_i} + phase - P_S\right) \tag{7.8}$$

Where:

- $Q_{ag,i}$ = above grade heat losses for month I (W)
- $Q_{bg,avg}$ = average below grade heat losses (W)
- $Q_{bg,var,I}$ = variable below grade heat losses (W)
- $T_{a,i}$ = the ambient outdoor temperature for month i $(°C)$
- $T_{g,avg}$ = annually averaged ground surface temperature $(°C)$
- $T_{basement}$ = basement temperature $(°C)$

- $middleday_i$ = number of days from the beginning of the year to the middle of month i $(days)$
- $phase$ = phase lag, $(\pi - phase)$ is the lag between the coldest ground surface temperature and the largest heat losses $(radians)$
- P_S = phase lag of ground surface temperature cosine $(radians)$

The total heat losses from the basement for month i is calculated by using:

$$Q_{basement,i} = Q_{ag,i} + Q_{bg,avg} + Q_{bg,var,i} \tag{7.9}$$

(Beausoleil-Morrison et al., 2007)

The boundary conditions BASECALC uses in its calculations is shown in Figure 7.4.

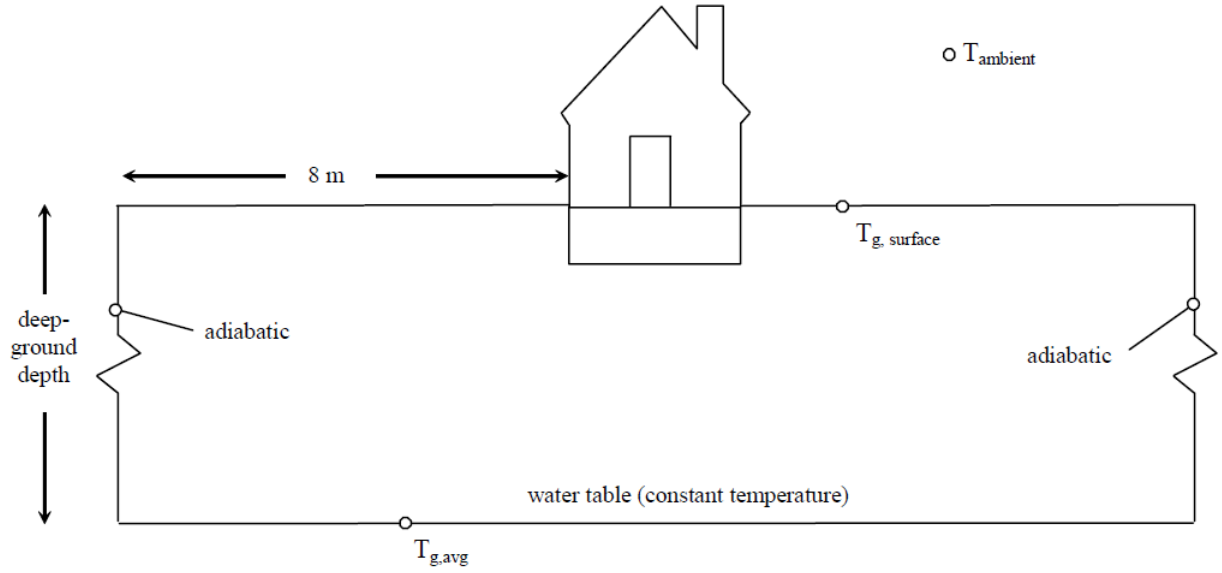

Figure 7.4: BASECALC heat loss model boundary conditions (Beausoleil-Morrison et al., 2007)

7.1.3 Nakhi's 3D conduction method

The ESRU team suggests this method for the passionate users. Abdullatif E. Nakhi's PhD from 1995 is available on the ESRU website and there is also an exemplar showing his theory implemented in the software.

Nakhi suggests that an imaginary zone should be created and placed under the building. This zone represents the ground and its surfaces should be similar to the 3-dimensional ground boundary surfaces.

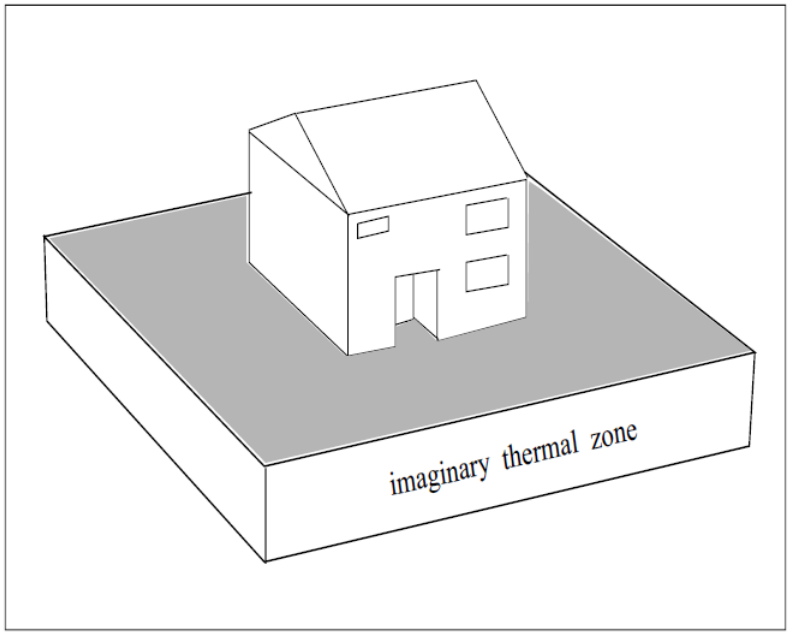

Figure 7.5: Imaginary thermal zone providing required boundary conditions for 3-dimensional ground model (Nakhi, 1995)

Figure 7.5 is from Nakhi's PhD and shows the imaginary thermal zone. All the bounding surfaces are assumed to have an adiabatic boundary condition, i.e. no heat flow between the surface nodes and the boundary. One exception is the top surface, which should be linked to all surfaces in the floor of the building. The remaining area of the top surfaces that is not linked to the building floor should have boundary conditions to the exterior environment. After all the surfaces are given their boundary condition, the connection between the building and the imaginary zone needs to be modified. Apparently the 1-dimensional modeling connects the floor surfaces to a point deep in the ground, and the 3-dimensinal modeling allows connection with the ground surface beneath the zone. The topology needs to be updated thus the floor surfaces must be linked to the 3-dimensional ground model.

After looking into the exemplar model in ESP-r, it seems like the imaginary thermal zone is built up by a construction called *fict_ grnd* at all surfaces. This construction is built up by the material called *common earth* and the layer is 100 *mm* thick. The zone also had negative z-values, which is mysterious since it is not possible to define negative z-values

when creating zones. According to Dr. Jon Hand the errors regarding this model is due to the fact that Nakhi's 3D ground conduction model not has been used very often in recent years and it needs some development work before it it ready for use (Hand, 2013). Hand suggested the BASESIMP feature for ground modeling in ESP-r.

7.2 Solar heating system

There at least two ways to model a solar heating system. A plant and system network can be defined where solar radiation data is obtained from the climate file, or a control loop can be established with input of solar radiation data converted to electrical data.

7.2.1 Plant and system network

In the network menu *plant and systems* there are several options for modeling mechanical ventilation systems, hydronic floors, electric heating systems and general HVAC components. The system that is to be modeled is created by choosing all the different components and define the connections between them. In the menu *containment* boundary conditions can be given to each component. If any of the components in the system needs electricity this information is given under the menu *electrical data* (Børset, 2009).

The different components are described below.

Simplified flat plate solar collector

There are several solar collectors available in the menu *Plant and systems*. The problem with some of these is that they require a significant number of inputs – inputs that not necessarily are available for the typical user. Therefore a simplified model has been developed. This model requires less information from the user, without reducing the accuracy of the calculations for the model significantly (Thevenard et al., 2004).

The simplified collector is a 1-node component, as shown in Figure 7.6. The node represents the outlet temperature of the solar collector.

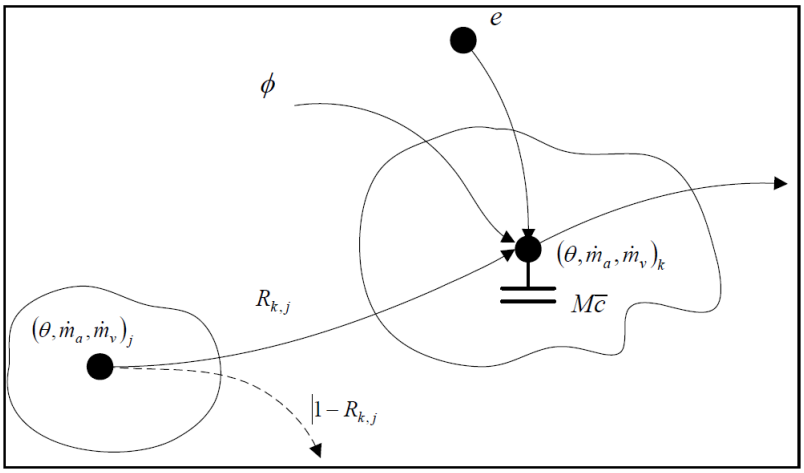

Figure 7.6: The collector model in ESP-r (Thevenard et al., 2004)

The collector is characterized by its efficiency. The efficiency is defined as the ratio of utilized energy over a given time period to the amount of solar radiation incident upon the collector over the same time period (Thevenard et al., 2004).

The collector efficiency is defined as:

$$\eta = \eta_{0,out} - \eta_{1,out}\frac{(\theta_{out} - \theta_e)}{G} \tag{7.10}$$

where $\eta_{0,out}$ and $\eta_{1,out}$ are characteristic parameters for the collector. G is the solar radiation incident upon the collector, θ_{out} is the outlet temperature of the collector and θ_e is the temperature of the environment.

An energy balance of the collector is expressed as:

$$M\bar{c}\frac{\partial\theta_{out}}{\partial t} = -\dot{m}C_p(\theta_{out} - \theta_{in}) + \eta AG \tag{7.11}$$

where M is the mass of the collector and fluid, $\bar{c}$ is the collector mass weighted average specific heat capacity, $\dot{m}$ is the flow rate through the collector. A is the gross area of the collector and θ_{in} is the inlet temperature of the collector (Thevenard et al., 2004).

This energy balance equation for the solar collector is not correct since it uses outlet temperature instead of average temperature on the left-hand side. However, this will not affect the model as the situation is treated as quasi steady-state.

If Equation 7.10 and Equation 7.11 are combined and identifying θ_{out} with the component's node temperature θ_k, and that θ_{in} with the node temperature θ_j of the component j which feeds into the collector,the equation can be rewritten as:

$$M\bar{c}\frac{\partial\theta_k}{\partial t} = -\dot{m}C_p(\theta_k - \theta_j) + \eta_{0,out}AG - \eta_{1,out}A(\theta_k - \theta_e) \tag{7.12}$$

This equation is ready to be programmed into ESP-r. However, the collector efficiencies are rarely reported as a function of outlet temperature. In North-America it is common to use the inlet temperature, while in Europe the average temperature is used. Also a quadratic equation is generally provided:

$$\eta = \eta_0 - \eta_1 \frac{\Delta\theta}{G} - \eta_2 \frac{\Delta\theta}{G} \tag{7.13}$$

where η_2 is heat loss coefficient based on average temperature, characteristic for solar collector type.

$\Delta\theta$ is defined by

$\Delta\theta = \theta_{in} - \theta_e$: North-American efficiency equation

$\Delta\theta = \theta_{avg} - \theta_e$: European efficiency equation

To take these two conditions into account, Equation 7.12 is converted into Equation 7.10 by the model. Further details can be found in the article *Development of a new solar collector model in ESP-r* by D. Thevenard, K. Haddad and J. Purdy (Thevenard et al., 2004).

Slab-on-grade hydronic floor

The hydronic floor is a 1-node model, which means that there is only one temperature for the whole surface. The injection node must be defined. The user chooses one of the nodes in the layers of the construction.

Variable speed domestic WCH pump

The pump in the solar heating system is controlled by a temperature difference between the node temperature in the solar collector and the node temperature in the hydronic floor.

7.2.2 Control loop with electric heating

Another approach to simulate a solar heating system with heat injection in the basement floor of the inner zone is to define a control loop for the zone. This can be defined in the menu *Controls* and further in the menu *zones*.

- Sensor details
- Actuator details

- Period data

The list above shows the different menus under *zones*. The user has to define where the sensor and actuator is placed. Then under *period data* control laws are defined. Periods are defined as day types in the year. A day is also divided into periods, and a control law is set for each period of the day.

The placement of the actuator is defined to be at a node within a construction. The heat injection will occur over the entire surface of the layer at the defined node.

7.3 Area of heat injection

To achieve frost proof conditions for the inner zones, without overheating in the summer, different areas of heat injection have been considered.

Figure 7.7 shows a plan view of the basement floor with alternative 1.

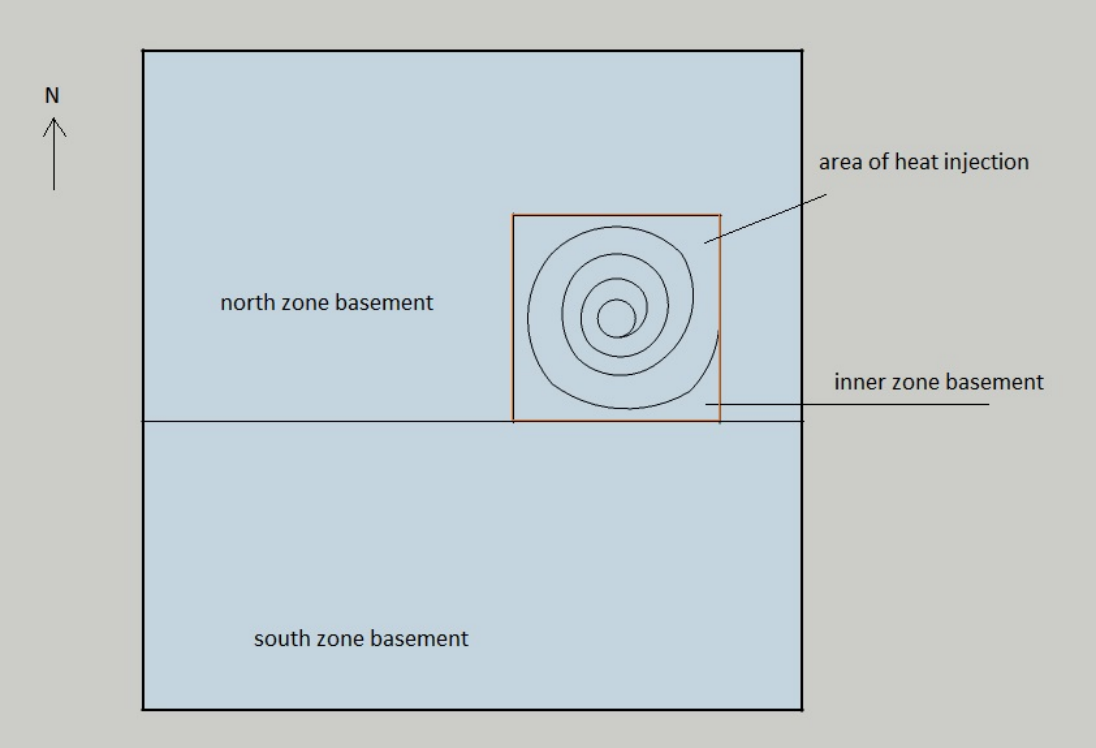

Figure 7.7: Alternative 1: Heat injection in the inner basement floor

Alternative 1 is to have all the heat injection in the inner zone of the basement. This is where the sanitary installations are placed, and this is the area that is to be kept frost proof. The heat injection will occur within a layer of the basement floor. Heat will disperse to the inner basement room and further up to the inner zone in 1st floor. The walls of the inner zone are constructed with extra insulation to prevent heat loss to the surrounding rooms.

In the project thesis, heat was injected at this point. A frost proof situation was obtained, but the temperature of the floor was very high in the summer months. The high temperatures are caused by an unrealistic large amount of injected by the control loop in the summer months. A distribution system with a heat transfer fluid would not be able to deliver the equivalent amount of solar heat available from the solar collectors. The temperature difference between the floor and the collectors would not be large enough for the heat transfer fluid to extract and deliver all the solar heat that is available.

Figure 7.8 shows a plan view of the basement floor with Alternative 2:

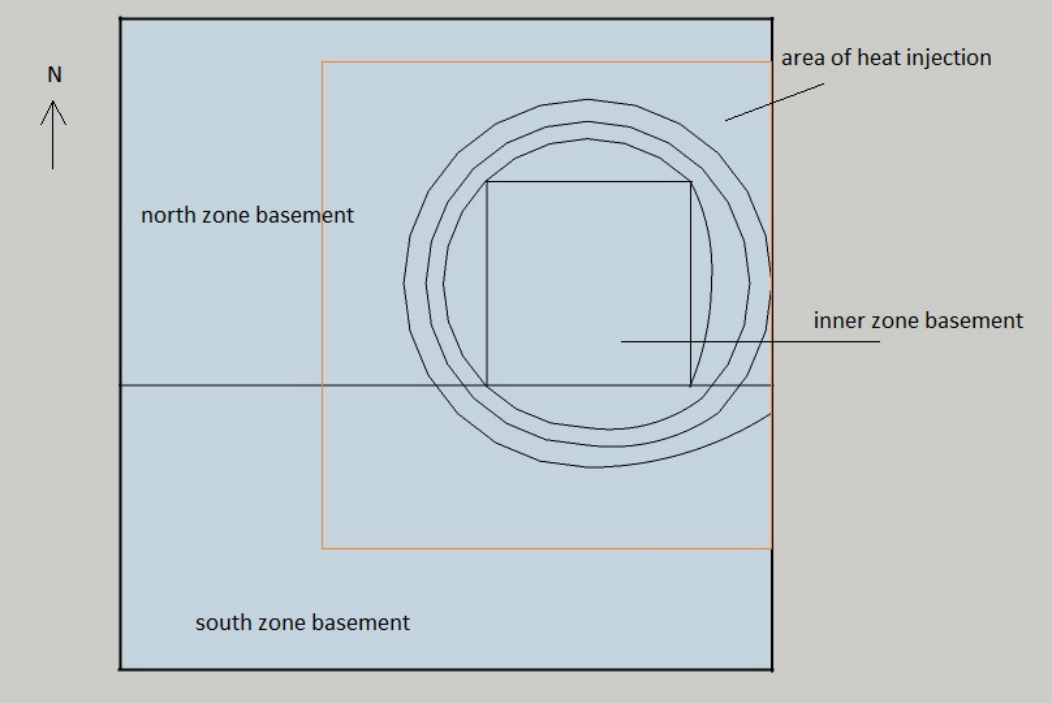

Figure 7.8: Alternative 2: Heat injection in the outer basement floor

Alternative 2 is to have heat injection in the surrounding floor around the inner zone. The heat injection will then occur in approximately 50 % of the floor area of the north and the south zone. The idea is that the floor in the outer zones with heat injection is in thermal contact with the floor in the inner basement and the ground. The heat will disperse through the concrete floor into the inner zone and downwards into the ground. The outer basement floor with heat injection will have layers of insulation at the top of the floor construction to prevent heat loss to the rooms.

Figure 7.9 shows a plan view of the basement floor with Alternative 3:

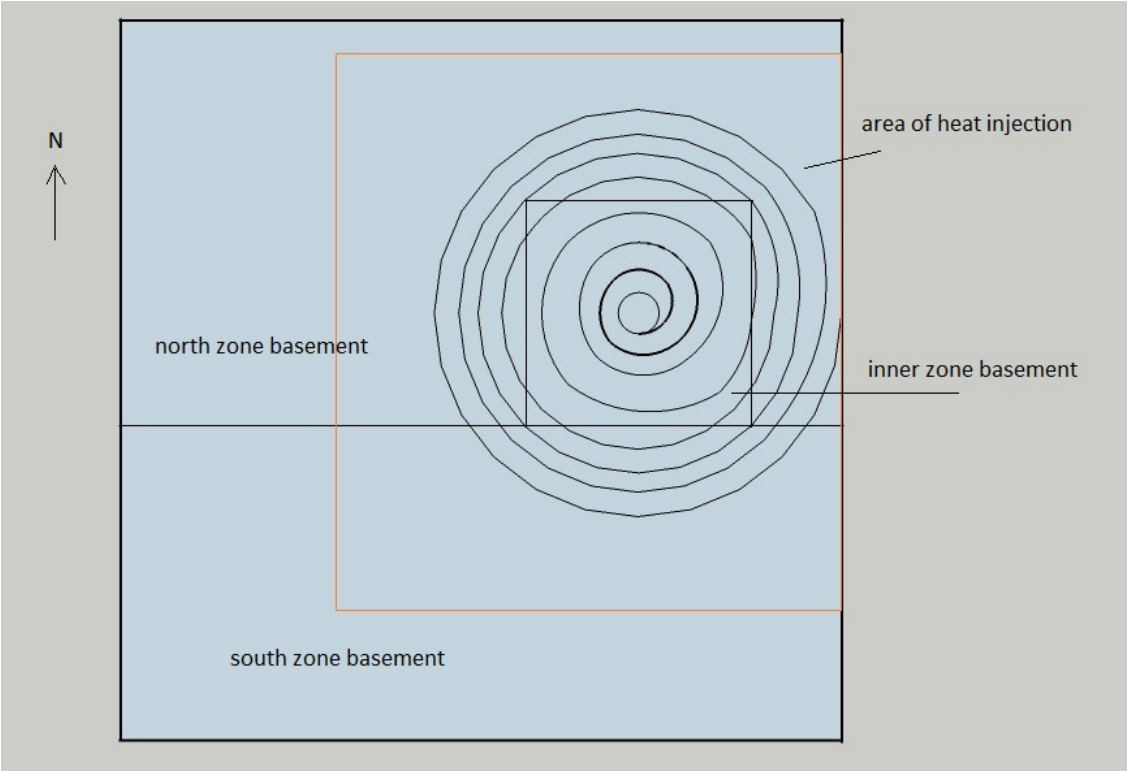

Figure 7.9: Alternative 3: Heat injection in both inner and outer zones of the basement floor

Alternative 3 is to have heat injection in the inner zone basement floor and in 50 % of the outer basement floor. This is a combination of Alternative 1 and 2.

With Alternative 2 and 3 the heat will be distributed over a larger area. The areas of heat injection would be in thermal contact with the ground and with the basement floor of the inner zone.

In the summer when there is a lot of solar radiation available, the circuit flow could go *from* the outer zones *to* the inner zone. In the winter time when there is little solar radiation available the circuit flow could go *from* the inner zone *to* the outer zones. This way the heat will be injected where it is most needed in the winter and for storage in the summer. With a longer distribution line for the heat transfer fluid, a greater temperature difference will be achieved and more heat will be extracted from the solar collectors.

If heat is to be injected in several surfaces, a control loop for each surface must be defined. A control loop is constructed with information about solar radiation data and time intervals for when solar radiation is available. If the heat injection is to happen in several zones via several control loops, the solar radiation data must be portioned out for each of the surfaces. Alternatively, heat could be injected where it is most needed, either in the upper part of the basement floor in the inner zone for immediate heating, or in the ground for storage. In order for several control loops to work, *nested functions* must

be defined. After discussions with the co-supervisor for ESP-r, it was suggested not to use this approach. Another problem with this approach is that the heat transfer is only calculated 1-dimensionally and perpendicular to the surfaces in ESP-r. That means that surfaces that lies adjacent to each other is not in thermal contact. So if heat is injected into the outer basement floors, this will only disperse into the rooms above or down to the ground below. Therefore, as in the project thesis, the point of heat injection is chosen to be as in alternative 1; in the basement floor of the inner zone.

7.4 Ground insulation

To prevent heat loss from the heat storage facility should insulation around the perimeter of the floor slab be implemented in the model.

Ideally it would be possible to create surfaces around the perimeter of the floor slab and construct it with insulation. However, it is not possible to create one single surface in ESP-r, but it is possible to create small zones. Figure 7.10 shows a plan view of the basement with ground insulation.

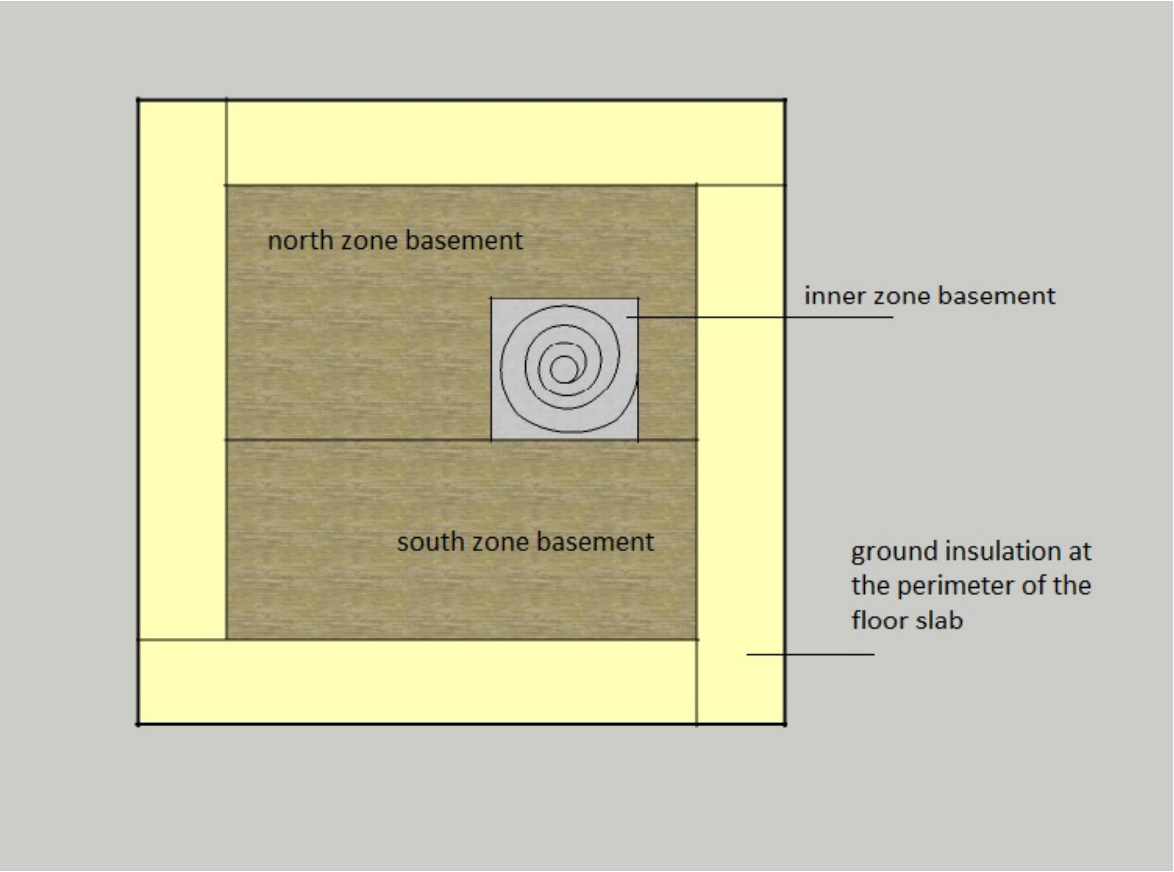

Figure 7.10: Ground insulation at the perimeter of the floor slab

The yellow area in Figure 7.10 shows the zones representing ground insulation. Each zone has 6 surfaces where each of them should be constructed only with insulation.

Another alternative for implementing ground insulation in the model is to investigate the BASESIMP configurations, as some of them are constructed with ground insulation.

Chapter 8

Modeling in ESP-r

After recommendations from Dr. Jon Hand from the ESRU team, further study of the BASESIMP configurations will be carried out (Hand, 2013). Nakhi's method will not be studied further. Two ways of modeling a solar heating system and how to implement a BASESIMP configuration will be presented in the following chapter.

8.1 The ground

To achieve a more realistic view of the ground, one of the BASESIMP configurations should be implemented as the boundary condition for the surfaces adjacent to the ground. BASESIMP can either be defined as the boundary condition for the surfaces adjacent to a basement, or the basement can be represented by a separate zone. When the basement is represented as a separate zone, the construction of the surfaces are defined and the transient response of these surfaces is considered. BASESIMP is then apportioned as a surface boundary for the floor and wall surfaces of the basement and the heat transfer is calculated (Beausoleil-Morrison, 2013).

After some test simulations it was discovered that the BASESIMP configuration only calculated the heat transfer between the building and the surrounding ground. It seems like the effect of heat storage not is taken into account.

An appropriate approach could be to create a separate zone as a basement, define the boundary conditions for the surfaces in the basement with BASESIMP and inject heat in the inner zone of the original basement. This way the heat storage will be taken into account in the massive concrete floor of inner zone 0. The heat transfer for the heat storage facility will be calculated 1-dimensionally as it is treated as a construction in the model. The heat transfer between the basement and the surrounding ground will be calculated quasi 3-dimensional by BASESIMP.

8.1.1 Basement zone

A new basement zone is created. The zone is placed directly under the leisure home with the same dimensions as the building above, 8 m wide and 8 m long. The basement is 2 m high and it is submerged 1.9 m into the ground. This zone and the new model is discussed further in Chapter 9.

8.1.2 BASESIMP

In the menu *Zones composition* and *geometry and attribution* the different zones and their surfaces can be linked to its boundary condition. By clicking into the basement zone, choosing *surface attributes*, selecting a surface and its environment a list of the different boundary conditions is shown. By choosing the option *BASESIMP foundation configuration* a new list of all the different basement configuration is shown. Option $BCIB\_6$ is chosen after discussions with the supervisor. BASESIMP is defined as boundary condition for the basement floor surface and 95 % of the basement walls.

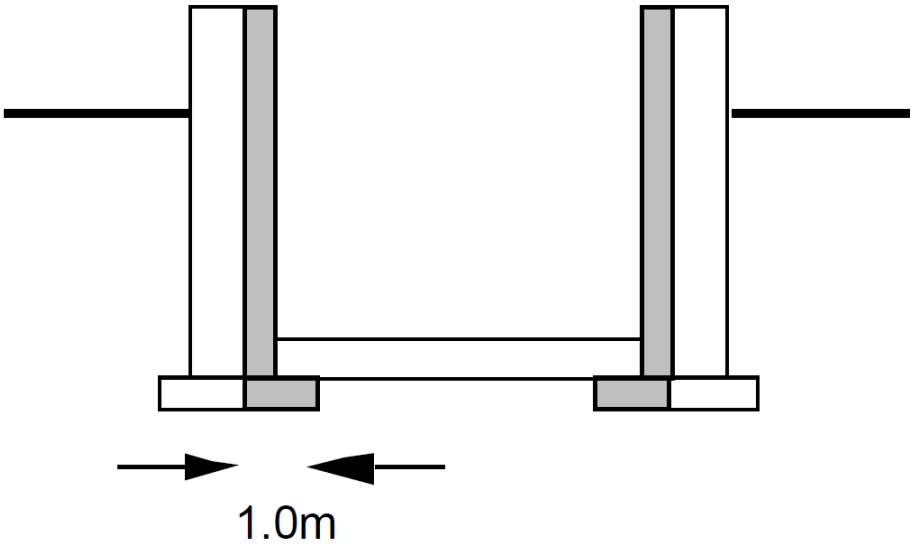

Figure 8.1: BASESIMP configuration $BCIB\_6$ (ESRU, 1999)

Figure 8.1 shows the configuration chosen for the leisure home model.

BASESIMP inputs

Below is a list of all the different inputs the user has to define for a BASESIMP configuration. The information is collected from the software and a report about BASESIMP found at the ESRU webpage (University of Strathclyde, Energy Systems Research Unit, 2013; ESRU, 2013).

Height
Distance from the top of the floor slab to the top of the basement structural wall. Value must be at least 0.1 m greater than the depth, and between 1 and 2.5 m.

Width
Exterior-of-structural-wall to exterior-of-structural-wall distance. Value must be less than or equal to the length, and between 2 and 20 m.

Length
Exterior-of-structural-wall to exterior-of-structural-wall distance. Value must be greater or equal to the width, and between 2 and 20 m.

Depth
Distance from the top of the floor slab to the grade level. Value must be between 0.05 and 2.4 m.

Wall insulation overlap
Height of the wall covered by both interior and exterior wall insulation. Value must be between 0 and 2.4 m. Only of interest for the configuration cases $BCCN\_1$ and $BCCN\_2$.

Insulation
Wall insulation RSI rating. Value must be between 0 and 20 m^2K/W.

Soil conductivity
Thermal conductivity of soil surrounding the foundation. Value must be between 0.1 and 1.9 W/mK.

Water table
Dictates the depth of horizontal thermal boundary. The deeper the water table, the lower the foundation heat loss will be. Value must be between 5 and 20 m.

Temperatures:

- TG_{avg}: Annually-averaged soil temperature. Value must be between -10 and 20 $°C$.
- TG_{amp}: Amplitude of ground-temperature's annual sine wave. Value must be between 0 and 25 $°C$.
- TG_{ps}: Phase lag of ground-temperature's annual sine wave. Value must be between 0 and 1 radians.

TG_{avg}, TG_{amp} and TG_{ps} are set using the weather file and the Moore model.

Moore method

The temperatures of the ground is set using Moore method and the climate file in ESP-r. The Moore method was originally developed for implementation in the software HOT2000. The method is a soil estimation model, which uses average monthly ambient dry air temperature and annual heating degree days to estimate the temperature of the soil at any depth at any time of year.

The first step in the development of this model was to create an appropriate time function to represent the temperature of the soil at any given depth. A simple cosine function was used to create this function (Moore, 1986):

$$T_s = A_s - B_s \cdot \cos\left(2 \cdot \pi \cdot \frac{n}{8766} - P_s\right) \tag{8.1}$$

Where:
T_s = temperature of soil at given depth and time of year ($°C$)
A_s = mean temperature of soil/ground ($°C$)
B_s = soil temperature at given depth ($°C$)
n = number of hours into year (note: there are 8766 hours per year)
P_s = phase angle at given depth (degrees)

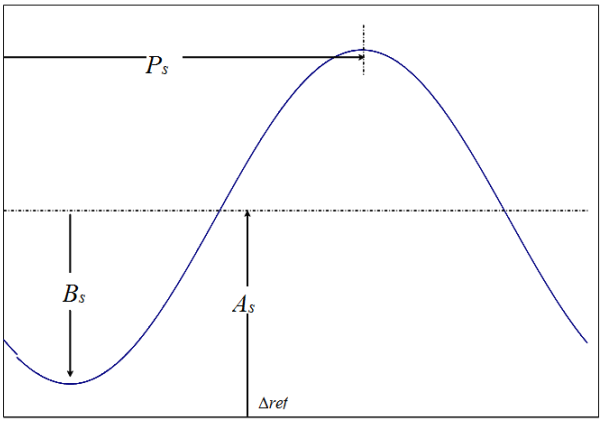

Figure 8.2: Time function for the temperature in the soil, cosine function (Purdy, 2013)

Soil temperature modeling procedures

The average monthly temperature and the number of heating degree days are collected from the weather file.

The basis for annual heating degree day calculations is 18.2 $°C$. The average temperature

is calculated by:

$$T_{average} = \frac{T_{max} - T_{min}}{2} \tag{8.2}$$

for any given day. If the average temperature of the day is less than 18.2 $^{\circ}C$, the number of degree days are

$$DD = 18.2 - T_{average} \tag{8.3}$$

If the average temperature of the day is greater than 18.2 $^{\circ}C$, the number of degree days for that day is 0.

The annual degree days is calculated by:

$$DD = \sum_{i=1}^{365} \left[18.2 - \left(\frac{T_{i,max} - T_{i,min}}{2} \right) \right] \tag{8.4}$$

The average monthly dry bulb temperatures are fitted into a cosine curve using a least square technique and values for A_a, B_a and P_a is obtained (Moore, 1986).

Ground parameters

Average ground temperature, A_s:

$$A_s = A_a - 1.438 + (9.189 \times 10^{-4})DD \tag{8.5}$$

Where

$$A_a = \frac{\sum_{i=1}^{12} T_{a,i}}{12} \tag{8.6}$$

i = month of the year
$T_{a,i}$ = monthly average outdoor air temperature

Ground temperature amplitude B_s

$$B_s = B_a - 7.875 + (1.97 \times 10^{-3})DD \tag{8.7}$$

Where

$$B_a = \frac{-\sqrt{S_1^2 + C_1^2}}{2} \tag{8.8}$$

$$S_1 = \sum_{i=1}^{12} \left\{ T_{a,i} \cdot \sin \left[\frac{2\pi}{12}(i - 0.5) \right] \right\} \tag{8.9}$$

$$C_1 = \sum_{i=1}^{12} \left\{ T_{a,i} \cdot \cos \left[\frac{2\pi}{12}(i - 0.5) \right] \right\} \tag{8.10}$$

Phase shift, P_s

$$P_s = P_a - 0.0756 + (2.128 \times 10^{-5})DD \tag{8.11}$$

Where

$$P_a = \tan^{-1} \left\{ \frac{S_1}{C_1} \right\} \tag{8.12}$$

Values for A_s, B_s and P_s are obtained for the soil at the surface using three correlations involving degree days. A_s, B_s and P_s represent the modified values of A_a, B_s and P_s (Moore, 1986).

The next step is to develop a temperature profile for any depth. As the depth of the ground increases, the temperature amplitude decreases, the phase shift angle shifts ahead in time and the mean soil temperature approaches a constant value.

$$T(x) = A_s - B_s \cdot b \cdot \cos \left(2 \cdot \pi \cdot \frac{n}{8766} - P_s - p \right) \tag{8.13}$$

Where:
$T(x)$ = temperature of soil at depth x ($^\circ C$)
A_s = mean temperature of soil/ground ($^\circ C$)
B_s = soil temperature at given depth ($^\circ C$)
n = number of hours into year (note: there are 8766 hours per year)
P_s = phase angle at given depth (degrees)
b = decrease in amplitude for depth x
p = shift in phase angle for depth x

How much the amplitude decreases and the phase shift increases with the depth is determined by the diffusivity of the soil (Moore, 1986). The diffusivity is a measure of how well the soil conducts heat. Correlations involving heating degree days are used to find the diffusivity of the soil at any location.

The ground diffusivity values A1, B1 and PH are determined for a location by the following correlations (Moore, 1986):

$$A1 = \frac{10^{(-8.74 \cdot 10^{-5}) \cdot DD - 0.0271}}{1000} \tag{8.14}$$

$$B1 = \frac{10^{(-1.678 \cdot 10^{-4}) \cdot DD - 0.7918}}{1000} \tag{8.15}$$

$$PH = \frac{10^{(-9.371 \cdot 10^{-5}) \cdot DD - 0.5865}}{1000} \tag{8.16}$$

The diffusivity values $D(amp)$ and $D(phase)$ are determined by:

$$D(amp) = A1 + B1 \cdot X \tag{8.17}$$

$$D(phase) = PH \tag{8.18}$$

where X (m) is the ground depth from the surface.

Finally, the diffusivity coefficients b and p can be determined:

$$b = e^{-X \cdot \sqrt{\frac{\pi}{D(amp) \cdot 8766}}} \tag{8.19}$$

$$p = -X \cdot \sqrt{\frac{\pi}{D(phase) \cdot 8766}} \tag{8.20}$$

The soil temperature equation, Equation 8.13, for any given depth at any time of the year is defined. This equation assumes the average monthly dry bulb temperature occurs at the middle of the month and that the ground is of constant permeability (Moore, 1986). Further information about Glenn Moore's article about this temperature estimation model can be found in the Appendix 14.

8.2 Solar heating

Two ways of modeling a solar heating system is presented in the following section.

8.2.1 Plant and system

The first method is to create a solar heating system by choosing components for the system and link them together. This is done in the menu *Plant and systems*.

The list below shows the different menus under *Plant and systems*:

- Components
- Connections
- Containments
- Electrical data
- Link to fluid flow network
- Link plant to zone(s)

There two last menus in the list are not used in this model.

Components in the solar heating system

The components in the solar heating system are solar collector, hydronic floor and a pump. The components have defined connections, but the distribution pipes between them are not included in the model, so heat loss from the pipes are neglected.

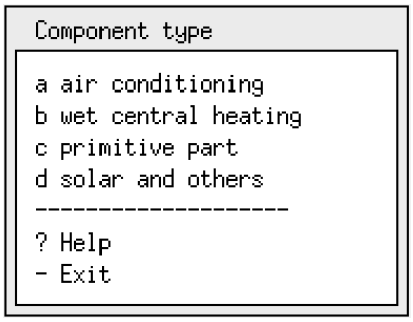

Figure 8.3: The different categories in the component menu in ESP-r

As Figure 8.3 shows there are 4 categories in the component menu. The components of the solar heating system is collected from *Solar and others* and *Wet central heating*.

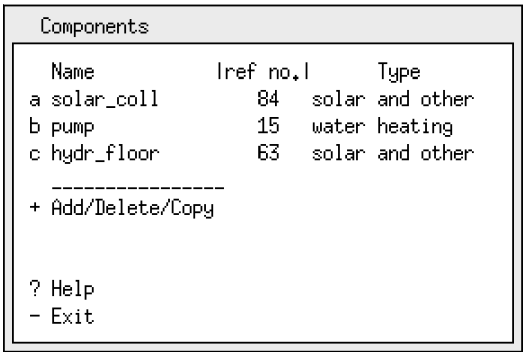

Figure 8.4: The different components of the solar heating system in ESP-r

The chosen solar collector is called *simplified flat plate solar collector*, the pump is called *variable speed domestic WCH pump* and the hydronic floor is called *slab-on-grade hydronic floor*.

Connections between the components in the solar heating system

The different connections between the components in the solar heating system are determined in the menu *connections*. The connections are created by first defining receiving component and node, and then choose the connection type. Finally, the sending component is defined together with the mass diversion ratio for the connection. An explanation of the input is available in the program which ways: *The mass diversion ratio is the amount of fluid coming from the sending component that reaches the receiving component* (University of Strathclyde, Energy Systems Research Unit, 2013). This can be used to specify leakage in the system.

Figure 8.5 shows the different connection types that are available in ESP-r.

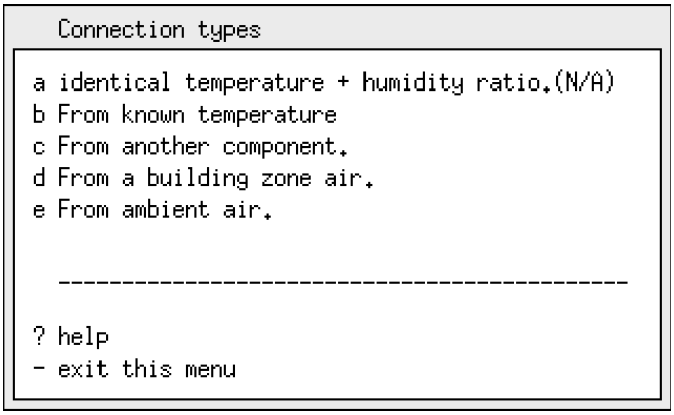

Figure 8.5: The different connection types available in ESP-r

For all the connections defined in this model, connection type *c: From another component* was chosen.

Figure 8.6 shows a list of the defined connections between the components:

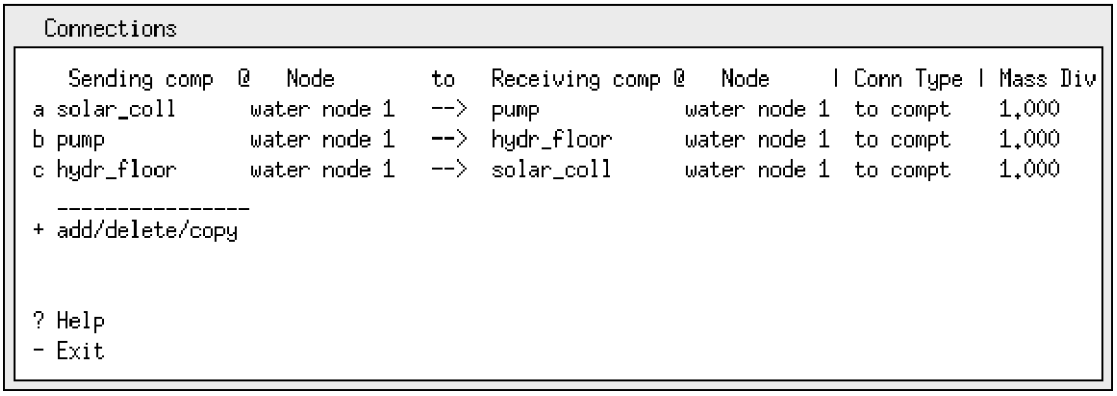

Figure 8.6: The defined connections between the components

Containments for the components in the solar heating system

Each component in the model is linked to its surroundings under the menu *containments*.

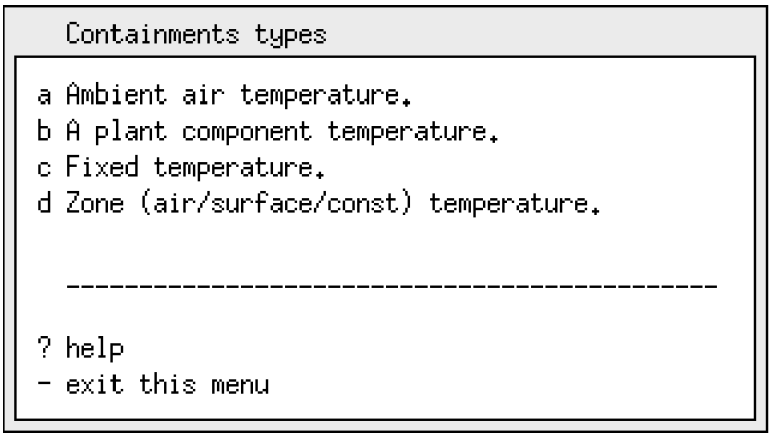

Figure 8.7: The different containment types available in ESP-r

The solar collector is linked to outside air, the hydronic floor is linked to the basement floor in the inner zone in the basement. The pump is not linked to anything and is assumed to be adiabatic for now.

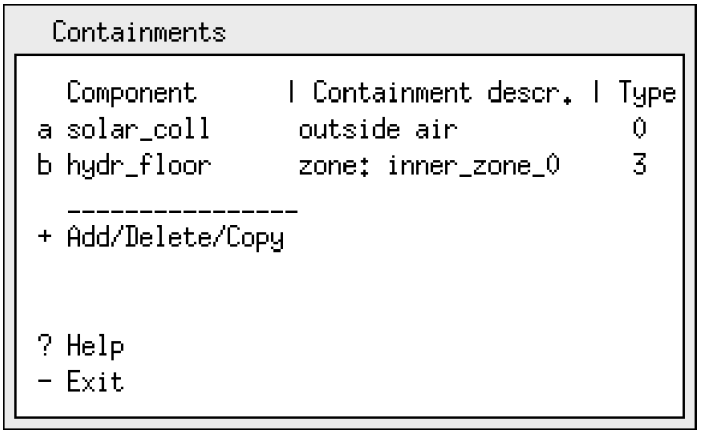

Figure 8.8: The defined containments

Control system for the solar heating system

The control system is defined under the menu *plant and systems*, and a control loop for the solar heating model must be defined. To achieve a good control system for the solar heating model, the heat transfer fluid should circulate only when there exists a temperature difference (Børset, 2009). The temperature difference is based on the difference between the solar collector and the hydronic floor. Period data, actuator and sensor details must be defined for the control loop.

Problems with this approach

Several attempts to run the simulations were carried out, but the described solar heating system did not work. A former student, Are Siljan Børset has done a similar study, only with a hot water tank instead of a hydronic floor. Børset used an additional connection between the hot water tank and the pump which he had found in an article (Børset, 2013). Unfortunately this was not transferable to a hydronic floor. Based on information obtained from the ESP-r user mailing list it became clear that this connection was unnecessary in such a simple system. It was also suggested to change the time-steps for the simulation (Geissler, 2013), but this did not work.

Given the main focus of this study which is to improve the ground model from the project thesis it was decided to use a control loop with electric heating. The control loop is based on solar radiation data and is further discussed in the following section.

8.2.2 Control loop - electric heating

The second method for modeling and simulating the solar heat injection is to create a control loop with electric heating.

A control loop is defined under the menu *Controls* and *zones*. A control loop has several options for defining periods. The first thing that needs to be established is what kind of day type is in the periods of the year. The list below shows the different options:

- Follow calender day types
- Just one day type
- Dates of validity

The option *Dates of validity* is chosen. This alternative gives the user the opportunity to define start-end periods within which to apply control e.g. summer and winter. *Dates of validity* should cover the whole year and be continuous (University of Strathclyde, Energy Systems Research Unit, 2013).

After *day type* is defined, the number of periods in the year is set. For the control loop used in the project thesis, from now on called Control loop 1, 8 periods was defined. For the new control loop, from now on called Control loop 2, 9 periods for the year was set. The next step is to define start period and duration of the periods and how many periods that is in the day type. For all the 8 or 9 periods in the year, 3 periods in the day type is defined for both control loops.

After the periods are defined, the heat injection for each period is set. For the 3 periods in a day type which is defined, a control law must be defined for each one of them. *Free floating* is defined by default for all the periods. For the period in the middle of the day, when solar radiation is available and heat injection occurs, the control law must be changed to *Basic controller for heating/cooling*.

The energy input is derived from solar radiation data from PVGIS (Joint Research Centre, IET, 2013). This is because the solar radiation data from the climate file in ESP-r is only available on a horizontal plate, while the PVGIS calculator has an incline option, so that data can be collected for different angles, see Appendix 14. The time interval is determined based on solar radiation data in ESP-r, see Appendix 14. For Control loop 1 some of the months are merged. An average value for incoming solar radiation is calculated for the merged months. As in the project thesis is a collector area of 4 m^2 and an efficiency of 45 % also chosen for this study.

Finally, sensor and actuator details are defined, and the control loop is linked to the basement inner zone.

Chapter 9

Simulation in ESP-r

9.1 The models

Both the old model from the project thesis and the new model is used in the simulations.

9.1.1 The old model

The old model from the project thesis is shown in Figure 3.4 in Chapter 3. The construction details for the leisure home are presented in Table 3.1 in the same chapter. The boundary conditions for the surfaces adjacent to the ground was monthly temperature profiles at 0.5 m depth for the basement floor in the outer zones, and at 4 m depth for the basement floor of the inner zone. As seen from the table with the construction details, the ground was presented in the inner basement floor as a 3.5 m thick concrete pillar.

9.1.2 The new model

The new model is based on the old model. The only difference in the geometry is that an additional zone has been added, a basement zone. A 3-D view of the model is shown in Figure 9.1.

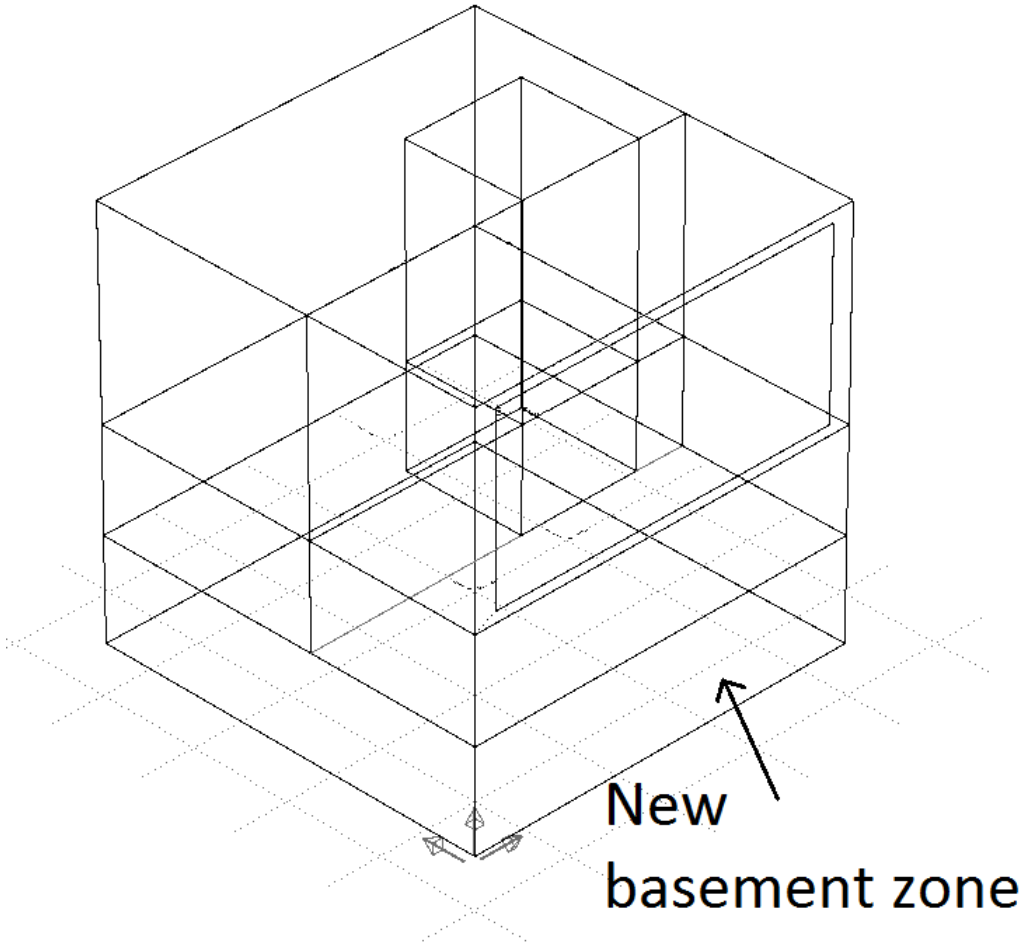

Figure 9.1: Leisure building model with the new basement zone

The new model has the same design as the old model, except for the inner basement floor. This new zone is not an *actual* basement in the model. This construction is discussed later in this chapter. The elements for the new basement zone are shown in the table below. They are based on the elements for the chosen BASESIMP configuration $BCIB\_6$.

Construction	**Material**	**Thickness** [mm]	**U-value** $[W/m^2K]$
Basement floor adjacent to the ground	heavy mix concrete	100	4.142
Basement wall adjacent to the ground	glasswool	100	0.356
	heavy mix concrete	200	

Table 9.1: Construction details for the new basement zone

9.2 The ground

The ground modeling has been improved by creating an additional zone and applying BASESIMP as boundary condition so that quasi 3D-calculations of the heat transfer is obtained. The heat storage is taken into account by representing thermal mass in the ground in the basement floor of the inner zone.

9.2.1 BASESIMP

The inputs for the chosen configuration $BCIB\_6$ is shown in Table 9.2. An explanation of the different inputs is found in Chapter 8.

	Input
Height	2 m
Width	8.6 m
Length	8.6 m
Depth	1.9 m
Overlap	0 m
Insulation	2.8 m^2K/W
Soil conductivity	1.9 W/mK
Water table	8 m
TG_{avg}	Set by Moore method
TG_{amp}	Set by Moore method
TG_{ps}	Set by Moore method

Table 9.2: Input values for the BASESIMP configuration $BCIB\_6$

The geometric inputs for the new basement zone are based on the geometry of the original basement in the leisure home model. The basement is defined to be submerged 1.9 m into the ground and the insulation is determined based on the materials used in the construction of the basement wall. This resistance to heat transfer is further discussed in Chapter 11. Soil conductivity is set to 1.9 W/mK as the ground is supposed to be constructed by rock such as granite. This is the maximum value ESP-r allows. The water table is defined to be at a depth of 8 m from the basement floor, which is 9.9 m from ground level. Below 10 m are the temperature somewhat stable as discussed in Chapter 5.

9.2.2 The ground construction

The heat storage in the ground is represented in the construction of the basement in the inner zone by 5 layers of concrete, which constitutes a thickness of 1.5 m. This corresponds to recommendations from Dr. Jon Hand from the ESRU team who suggests a thickness of 1.5 m when the ground is represented in the slab construction (ESRU & users, 2006-2013).

The material *heavy mix concrete* is copied and named *ground*. The importance of available thermal mass is to be studied and by copy and create a new material, it is a simple maneuver to change the thermal properties for the material - hence the construction. Table 9.3 shows 4 different cases where the product of the density and the specific heat capacity is multiplied with a factor of 1, 4, 7 and 10.

	Density (kg/m^3)	**Specific heat capacity** (J/kgK)
Standard values in ESP-r	2100	653
Maximum values in ESP-r	*9000*	*2000*
Case 1 $(\rho \cdot c) \cdot 1$	2100	653
Case 2 $(\rho \cdot c) \cdot 4$	8400	653
Case 3 $(\rho \cdot c) \cdot 7$	9000	1067
Case 4 $(\rho \cdot c) \cdot 10$	9000	1524

Table 9.3: Different thermal properties for the ground construction

The area under the outer zones of the basement is not represented as a part of the heat storage in the simulations. To take this area into account, the thermal properties are multiplied with different factors to accommodate for a larger storage volume. Table 9.3 shows the thermal properties for the different cases that are to be studied.

9.3 Solar heat - Control loop

Control loops are established to represent the solar heating system. To compare the results from the project thesis, both the *old* and the *new* control loop are presented as Control loop 1 and Control 2. The steps for how a control loop is established are demonstrated below.

The inputs for the control loops are shown in Table 9.4 and Table 9.5.

Period	Month(s)	Time interval	No of start hours	45 ° (W/m^2)	Heat injection (W)	Day periods in year
1	Jan	10.00-15.00	5	120.6	217	1-31
2	Feb	09.00-17.00	8	241.3	434	32-59
3	Mar & Apr	06.00-19.00	13	290.8	523	60-120
4	May & June	05.00-20.00	15	346.3	623	121-181
5	July & Aug	05.00-20.00	15	286.3	515	182-243
6	Sept & Oct	07.00-18.00	11	202.7	365	244-304
7	Nov	09.00-15.00	6	151.8	273	305-334
8	Dec	11.00-14.00	3	113.7	205	335-365

Table 9.4: Solar radiation data for Control loop 1

Period	Month(s)	Time interval	No of start hours	70 ° (W/m^2)	Heat injection (W)	Day periods in year
1	Jan	10.00-15.00	5	144.2	260	1-31
2	Feb	09.00-17.00	8	272.5	491	32-59
3	March	07.00-18.00	11	305.5	550	60-90
4	April	06.00-19.00	13	304.6	548	91-120
5	May, June, July & Aug	05.00-20.00	15	-	0	121-243
6	Sept	07.00-18.00	11	240.0	432	244-273
7	Oct	08.00-17.00	9	205.6	370	274-304
8	Nov	09.00-15.00	6	178.3	321	305-334
9	Dec	11.00-14.00	3	138.7	250	335-365

Table 9.5: Solar radiation data for Control loop 2

The time intervals for the days in the different periods are defined when creating a new control loop. First, number of periods in a year is determined, and then periods for the days in that particular period. Then the time intervals must be established and a control law is defined for each period of the day.

The heat input is defined under the menu *period data* and by changing the control law for the period in the middle of the day to *Basic controller for heating/cooling*.

The first and the third period of the day has *free floating* as control law, which means that nothing special is happening during this time. The second period however, has the control law *Basic controller for heating/cooling* and this is when heat injection occurs.

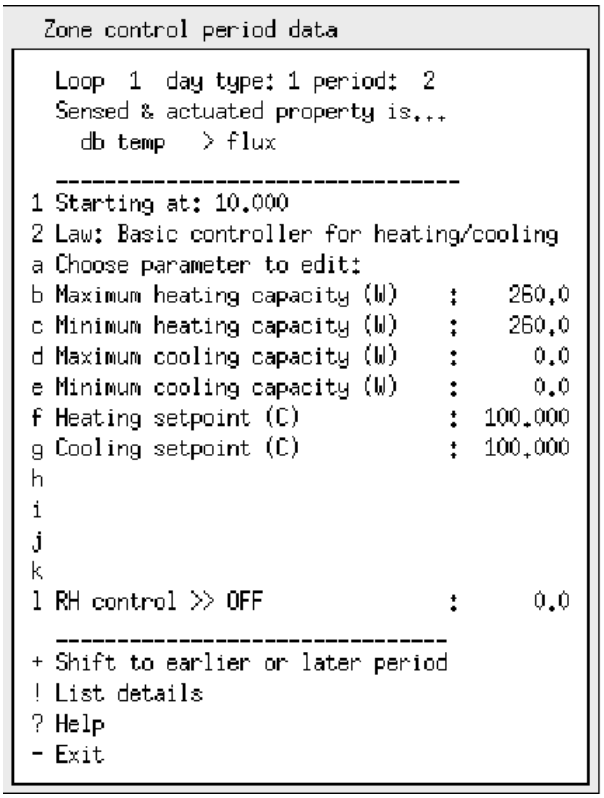

Figure 9.2: The input for Period 1: January, the second period of the day

Figure 9.2 shows an example of how the heat input is defined in the control law *Basic controller for heating/cooling*. Only heating is defined, and the cooling capacity is set to zero, since this represents a solar heating system. The set point are defined in a way so that all the heat available will be transferred to the floor.

The sensor and actuator details need to be defined, and finally the control loop has to be linked to a zone. For the zone sensor, option *a: senses current zone db temp* is chosen. A question about nested control functions pops up, the answer to this is *NO*. Nested functions are used when a MLC switching controller is defined (University of Strathclyde, Energy Systems Research Unit, 2013). For the zone actuator, option *d: air point or surf in inner zone 0* is chosen. Further is the inner basement floor chosen and a node. The location of the node defines where in the construction the heat injection occurs. The heat is injected for the whole surface area. The control loop is linked to the inner zone in the basement, since this is where the sensor and the actuator is placed.

The heat injected by the control loop

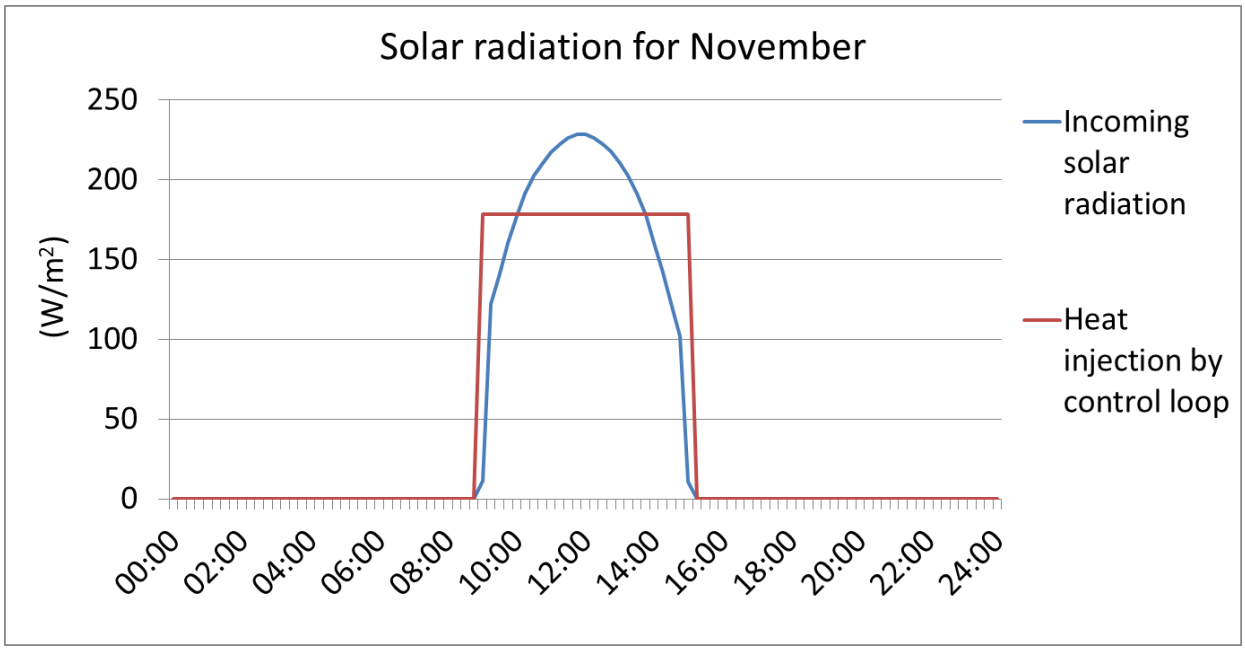

Figure 9.3: Incoming solar radiation converted to heat input by Control loop 2 for a day in November

Figure 9.3 shows how the solar heat is injected by the control loop and the difference between actual incoming solar radiation and solar heat injected by the control loop.

Chapter 10

Results and discussion

Different aspects of available solar radiation and thermal mass have been considered in the simulations. The collector area and incline have been studied. Available thermal mass and point of heat injection have also been studied.

For the simulations of the leisure home, 100 start-up days have been chosen. Ideally it would be better to perform simulations with more start-up days for more realistic results. For seasonal storage it would probably take several years before the ground is heated up to stable conditions, but the maximum allowed number of start-up days in ESP-r is 100 and this will be used in the simulation. The number of start-up days lets the simulation include data about conditions in previous days before the period of interest starts. In this way, past climate data and ground conditions are accounted for when the simulation period starts.

10.1 Solar radiation at different inclines

Solar radiation can be collected at different inclines. For heat storage in the ground it is preferable to collect as much energy as possible over the year and maintain frost proof conditions in the inner zone. In the project thesis an incline of 45 ° was used. It resulted in frost proof conditions in the winter and very high temperatures during the summer.

If a hot water tank is used for storage it is important that the water temperature is kept sufficiently high throughout the year, especially in the most critical months such as December, January and February. Since water does not have the same ability to store heat as the ground does, the hot water tank needs to be supplied with heat continuously over the year. Therefore, a solar collector placed at a steeper incline would be more suitable in order to maintain frost proof conditions. This is because the sun is lower in the sky during the winter than in the summer, so in order to catch the solar rays the angle must be increased.

The most critical period for keeping the inner zones above 0 $°C$ is mid-winter, in the month of February. An incline of 45 ° was used in the project thesis. A new control loop has been developed with an incline of 70 °. By collecting solar radiation at 70 ° instead of

45 ° more heat is collected in the spring and in the fall. This seems like a good approach for storing heat to the critical periods. The figure below shows how much solar radiation that is available for inclines of 45 ° and 70 ° over the year.

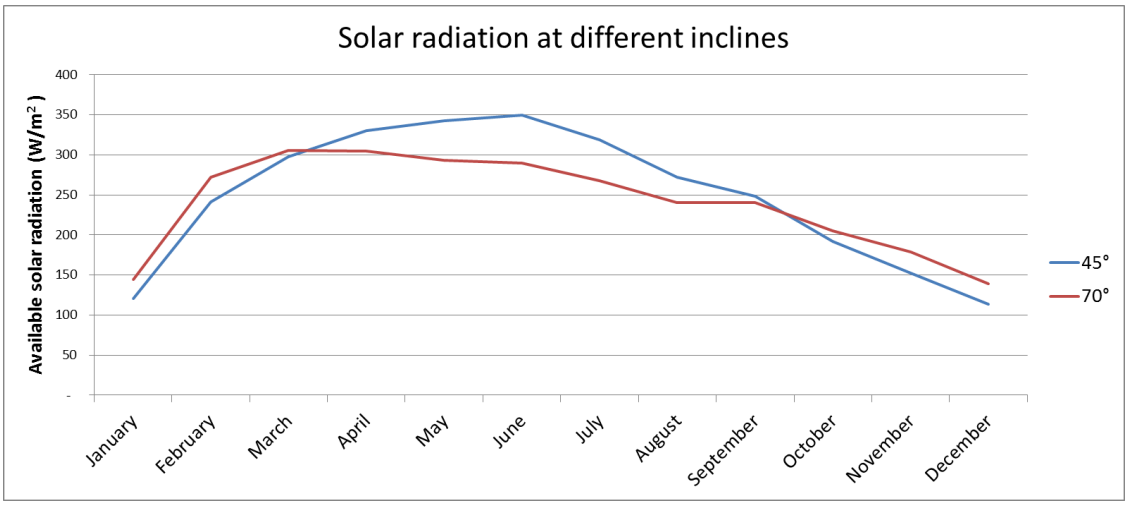

Figure 10.1: Solar radiation for an incline of 45 ° and 70 °

Figure 10.2 shows how much energy which is delivered by the two control loops that is studied further. Control loop 1 is collected energy with an incline of 45 ° and Control loop 2 is collected energy with an incline of 70 °. Control loop 1 was used in the project thesis.

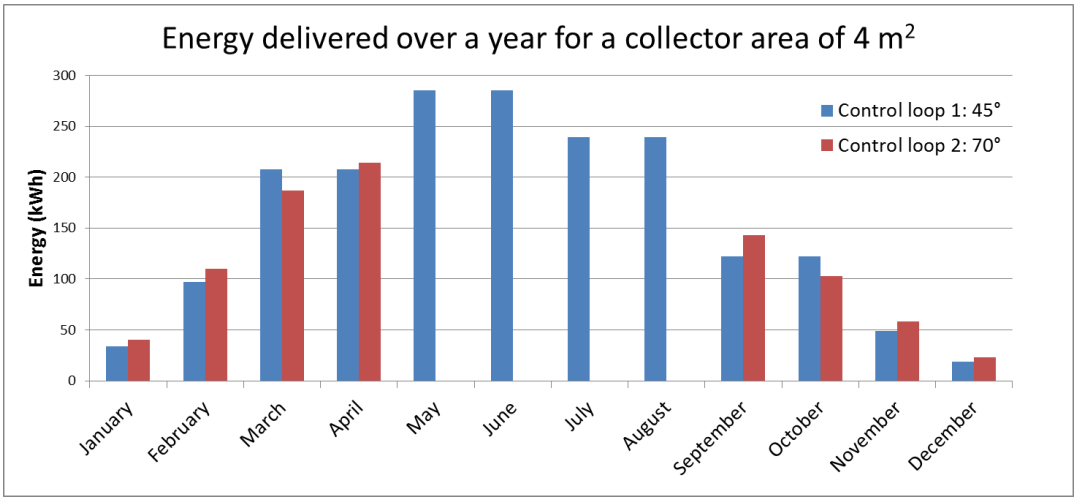

Figure 10.2: Energy delivered over a year for a solar collector area of 4 m^2 and an efficiency of 45 % for Control loop 1: 45 ° and Control loop 2: 70 °

The control loops are based on a collector area of 4 m^2 and an efficiency of 45 %. The efficiency is determined from Figure 4.9 in Chapter 4. The basis for the control loops is solar radiation data collected from PVGIS and the data is attached in Appendix 14. Control loop 1 is from the project thesis and is based on an incline of 45 ° and heat

injection throughout the year. Control loop 2 is based on an incline of 70 ° and has no heat injection during May, June, July and August. This is to avoid that an unrealistic amount of heat is being transferred to the ground construction in the summer. The effect of neglecting the heat injection during the summer months will be studied in the next section.

10.2 The old model

The old model from the project thesis is shown in Figure 3.4 in Chapter 3 and the building elements used is shown in Table 3.1. The boundary conditions towards the ground is a monthly temperature profile at 0.5 m depth for the floors in the outer zones and at 4 m depth for the concrete pillar representing the ground. The temperature profiles is shown in Figure 5.8 in Chapter 5. The simulations are done with normal thermal properties for the concrete. Heat is being injected at a depth of 0.5 m into the concrete pillar.

There has been done simulations with the old model for both Control loop 1 and Control loop 2.

10.2.1 The old model with Control loop 1: 45 °

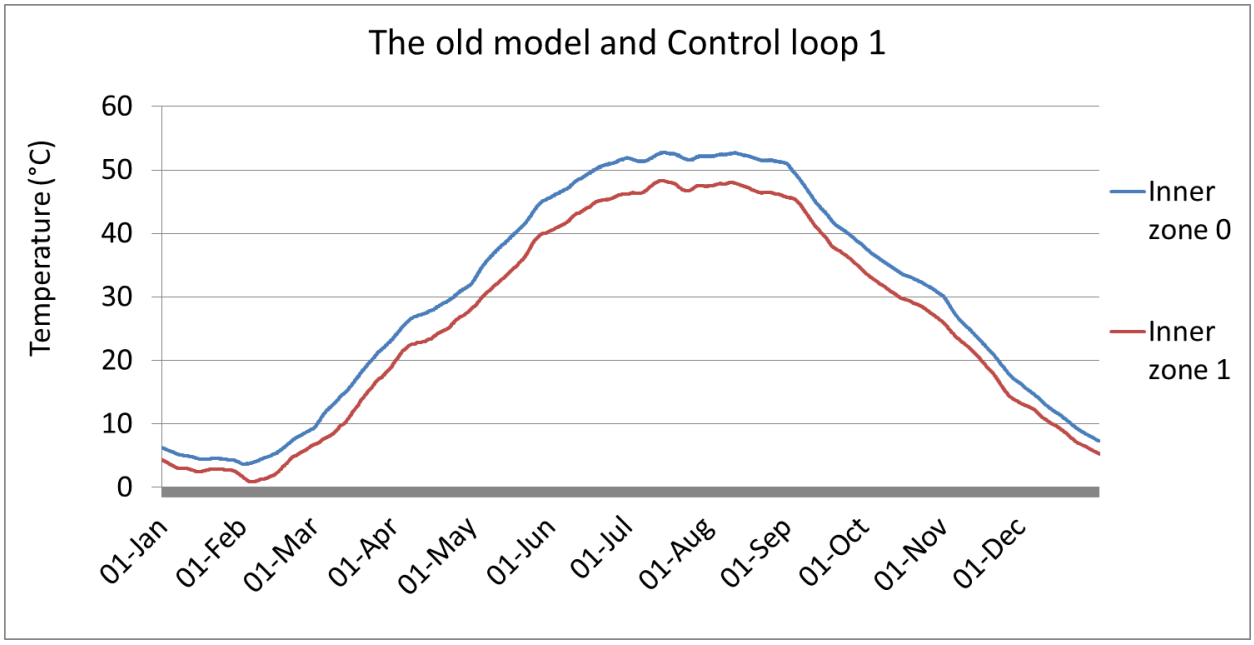

Figure 10.3: Temperature profiles for the inner zones with the old model and Control loop 1: 45 °

The temperatures for the inner zones for the old model with Control loop 1 is shown in Figure 10.3. Frost proof conditions are barely reached for the winter with a minimum temperature of 0.9 °C for the inner zone 1 at the 4th of February. A safety margin of 0.9

$°C$ is probably not sufficient to keep the sanitary installations frost proof. There will be temperature differences within the room, and they might be larger than 0.9 $°C$. In years with extremely cold weather frost proof conditions are probably not reached. Minimum and maximum temperatures and time of peak values for this case with the old model and Control loop 1 can be seen in Table 10.1.

	Minimum temperature and occurrence	**Maximum temperature and occurrence**
Inner zone 0	3.6 $°C$ at 01-Feb	52.8 $°C$ at 15-Jul
Inner zone 1	0.9 $°C$ at 04-Feb	48.3 $°C$ at 15-Jul

Table 10.1: Peak values for the old model with Control loop 1

10.2.2 The old model with Control loop 2: 70 °

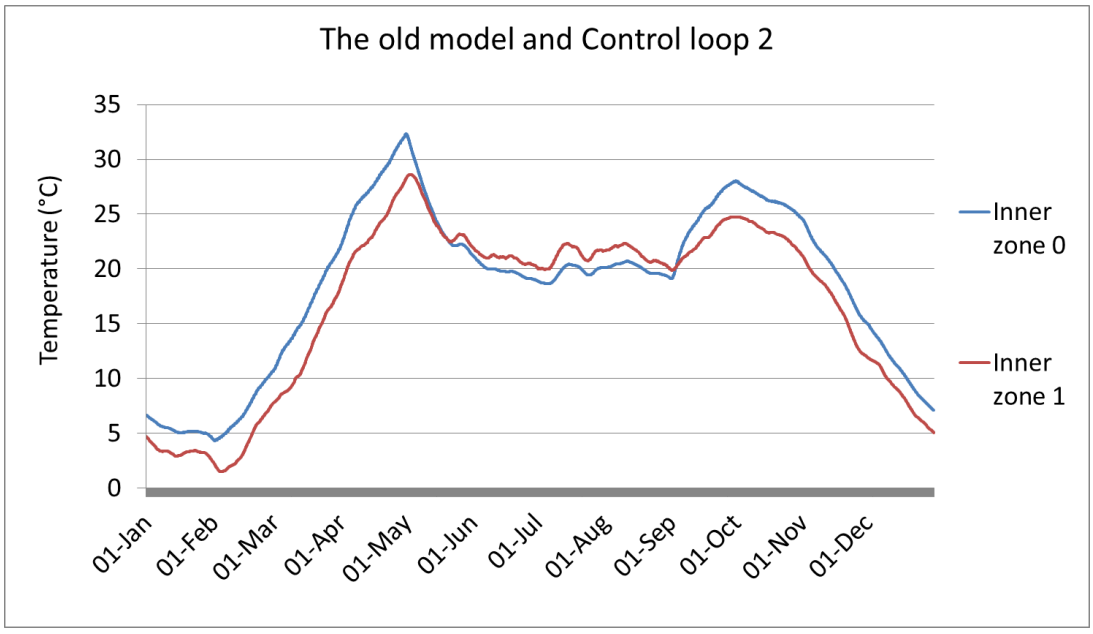

Figure 10.4: Temperature profiles for the inner zones with the old model and Control loop 2: 70 °

Figure 10.4 shows the temperature profiles with Control loop 2. The minimum temperature is 1.5 $°C$ for the inner zone 1 at the 4th of February. This is slightly higher than what was achieved with Control loop 1 as expected. More heat is being collected during the winter season. Since no heat injection occurs in the summer, lower maximum temperatures are achieved for this case. The maximum temperature for this case is 32.3 $°C$ for the inner zone 0 at 1st of May. The temperature in the inner zone 1 is higher than for the inner zone 0 in the summer months. This is because of the large south-facing window

on the 1st floor. Minimum and maximum temperatures and time of peak values for this case with the old model and Control loop 2 can be seen in Table 10.2.

	Minimum temperature and occurrence	**Maximum temperature and occurrence**
Inner zone 0	4.3 $°C$ at 01-Feb	32.3 $°C$ at 01-May
Inner zone 1	1.5 $°C$ at 04-Feb	28.3 $°C$ at 03-May

Table 10.2: Peak values for the old model with Control loop 2

10.2.3 Comparison of the different control loops

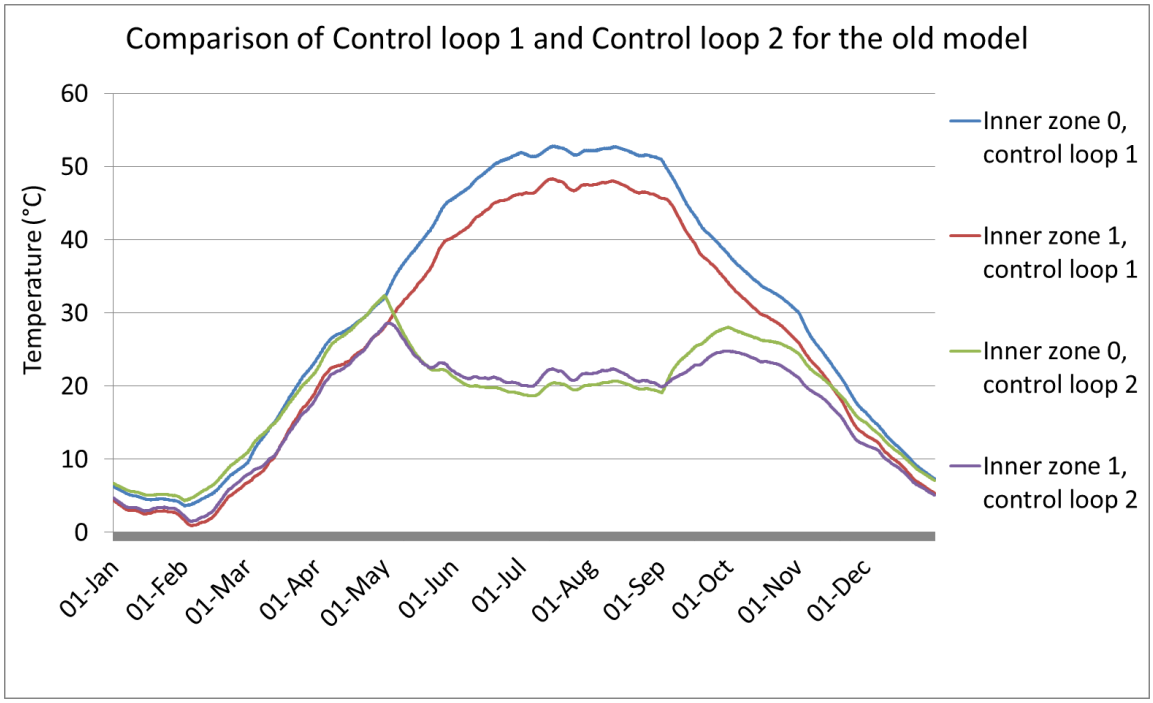

Figure 10.5: Temperature profiles for the inner zones with the old model with Control loop 1 and Control loop 2

Figure 10.5 shows the temperature profiles for the old model with both control loops. The inner zones are kept at higher temperatures with Control loop 2 in January until May. Since Control loop 2 has no heat injection during the summer months, the inner zones have a much lower temperatures during this period compared to the case with Control loop 1. In the fall and until New Years, the temperatures are lower with Control loop 2. Even if more heat is collected with Control loop 2 for this period, the storage over the summer with Control loop 1 gives higher temperatures. This is due to inert thermal mass.

Control loop 1 delivers 1909 kWh over the year, while Control loop 2 delivers 878 kWh which is only 46 % the amount of heat of what Control loop 1 does. Despite of less heat delivery, Control loop 2 is able to keep the inner zones at higher temperatures in the critical months. Control loop 2 gives more realistic results of the actual case, or at least more conservative results of the case where an actual solar heating system is installed. The heat during the summer might be used for hot water if the leisure home is being used. Control loop 2 is used in the further simulations.

10.3 The new model

A new model has been developed to achieve more accurate heat transfer calculations between the building and the ground. The new model is shown in Figure 9.1. An additional zone, a basement, has been constructed. The heat transfer is calculated quasi 3-dimensional between the basement and the surrounding ground. Since BASESIMP only calculates the heat transfer and does not take storage of heat into account, the storage is represented in the basement floor of the inner zone. The ground construction is built up by 5 layers of concrete with a total thickness of 1.5 m. Heat injection occurs at a depth of 0.3 m into this block.

Simulations for the new model will be carried out for the scenarios described in the list below:

- The new model without any heat injection
- The new model with heat injection by Control loop 2
- The new model with heat injection by Control loop 2 *and* with additional summer heat

10.3.1 Temperature profiles with no heat injection

A simulation of the new model without any heat injection was done. Figure 14.5 shows the temperature profiles for all the zones in the leisure home building and the ambient temperature.

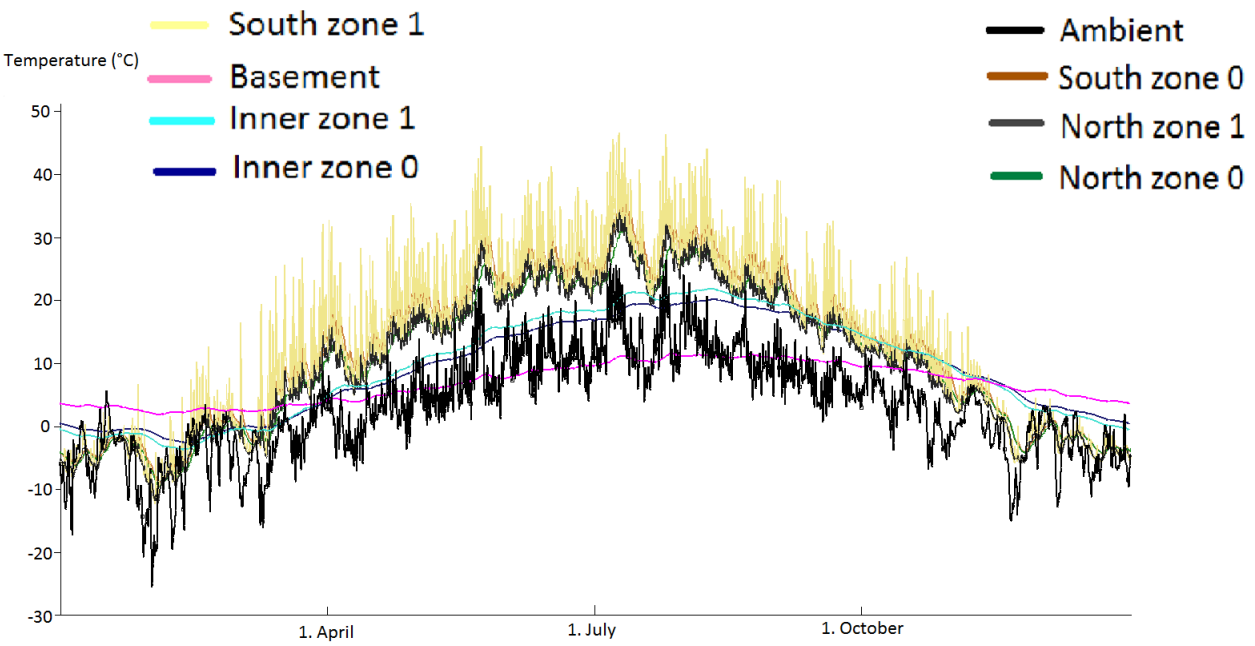

Figure 10.6: Temperature profiles for the new model for all zones with no heat injection

The most critical period over the year is shown in Figure 14.6.

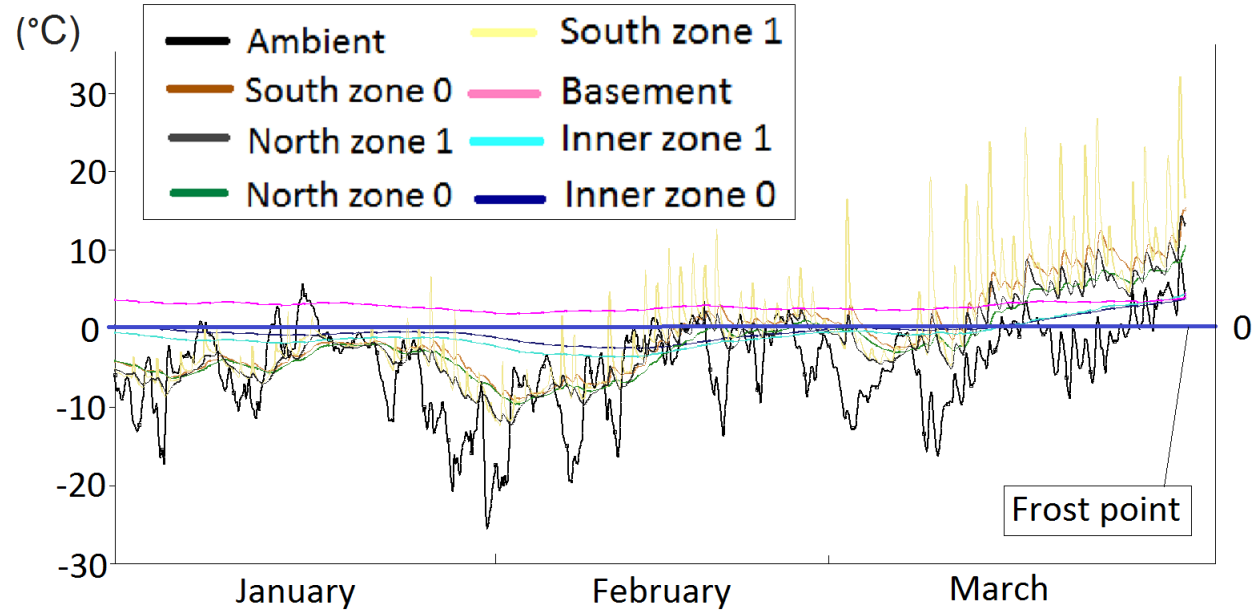

Figure 10.7: Temperature profiles for all the zones in the new model for the critical period January-March *without* any heat injection over the year

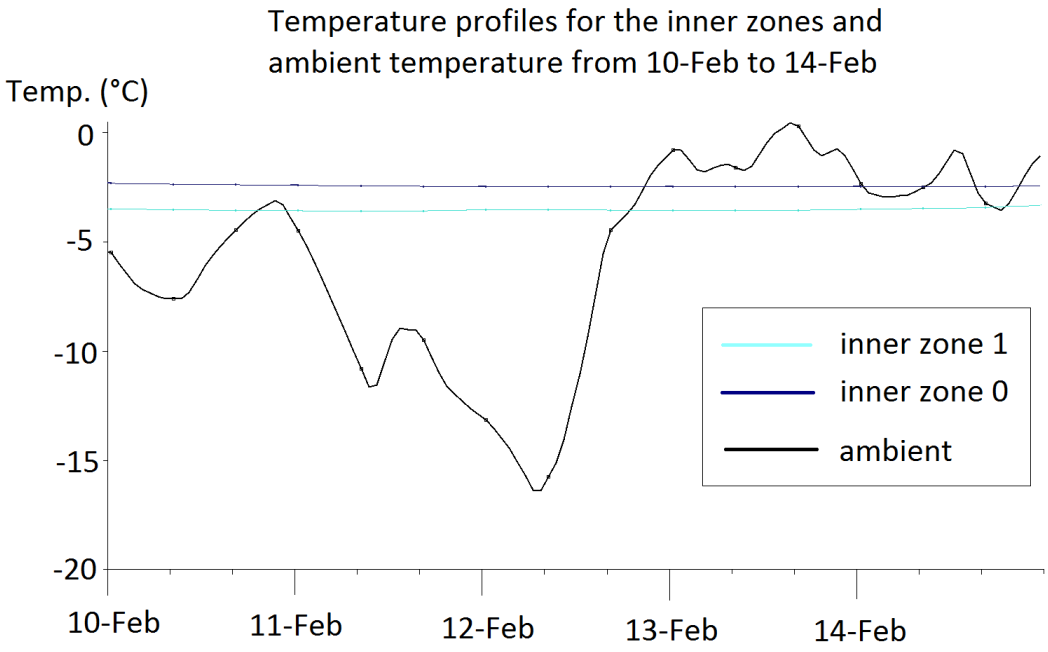

Figure 10.8: Temperature profiles for the inner zones in the new model for the period when the lowest temperatures in the inner zones occur - *without* any heat injection over the year

The inner zones are represented by the blue graphs in the figure above. It can be seen that frost proof conditions are not achieved, and there is a need for heating. The aim for this study is to develop a concept for a leisure home with frost proof sanitary installations without the use of primary energy sources. Therefore renewable energy such as solar heat should be used in the aim to keep the inner zones frost proof.

This simulation is done with the inner zone basement floor consisting of heavy mix concrete with normal thermal properties. The inner zones of the cabin are well-insulated and the walls have a U-value of 0.117 W/m^2K. The well-insulated inner zones appear to have a much more stable temperature profile than the other zones, and are thus less sensitive to sudden changes in ambient temperature than the outer zones. This shows that by isolating the sanitary installations in a well-insulated internal zone the risk of frost within these zones is significantly reduced. As mentioned in Chapter 2, SINTEF recommends a minimum temperature of 10 $°C$ inside leisure homes to assure that frost damages are avoided. This is a general recommendation for standard insulated leisure homes. For this case where the sanitary installations are placed in a well-insulated inner zone the safety margin can probably be set lower than $\Delta T = 10\ °C$ as SINTEF recommends. Figure 14.5, Figure 14.6 and Figure 14.7 are also attached in Appendix 14.

The highest temperatures occur on the 1st floor in the south zone for most of the year. This is due to passive solar heating through the window. Minimum and maximum temperatures and time of peak values for this case with the new model and no heat injection can be seen in Table 10.3.

	Minimum temperature and occurrence	Maximum temperature and occurrence
Inner zone 0	-2.5 $^{\circ}C$ at 13-Feb	20.2 $^{\circ}C$ at 11-Aug
Inner zone 1	-3.6 $^{\circ}C$ at 11-Feb	21.9 $^{\circ}C$ at 10-Aug
South zone 0	-9.1 $^{\circ}C$ at 03-Feb	35.6 $^{\circ}C$ at 12-Jul
South zone 1	-12.4 $^{\circ}C$ at 02-Feb	46.6 $^{\circ}C$ at 10-Jul
North zone 0	-9.7 $^{\circ}C$ at 03-Feb	31.5 $^{\circ}C$ at 12-Jul
North zone 1	-12.2 $^{\circ}C$ at 03-Feb	33.9 $^{\circ}C$ at 10-Jul
Basement	1.9 $^{\circ}C$ at 03-Feb	11.6 $^{\circ}C$ at 28-Jul
Ambient	-25.5 $^{\circ}C$ at 01-Feb	26.4 $^{\circ}C$ at 26-Jul

Table 10.3: Peak values for the new model with no heat injection

10.3.2 New model with Control loop 2 and *with* heat injection during the summer months

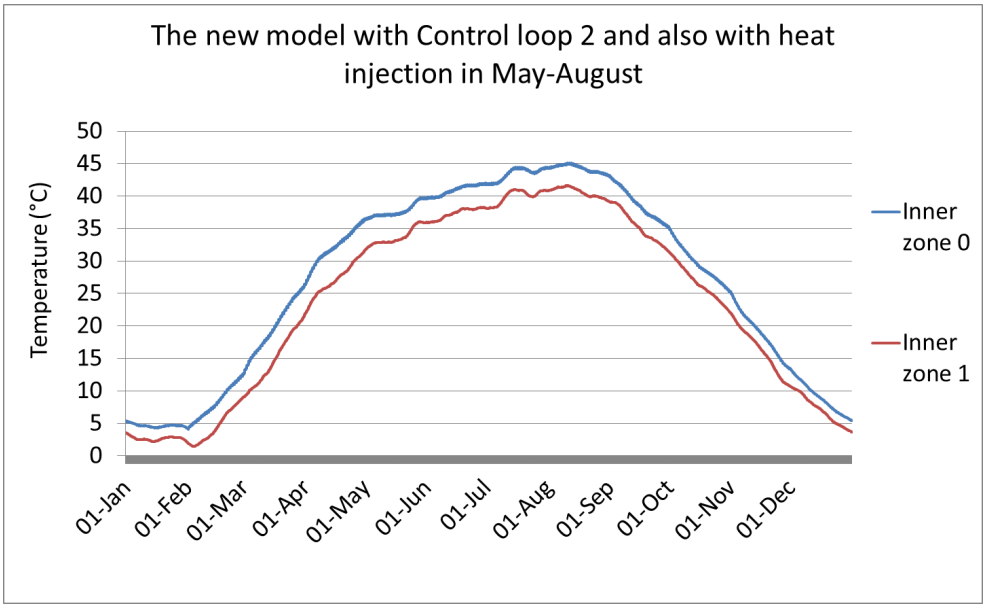

Figure 10.9: Temperature profiles for the new model with Control loop 2 and heat injection during the summer months May-August

The effect of neglecting the summer heat in Control loop 2 is studied. Figure 10.9 shows the new model with Control loop 2 and also with heat injection during the summer months. The heat injection for May-August in this simulation was set to the solar radi-

ation available in August, which is 404 W for an incline of 70 °, efficiency of 45 % and a collector area of 4 m^2.

Table 10.4 shows the peak values for this results *with* summer heat.

	Minimum temperature and occurrence	**Maximum temperature and occurrence**
Inner zone 0	4.1 °C at 01-Feb	45.1 °C at 01-May
Inner zone 1	1.5°C at 03-Feb	41.6 °C at 02-May

Table 10.4: Peak values for the new model with Control loop 2 and *with* heat injection during the summer months

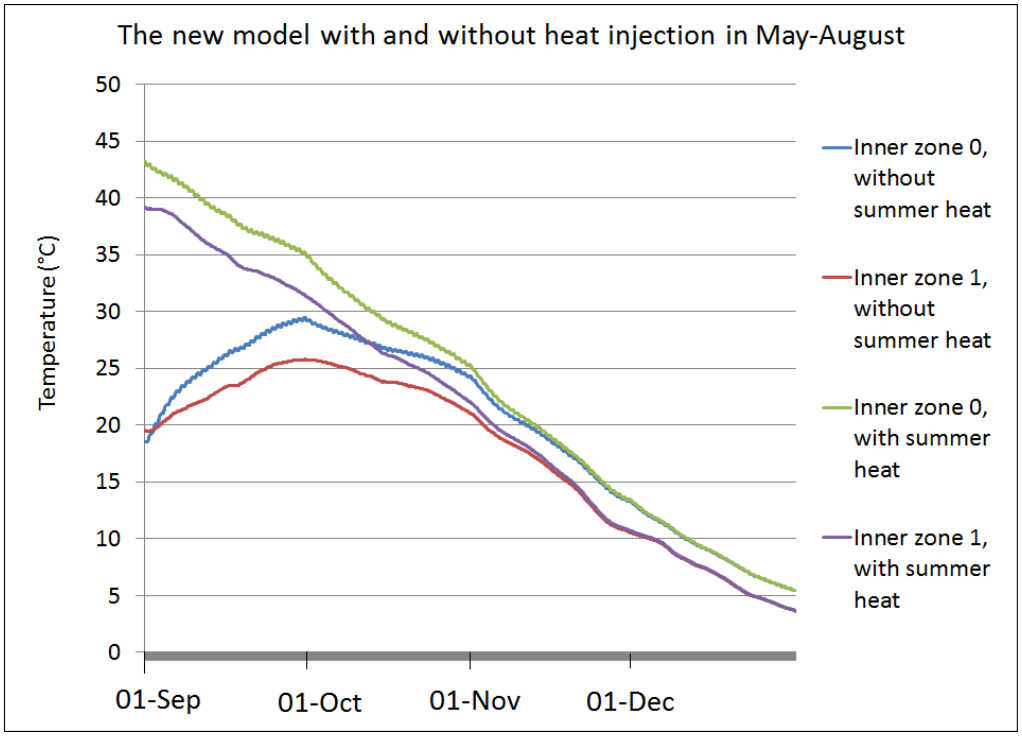

Figure 10.10: Temperature profiles for the fall for the new model *with* and *without* heat injection during the summer months May-August

Figure 10.10 shows the temperature profiles in the fall for the inner zones for both cases *with* and *without* heat injection during the summer months with Control loop 2. For the case with heat injection during the summer, the inner zones are kept at a higher temperature in the early fall. However, in the late fall and in the winter, there are almost no difference between the two cases. The simulations were done with normal thermal properties, the result might have been different if more thermal mass was available.

For this result, shown in Figure 10.10 and in Table 10.5 it can be seen that for this amount of thermal mass, the effect of summer heating is not of great importance.

	Minimum temperature and occurrence	**Maximum temperature and occurrence**
Inner zone 0 with summer heat	5.5 $^{\circ}C$ at 31-Dec	43.2 $^{\circ}C$ at 01-Sep
Inner zone 1 with summer heat	3.7 $^{\circ}C$ at 31-Dec	39.1 $^{\circ}C$ at 01-Sep
Inner zone 0 without summer heat	5.4 $^{\circ}C$ at 31-Dec	29.4 $^{\circ}C$ at 30-Sep
Inner zone 1 without summer heat	3.6 $^{\circ}C$ at 31-Dec	25.7 $^{\circ}C$ at 01-Oct

Table 10.5: Peak values for the new model with Control loop 2 *with* and *without* heat injection during the summer months for the period 1st of September until 31st of December

10.3.3 New model with Control loop 2

Simulations with Control loop 2 has been carried out and the result is shown in the figure below.

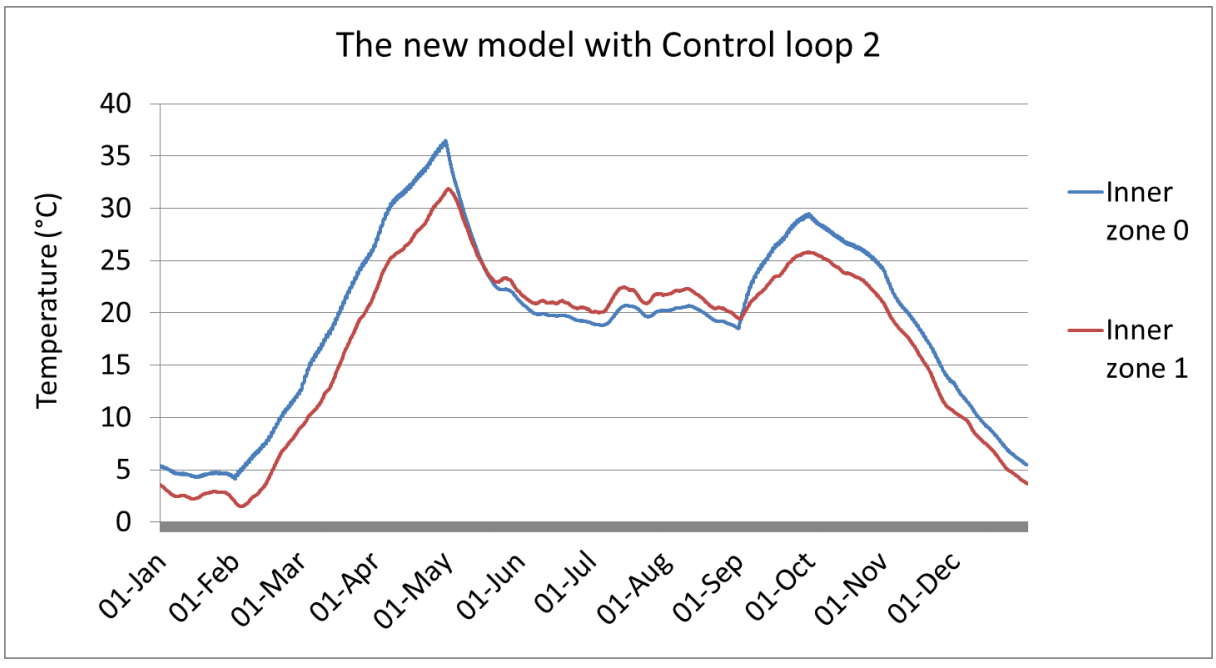

Figure 10.11: Temperature profiles for the new model with Control loop 2

The minimum temperature is 1.5 $°C$ and occurs in inner zone 1 at 3rd of February for this simulation. Inner zone 1 experiences a higher temperature than inner zone 0 in the summer months. This is probably because of passive solar heat gained from the large south-facing window in the same floor. Minimum and maximum temperatures and time of peak values for this case with the new model and Control loop 2 can be seen in Table 10.6.

	Minimum temperature and occurrence	**Maximum temperature and occurrence**
Inner zone 0	4.1 $°C$ at 01-Feb	36.1 $°C$ at 01-May
Inner zone 1	1.5 $°C$ at 03-Feb	31.9 $°C$ at 02-May

Table 10.6: Peak values for the new model with Control loop 2

10.3.4 Comparison of the old and the new model with Control loop 2

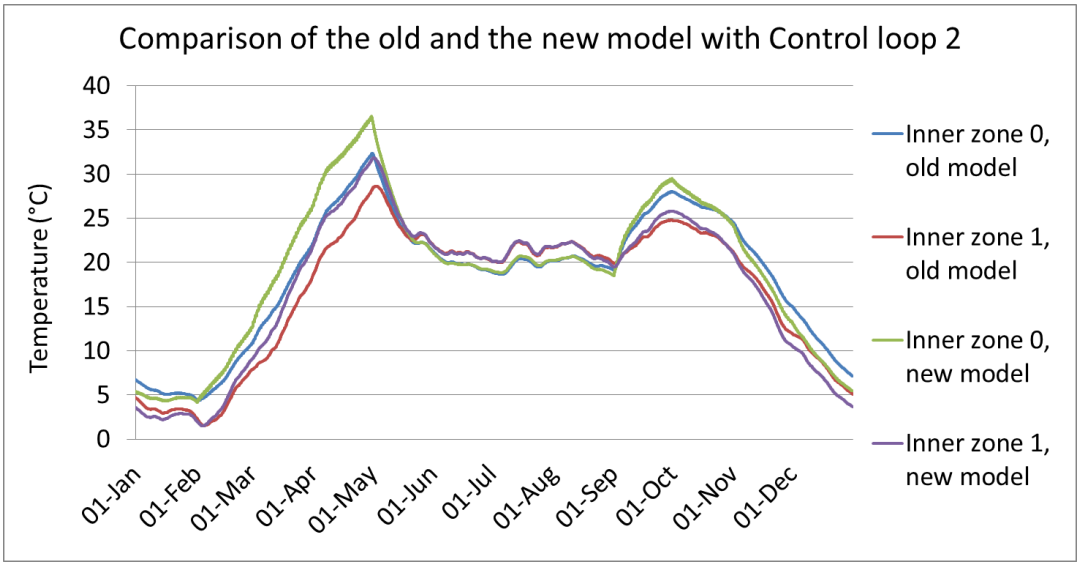

Figure 10.12: Temperature profiles for the inner zones for the old and the new model with Control loop 2

The results are surprisingly similar, considering that the ground construction and the boundary conditions for the two cases are quite different. The two models obtain the same minimum temperature of 1.5 $°C$ in the inner zone 1 in February, and the maximum temperature only differs by 3.8 $°C$ for the inner zone 0 in May.

In January the temperature for the new model is lower than for the old model. A reason for this might be that the old model has a larger thermal mass, and is able to store more

heat in the fall than the new model and also that heat is emitted from the storage. Little heat is injected in January, as there is only a small amount of solar radiation available. From February to May the temperatures are higher for the new model than for the old one. This is probably because more solar radiation is available, and the heat injection for the new model occurs at 0.3 m depth, while for the old model it occurs at 0.5 m depth. Heat is more easily transferred to the inner zones for the new model because of the depth of heat injection and the amount of thermal mass. In the summer months, when no heat injection occurs, the temperatures are almost the same for both models. From September to October the temperature is higher for the new model than for the old model, but changes back again and the temperature is lower until New Years for the new model. This is probably for the same reasons as in January, the storage capacity and the depth of heat injection together with available solar radiation.

The new model with Control loop 2 is further used, as this gives a more realistic view of the real case.

10.4 Thermal mass

The thermal storage in the ground is represented in the basement floor of the inner zone. Several simulations have been carried out with different thermal properties for the concrete floor. The effect of available thermal mass have been studied by changing the thermal properties to account for a larger storage volume. The thermal properties for the different cases are shown in Table 9.3 in Chapter 9. The area under the outer zones of the basement is not represented in the ground construction. The area is taken into account by multiplying the thermal properties with different factors.

The heat from the control loop is injected at a depth of 0.3 m. Figure 10.11, Figure 10.13, Figure 10.14 and Figure 10.15 show the temperature profiles with the thermal properties for Case 1, 2, 3 and 4 respectively. The figures illustrate the effect of changing the properties of the thermal mass under the leisure home. It can be seen that by increasing the density and the specific heat capacity of the thermal mass, i.e. increasing the volume of the storage, the possibility for heat storage increases.

10.4.1 Case 1

The results for the simulation for Case 1 is already presented in Figure 10.11 as the new model with Control loop 2. The ground construction has normal thermal properties for Case 1. Minimum and maximum temperatures and time of peak values for Case 1 can be seen in Table 10.6.

10.4.2 Case 2

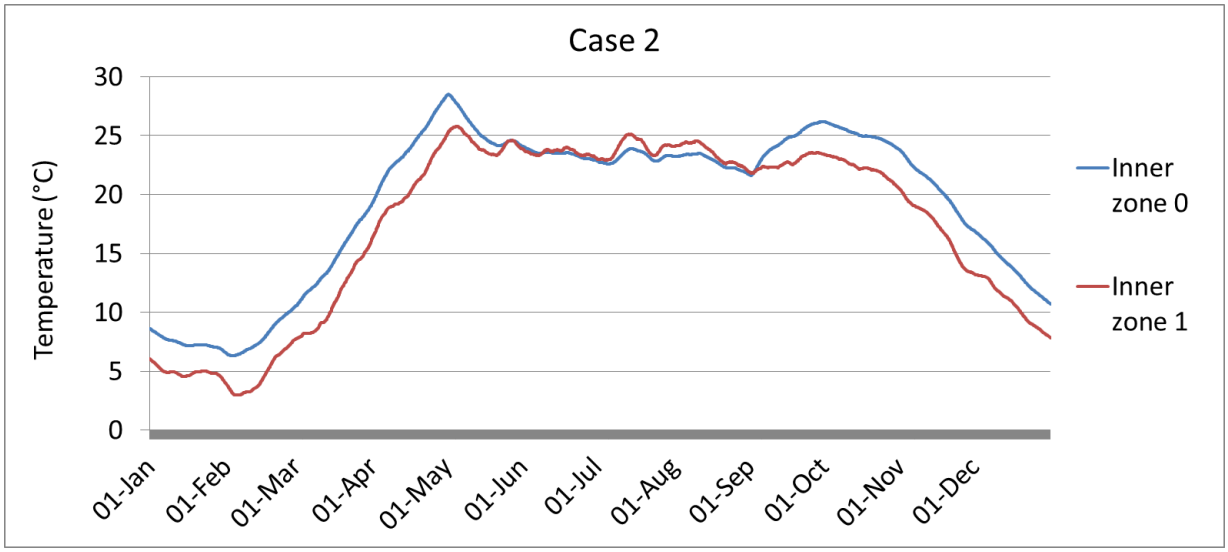

Figure 10.13: Temperature profiles for the inner zones for Case 2

Figure 10.13 shows the temperature profiles for Case 2, when the thermal properties is multiplied with a factor of 4. Case 2 maintain frost proof conditions for the inner zones and achieves slightly higher minimum temperatures than Case 1. For Case 2 the minimum temperature is 3 $°C$, occurring the 5th of February in inner zone 0. For Case 1 it is 1.5 $°C$, occurring the 3rd of February in the same zone. The maximum temperature for Case 2 is slightly less than for Case 1 and it occurs one day later. This indicates that the ground has a greater capacity to store heat in Case 2 than in Case 1 and the peak values has been shifted slightly ahead in time. Minimum and maximum temperatures and time of peak values for Case 2 can be seen in Table 10.7.

	Minimum temperature and occurrence	**Maximum temperature and occurrence**
Inner zone 0	6.3 $°C$ at 03-Feb	28.5 $°C$ at 02-May
Inner zone 1	3.0 $°C$ at 05-Feb	25.8 $°C$ at 05-May

Table 10.7: Peak values for Case 2

10.4.3 Case 3

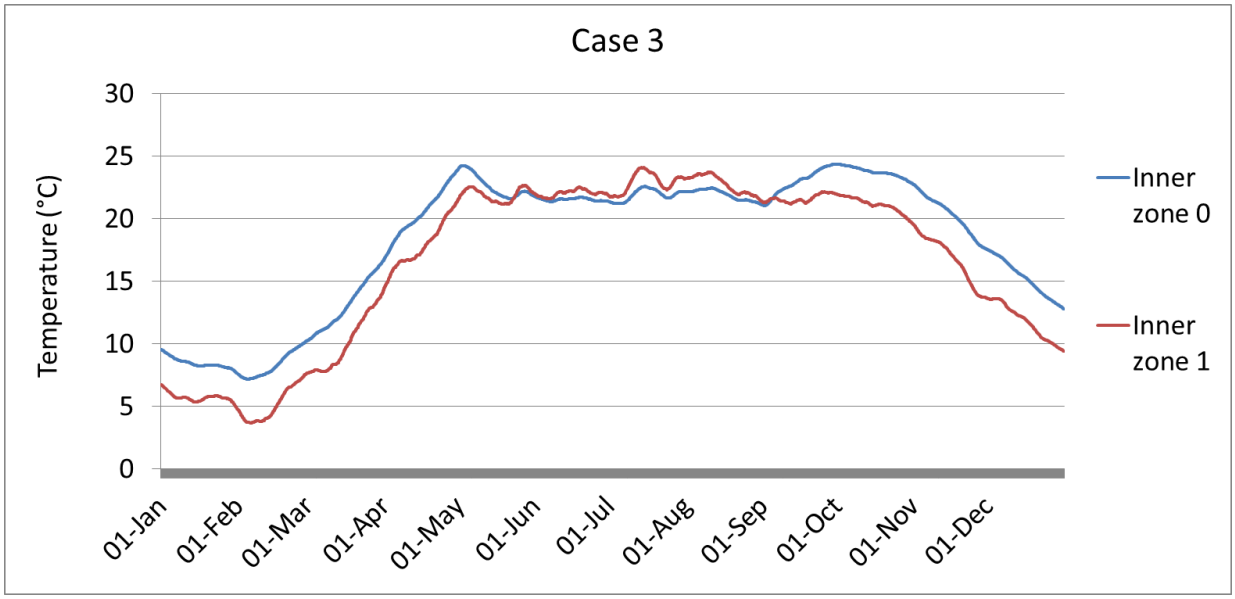

Figure 10.14: Temperature profiles for the inner zones for Case 3

The results for Case 3 is shown in Figure 10.14. In Case 3 the maximum temperatures continue to decrease, and the minimum temperatures to increase slightly. The maximum temperature for Case 3 is 24.4 $°C$ in inner zone 0 at 30th of September. The time of maximum temperature has shifted from May to September from Case 2 to Case 3. A reason for such a large shift is probably because there is no heat injection during the summer. Case 3 also has a higher storage capacity than Case 2 which also explains the delay of heat release. Minimum and maximum temperatures and time of peak values for Case 3 can be seen in Table 10.8.

	Minimum temperature and occurrence	**Maximum temperature and occurrence**
Inner zone 0	7.2 $°C$ at 04-Feb	24.4 $°C$ at 30-Sep
Inner zone 1	3.7 $°C$ at 06-Feb	24.1$°C$ at 15-Jul

Table 10.8: Peak values for Case 3

10.4.4 Case 4

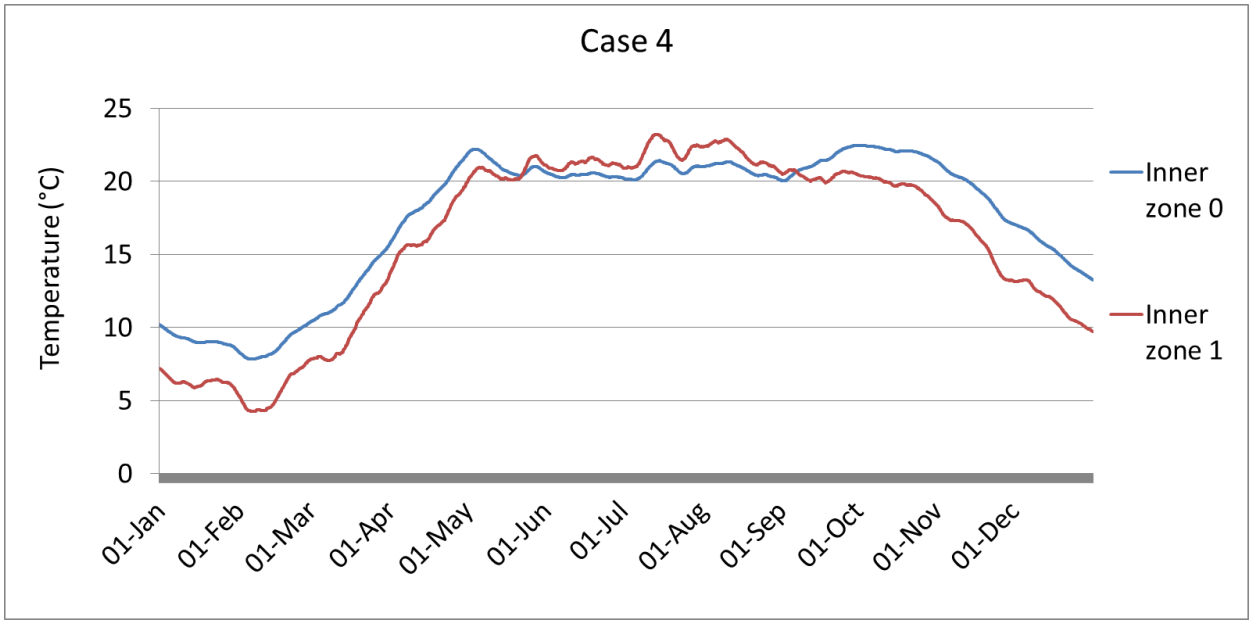

Figure 10.15: Temperature profiles for the inner zones for Case 4

The thermal mass with the highest density and the highest specific heat capacity represents Case 4, and the temperature profiles for this case are shown in Figure 10.15. The minimum temperature for this case is 4.2 $°C$ in the inner zone 1 at the 6th of February. The minimum temperature does not meet the recommendations from SINTEF, but a safety margin of 4.2 $°C$ is achieved. For a well-insulated inner zone this safety margin might still be acceptable.

It is important to note here that the number of start-up days used in the simulation is 100. If the number of start-up days were several years, the minimum temperature would most likely be higher. The ground would then have been heated up several years in advance and reached more stable conditions. The starting temperature and the final temperature in the figure should be almost the same as they represent the last hour of the last day in December and the first hour of the first day in January. This is based on the fact that the simulations have been carried out with the same climate data for a longer period of time. This emphasises the importance of start-up days.

The maximum temperatures in both zones are lower than in the previous cases. The maximum temperature is 23.2 $°C$ in the inner zone 1 at 14th of July. For the other cases, the maximum temperature has occurred in the inner zone 0. When the heat storage has a larger volume, the release of heat is more inert. Therefore, in Case 4 where the thermal properties are multiplied with 10, the maximum temperature occurs in inner zone 1 due to passive solar heat in the 1st floor. Minimum and maximum temperatures and time of peak values for Case 4 can be seen in Table 10.9.

	Minimum temperature and occurrence	Maximum temperature and occurrence
Inner zone 0	7.8 $°C$ at 06-Feb	22.5 $°C$ at 30-Sep
Inner zone 1	4.2 $°C$ at 06-Feb	23.2 $°C$ at 14-Jul

Table 10.9: Peak values for Case 4

10.4.5 Comparison of Case 1 and Case 4

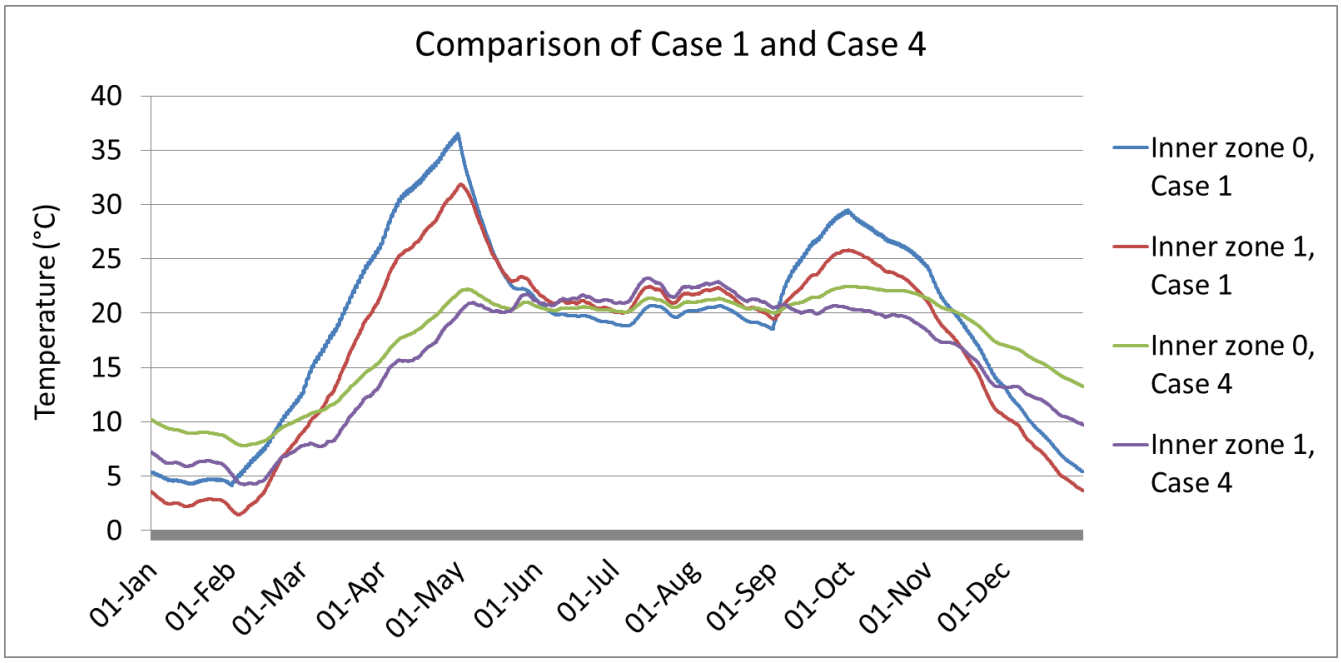

Figure 10.16: Temperature profiles for the inner zones for Case 1 and Case 4

Figure 10.16 shows the temperature profiles for both Case 1 with normal thermal properties and for Case 4 with the thermal properties multiplied with a factor of 10. The minimum temperature for both cases occurs in the inner zone 1. The temperature for Case 1 is 1.5 $°C$ at the 3rd of February and for Case 4 it is 4.2 $°C$ at the 6th of February. Figure 10.16 demonstrates the effect of thermal inertia from Case 1 to Case 4.

10.5 Depth of heat injection

Another simulation was performed where the heat was injected at a depth of 0.75 m instead of 0.3 m as for the cases above. The reason for this was to investigate the effect of injecting heat at a greater depth. The results of this simulation can be seen in Figure 10.17.

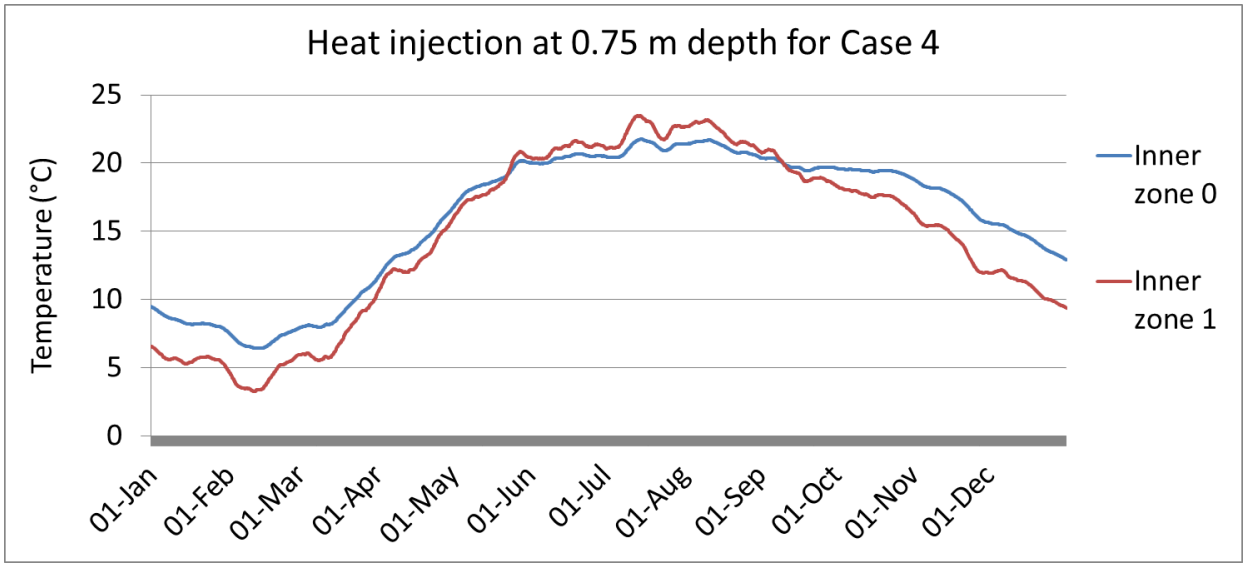

Figure 10.17: Temperature profiles with heat injection at 0.75 m for Case 4

Figure 10.17 and Table 10.10 shows that the temperatures are lower in this case than for the case with heat injection at 0.3 m. The heat transfer resistance is now greater upwards, resulting in lower temperatures. The main focus of this study is raising the minimum temperatures of the inner zones, therefore injecting heat at 0.3 m is a better alternative. Minimum and maximum temperatures and time of peak values for Case 4 with heat injection at a depth of 0.75 m can be seen in Table 10.10

	Minimum temperature and occurrence	**Maximum temperature and occurrence**
Inner zone 0	6.4 $°C$ at 13-Feb	21.8 $°C$ at 30-Sep
Inner zone 1	3.3 $°C$ at 11-Feb	23.5 $°C$ at 14-Jul

Table 10.10: Peak values for Case 4 with heat injection at 0.75 m depth

10.6 Solar collector area

A simulation was carried out using solar radiation data in the control loop for a collector area of 6 m^2 together with Case 4 in order to investigate the impact it would have on the temperature profiles in the inner zones. The result is shown in Figure 10.18.

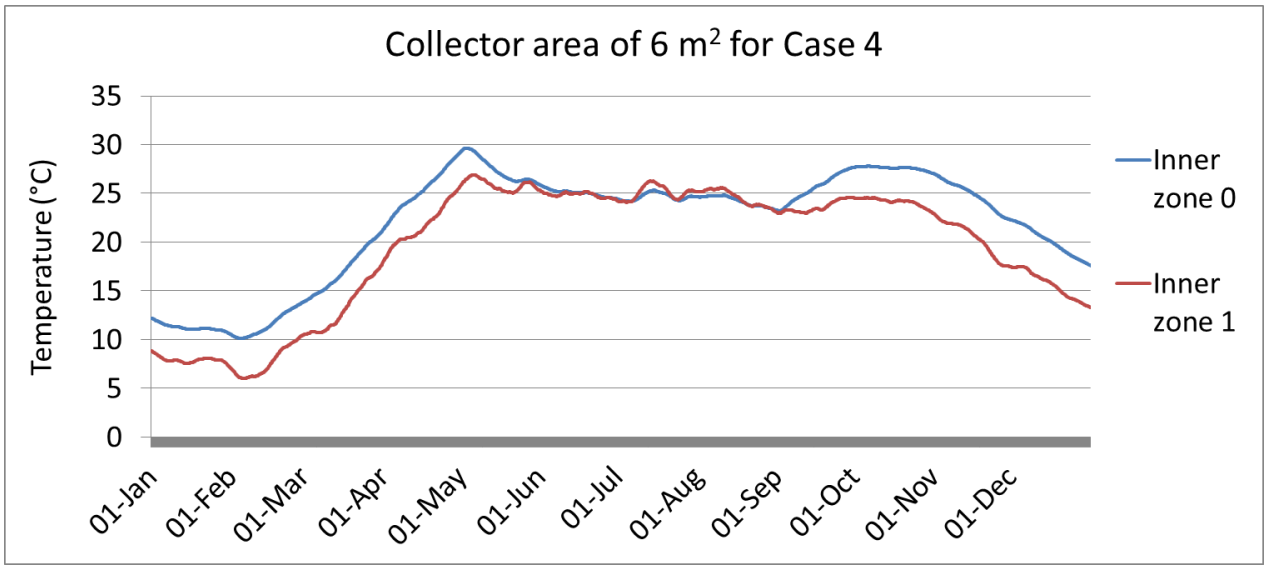

Figure 10.18: Temperature profiles with a collector area of 6 m^2 for Case 4

As expected the minimum temperatures in the internal zones turned out to be higher when using a larger collector area. To achieve frost proof conditions for the inner zones with a greater safety margin, a larger collector area may be installed. Minimum and maximum temperatures and time of peak values for Case 4 with a collector area of 6 m^2 can be seen in Table 10.11.

	Minimum temperature and occurrence	**Maximum temperature and occurrence**
Inner zone 0	10.4 °C at 13-Feb	29.6 °C at 30-Sep
Inner zone 1	6.0 °C at 11-Feb	26.9 °C at 14-Jul

Table 10.11: Peak values for Case 4 with a collector area of 6 m^2

10.7 Heat transfer

The simulations for Case 1 and Case 4 with Control loop 2, based on a collector area of 4 m^2, and heat injection at 0.3 m depth has been studied further. The solar heat delivered by Control loop 2 is shown in Figure 10.2. The heat transfer is calculated 1-dimensionally through the constructions in ESP-r.

Temperatures at the heat injection point, and the inside and outside face of the basement floor of the inner zone has been collected to study the direction of the heat transfer throughout the year. Further has the temperature for the basement floors inside and outside face of south and north zone been collected. This is of interest when examining how much of the heat transferred from the heat injection point to the basement zone have been transferred further to the outer basement zones. Values for the thermal conductivity for the different materials in the constructions has been collected from the material database in ESP-r. The heat transfer through the constructions are calculated by the following equation:

$$Q = \frac{k}{x} A \Delta T \tag{10.1}$$

where k is the thermal conductivity of the material used in the constructions, x is the material thickness and A is the surface area of the construction.

10.7.1 Heat transfer in the basement floor of the inner zone

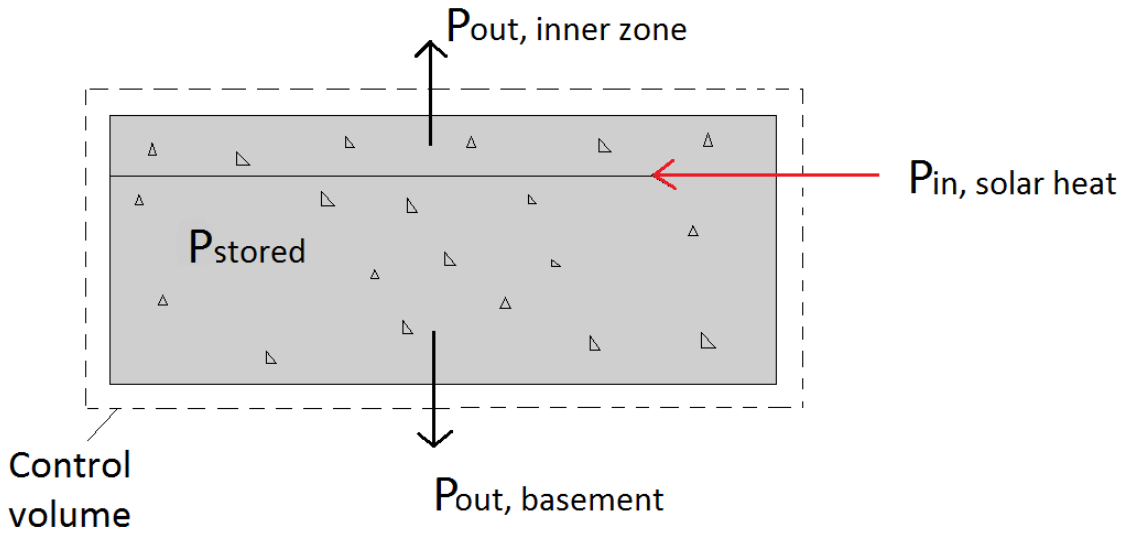

Figure 10.19: Heat transfer in the basement floor of inner zone

Figure 10.19 shows the heat transfer for the inner basement floor. Solar heat is being injected at 0.3 m depth into the construction. The heat will either be transferred to the

inner zone or the basement zone, or it will be stored within the construction.

The amount of stored heat is calculated based on the following equation:

$$P_{stored} = P_{in} - P_{out,innerzone} - P_{out,basement} \tag{10.2}$$

The storage capacity of the ground construction (the inner basement floor) is studied through Case 1 with normal thermal properties and Case 4 where the thermal properties have been multiplied with a factor of 10. The power is summarized for each month and the sum of P_{stored}, $P_{out,basement}$ and $P_{out,innerzone}$ is the $P_{in,solarheat}$.

Heat transfer in the basement floor of the inner zone for Case 1

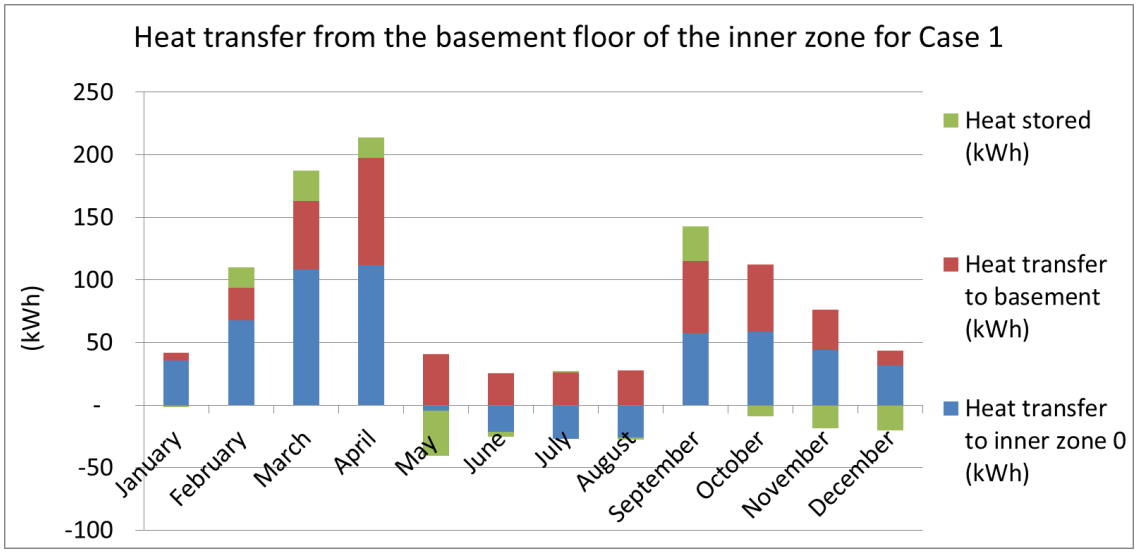

Figure 10.20: Heat transfer from basement floor of the inner zone for Case 1

Figure 10.20 shows the distribution of the power injected to the basement floor for Case 1. For the periods when heat injection occurs, the heat transfer to the inner zone is always larger than the heat transfer to the basement. The distance from the heat injection point to the inner zone is shorter than the distance from the heat injection point to the basement, hence there is a larger resistance to heat downwards to the basement. This is beneficial since it is the inner zone that is to be heated.

The heat storage is negative in January, but increases in the spring time when there is more solar radiation available. It is also negative when no heat injection occurs, except in the month of July where 1 kWh is stored. Heat is also stored in September, but when less solar heat is available in the late fall, the heat storage is negative.

The power delivered to the different zones, the power delivered by the control loop and the storage in the construction is shown in Table 10.12. These values are the basis of Figure 10.20.

	Solar heat injected by control loop *(kWh)*	**Heat transfer to inner zone 0** *(kWh)*	**Heat transfer to basement** *(kWh)*	**Heat stored** *(kWh)*
January	40.2	35.7	6.3	-1.7
February	109.9	67.9	25.6	16.4
March	187.5	108.5	54.6	24.3
April	213.8	111.9	85.5	16.4
May	-	-4.6	40.7	-36.1
June	-	-21.2	25.5	-4.2
July	-	-26.9	25.9	1.0
August	-	-25.9	27.5	-1.6
September	142.6	57.8	57.2	27.6
October	103.2	58.8	53.3	-8.9
November	57.8	44.2	31.9	-18.4
December	23.2	31.9	11.5	-20.1

Table 10.12: Heat transfer from basement floor in inner zone 0 for Case 1

Heat transfer in the basement floor of the inner zone for Case 4

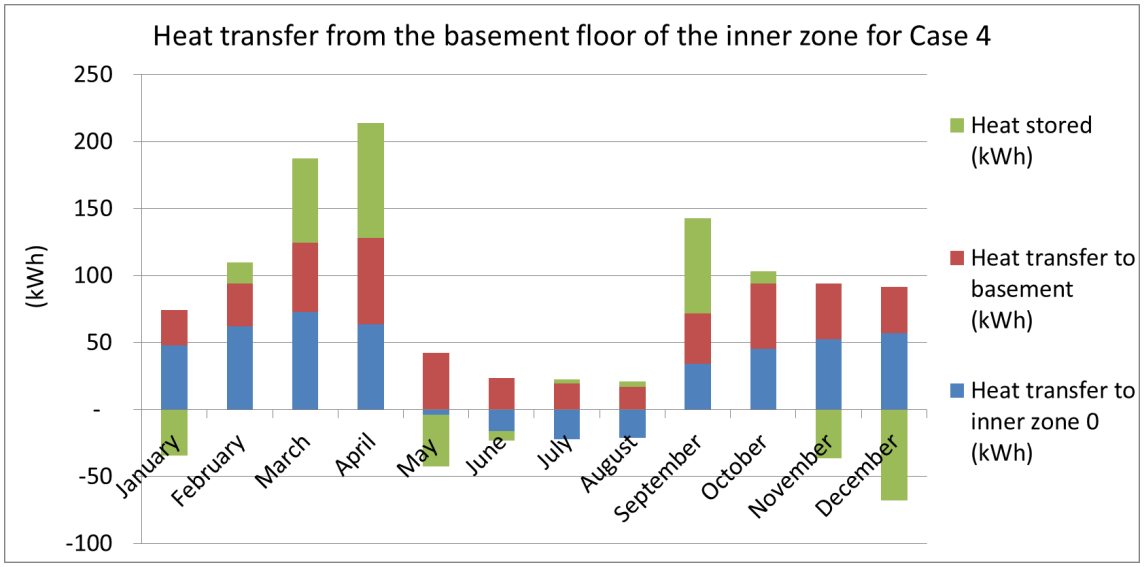

Figure 10.21: Heat transfer from basement floor of the inner zone for Case 4

Figure 10.21 shows the distribution of the power injected to the basement floor for Case 4. The heat storage has a bigger increase in the spring for Case 4 than for Case 1, as Case 1 releases more heat continuously. The ground construction in Case 4 has a larger storage capacity, hence it is more inert and less sensitive to sudden changes in temperature than the ground construction in Case 1. More heat is stored for Case 4.

The power delivered to the different zones, the power delivered by the control loop and the storage in the construction is shown in Table 10.13. These values are the basis of Figure 10.21.

	Solar heat injected by control loop *(kWh)*	**Heat transfer to inner zone 0** *(kWh)*	**Heat transfer to basement** *(kWh)*	**Heat stored** *(kWh)*
January	40.2	48.0	26.5	-34.2
February	109.9	61.8	32.2	15.9
March	187.5	72.7	51.9	63.0
April	213.8	63.7	64.4	85.7
May	-	-4.0	42.4	-38.5
June	-	-16.1	23.3	-7.3
July	-	-22.4	19.3	3.1
August	-	-21.1	17.0	4.1
September	142.6	34.1	37.4	71.1
October	103.2	45.3	48.9	9.0
November	57.8	52.5	41.5	-36.2
December	23.2	54.8	30.4	-62.0

Table 10.13: Heat transfer from basement floor in inner zone 0 for Case 4

10.7.2 Heat transfer in the basement zone

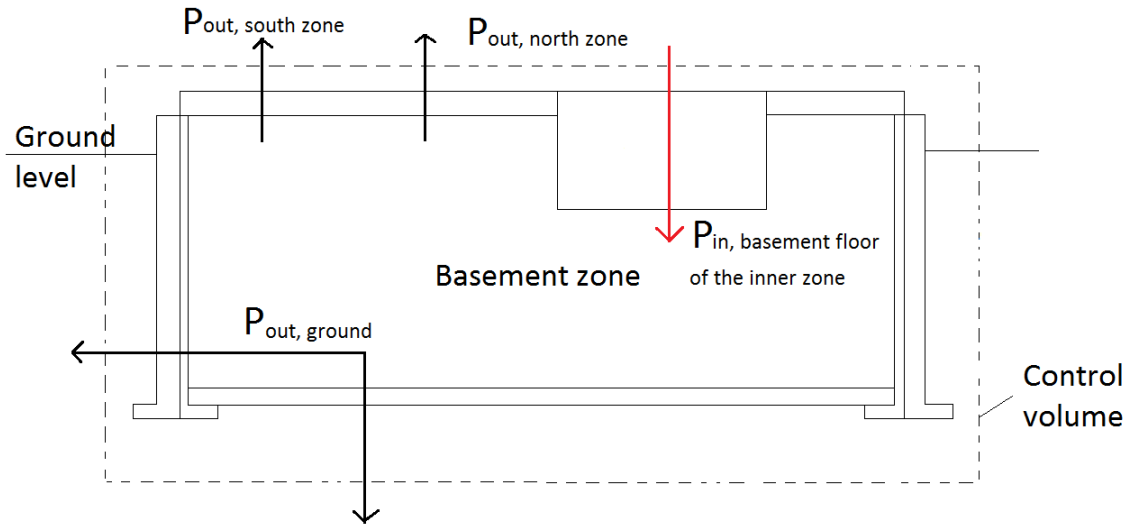

Figure 10.22: Heat transfer in the basement zone

Figure 10.22 shows the heat transfer for the basement zone. Heat is transferred from the control loop via the basement floor of the inner zone downwards to the basement zone. Further, this heat is transferred upwards to the outer zones or to the surrounding ground.

The heat transfer to the ground is calculated based on the following equation:

$$P_{out,ground} = P_{in,basementfloorof theinnerzone} - P_{out,northzone} - P_{out,southzone} \tag{10.3}$$

The heat transfer to the ground is studied for Case 1 and for Case 4. The power is summarized for each month and the sum of $P_{out,southzone}$, $P_{out,northzone}$ and $P_{out,ground}$ is the $P_{in,basementfloorof theinnerzone}$.

Heat transfer in the basement zone for Case 1

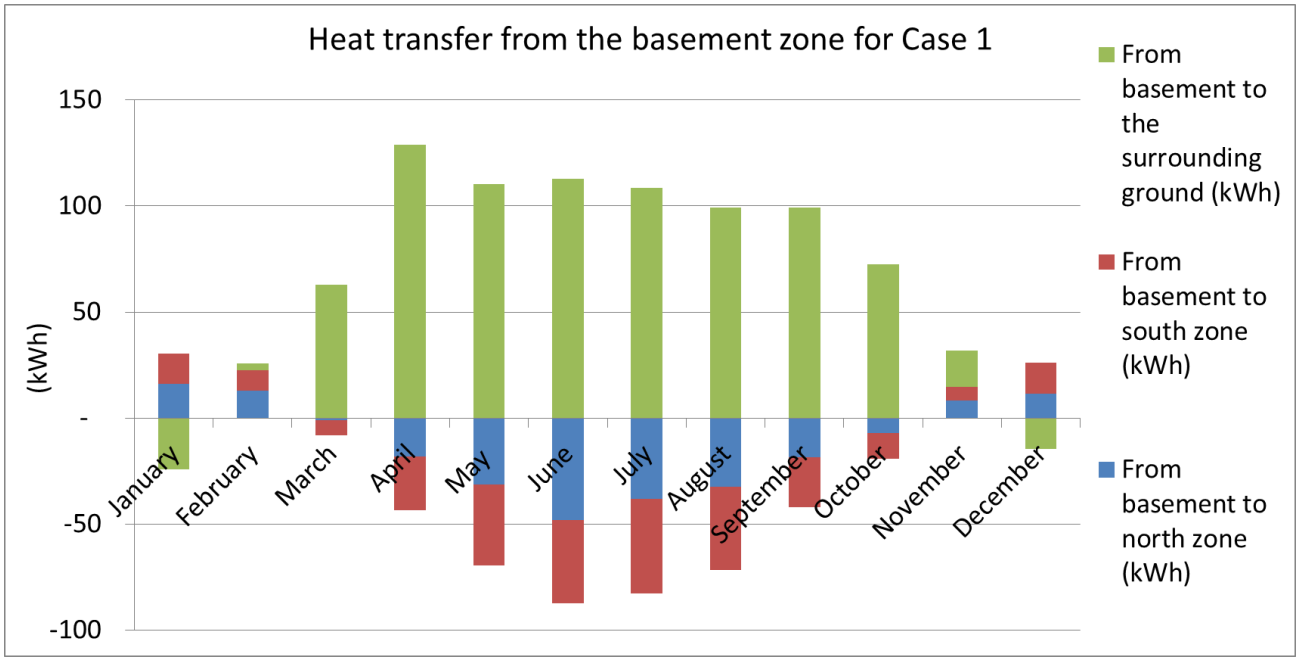

Figure 10.23: Heat transfer in the basement zone for Case 1

Figure 10.23 shows the heat transfer from the basement zone for Case 1. The heat transfer between the south zone and the basement are almost equal to the heat transfer between the north zone and the basement. North zone 0 receives a bit more heat from the basement than south zone 0. This is probably because north zone 0 has a slightly larger surface area. Another reason might be that south zone 0 receives more heat from south zone 1 than what north zone 0 does from north zone 1. There is a large window in south zone 1 and the floor separation is made of concrete. The temperatures in both south zones are probably a bit higher in the summer and a bit lower in the winter than for the north zones, however the differences are small. It seems reasonable that the heat transfer by conduction through the structure between the basement and the south zone and the north zone are alike. The heat transfer rate *from* the basement *to* the outer zones is negative most of the year.

Heat is lost from the basement to the ground for all periods, except for January and December. The basement has a rather stable temperature throughout the year compared to the rest of the zones. (REF en oversiktsfigur? Med alle temp for alle zoner for et valg tilfelle med heat inj). Only in the winter months is the temperature lower in the outer zones than in the basement, and the heat transfer rate is positive.

The power delivered to the different zones is shown in Table 10.14. These values are the basis of Figure 10.23.

	Heat transfer to basement *(kWh)*	**Heat transfer to north zone from basement** *(kWh)*	**Heat transfer to south zone from basement** *(kWh)*	**Heat transfer to the ground** *(kWh)*
January	6.3	16.1	14.3	-24.1
February	25.6	13.0	9.4	3.2
March	54.6	-0.9	-7.3	62.9
April	85.5	-18.2	-25.3	129.0
May	40.7	-31.3	-38.3	110.3
June	25.5	-48.2	-39.0	112.7
July	25.9	-38.1	-44.6	108.6
August	27.5	-32.4	-39.3	99.2
September	57.2	-18.3	-23.7	99.3
October	53.3	-7.2	-12.0	72.5
November	31.9	8.2	6.6	17.1
December	11.5	11.3	14.7	-14.6

Table 10.14: Heat transfer from basement zone for Case 1

Heat transfer in the basement zone for Case 4

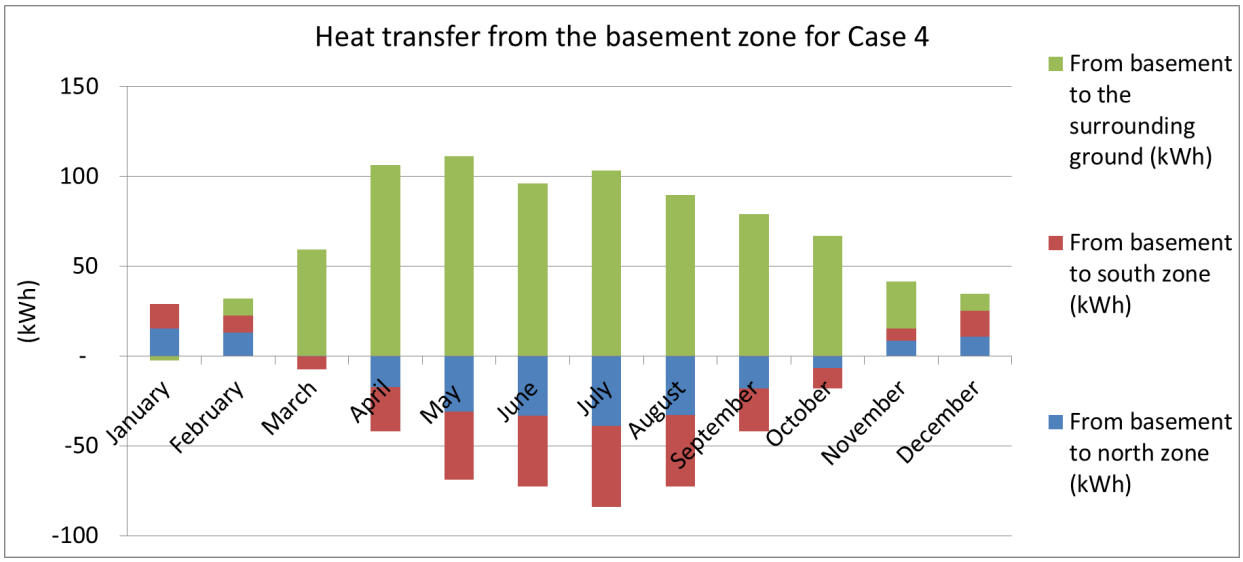

Figure 10.24: Heat transfer in the basement zone for Case 4

The same tendency regarding south zone and north zone is seen in Figure 10.24 for Case 4 as for Case 1. More heat is transferred to the basement in the winter months for Case 4 than for Case 1, hence is the heat loss to the ground greater in the winter for Case 4 than for Case 1. The opposite happens in the summer months, when Case 1 experience more heat loss to the ground due to a grater heat transfer to the basement zone.

The power delivered to the different zones is shown in Table 10.15. These values are the basis of Figure 10.24.

	Heat transfer to basement *(kWh)*	**Heat transfer to north zone from basement** *(kWh)*	**Heat transfer to south zone from basement** *(kWh)*	**Heat transfer to the ground** *(kWh)*
January	26.5	15.3	13.6	-2.4
February	32.2	13.0	9.5	9.7
March	51.9	-0.3	-7.1	59.3
April	64.4	-17.2	-24.9	106.5
May	42.4	-30.7	-38.0	111.2
June	23.3	-33.3	-39.4	96.1
July	19.3	-38.8	-45.2	103.2
August	17.0	-32.9	-39.7	89.5
September	37.4	-18.1	-23.6	79.1
October	48.9	-6.5	-11.5	66.8
November	41.5	8.6	6.9	26.0
December	30.4	10.7	14.6	5.1

Table 10.15: Heat transfer from basement zone for Case 4

Heat transfer for the model without heat injection

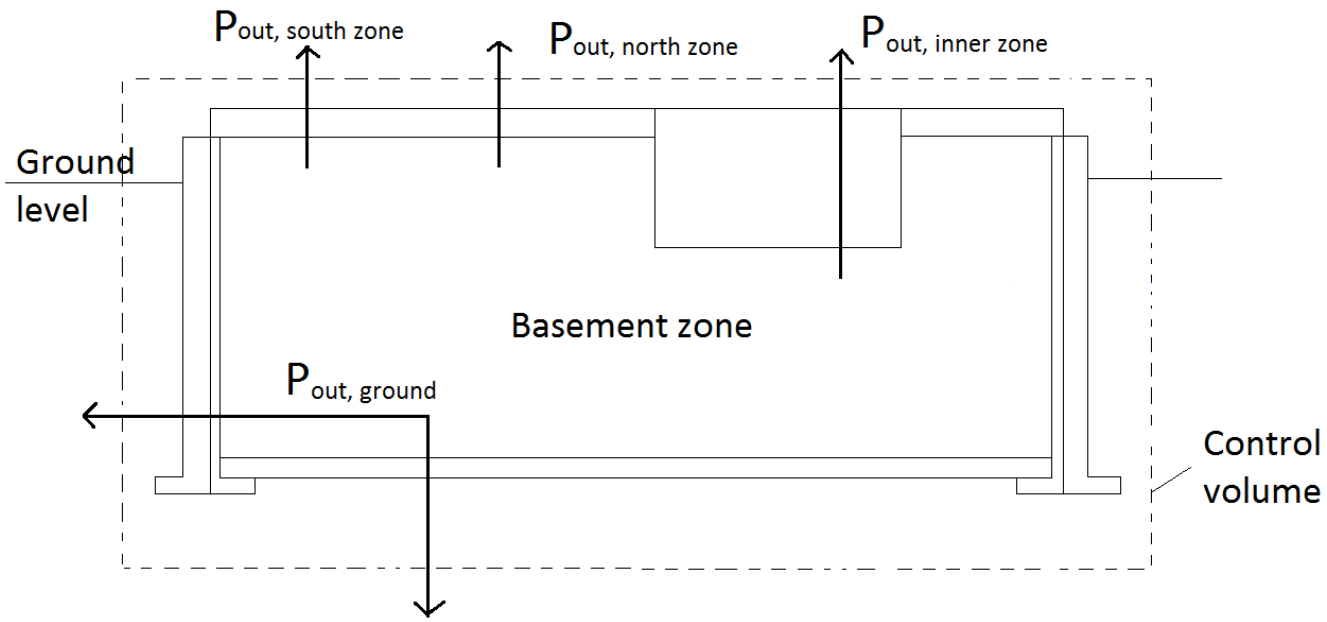

Figure 10.25: Heat transfer in the basement for the model without heat injection

Figure 10.25 shows the heat transfer for the basement zone. There is no solar heat being injected into the basement floor of the inner zone.

The heat transfer between the basement zone and the ground is calculated based on the following equation:

$$-P_{out,ground} = P_{out,northzone} + P_{out,southzone} + P_{out,innerzone} \tag{10.4}$$

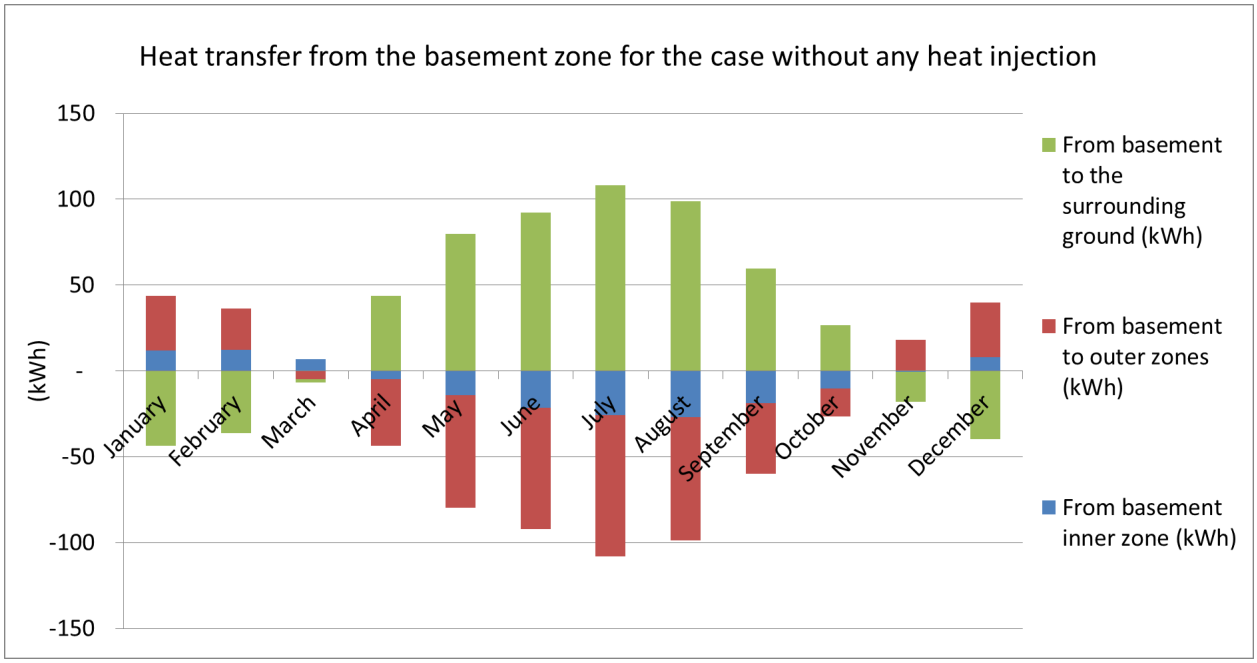

Figure 10.26: Heat transfer from the basement for the case without any heat injection

Figure 10.26 shows the transport of heat in the basement zone for a case where no heat is being injected to the basement floor of the inner zone. In the winter when the ambient temperature is low, hence the dry bulb temperature of the zones in the building is low, the only source of heat is the ground. As seen in the figure above is heat collected from the ground in the winter months. In the summer when the ambient temperature rises and solar radiation is available, the temperature increases in the zones of the building and heat is lost to the ground.

The power delivered to the different zones is shown in Table 10.16. These values are the basis of Figure 10.26.

	Heat transfer to inner zone *(kWh)*	**Heat transfer to outer zones** *(kWh)*	**Heat transfer to the ground** *(kWh)*
January	11.7	31.8	-43.5
February	12.2	24.1	-36.3
March	6.9	-4.8	-2.1
April	-4.7	-38.8	43.5
May	-14.1	-65.5	79.6
June	-21.6	-70.6	92.2
July	-25.7	-82.3	108.0
August	-27.1	-71.6	98.7
September	-19.0	-40.8	59.8
October	-10.3	-16.3	26.6
November	-0.4	17.9	-17.6
December	8.1	31.8	-39.9

Table 10.16: Heat transfer from basement zone for the case without any heat injection

10.7.3 Heat storage

The heat storage has been calculated using two methods.

The first method, Method 1 is already explained earlier in this chapter. Figure 10.19, Equation 10.1 and Equation 10.2 illustrates how the heat storage has been calculated.

Comparison of stored heat for Case 1 and Case 4 calculated by Method 1

The heat storage is studied for the two cases.

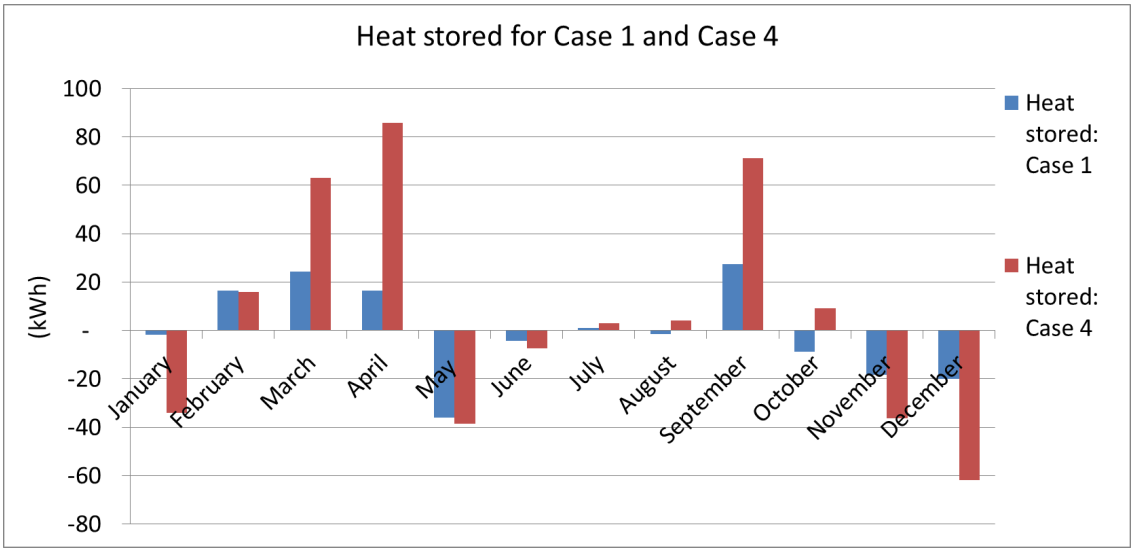

Figure 10.27: Comparison of the heat stored per month for Case 1 and Case 4 by Method 1

Figure 10.28 shows the heat storage summarized.

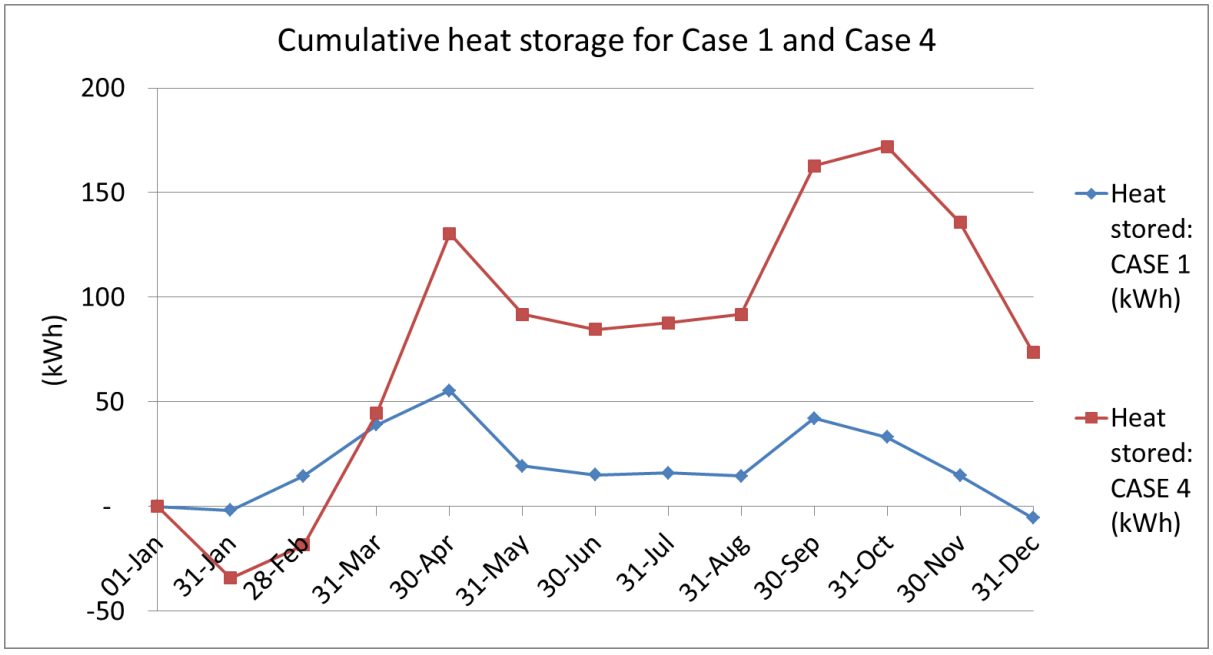

Figure 10.28: Comparison of the cumulative heat storage for Case 1 and Case 4 by Method 1

Figure 10.27 and Figure 10.28 shows the heat storage for Case 1 and for Case 4. The heat storage capacity is shown to be much larger for Case 4 than for Case 1 as expected. Figure 10.28 shows the cumulative heat storage for the two cases.

To compare Case 1 and Case 4, the month of November is studied.

	Hear transfer to inner zone	Heat transfer to basement	Heat storage in the construction
Case 1	44.2 kWh	31.9 kWh	-18.4 kWh
Case 4	52.5 kWh	41.5 kWh	-36.2 kWh

Table 10.17: Heat transfer in November for Case 1 and Case 4

Table 10.17 shows the heat transfer from the basement floor of the inner zone for Case 1 and Case 4 in November. Case 4 has a greater ability to store heat, hence it has more heat stored than Case 1 in the month of November. There is a great difference in the amount of heat stored in the late fall for the two cases as seen in Figure 10.28. The effect is also seen in the temperature profiles for Case 1 and Case 4 in Figure 10.11 and Figure 10.15 respectively.

Calculated heat storage with Method 2

To verify and compare the results of calculations for heat storage, another calculation has been carried out. Temperatures have been collected for all the layers in the ground construction for each hour over the year. The ground construction with its layers and nodes is shown in Figure 10.29.

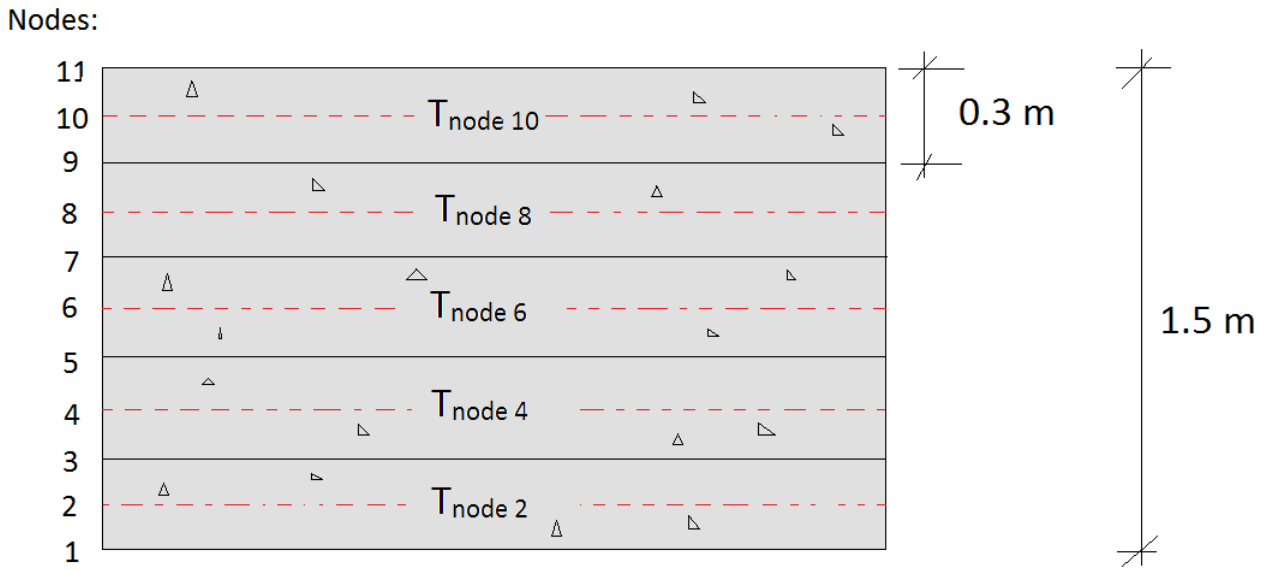

Figure 10.29: The basement floor of the inner zone showing the layers of the construction and the nodes within the layers

The heat storage has been calculated using the following equation:

$$Q = \rho c V \frac{\Delta T}{\Delta t} \tag{10.5}$$

where ρ and c is the thermal properties for the material, V is the volume of the layer, Δt is the time interval and ΔT is defined as:

$\Delta T = T_{node}$ - 0 $^{\circ}C$

There is positive storage as long as the construction is above the frost point. The stored heat has been calculated for each hour and plotted in Figure 10.30.

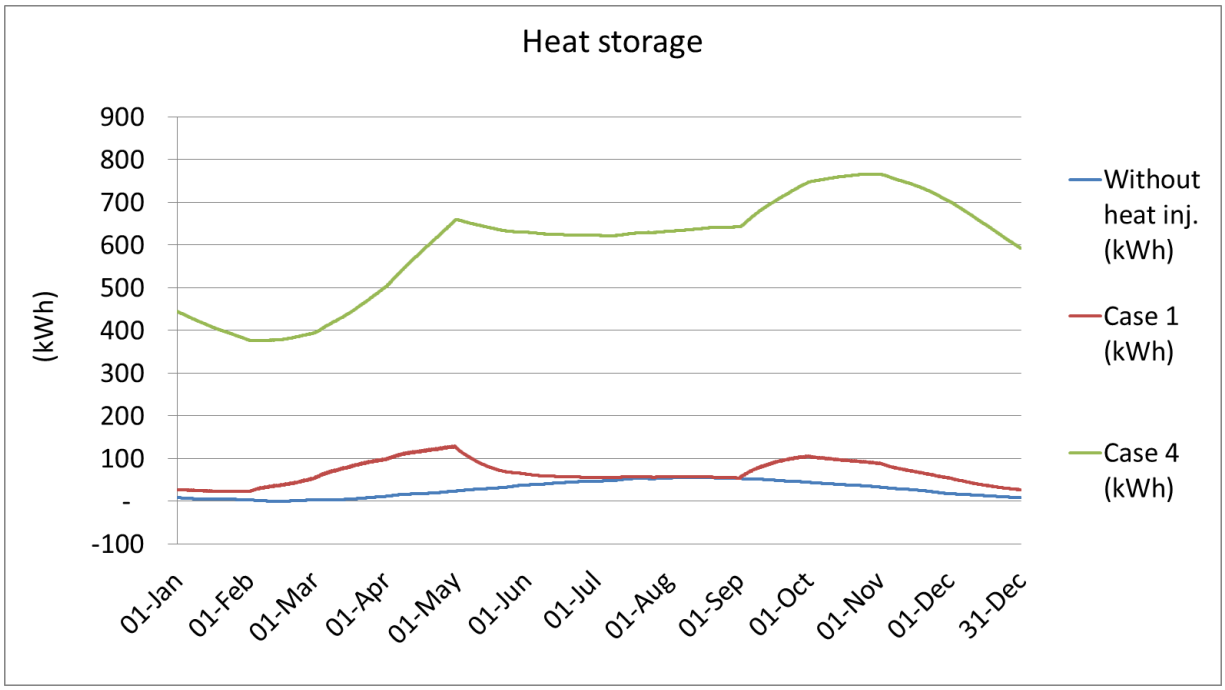

Figure 10.30: Calculated heat storage by Method 2 for Case 1, Case 4 and the case without any heat injection

	Heat storage the 1st of January	**Heat storage the 31st of December**	**Heat storage over the year**
Without any heat inj.	8 kWh	8 kWh	0 kWh
Case 1	27 kWh	27 kWh	0 kWh
Case 4	444 kWh	592 kWh	148 kWh

Table 10.18: Heat storage over the year for the case without any heat injection, Case 1 and Case 4

Comparison of the two methods for calculating heat storage

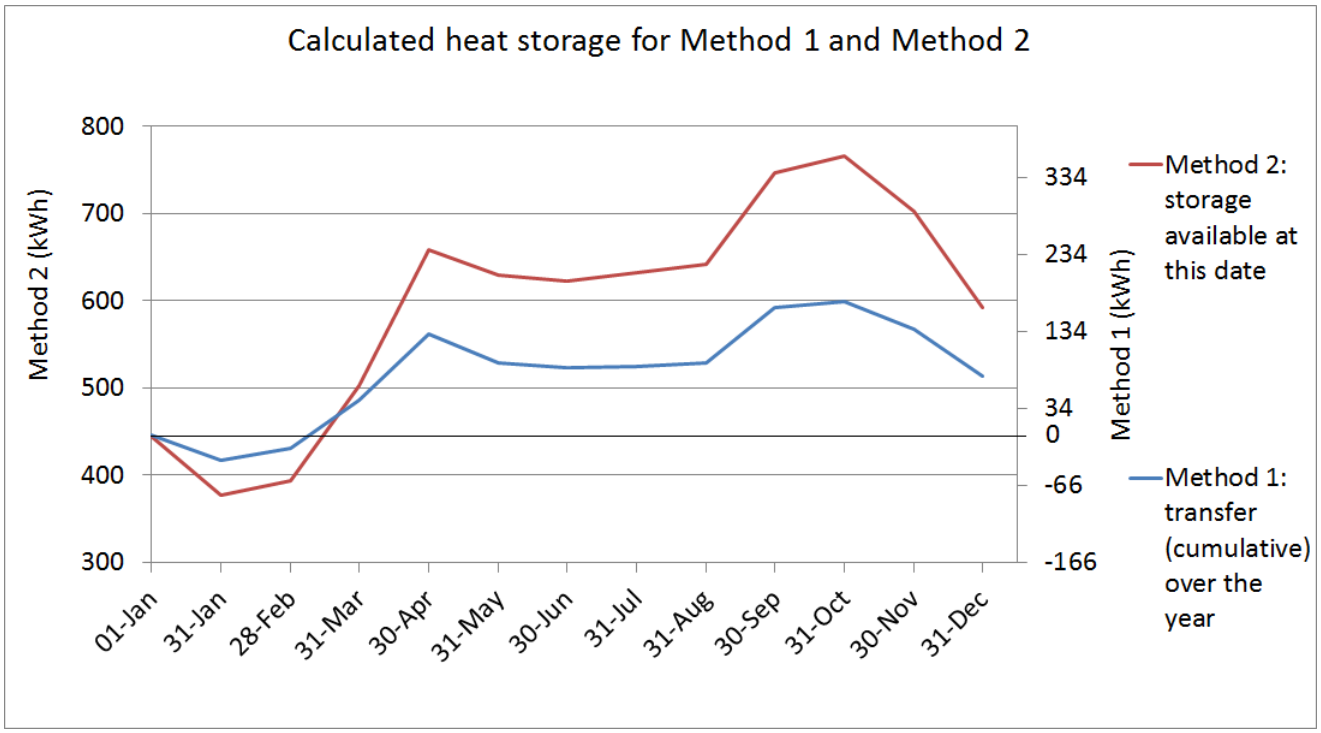

Figure 10.31: Calculated heat storage for Case 4 with Method 1 and Method 2

Figure 10.31 shows the variation in the heat storage throughout the year calculated using both methods.

Method 1 calculates the heat storage based on how much solar heat that is injected by the control loop, and how much heat that is transferred to the inner zone and the basement zone. This is based on monthly values, and the starting point is defined to be 0, since this method of calculating the heat storage only calculates the variation from month to month.

Method 2 calculates the heat storage available each hour of each day. In the figure above, it is the variation from one month to the other that is to be studied, therefore the values has been collected for each month.

The tendency are similar for the two methods, but the derivative is quite different for some of the months.

Method 2 looses more heat from the storage the first month, while the variation is almost the same in the second month of the year. From 1st of March to 30th of April more heat is stored for Method 2. In the summer months, no heat injection occurs, and the difference between the two methods are small. In the fall, when more solar radiation is injected by the control loop, Method 2 stores more heat.

Table 10.19 shows the variation in the heat storage calculated by the two methods:

	Heat storage the 1st of January	**Heat storage the 31st of December**	**Heat storage over the year**
Method 1	0 kWh	74 kWh	74 kWh
Method 2	444 kWh	592 kWh	148 kWh

Table 10.19: Calculated heat storage for Case 4 with two different methods

Method 2 gives twice as much storage throughout the year.

The ground construction is constructed by inert thermal mass. Case 4 is less sensitive to sudden changes in temperatures than Case 1. Method 1 calculated the variation in the heat storage based on how much heat that is transferred to the inner zone and to the basement zone. It is assumed a linear temperature distribution and steady-state conditions for the calculations in Method 1. The heat transfer from the ground construction is calculated based on hourly values of the temperature.

Method 2 is also based on hourly values for the temperature, but for this method, the layers have been studied in more detail. The temperature of each layer is collected, and summarized for the construction. This result from Method 2 shows the available heat in the storage at any time.

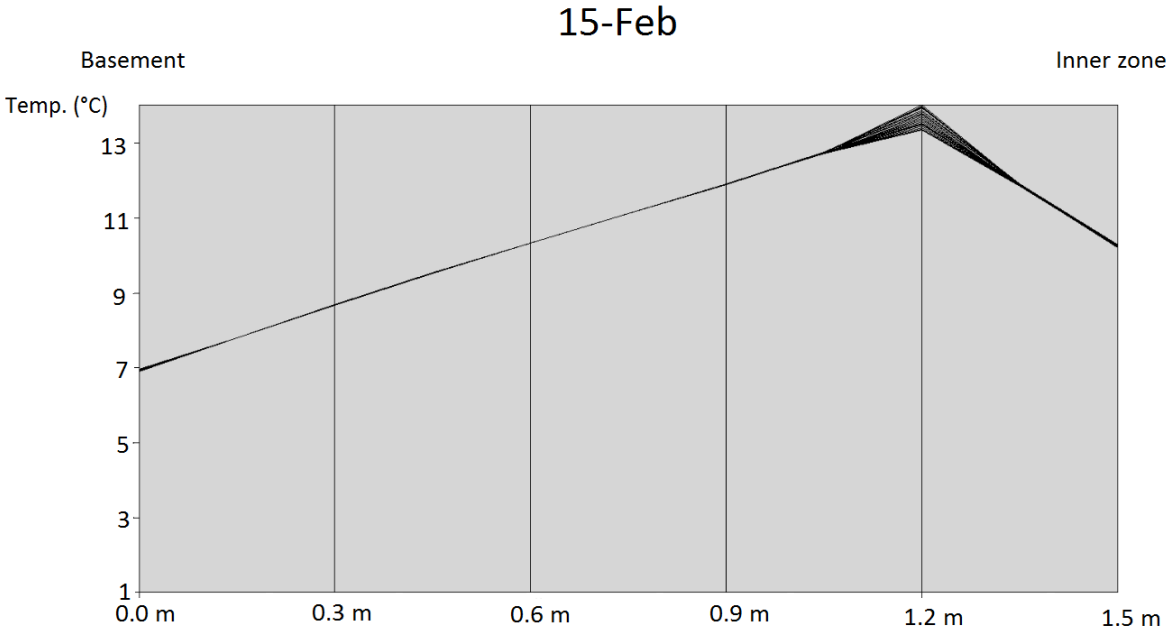

Figure 10.32: Temperature distribution in the ground construction (the basement floor of the inner zone) at 15th of February

Figure 10.32 shows the temperature distribution in the basement floor of the inner zone 15th of February. A source of error in the calculations using Method 1 could be to assume

linear temperature distribution through the construction. The solar heat injected by the control loop occurs for a given period each day. This is a dynamic system with great variations throughout the day. As seen from the figure above, this assumption of linear temperature distribution seems to be valid in this case, and it should not be the greatest source of error. Case 1 which do not experience the same inertia as Case 4, may have more variations in the temperature distribution and the assumption of linear temperature distribution may be a larger source of error than for Case 4.

Since the layers are studied in more detail for Method 2, and the storage are calculated directly, this Method seems more reliable. Method 1 calculates the heat transfer to the zones, and calculates the storage based on how much heat that is transferred away from the construction.

10.7.4 Heat delivered to inner zone 0

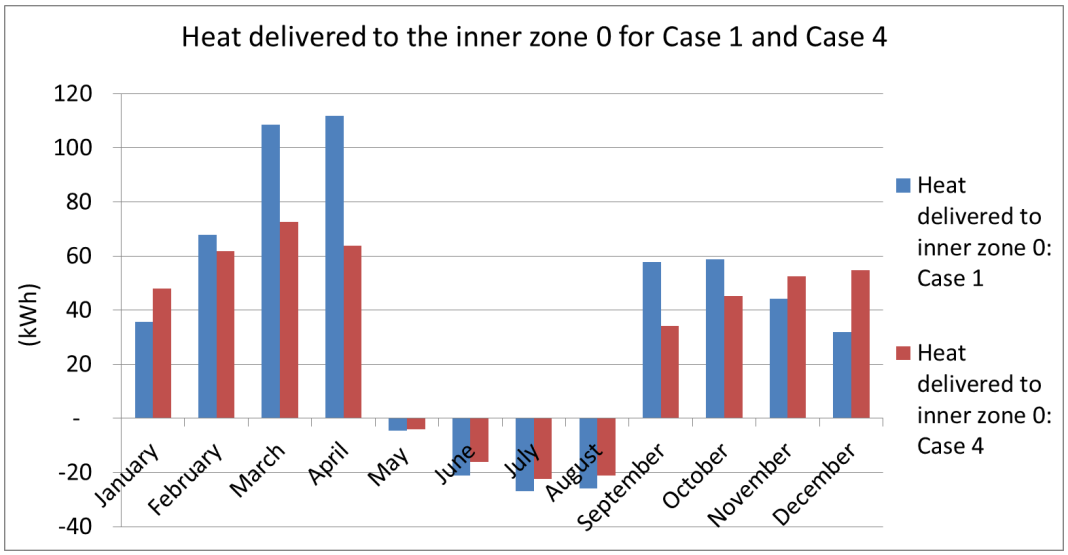

Figure 10.33: Comparison of the heat delivered to the inner zone 0 for Case 1 and Case 4

Figure 10.33 shows a comparison of the heat delivered to the inner zone for Case 1 and Case 4. More heat is delivered to the inner zone in Case 1 when there is solar radiation available, in the spring time and in the first two months after the summer. Case 4 delivers more heat than Case 1 in the winter. This shows that the ground construction in Case 4 is more inert and has more heat to release from the storage in the winter months.

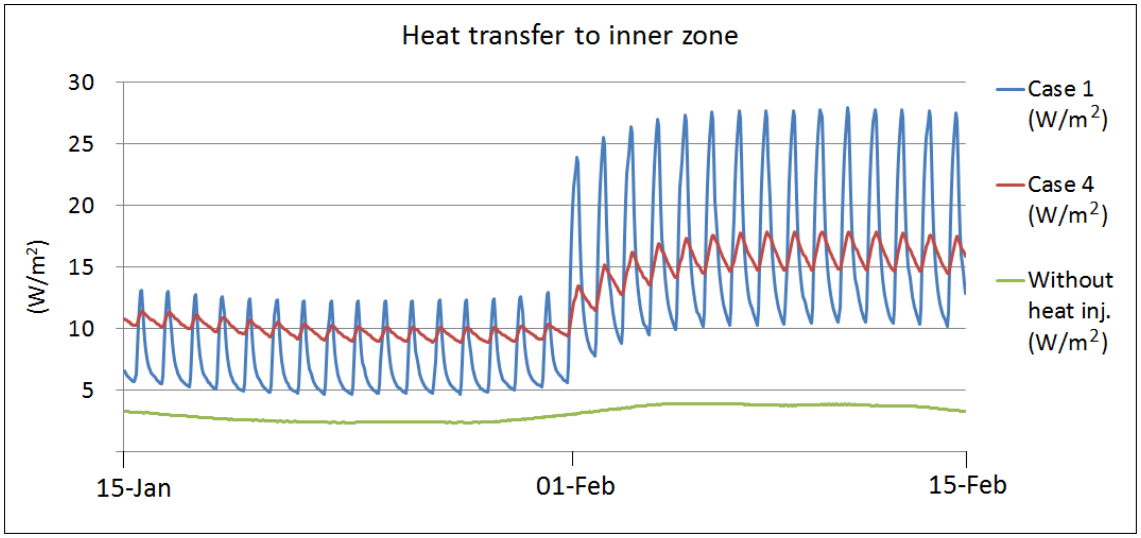

Figure 10.34: Heat transfer to inner zone for Case 1, Case 4 and the case *without* any heat injection from the ground construction for 15th of January to 15th of February. The heat transfer is calculated based on Figure 10.19.

The heat transfer from the ground construction, the massive basement floor of the inner zone and the basement zone, to the inner zone is studied for the period 15th of January to 15th of February in Figure 10.34. The peaks for Case 1 and Case 4 is due to the heat injection that occurs in the middle of the day and not during night. The jump in the graphs at 1st of February is due to the change in solar heat input from the control loop as seen in Figure 9.3 in Chapter 9.

The green line represents the case without any heat injection. The only heat that is available in this case is geothermal heat from the earth. A former student, Ole-Jørgen Feiring Myrtrøen studied the heat transfer between a basement in a building and the ground, his findings showed that the heat flux from the earth is between 1.94 to 3.34 W/m^2 and is contributing to keeping a basement zone with an area of 80 m^2 above freezing point (Myrtrøen, 2006). Myrtrøen is referring to an article by Krarti and Choi who suggest a heat flux of 3.34 W/m^2 from the earth (Krarti & Choi, 1996). Unfortunately this article could not be obtained.

10.7.5 Heat transfer to the basement zone

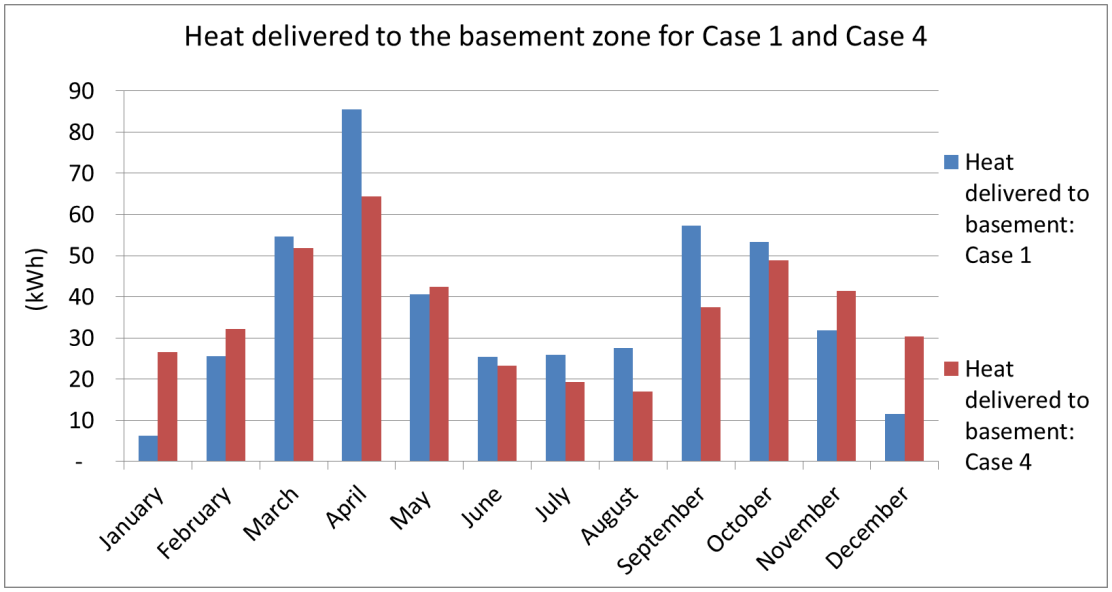

Figure 10.35: Comparison of the heat delivered to the basement zone for Case 1 and Case 4 based on Figure 10.19

Figure 10.35 shows a comparison of the heat delivered to the basement for Case 1 and Case 4. The same tendency is shown for the heat delivered to the basement as for the heat delivered to the inner zone.

Heat delivered to the outer zones

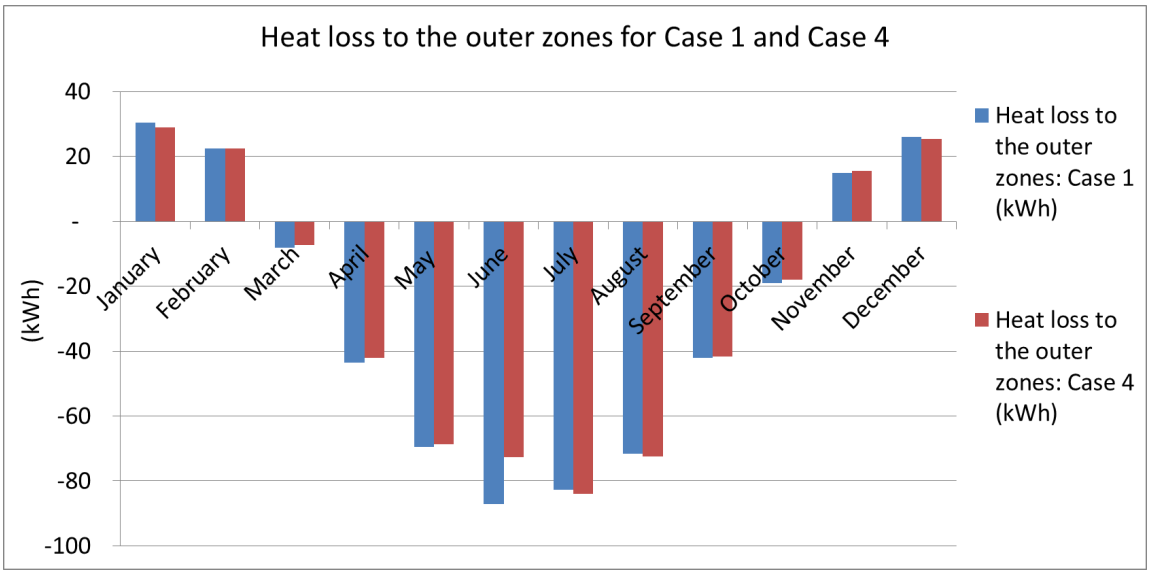

Figure 10.36: Comparison of the heat loss to the outer zones from the basement zone for Case 1 and Case 4 based on Figure 10.22

Heat transfer to the ground

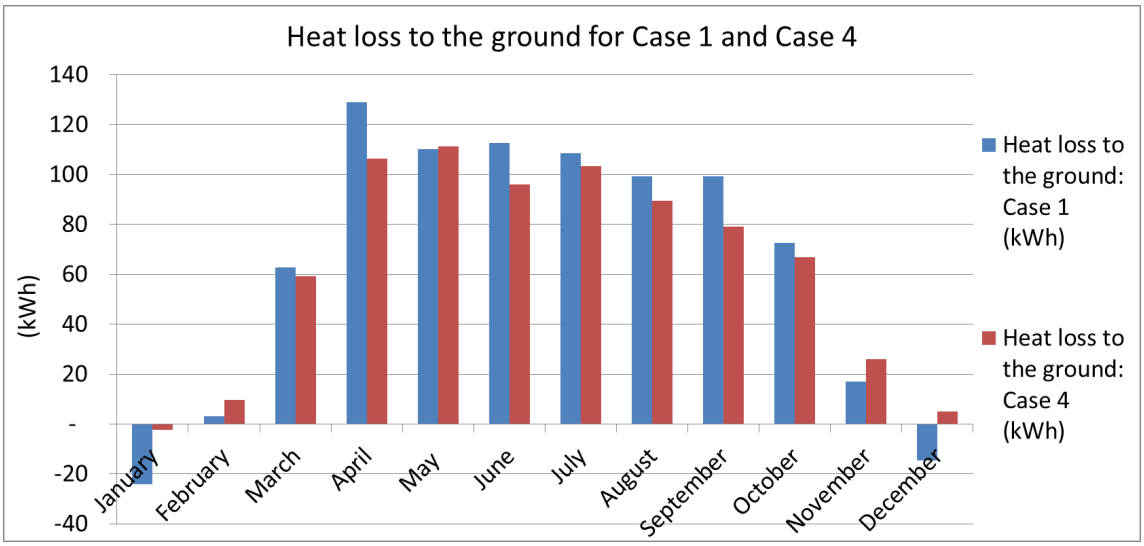

Figure 10.37: Comparison of the heat loss to the ground from the basement zone for Case 1 and Case 4 based on Figure 10.22

Chapter 11

Discussion and analysis of the heat exchange

Heat transfer occurs where there is a temperature difference. The heat flux which is the rate of heat transfer, is determined by the resistance of the material heat is being transferred through. In this chapter heat transfer between the different elements in the model will be analysed.

11.1 Heat transfer in the building

A building experiences different modes of heat transfer, infiltration and other climatic effects. Some of these effects are not taken into account in the simulations. It is important to be aware of the influence that might have on the results of the simulations.

11.1.1 The *actual* building

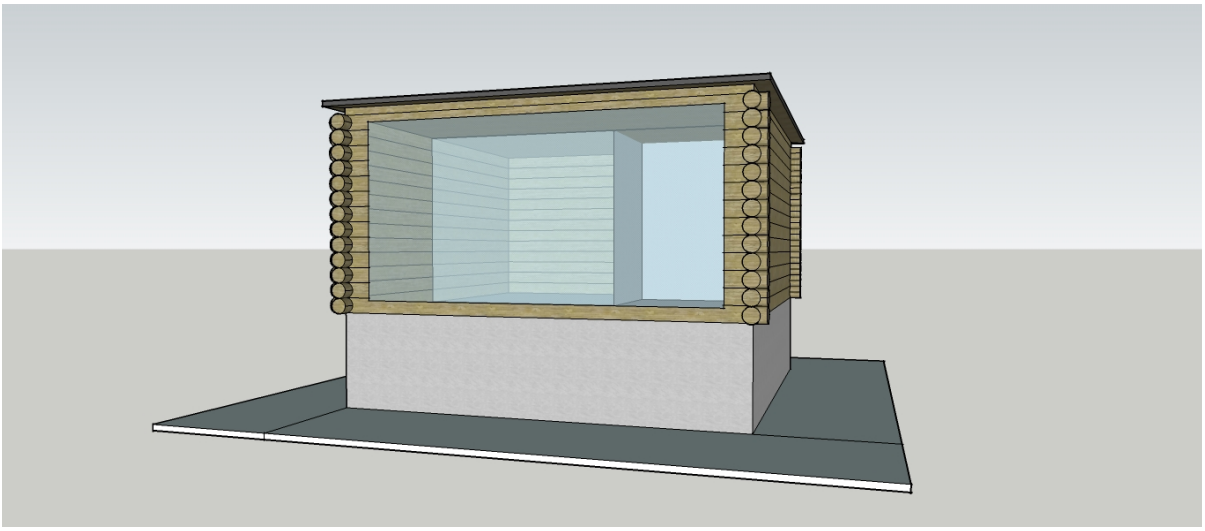

Figure 11.1: The actual building without solar collectors shown

Figure 11.1 shows the actual building with ground insulation around the perimeter of the floor slab, log walls, a large south-facing window and an internal zone. The ground insulation would be buried approximately 0.3 m into the ground as shown in Figure 11.3 and Figure 11.4.

There are several modes of heat transfer occurring between a building and its surroundings. In the northern hemisphere, where winter conditions tend to govern building design, it is usually assumed that the heat transfer rate from the building to the outside is positive.

Fabric heat loss due to temperature differences between outside and inside the building envelope, is calculated by the following equation for steady state, 1-dimensional heat transfer:

$$Q = UA\Delta T \tag{11.1}$$

where A is the surface area of the fabric and ΔT is the temperature difference between the inside and outside. U is the thermal transmittance defined by:

$$\frac{1}{U} = \frac{1}{\alpha_i} + \Sigma(R) + \frac{1}{\alpha_o} \tag{11.2}$$

α_i and α_o is the inside and outside surface heat transfer coefficients and $\Sigma(R)$ is the sum of the resistances of the individual layers of fabric – the thermal conductance (Eastop & Watson, 1991).

In any building there will be infiltration and exfiltration of air. Gaps in the construction causes air movement, and the rate of air movement is determined by pressure differences which is dependent of the wind direction and velocity.

Heavy constructions such as the floor separation between 1st floor and ground floor for north zone and south zone, and the basement floor of the inner zone may store heat for a longer period as shown in Figure 5.12 in Chapter 5. The floor slab in the 1st floor is exposed to solar radiation through the large south-facing window and its design works as a passive solar heating system as seen in Figure 5.11 in Chapter 5.The wall that separates the north and the south zone is constructed by glass. This is to allow solar radiation to reach as far in as possible and heat up the concrete floor. The basement floor of the inner zone is where heat is injected from the solar collectors as seen in Figure 5.11 in Chapter 5. When the surface temperature is higher than the surrounding air it loses heat by convection. If the surface temperature is higher than the mean temperature of the surrounding surfaces then heat is also transferred by radiation (Eastop & Watson, 1991).

It is the inner zones where the sanitary installations are placed, that are to be kept frost proof. The walls of the inner zones are well insulated and has a U-value of 0.117 W/m^2K to minimize the fabric heat loss to the outer zones. To achieve better heat transfer between the internal zones, holes could be created in the floor/roof that separates them. Warm air is lighter than cold air, and the difference in the density because of this temperature difference creates a pressure difference. This means that the warm air will arise from the bottom inner zone to the upper inner zone.

11.1.2 The *modeled* building

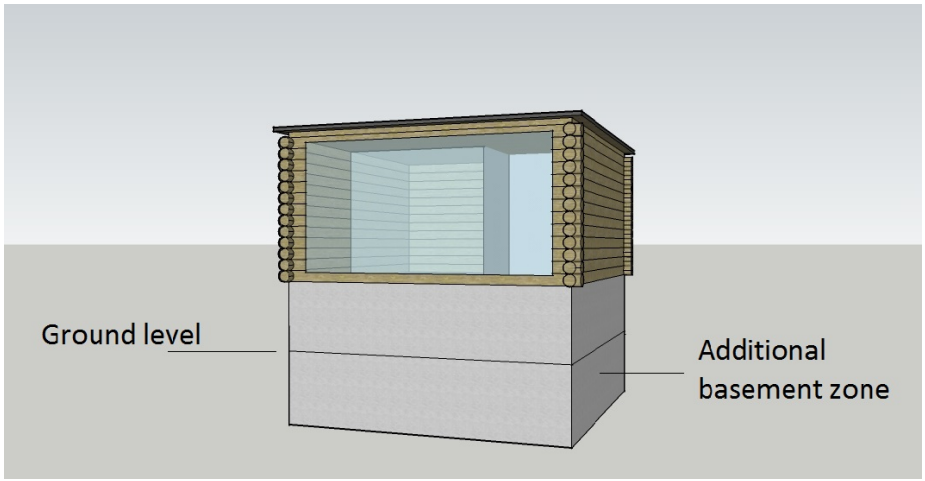

Figure 11.2: The modeled building without solar collectors

Figure 11.2 shows the modeled building with an additional basement zone. There are some differences between the actual and modeled building and this is discussed further below.

All the constructions are defined with materials with a given thickness. Thermally, the thickness of the constructions are taken into account when modeling the heat transfer. However, the program does not account for the geometric thickness of a construction and it is zero in the simulations. Corners for example, are not defined, and the room volume will be calculated based on the given coordinates of each zone. The different constructions are not in thermal contact with each other. The heat transfer is calculated 1-dimensional and perpendicular through each construction. There are not defined any thermal bridges, hence this is not taken into account in the simulations.

Infiltration is not implemented in the model. It is possible to define cracks in the constructions, and infiltration rates in the program, but since the ground modeling was the main focus of this report, this have not been studied further. The heating demand is therefore greater in reality than what the results from the simulations are showing.

The passive solar heat through the window is modeled in the simulations.

However, the albedo effect from the snow is not taken into account, as snow lying on the ground not is considered in the simulations. At a location as Östersund, there will be snow lying on the ground for a significant time over the year, and snow has the ability to reflect up to 90 % of the solar radiation. This would have contributed to heat up the floor slab in the 1st floor through the window.

Occupancy patterns has not been defined, although there are possibilities for this in ESP-r. The idea is that this is a leisure home used during the summer. Occupancy during this time will not have much effect on the heat storage and release during the winter. However, the leisure home is supposed to have a heat storage tank in one of the inner zones. When the leisure home is being used, there will be a need for hot water. The solar heating system should be designed in a way that excess heat can be transferred to the tank. The simulations are done without heat transfer to the basement floor of the inner zone from May until August. This heat can easily be transferred to a hot water tank without having any negative effects on the heat storage.

11.2 The heat storage facility

11.2.1 The *actual* heat storage facility

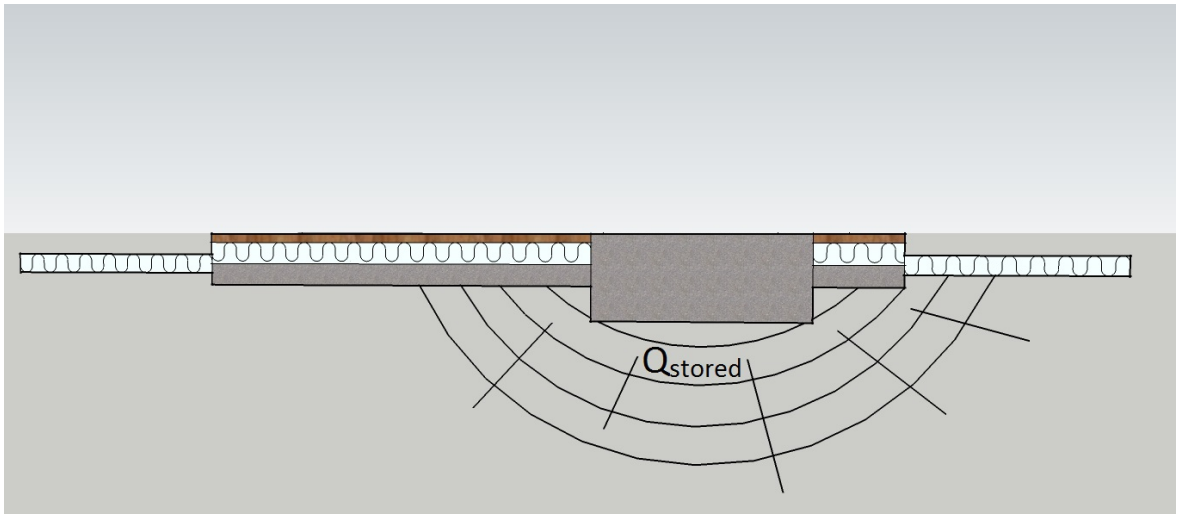

Figure 11.3: The actual heat storage facility

Figure 11.3 shows the heat storage facility placed underneath the basement floor of the inner zone. The basement floor is to be in thermal contact with the ground, so heat injected to the floor will disperse into the ground, and back again. The ground should ideally be constructed by rock such as granite. It is reasonable to assume a rocky ground in Norway. The composition of minerals, the water content, air gaps and porosity determines the rate at which heat is transferred in and out of the storage facility. It might be an inhomogeneous mass, so the thermal properties changes in the storage volume.

Figure 11.4 shows different heat flow paths around the floor slab.

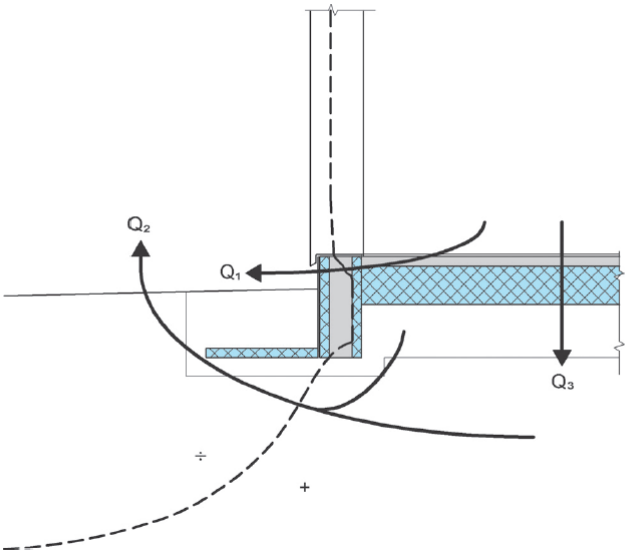

Figure 11.4: Different heat flow paths around the floor slab of a building (Gundersen, 2005)

With ground insulation around the perimeter of the building, the heat loss in upwards direction will be minimized. Snow also works as insulation and will contribute to minimizing this heat loss.

The amount of lost heat to the surrounding ground compared to utilized heat from the ground to the inner zone will vary depending on time. The ground and the heat storage facility needs time to heat up and with a so-called *cold start* the amount of lost heat to the surrounding ground would be a lot more than for a *warm start* where less heat is lost, and more is utilized to heat up the building. This is studied by Shelton, and it is discussed in Section 5.5 in Chapter 5 (Shelton, 1974). The season will also have an effect on how much heat that is utilized compared to lost heat to the surroundings, as the ground temperature varies over the year, with a delay of approximately 3 months from the curve of the ambient temperature.

11.2.2 The *modeled* heat storage facility

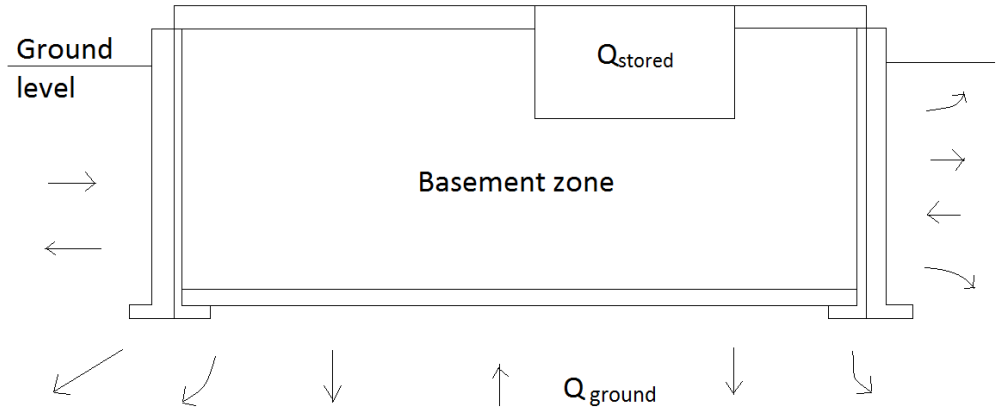

Figure 11.5: The modeled heat storage facility

The modeled heat storage facility is illustrated in Figure 11.5. A BASESIMP configuration was used to calculate the heat transfer from the building to the ground quasi 3-dimensional. Since BASESIMP only calculates the heat transfer and do not take heat storage in the ground into account, the heat storage is represented in the basement floor of the inner zone. A basement zone was created, so the heat transfer to the ground is calculated from the walls and the floor of the basement zone. The heat storage is adjacent to the basement room. The basement floor of the inner zone is a construction in the model, hence the heat transfer is calculated 1-dimensional and perpendicular through the construction. Dr. Jon Hand from the ESRU team suggest a thickness of 1.5 m when representing the ground in a floor slab construction, therefore is this thickness chosen for the basement floor of the inner zone (Hand, 2013). The basement floor of the inner zone has a surface area of 6.25 m^2 and is constructed by concrete. The availability of thermal mass in the heat storage facility was studied by multiplying the thermal properties with different factors.

There are not many possibilities for adding ground insulation to a model in ESP-r. Some of the BASESIMP configurations are constructed with ground insulation, and it has been suggested by members on the ESP-r user mailing list to create additional zones around the perimeter of the floor slab and construct them with insulation. However, this new basement zone, which does not exist in the actual model, creates a resistance to heat transfer in the basement wall in the same way ground insulation would do. The basement wall is immersed 1.9 m into the ground and it is constructed by 200 mm concrete and 100 mm insulation. This gives a resistance to heat of 2.64 m^2K/W for the wall.

Tynset, Norway has a frost index of 65 000 h°C, while Ringsaker, Norway has an index of 51 000 h°C (Rockwool, 2013). With a frost index of 60 000 h°C, a ground insulation thickness of 100 mm and a width of 2.4 m for critical areas of the building is

recommended by Byggforsk (Gundersen, 2005). It seems reasonable to assume that this recommendation is valid for Östersund, Sweden. Ground insulation constructed by extruded polystyrene (XPS) has a conductivity of 0.037 W/mK, which gives a resistance to heat of 2.70 m^2K/W. This correlates well with a resistance of 2.64 m^2K/W for the wall.

Table 11.1 shows the materials and values used in the calculations for the ground insulation heat resistance.

Construction	**k-value** (W/mK)	**Thickness** (mm)	**Resistance** $[m^2K/W]$
Ground insulation	0.037	100	2.70
Basement wall:			2.64
concrete	1.4	200	
insulation	0.04	100	

Table 11.1: Heat resistance for basement wall and ground insulation

It was uncertain if snow was accounted for in the simulations. After raising the question on the ESP-r mailing list it was revealed that snow was not implemented in the program 10 years ago, and that it is rather doubtful that it has been implemented since. ESP-r and most of other building simulation tools does not have precipitation implemented for simulations. However, some of the climate files available from U.S Department of Energy do contain information about this, and apparently the file for Östersund does have this information (Spitler, 2013).

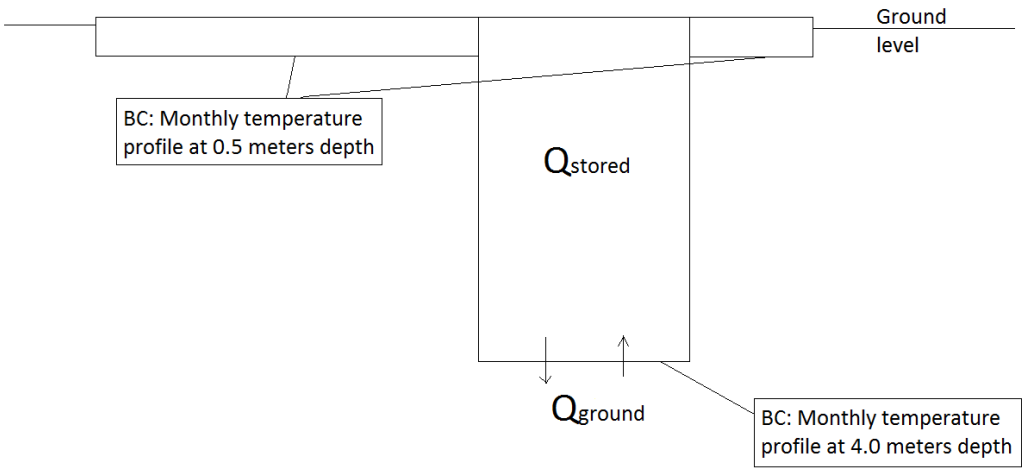

Figure 11.6: The modeled heat storage facility in the project thesis

Figure 11.6 shows how the heat storage facility was modeled in the project thesis. The ground was represented in the floor slab construction as a 3.5 m concrete pillar. The boundary conditions for the basement floors was monthly ground temperature profiles as seen in Figure 11.6 and Figure 5.8.

The differences in the temperature profiles for the inner zones over the year for the old and the new model are surprisingly small.

The heat transfer through the ground construction is calculated 1-dimensional as it is defined as a construction in the model. There is no ground insulation implemented in this model.

11.3 The solar heating system

11.3.1 The *actual* solar heating system

Figure 3.11 in Chapter 3 illustrates an actual solar heating system that should be implemented in the leisure home. It contains of solar collectors, a pump and distribution pipes.

The system will experience heat loss both in the solar collectors, in the pump and in the distribution pipes. Figure 4.9 in Chapter 4 shows efficiency curves for different collectors and the topic is discussed in this chapter. The pump should be installed in a way where it only will run when there is a positive temperature difference to minimize the use of electricity and to avoid that heat is transferred *from* the basement floor out *to* the collectors. The distribution pipes will also experience some heat loss along the way. If it is possible, they should be mounted inside the inner zones, so that the heat loss from the pipes will be utilized.

There would be a hot water tank placed in the inner zones which should be attached to the the solar heating system to supply the users with hot water when needed.

11.3.2 The *modeled* solar heating system

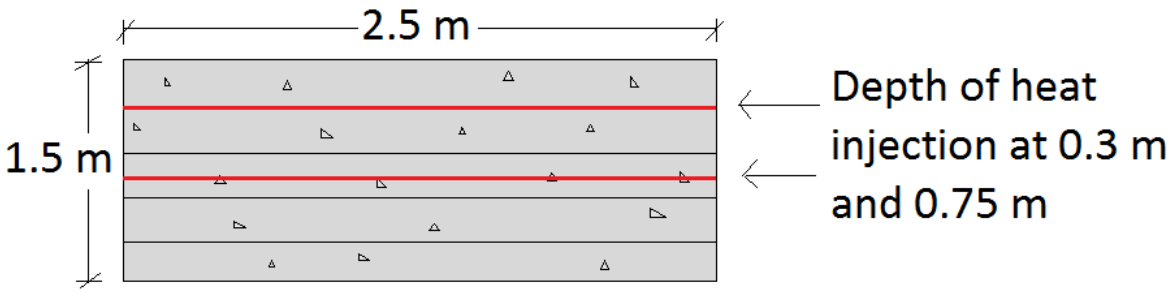

Figure 11.7: Electric heated basement floor

Figure 11.7 shows how the solar heating system was modeled. Since there was some difficulties building up a solar heating model in ESP-r, a control loop with electric heating was used instead. The electric heat injection is based on solar radiation data from PVGIS and the time intervals is set by studying when there is solar radiation available.

Heat is injected as a certain amount of watts for the given period. A solar heating system will have a heat transfer fluid at a certain temperature delivering the heat to the basement floor. The amount of heat received at the basement floor is dependent of the temperature difference between the heat transfer fluid and the basement floor. This is a source of error when using electric heat instead of a solar heating model. However, the error will be largest in the late summer, when there is a lot of solar radiation available and the floor would have been heated for a while. The floor would not be able to extract all the heat since it already has been heated. Control loop 2 has no heat injection during the summer months, and therefore is the largest error avoided.

How much solar radiation that is available varies from one year to another. There is no such thing as a standard year. This should be kept in mind when studying the results. This applies to all climate data used in any simulation tool.

Chapter 12

Discussion

The modeling of buildings and climate in simulation tools will never present the real case to full extent. The accuracy will increase with more advanced simulation tools, but independent of what tool that is used, simplifications and adjustments are usually done along the way. It is important to consider to what degree the results of this study can be useful.

12.1 Solar heat

There have been done simulations for the leisure home model without any heat injection, and it is shown that frost proof conditions are not achieved. This is shown in Figure 14.6 and Table 10.3. Solar energy, which is not associated with CO_2-emissions, are implemented in the model to keep the inner zones frost proof.

The control loop from the project thesis, Control loop 1 which was based on a solar collector with an incline of 45 ° have been replaced with Control loop 2. A steeper incline was chosen for the new solar control loop in order to collect more solar heat in the spring and in the fall. It is shown in Figure 10.5 that the inner zones are kept at higher temperatures with Control loop 2 in the critical periods, around the beginning of February. Control loop 2 has no heat injection from May until August. Neglecting the summer heat is a conservative approach to not exaggerate the input of solar heat in means of electric heat, since a solar heating system will behave differently than electric floor heating. The amount of heat released or extracted by a heat transfer fluid in a solar heating system is dependent on the temperature difference between the collector and the basement floor. When there is a longer period with a lot of solar radiation available, the basement floor would already be heated and the heat transfer fluid would not be able to release all the heat that it is carrying, because the temperature difference between the floor and the collector is too small.

The effect of not injecting heat during the summer months is shown in Figure 10.10, and for a thermal mass with normal properties, seems to have no effect on the temperatures of the inner zones in the winter. The collector efficiency is another factor that needs to

be evaluated. A collector efficiency of 45 % corresponds to an average efficiency, but this will vary depending on collector type, temperature differences and weather conditions.

There have been done simulations with a collector area of 4 m^2 and 6 m^2. With an area of 4 m^2 with Case 4, the minimum temperature over the year is 4.2 $°C$ in the inner zone 1 and with a collector area of 6 m^2 the minimum temperature is 6.0 $°C$ in the same zone. To assure that frost proof conditions are achieved in extremely cold winters, a collector area of 6 m^2 might be considered. But one should also keep in mind that the inner zones are well-insulated and less sensitive to sudden changes in ambient temperature.

12.2 Heat storage by the ground

The modeling of the ground has been done by representing the heat storage in the basement floor of the inner zone by creating a new basement zone to implement the BASESIMP configurations as boundary conditions for the surfaces adjacent to the ground. This way of modeling the interactions between the leisure home building and the ground seems more accurate than the approach used in the project thesis, although the results for the two models were surprisingly similar. The modeling of the heat storage facility for the new model compared to the old model differs by the thickness of the ground construction and the boundary condition for the outside surface of this construction. In the project thesis, the ground construction was 3.5 m thick with a monthly temperature profile at 4 m depth as boundary condition. For the new model, the thickness is reduced to 1.5 m after recommendations from Dr. Jon Hand, see Chapter 9, and the boundary condition for the heat storage is the new basement zone. The BASESIMP configuration which is set as boundary condition for the surfaces adjacent to the ground calculates the heat transfer between the basement and the ground quasi 3-dimensional, but it does not include modeling of thermal mass.

The modeled ground construction is a rough approximation of the heat storage facility. The designed ground construction is supposed to account for the entire ground under the cabin. The thermal properties were therefore multiplied with a factor of 10 in Case 4, and is represented unrealistically dense for this case to account for a larger volume. The heat transfer and storage is calculated 1-dimensional in this construction. The heat stored in the ground construction over the year has been calculated using two methods, based on collected temperatures at different points in the ground construction. Method 1 suggests a heat storage of 74 kWh over the year, while Method 2 suggests a heat storage of 148 kWh. It is a large gap between these two results, which in theory should be the same. Since the layers are studied in more detail for Method 2, and the storage are calculated directly, this method seems more reliable. Method 1 calculates the heat transfer to the zones, and calculates the storage based on how much heat that is transferred away from the construction. Method 2 seems more trustworthy, but since there is a such great difference in the results, this has to be considered with a pinch of salt. Further analysis of the heat storage should be carried out in future studies. It would have been convenient if the BASESIMP configuration also accounted for heat storage, hence given a more realistic picture of what happens in the surrounding ground. Since this is not the case,

the heat storage should be studied further in another simulation tool. A simulation tool called HEAT3 (BLOCON, 2011) studies 3-dimensional heat conduction problems. This may give a better view of how the storage will behave in the ground. However, it is uncertain how well this simulation tool will model the interactions between a building and the ground.

The heat transfer to the inner zone was studied for the critical period of 15th January to 15th of February. The contribution from the surrounding ground when no heat is injected was found to be around 3.3 W/m^2 in this period. This correlates well with earlier studies and implies that the heat flux from the earth is taken into account in the BASESIMP configuration.

12.3 Climate and location

A leisure home that is to be frost proof by solar heat and seasonal storage in the ground is dependent on a location where the climate make this possible. The solar availability is important, but also the ground conditions. A good solution is to place the leisure home on a rocky ground in a south oriented hillside.

The most suitable climate file available for implementation in ESP-r for the leisure home placed in the southern mountain regions in Norway, was found to be for Östersund, Sweden. An earlier study has shown that it seems reasonable to use this climate data (Børset, 2009). The monthly mean temperature is lower for the southern mountain regions in Norway than for Östersund in the critical periods of February. The southern mountain regions of Norway seems to have more solar radiation available than in Östersund. The climate file for Östersund contains data for the year of 1995. In real life, no years are the same in means of weather and climate. Extremely cold winters, or a overcast year would give a higher heating demand to keep the inner zones frost proof. This should be kept in mind when sizing the solar collector.

The ground properties of Östersund was not studied in detail since the ground construction was chosen to be represented by a concrete block. If a system with heat storage is to be implemented for a building, the ground should be studied in advance. The thermal properties of the ground, its composition of minerals, the water content, porosity and air gaps are things that should be studied before the building is put in thermal contact with the ground. The ideal ground is constructed mainly by granite or a similar rock, and the basement floor of the inner zone is put in thermal contact with the ground by casting a concrete floor directly on the rocky ground.

For a heat storage in the ground, the presence of ground insulation will be important. This has been implemented in the model via the basement walls of the new zone. These walls have a resistance to heat transfer in the same extent as the amount of ground insulation needed for this type of building in this climate recommended by Byggforsk (Gundersen, 2005). Snow on the ground will also contribute to the insulation of the heat storage in the ground and prevent the surrounding ground from freezing. Snow is not taken into account in the simulations. This indicates that the surrounding ground will

experience temperatures below 0 $^{\circ}C$ at greater depths, than what would be the case *with* layers of snow on the ground. The heat loss from the basement zone to the surrounding ground may be larger than what it would have been if snow was implemented in the model. Possibilities for implementing snow in the model should be studied further.

12.4 Heating demand

Total delivered energy over a year by Control loop 2 turned out to be 878 kWh with a collector area of 4 m^2, efficiency of 45 % and an incline of 70 °. This is without collecting any solar heat from May until August. If the solar heat in the summer also were collected, the amount of energy delivered would have been 1778 kWh. According to Energibo (Energibo, 2013), a south oriented collector at an angle of 30 ° in Sweden will receive approximately 1000 kWh/m^2. With a solar collector area of 4 m^2 and an efficiency of 45 % the useful energy collected would be 1800 kWh. This is not very different from what Control loop 2 *with* summer heat would have delivered. According to Energilink (Teknisk Ukeblad Media AS, 2013) is the average incoming solar radiation over a year for the northern parts of Norway 700 kWh/m^2, while for the southern parts of Norway it is 1100 kWh/m^2. With a collector area of 4 m^2 and an efficiency of 45 %, the delivered energy over the year is 1260 kWh for the northern parts and 1980 kWh for the southern parts. Both Norway and Sweden are geographically long countries, and the solar radiation will have a great variation from the south to the north of the country.

With the solar heat injected by Control loop 2 are the inner zones kept frost proof. Infiltration has not been taken into account in the simulations. Some heat will be lost through cracks and unevenness in the building envelope. The heating demand may therefore be higher than what the results are suggesting. However, the zones that are to be kept frost proof are well-insulated, and airtight, inside the building envelope.

Chapter 13

Conclusion

The focus on reducing CO_2 emissions in the building sector has increased greatly during the last decade, and it is desirable to utilize renewable energy sources for heating buildings. Unnecessary amounts of energy are required to maintain frost proof conditions in uninhabited leisure homes through the winter season. A concept for a leisure home with frost proof sanitary installations without the use of electricity or primary energy has been developed. This is achieved by modeling an active solar heating system and by utilizing seasonal heat storage in the ground. The model from the project thesis has been continued and improved using the dynamic simulation tool ESP-r.

The results from simulations with well-insulated internal zones, and the modeled ground conditions showed that it is possible to maintain frost proof conditions in the inner zones throughout the year using the modeled active solar heating system and exploiting stored heat from the ground. The chosen solar heating system had an incline of 70 ° and a collector area of 4 m^2 with no heat collected for the summer months. With the ground constructions from Case 4, where the thermal properties are multiplied with a factor of 10, and heat injected at 0.3 m depth, the minimum temperature occurred in the first floor of the inner zone at a temperature of 4.2 $°C$. This temperature does not meet the recommendations from SINTEF requiring a minimum temperature of 10 $°C$ in leisure homes. However the safety margin of 4.2 $°C$ is probably sufficient to obtain frost proof conditions for sanitary installations in the well-insulated internal zones. If the number of start-up days had been several years instead of 100 days, the minimum temperature would most likely have been higher. The minimum temperature in the ground floor of the inner zone is 7.8 $°C$. To achieve a more even temperature distribution between the zones, holes could be established in the separation floor creating buoyancy driven air flow between the zones.

Results show that the inner zones maintained a much more stable temperature throughout the year than the outer zones. This shows that by isolating the sanitary installations in a well-insulated internal zone, sudden variations in outdoor temperatures will not affect the temperatures in these zones to the same degree as the outer zones.

The model responded to change in different system parameters as expected. The quality of the thermal mass had a great impact on the heat storage potential and on the amount of heat arising in the winter. A steeper incline on the collector had a positive effect on the temperatures for the inner zones in the critical period. Increasing the size of the solar collector, also contributed to higher temperatures for the inner zones.

A solar heating system will require a pump to function, and the pump needs electricity to run. The amount of electricity needed to run such a pump has not been studied in this report. To reach the goal of implementing a system which does not require electricity or use of primary energy sources, this pump should be operated by the use of photovoltaic panels and batteries. Implementing PV-panels for the leisure home have been studied earlier by Are Siljan Børset (Børset, 2009).

The heat stored in the ground construction has been calculated using two different methods for Case 4. Method 1 gives a heat storage of 74 kWh over the year, while Method 2 gives a storage of 148 kWh. Method 2 seems more accurate in the way the heat storage is calculated and it studies the ground construction in more detail than Method 1. The actual heat storage over the year is probably closer to the results from Method 2, but because there is such a great difference in the results it must be considered with a pinch of salt. It should be investigated if there are other possibilities for collecting information about the heat transfer rate directly from ESP-r.

The heat transfer to the inner zone was studied for Case 1, Case 4 and the case without any heat injection. For the case without any heat injection there was found that heat is transferred at a rate of approximately 3.3 W/m^2 in the most critical months. This corresponds well with earlier studies, and this implies that the heat flux from the earth is implemented in the BASESIMP configuration.

The largest uncertainty in this model is the calculations for the heat storage and the heat loss to the surrounding ground. The BASESIMP configurations should be studied further to see how this boundary condition changes over the year in terms of ground temperatures and the heat transfer rates should be studied further in ESP-r. A layer of insulation to account for snow should somehow be implemented to decrease the depth of frozen ground. Emphasis should be placed on the study of the surrounding ground and the heat storage. There is potential for improving the model in ESP-r in terms of solar heating system and the construction of the leisure home. Other simulation tools should be used to study the interactions between the surrounding ground and the heat storage, preferably a 3-D conduction modeling program.

The conclusion is that it is considered to be possible to achieve the goal of maintaining frost proof conditions for sanitary installations placed in an internal zone, without the use of electricity or primary energy sources resulting in net CO_2 emissions.

Chapter 14

Further studies

In this project, a significant amount of time was spent to explore different modeling methods and theories regarding heat storage in the ground. Different ways to implement a solar heating system have also been studied. Simplifications have been made along the way, and there is a potential for improving the model.

There are room for improvements regarding the construction of the building. Today, the leisure home is modeled like a rectangular box without any doors and only with one window. The building elements are constructed only by their main parts. Infiltration has not been implemented in the model causing a lower heating demand, since the building is modeled as it was air tight. It should be considered to create a more realistic model in the extended work. It is considered possible to make the inner zones airtight. But the outer zones should be modeled with infiltration.

The solar control loop without summer heat is a simplified way to model the solar heating system. It was attempted to implement a solar heating system consisting of solar collectors, pump and hydronic floor, but the attempt was not successful. With the thesis written by Are Siljan Børset (Børset, 2009) and also this report as a basis, a more thorough study of the solar system available in ESP-r should be carried out.

The interactions between the heat storage and the surrounding ground should be studied further. It seems like there is no way to model a heat storage facility in direct contact with the ground 3-dimensionally in ESP-r. Another simulation tool, like HEAT3 for example could be used for this study. HEAT 3 deals with 3-dimensional conduction problems (BLOCON, 2011).

Apparently the IWEC-2 climate file for Östersund used in ESP-r contains data of precipitation depth in liquid equivalents (Spitler, 2013). This information can be used, in combination with information about when the ambient temperature falls below 0 $^{\circ}C$, to estimate when it will snow. However, this information is only valid for the year of 1995 when the climate data was collected. The depth of frozen ground is dependent of when it will snow and if it has been minus degrees a long time in advance. This varies from one year to another. The insulation effect of snow should be studied further to see how it affects the heat storage in the ground.

References

Adam Solar Resources. (2012). *Adam solar resources: Solar thermal.* Retrieved 16th of February 2013, from `www.adamsolarresources.com`

Amble, A. K. (2008). *Analysis of energy use for building with solar heating and heat exchange with the ground.* Project thesis.

Andresen, I. (2008). *Planlegging av solvarmeanlegg for lavenergiboliger og passivhus. en introduksjon* (Tech. Rep.). SINTEF Byggforsk.

Beausoleil-Morrison, I. (2013, 25th of April). *Basesimp.* email. (Email contact with Associate Professor Ian Beausoleil-Morrison who is one of the developers of BASESIMP)

Beausoleil-Morrison, I., & Mitalas, G. (1997). *Basesimp: A residential-foundation heat-loss algorithm for incorporating into whole-building energy-analysis programs* (Tech. Rep.). Int Building Performance Simulation Association.

Beausoleil-Morrison, I., Mitalas, G., & Chin, H. (1995). *Estimating three-dimensional below-grade heat losses from houses using two-dimensional calculations* (Tech.

Rep.). Buildings Group, Energy Efficiency Division, CANMET, Natural Resources Canada and Institute for Research Council Canada.

Beausoleil-Morrison, I., Pinel, P., & Ribberink, H. (2007). *Modeler report for bestest cases gc10a-gc80c basecalc version 1.0e and basesimp/esp-r* (Tech. Rep.). CANMET Energy Technology Centre, Natural Resources Canada.

BLOCON. (2011). *Heat2 - heat transfer in three dimensions.* Retrieved 3rd of March 2013, from `http://www.buildingphysics.com/`

Bodenkunde. (1983). Ulmer Verlag.

Børset, A. S. (2009). *Development of a zero emission leisure home with a thermally insulated, frost-free, inner zone and solar-heated water storage.* Master thesis.

Børset, A. S. (2013, 19th of March). *Previos master thesis, simulation of solar heating system.* email. (Email contact with Are Siljan Børset who has studied a similar problem; simulating a solar heating system with a hot water tank)

Chuangchid, P., & Krarti, M. (2001). Foundation heat loss from heated concrete slab-on-grade floors. In *Building and environment; 36(5):637-655.*

dsb. (2010). *Regelverk: Oppslagsverk: Historisk arkiv: Plan/bygg: Byggesforskrift.* Retrieved 31st of January 2013, from `www.dsb.no`

Eastop, T. D., & Watson, W. E. (1991). *Mechanical services for buildings.* Longman Group UK.

Energibo. (2013). *Info: Solenergi.* Retrieved 1st of June, 2013, from `http://www.energibo.se`

EQUA. (2013a). IDA ICE 4: Getting Started [Computer software manual].

EQUA. (2013b). IDA Indoor Climate and Energy 4: Fortsättningskurs: Kursmaterial [Computer software manual].

EQUA. (2013c). *Software.* Retrieved 22th of April 2013, from `http://www.equa-solutions.co.uk/`

ESRU. (1999). *Released documents, esp-r.* Retrieved 14th of February 2013, from `www.esru.strath.ac.uk`

ESRU. (2013). *Basesimp foundation model.* Retrieved 14th of February 2013, from `www.esru.strath.ac.uk`

ESRU, & users, E.-r. (2006-2013). *Esp-r mailing list.* Retrieved 20th of January - 1st of June 2013, from `www.esru.strath.ac.uk`

Fundamentals of heat and mass transfer. (2007). John Wiley & sons.

Geissler, A. (2013, 9th of April). *slab-on-grade hydronic floor in a solar heating system.* email. (Email contact with Achim Geissler via the ESP-r user mailinglist)

Givoni, B. (1977). *Underground longterm storage of solar energy - an overview* (Tech. Rep.). Desert Research Insitute, Ben-Gurion University.

Google. (2013). *maps.* Retrieved 2nd of February 2013, from `www.maps.google.com`

Gundersen, P. (2005). Golv på grunnen med ringmur. varmeisolering, frostsikring og beregning av varmetap. In K. I. Edvardsen (Ed.), *Byggforskserien.*

Hand, J. (2013, 18th of April). *A question about ground heat transfer.* email. (Email contact with Dr. Jon Hand from the ESRU team via the ESP-r user mailinglist)

Joint Research Centre, IET. (2013). *Interactive access to solar resources and photvoltaic potential: Europe.* Retrieved 3rd of March 2013, from `http://re.jrc.ec.europa.eu/pvgis/`

Knoblich, K., Rammer, R., & Martin, G. (n.d.). Proceedings of the workshop on seasonal thermal energy storage in duct systems. In *Zeitschrift für angewandte geowissenschaften, volume 9.*

Krarti, & Choi. (1996). Simplified method for foundation heat loss calculation. *ASHRAE Transactions, 102: 140-152.*

Lovdata. (2010). *Byggteknisk forskrift - tek 10.* Retrieved 31st of January 2013, from `www.lovdata.no`

Moore, G. (1986). *Hot-2000 energy analysis program, soil temperature estimation model.* (This report was collected after email contact with Julia Purdy at Building Energy Simulation Research, Natural Resources Canada)

Myrtrøen, O.-J. F. (2006). *Analyses of heat exchange between a basement in a building and the ground.* Project thesis.

Nakhi, A. E. (1995). *Adaptive construction modelling within whole building dynamic simulation.* Unpublished doctoral dissertation, University of Strathclyde.

Novakovic, V., Hanssen, S. O., Thue, J. V., Wangsteen, I., & Gjerstad, F. O. (2007). *Enøk i bygninger.* Gyldendal.

Planning an installing solar thermal systems: A guide for installers, architects and engineers. (2005). James & James.

Professor Per Olaf Tjelflaat. (2013). *Department of energy and process engineering, ntnu. Modeling of heat exchange and analyses of energy use for a frost proof leisure building with active solar heating.* Personal contact.

Purdy, J. (2013, 3rd of June). *Moore model basesimp.* email. (Email contact with Julia Purdy from the National Resources Canada, via the ESP-r user mailinglist)

Reuss, M., Beck, M., & Müller, J. (1997). *Design of a seasonal thermal energy storage in the ground* (Tech. Rep.). Insititute of Agricultural Engineering, Technical University Munich.

Rockwool. (2013). *Frostmengde og årsmiddeltemperaturer.* Retrieved 4th of April 2013, from `http://www.rockwool.no/`

Shelton, J. (1974). *Underground storage of heat in solar heating systems* (Tech. Rep.). Physics Department, Williams College.

SINTEF. (2007). *Fornybar energi.* Retrieved 16th of February 2013, from `www.fornybar`

.no

SINTEF. (2011). *Byggforsk, vannskadekontoret* (Tech. Rep.). Author.

Solar water heating. (2006). New Society Publishers.

Spitler, J. (2013, 24th of May). *climate and snow.* email. (Email contact with Dr. Jeffrey Spitler via the ESP-r user mailinglist)

Statistisk sentralbyrå. (2013a). *Statistikkbanken: Emne: 10 næringsvirksomhet: Tabell: 03174: Eksisterende bygningsmasse. fritidsbygg, etter bygningstype (f).* Retrieved 15th of May 2013, from www.ssb.no

Statistisk sentralbyrå. (2013b). *Statistikkbanken: Emne 10: Næringsvirksomhet: Tabell 06952: Byggeareal. fritidsboliger (k).* Retrieved 15th of May 2013, from www.ssb.no

Teknisk Ukeblad Media AS. (2013). *leksikon: solinnstråling.* Retrieved 1st of June, 2013, from http://energilink.tu.no

TESS Components Libraries, General Descriptions [Computer software manual]. (2013).

Thermal Energy System Specialists, LLC. (2013a). *Tess libraries.* Retrieved 22nd of April 2013, from http://www.trnsys.com/

Thermal Energy System Specialists, LLC. (2013b). *What is trnsys?* Retrieved 22nd of April 2013, from http://www.trnsys.com/

Thevenard, D., Haddad, K., & Purdy, J. (2004). Development of a new solar collector

model in esp-r. In *Canadian solar building conference.*

University of Strathclyde, Energy Systems Research Unit. (2013). *Software: Esp-r.* Retrieved 5th of April 2013, from `www.esru.strath.ac.uk`

U.S. Department of Energy. (2012). *Home: Energy saver: Geothermal heat pumps.* Retrieved 16th of February 2013, from `energy.gov`

Appendix

Appendix A: Detailed description of the new model in ESP-r

Appendix A: Detailed description of the new model in ESP-r

A.1 Appendix comment

To allow for a replication of the simulation, the description of the model is restored as in ESP-r.

A.2 Location and climate

The model is located at latitude 63.18 with a longitude difference of 14.64 from the local time meridian. The year used in simulations is 2012 and weekends occur on Saturday and Sunday. The site exposure is typical city centre and the ground reflectance is 0.20.

The climate is: OSTERSUND/FROSON - SWE

Calculated ground temp at 0.5m depth
-1.9597 -5.0454 -5.8853 -5.1568 -0.99080 3.6750 8.0648 11.243 12.171 10.678 7.0813 2.5468

Calculated ground temp at 1.0m depth
-0.86512 -3.9428 -5.0408 -4.6372 -1.2336 2.8999 6.9788 10.134 11.347 10.349 7.3528 3.3290

Calculated ground temp at 2.0m depth
0.81430 -2.0766 -3.4534 -3.5032 -1.3041 1.8879 5.3212 8.2645 9.7855 9.5010 7.4716 4.3546

Calculated ground temp at 4.0m depth
2.6250 0.38079 -0.99802 -1.4214 -0.60971 1.2485 3.5568 5.8234 7.3466 7.7115 6.8402 5.0151

A.3 Controls

The model includes ideal controls as follows:
Control description: Base case control

Zones control includes 1 function.

The sensor for function 1 senses the temperature of the current zone. The actuator for function 1 is within ifloor0 in inner_zone_0. There have been 9 periods of validity defined during the year.

A.3.1 Control is valid Sun-01-Jan to Tue-31-Jan, 2013 with 3 periods.

```
Per|Start|Sensing|Actuating|Control law description

1  0.00 db temp   > flux      free floating

2 10.00 db temp   > flux      basic control:
                                   max heating capacity 260.0W
                                   min heating capacity 260.0W
                                   max cooling capacity 0.0W
                                   min cooling capacity 0.0W.
                                   Heating setpoint 100.00C
                                   cooling setpoint 100.00C.

3 15.00 db temp   > flux      free floating
```

A.3.2 Control is valid Wed-01-Feb to Tue-28-Feb, 2012 with 3 periods.

```
 Per|Start|Sensing|Actuating|Control law description

1  0.00 db temp   > flux      free floating

2  9.00 db temp   > flux      basic control:
                                   max heating capacity 491.0W
                                   min  heating capacity 491.0W
                                   max cooling capacity 0.0W
                                   min cooling capacity 0.0W.
                                   Heating setpoint 100.00C
                                   cooling setpoint 100.00C.

   3 17.00 db temp   > flux      free floating
```

A.3.3 Control is valid Thu-01-Mar to Sat-31-Mar, 2012 with 3 periods.

```
 Per|Start|Sensing|Actuating| Control law description

1  0.00 db temp   > flux      free floating

2  7.00 db temp   > flux      basic control:
                                   max heating capacity 550.0W
                                   min heating capacity 550.0W
                                   max cooling capacity 0.0W
```

```
                                    min cooling capacity 0.0W.
                                    Heating setpoint 100.00C
                                    cooling setpoint 100.00C.

3 18.00 db temp   > flux      free floating
```

A.3.4 Control is valid Sun-01-Apr to Mon-30-Apr, 2012 with 3 periods.

```
Per|Start|Sensing |Actuating| Control law description

1  0.00 db temp   > flux      free floating

2  6.00 db temp   > flux      basic control:
                                    max heating capacity 548.0W
                                    min heating capacity 548.0W
                                    max cooling capacity 0.0W
                                    min cooling capacity 0.0W.
                                    Heating setpoint 100.00C
                                    cooling setpoint 100.00C.

3 19.00 db temp   > flux      free floating
```

A.3.5 Control is valid Tue-01-May to Fri-31-Aug, 2012 with 3 periods.

```
Per|Start|Sensing|Actuating | Control law description

1  0.00 db temp   > flux      free floating

2  5.00 db temp   > flux      basic control:
                                    max heating capacity 0.0W
                                    min heating capacity 0.0W
                                    max cooling capacity 0.0W
                                    min cooling capacity 0.0W
                                    Heating setpoint 100.00C
                                    cooling setpoint 100.00C.

3 20.00 db temp   > flux      free floating
```

A.3.6 Control is valid Sat-01-Sep to Sun-30-Sep, 2012 with 3 periods.

```
 Per|Start|Sensing  |Actuating|Control law description

1  0.00 db temp   > flux      free floating
```

2 7.00 db temp > flux basic control:
max heating capacity 432.0W
min heating capacity 432.0W
max cooling capacity 0.0W min
cooling capacity 0.0W.
Heating setpoint 100.00C
cooling setpoint 100.00C.

3 18.00 db temp > flux free floating

A.3.7 Control is valid Mon-01-Oct to Wed-31-Oct, 2012 with 3 periods.

Per|Start|Sensing|Actuating| Control law description

1 0.00 db temp > flux free floating

2 8.00 db temp > flux basic control:
max heating capacity 370.0W
min heating capacity 370.0W
max cooling capacity 0.0W min
cooling capacity 0.0W.
Heating setpoint 100.00C
cooling setpoint 100.00C.

3 17.00 db temp > flux free floating

A.3.8 Control is valid Thu-01-Nov to Fri-30-Nov, 2012 with 3 periods.

Per|Start|Sensing |Actuating| Control law description

1 0.00 db temp > flux free floating

2 9.00 db temp > flux basic control:
max heating capacity 321.0W
min heating capacity 321.0W
max cooling capacity 0.0W min
cooling capacity 0.0W.
Heating setpoint 100.00C
cooling setpoint 100.00C.

3 15.00 db temp > flux free floating

A.3.9 Control is valid Sat-01-Dec to Mon-31-Dec, 2012 with 3 periods.

Per	Start	Sensing	Actuating	Control law description
1	0.00	db temp	> flux	free floating
2	11.00	db temp	> flux	basic control: max heating capacity 250.0W min heating capacity 250.0W max cooling capacity 0.0W min cooling capacity 0.0W. Heating setpoint 100.00C cooling setpoint 100.00C.
3	14.00	db temp	> flux	free floating

A.3.10 Control loop linkages

Zone to control loop linkages:

```
 zone ( 1) inner_zone_0 << control  1
 zone ( 2) soth_zone_0  << control  0
 zone ( 3) north_zone_0 << control  0
 zone ( 4) south_zone_1 << control  0
 zone ( 5) north_zone_1 << control  0
 zone ( 6) inner_zone_1 << control  0
 zone ( 7) basement     << control  0
```

A.4: Zones

ID	Zone Name	Volume m^3	Surface No.	Opaque	Transp	~Floor
1	inner_zone_0	12.5	6	32.5	0.0	6.3
2	south_zone_0	56.0	8	91.0	11.0	28.0
3	north_zone_0	59.5	10	108.5	11.0	29.8
4	south_zone_1	112.0	9	100.4	47.6	28.0
5	north_zone_1	119.0	10	157.5	22.0	29.8

6	inner_zone_1	25.0	6	52.5	0.0	6.3
7	basement	128.0	8	192.0	0.0	64.0
	all	512.	57	734.	92.	192.

A.4.1 Geometry and attribution details for inner_zone_0

Zone inner_zone_0 (1) is composed of 6 surfaces and 8 vertices. It encloses a volume of 12.5m^3 of space, with a total surface area of 32.5m^2 & user edited floor area of 6.25m^2

A summary of the surfaces in inner_zone_0(1) follows:

Sur | Area |Azim |Elev|surface|geom|constr env |m^2 |deg |deg | name|optical|locat| use | name |other side
1 5.00 180. 0. south0 OPAQUE VERT PARTN internal_wal ||< north0_part:soth_zone_0
2 5.00 90. 0. east0 OPAQUE VERT PARTN internal_wal ||< east0_in:north_zone_0
3 5.00 0. 0. north0 OPAQUE VERT PARTN internal_wal ||< north0_in:north_zone_0
4 5.00 270. 0. west0 OPAQUE VERT PARTN internal_wal ||< west0_in:north_zone_0
5 6.25 0. 90. roof0 OPAQUE CEIL PARTN fl_seperatio ||< floor1:inner_zone_1
6 6.25 0. -90. ifloor0 OPAQUE FLOR FLOOR new02_ifloor ||< floor0:basement

All surfaces will receive diffuse insolation (if shading not calculated).

Notes: nothing happens in this zone in terms of occupants lights and small power. There is not infiltration or ventilation.

A.4.2 Geometry and attribution details for south_zone_0

Zone south_zone_0 (2) is composed of 8 surfaces and 12 vertices. It encloses a volume of 56.0m^3 of space, with a total surface area of 102.m^2 & approx floor area of 28.0m^2. There is 30.000m2 of exposed surface area, 30.000m2 of which is vertical. Outside walls are 107.14 % of floor area & average U of 0.128 & UA of 3.8398

A summary of the surfaces in south_zone_0(2) follows:

Sur	Area	Azim	Elev	surface	geom	constr	env
	m^2	deg	deg	name	optical	locat	use	name	other side
1	16.0	180.	0.	south0	OPAQUE	VERT	WALL	0ext_wall	||< external
2	7.00	90.	0.	east0	OPAQUE	VERT	WALL	0ext_wall	||< external
3	7.00	270.	0.	west0	OPAQUE	VERT	WALL	0ext_wall	||< external
4	28.0	0.	90.	roof0	OPAQUE	CEIL	-	fl_seperatio	||< floor1:south_zone_1
5	28.0	0.	-90.	sfloor0	OPAQUE	FLOR	FLOOR	base_floor	||< floor0:basement
6	5.00	0.	0.	north0_part	OPAQUE	VERT	PARTN	internal_inv	||< south0:inner_zone_0
7	9.00	0.	0.	north0_west	DCF7671_	VERT	PARTN	part_wall	||< south0_west:north_zone_0
8	2.00	0.	0.	north0_east	DCF7671_	VERT	PARTN	part_wall	||< south0_east:north_zone_0

All surfaces will receive diffuse insolation (if shading not calculated).

Surface sfloor0 has a nonsymmetric construction base_floor. It faces floor0 which is composed of base_floor.

Notes: nothing happens in this zone in terms of occupants lights and small power. There is not infiltration or ventilation.

A.4.3 Geometry and attribution details for north_zone_0

Zone north_zone_0 (3) is composed of 10 surfaces and 16 vertices. It encloses a volume of 59.5m^3 of space, with a total surface area of 120.m^2 & approx floor area of 29.8m^2. There is 34.000m2 of exposed surface area, 34.000m2 of which is vertical. Outside walls are 114.29 % of floor area & average U of 0.128 & UA of 4.3518

A summary of the surfaces in north_zone_0(3) follows:

```
Sur| Area |Azim |Elev|surface|geom|constr env
|m^2 |deg |deg | name|optical|locat| use | name|other side

  1  9.00    180.   0. south0_west  DCF7671_ VERT PARTN
part_wall    ||< north0_west:south_zone_0

  2  5.00     90.   0. west0_in     OPAQUE   VERT PARTN
internal_inv ||< west0:inner_zone_0

  3  5.00    180.   0. north0_in    OPAQUE   VERT PARTN
internal_inv ||< north0:inner_zone_0

  4  5.00    270.   0. east0_in     OPAQUE   VERT PARTN
internal_inv ||< east0:inner_zone_0

  5  2.00    180.   0. south0_east  DCF7671_ VERT PARTN
part_wall    ||< north0_east:soth_zone_0

  6  9.00     90.   0. east0        OPAQUE   VERT WALL
0ext_wall    ||< external

  7  16.0      0.   0. north0       OPAQUE   VERT WALL
0ext_wall    ||< external

  8  9.00    270.   0. west0        OPAQUE   VERT WALL
0ext_wall    ||< external

  9  29.8      0.  90. roof0        OPAQUE   CEIL PARTN
fl_seperatio ||< floor1:north_zone_1

 10  29.8      0. -90. nfloor0      OPAQUE   FLOR FLOOR
base_floor   ||< floor_n0:basement
```

All surfaces will receive diffuse insolation (if shading not calculated).

Surface nfloor0 has a nonsymmetric construction base_floor. It faces floor_n0 which is composed of base_floor.

Notes: nothing happens in this zone in terms of occupants lights and smallpower. There is not infiltration or ventilation.

A.4.4 Geometry and attribution details for south_zone_1

Zone south_zone_1 (4) is composed of 9 surfaces and 16 vertices. It encloses a volume of 112.m^3 of space, with a total surface area of 148.m^2 & user edited floor area of 28.0m^2 There is 88.000m2 of exposed surface area, 60.000m2 of which is vertical. Outside walls are 122.86 % of floor area & average U of 0.806 & UA of 27.710 Flat roof is 100.00 % of floor area & average U of 0.052 & UA of 1.4681. Glazing is 91.428 % of floor & 42.667 % facade with average U of 1.458 & UA of 37.329

A summary of the surfaces in south_zone_1(4) follows:

```
Sur| Area |Azim |Elev|surface|geom|constr env
|m^2 |deg |deg | name|optical|locat| use | name|other side

  1  6.40    180.   0. south1       OPAQUE   VERT WALL
1external_wa ||< external

  2  14.0     90.   0. east1        OPAQUE   VERT WALL
1external_wa ||< external

  3  14.0    270.   0. west1        OPAQUE   VERT WALL
1external_wa ||< external

  4  28.0      0.  90. roof1        OPAQUE   CEIL ROOF  roof
||< external

  5  28.0      0. -90. floor1       OPAQUE   FLOR PARTN
fl_seperatio ||< roof0:soth_zone_0

  6  25.6    180.   0. win_south    DAG6349_ VERT C-WIN window
||< external
  7  10.0      0.   0. north1_part  OPAQUE   VERT PARTN
internal_inv ||< south1:inner_zone_1

  8  18.0      0.   0. north1_west  DCF7671_ VERT PARTN
part_wall    ||< south1_west:north_zone_1

  9  4.00      0.   0. north1_east  DCF7671_ VERT PARTN
part_wall    ||< south1_east:north_zone_1
```

All surfaces will receive diffuse insolation (if shading not calculated).

Notes: nothing happens in this zone in terms of occupants lights and small power. There is not infiltration or ventilation.

A.4.5 Geometry and attribution details for north_zone_1

Zone north_zone_1 (5) is composed of 10 surfaces and 16 vertices. It encloses a volume of 119.m^3 of space, with a total surface area of 180.m^2 & approx floor area of 29.8m^2
There is 97.750m2 of exposed surface area, 68.000m2 of which is vertical. Outside walls are 228.57 % of floor area & average U of 0.806 & UA of 54.776. Flat roof is 100.00 % of floor area & average U of 0.052 & UA of 1.5599.

A summary of the surfaces in north_zone_1(5) follows:

Sur	Area	Azim	Elev	surface	geom	constr	env
	m^2	deg	deg	name	optical	locat	use	name	other side
1	18.0	180.	0.	south1_west	DCF7671_	VERT	-	part_wall	||< north1_west:south_zone_1
2	10.0	90.	0.	west1_in	OPAQUE	VERT	PARTN	internal_inv	||< west1:inner_zone_1
3	10.0	180.	0.	north1_in	OPAQUE	VERT	PARTN	internal_inv	||< north1:inner_zone_1
4	10.0	270.	0.	east1_in	OPAQUE	VERT	PARTN	internal_inv	||< east1:inner_zone_1
5	4.00	180.	0.	south1_east	DCF7671_	VERT	-	part_wall	||< north1_east:south_zone_1
6	18.0	90.	0.	east1	OPAQUE	VERT	WALL	1external_wa	||< external
7	32.0	0.	0.	north1	OPAQUE	VERT	WALL	1external_wa	||< external
8	18.0	270.	0.	west1	OPAQUE	VERT	WALL	1external_wa	||< external
9	29.8	0.	90.	roof1	OPAQUE	CEIL	ROOF	roof	||< external
10	29.8	0.	-90.	floor1	OPAQUE	FLOR	PARTN	fl_seperatio	||< roof0:north_zone_0

All surfaces will receive diffuse insolation (if shading not calculated).

Notes: nothing happens in this zone in terms of occupants lights and small power. There is not infiltration or ventilation.

A.4.6 Geometry and attribution details for inner_zone_1

Zone inner_zone_1 (6) is composed of 6 surfaces and 8 vertices. It encloses a volume of 25.0m^3 of space, with a total surface area of 52.5m^2 & approx floor area of 6.25m^2. There is 6.2500m2 of exposed surface area. Flat roof is 100.00 % of floor area & average U of 0.052 & UA of 0.32771.

A summary of the surfaces in inner_zone_1(6) follows:

Sur	Area m^2	Azim deg	Elev deg	surface name	geom optical	constr locat	env use	name other side
1	10.0	180.	0.	south1	OPAQUE	VERT	PARTN	internal_wal ||< north1_part:south_zone_1
2	10.0	90.	0.	east1	OPAQUE	VERT	PARTN	internal_wal ||< east1_in:north_zone_1
3	10.0	0.	0.	north1	OPAQUE	VERT	PARTN	internal_wal ||< north1_in:north_zone_1
4	10.0	270.	0.	west1	OPAQUE	VERT	PARTN	internal_wal ||< west1_in:north_zone_1
5	6.25	0.	90.	roof1	OPAQUE	CEIL	ROOF	roof ||< external
6	6.25	0.	-90.	floor1	OPAQUE	FLOR	PARTN	fl_seperatio ||< roof0:inner_zone_0

All surfaces will receive diffuse insolation (if shading not calculated).

Notes: nothing happens in this zone in terms of occupants lights and small power. There is not infiltration or ventilation.

A.4.7 Geometry and attribution details for basement

Zone basement (7) is composed of 8 surfaces and 14 vertices. It encloses a volume of 128.m^3 of space, with a total surface area of 192.m^2 & approx floor area of 64.0m^2.

A summary of the surfaces in basement(7) follows:

```
Sur| Area |Azim |Elev|surface|geom|constr env
|m^2 |deg |deg | name|optical|locat| use | name|other side

  1  16.0    180.   0. Wall-1       OPAQUE   VERT -
0base_wall   ||< BASESIMP config type  24

  2  16.0     90.   0. Wall-2       OPAQUE   VERT -
0base_wall   ||< BASESIMP config type  24

  3  16.0      0.   0. Wall-3       OPAQUE   VERT -
0base_wall   ||< BASESIMP config type  24

  4  16.0    270.   0. Wall-4       OPAQUE   VERT -
0base_wall   ||< BASESIMP config type  24

  5  64.0      0. -90. Base-6       OPAQUE   FLOR -
0base_floor  ||< BASESIMP config type  24

  6  6.25      0.  90. floor0       OPAQUE   CEIL FLOOR
new02_ifloor ||< ifloor0:inner_zone_0

  7  28.0      0.  90. floor0       OPAQUE   CEIL FLOOR
base_floor   ||< sfloor0:soth_zone_0

  8  29.8      0.  90. floor_n0     OPAQUE   CEIL FLOOR
base_floor   ||< nfloor0:north_zone_0
```

All surfaces will receive diffuse insolation (if shading not calculated).

Notes: nothing happens in this zone in terms of occupants lights and small power. There is not infiltration or ventilation.

A.5 Constructions

A.5.1 Construction areas

Project floor area is 192.00m2, wall area is 166.40m2, window area is 25.600m2. Sloped roof area is 0.00m2, flat roof area is 64.000m2, skylight area is 0.00m2. In contact with ground 0.00m2. There is 256.00m2 of outside surface area, 192.00m2 of which is vertical. Outside walls are 86.667 % of floor area & average U of 0.545 & UA of 90.677 & max MLC thickness 0.500
Flat roof is 33.333 % of floor area & average U of 0.052 & UA of 3.3557. Glazing is 13.333 % of floor & 13.333 % facade with average U of 1.458 & UA of 37.329.

A.5.2 Construction details: roof

Multi-layer constructions used:

Details of opaque construction: roof and overall thickness 0.810

Layer	Matr	Thick (mm)	Conduc-tivity	Density db	Specif heat	IR emis	Solar abs	Diffu resis	R m^2K/W	Description
Ext	234	300.0	0.049	110.	1.	0.90	0.13	10.	6.12	snow: snow
2	64	160.0	0.140	419.	2720.	0.90	0.65	12.	1.14	fir: Fir (20% mc)
Int	205	350.0	0.030	30.	837.	0.90	0.50	90.	11.67	Polyurethane foam bd: Polyurethane foam board

ISO 6946 U values (horiz/upward/downward heat flow)= 0.052 0.052 0.052 (partition) 0.052

A.5.3 Construction details: 1external_wall

Details of opaque construction: 1external_wa and overall thickness 0.150

Layer	Matr	Thick (mm)	Conduc-tivity	Density db	Specif heat	IR emis	Solar abs	Diffu resis	R m^2K/W	Description
1	64	150.0	0.140	419.	2720.	0.90	0.65	12.	1.07	fir : Fir (20% mc)

ISO 6946 U values (horiz/upward/downward heat flow)= 0.806 0.825 0.780 (partition) 0.751

A.5.4 Construction details: internal_wall

Details of opaque construction: internal_wal linked to internal_inv & with overall thickness 0.350

Layer|Matr|Thick |Conduc-|Density|Specif|IR |Solar|Diffu| R |Description |db |(mm) |tivity | |heat|emis|abs|resis|m^2K/W

Ext 205 250.0 0.030 30. 837. 0.90 0.50 90. 8.33 Polyurethane foam bd : Polyurethane foam board

Int 32 100.0 1.400 2100. 653. 0.90 0.65 19. 0.07 heavy mix concrete : Heavy mix concrete

ISO 6946 U values (horiz/upward/downward heat flow)= 0.117 0.117 0.116 (partition) 0.115

A.5.5 Construction details: window

Details of transparent construction: window with DAG6349_06nb optics and overall thickness 0.028

Layer|Matr|Thick |Conduc-|Density|Specif|IR |Solar|Diffu| R |Description |db |(mm) |tivity | |heat|emis|abs|resis|m^2K/W

Ext 242 6.0 0.760 2710. 837. 0.83 0.05 19200. 0.01 plate glass : Plate glass with placeholder single layer optics

2 0 16.0 0.000 0. 0. 0.99 0.99 1. 0.50 air 0.50 0.50 0.50

Int 242 6.0 0.760 2710. 837. 0.83 0.05 19200. 0.01 plate glass : Plate glass with placeholder single layer optics

ISO 6946 U values (horiz/upward/downward heat flow)= 1.458 1.525 1.378 (partition) 1.289

A.5.6 Construction details: partition_wall

Details of transparent construction: part_wall with DCF7671_06nb optics and overall thickness 0.024

Layer|Matr|Thick |Conduc-|Density|Specif|IR |Solar|Diffu| R |Description |db |(mm) |tivity | |heat|emis|abs|resis|m^2K/W

Ext 242 6.0 0.760 2710. 837. 0.83 0.05 19200. 0.01 plate glass : Plate glass with placeholder single layer optics

2 0 12.0 0.000 0. 0. 0.99 0.99 1. 0.17 air 0.17 0.17 0.17

Int 242 6.0 0.760 2710. 837. 0.83 0.05 19200. 0.01 plate glass : Plate glass with placeholder single layer optics

ISO 6946 U values (horiz/upward/downward heat flow)= 2.811 3.069 2.527 (partition) 2.243

A.5.7 Construction details: floor_separation

Details of opaque construction: fl_seperatio and overall thickness 0.150

Layer|Matr|Thick |Conduc-|Density|Specif|IR |Solar|Diffu| R |Description |db |(mm) |tivity | |heat|emis|abs|resis|m^2K/W

1 32 150.0 1.400 2100. 653. 0.90 0.65 19. 0.11 heavy mix concrete : Heavy mix concrete

ISO 6946 U values (horiz/upward/downward heat flow)= 3.608 4.046 3.153 (partition) 2.724

A.5.8 Construction details: 0external_wall

Details of opaque construction: 0ext_wall and overall thickness 0.500

Layer|Matr|Thick |Conduc-|Density|Specif|IR |Solar|Diffu| R |Description |db |(mm) |tivity | |heat|emis|abs|resis|m^2K/W

Ext 32 200.0 1.400 2100. 653. 0.90 0.65 19. 0.14 heavy mix concrete : Heavy mix concrete

Int 211 300.0 0.040 250. 840. 0.90 0.30 4. 7.50 glasswool : Glasswool (generic)
ISO 6946 U values (horiz/upward/downward heat flow)= 0.128 0.128 0.127 (partition) 0.127

A.5.9 Construction details: base_floor

Details of opaque construction: base_floor and overall thickness 0.500

Layer|Matr|Thick |Conduc-|Density|Specif|IR |Solar|Diffu| R |Description |db |(mm) |tivity | |heat|emis|abs|resis|m^2K/W

Ext 214 250.0 0.030 25. 1000. 0.90 0.30 67. 8.33
EPS : EPS (expanded polystyrene)

Int 32 250.0 1.400 2100. 653. 0.90 0.65 19. 0.18
heavy mix concrete : Heavy mix concrete

ISO 6946 U values (horiz/upward/downward heat flow)= 0.115 0.116 0.115 (partition) 0.114

A.5.10 Construction details: internal_wall

Details of opaque construction: internal_inv linked to internal_wal & with overall thickness 0.350

Layer|Matr|Thick |Conduc-|Density|Specif|IR |Solar|Diffu| R |Description |db |(mm) |tivity | |heat|emis|abs|resis|m^2K/W

Ext 32 100.0 1.400 2100. 653. 0.90 0.65 19. 0.07
heavy mix concrete : Heavy mix concrete

Int 205 250.0 0.030 30. 837. 0.90 0.50 90. 8.33
Polyurethane foam bd : Polyurethane foam board

ISO 6946 U values (horiz/upward/downward heat flow)= 0.117 0.117 0.116 (partition) 0.115

A.5.11 Construction details: 0base_floor

Details of opaque construction: 0base_floor and overall thickness 0.100

Layer|Matr|Thick |Conduc-|Density|Specif|IR |Solar|Diffu| R |Description |db |(mm) |tivity | |heat|emis|abs|resis|m^2K/W

Ext 32 50.0 1.400 2100. 653. 0.90 0.65 19. 0.04
heavy mix concrete : Heavy mix concrete

Int 32 50.0 1.400 2100. 653. 0.90 0.65 19. 0.04
heavy mix concrete : Heavy mix concrete

ISO 6946 U values (horiz/upward/downward heat flow)= 4.142
4.730 3.553 (partition) 3.017

A.5.12 Construction details: 0base_wall

Details of opaque construction: 0base_wall and overall thickness
0.300

Layer|Matr|Thick |Conduc-|Density|Specif|IR |Solar|Diffu| R
|Description |db |(mm) |tivity | |heat|emis|abs|resis|m^2K/W

Ext 32 200.0 1.400 2100. 653. 0.90 0.65 19. 0.14
heavy mix concrete : Heavy mix concrete

Int 211 100.0 0.040 250. 840. 0.90 0.30 4. 2.50
glasswool : Glasswool (generic)

ISO 6946 U values (horiz/upward/downward heat flow)= 0.356
0.359 0.351 (partition) 0.344

A.5.13 Construction details: new02_ifloor

Details of opaque construction: new02_ifloor and overall
thickness 1.500

Layer|Matr|Thick |Conduc-|Density|Specif|IR |Solar|Diffu| R
|Description |db |(mm) |tivity | |heat|emis|abs|resis|m^2K/W

Ext 50 300.0 1.400 9000. 1524. 0.90 0.65 19. 0.21
ground01 : Heavy mix concrete (copy of heavy mix concrete)

2 50 300.0 1.400 9000. 1524. 0.90 0.65 19. 0.21
ground01 : Heavy mix concrete (copy of heavy mix concrete)

3 50 300.0 1.400 9000. 1524. 0.90 0.65 19. 0.21
ground01 : Heavy mix concrete (copy of heavy mix concrete)

4 50 300.0 1.400 9000. 1524. 0.90 0.65 19. 0.21
ground01 : Heavy mix concrete (copy of heavy mix concrete)

Int 50 300.0 1.400 9000. 1524. 0.90 0.65 19. 0.21
ground01 : Heavy mix concrete (copy of heavy mix concrete)

ISO 6946 U values (horiz/upward/downward heat flow)= 0.806
0.825 0.780 (partition) 0.751

Appendix B: Solar radiation data from ESP-r

Appendix B: Solar radiation data from ESP-r

B.1 Appendix comment

Direct normal solar radiation and diffuse horizontal radiation for each month, and an average time interval per month.

This data has been used to determine the periods and time intervals for when heat is injected into the ground under the inner zone.

B.2 Solar radiation data from ESP-r

Period 1 and 2

	January		*February*	
kl	Diffuse horizontal radiation mean (W/m2)	Direct normal radiation mean (W/m2)	Diffuse horizontal radiation mean (W/m2)	Direct normal radiation mean (W/m2)
8			1	0
9			14,1	2,1
10	5,5	0,5	42,1	24,4
11	23,5	32	67,3	93,9
12	34,2	88,1	82,1	133,9
13	35,5	97,9	86,6	127,4
14	27,4	71,1	82,9	120,5
15	10,9	36,4	59,4	99,5
16	1,3	0	31,2	25,2
17			5,8	0,5

Period 3 and 4

kl	*March* Diffuse horizontal radiation mean (W/m2)	*March* Direct normal radiation mean (W/m2)	*April* Diffuse horizontal radiation mean (W/m2)	*April* Direct normal radiation mean (W/m2)
5			4,4	0
6	0,4	0	32,8	22,4
7	10	16,2	69,3	158,1
8	36,9	112,9	111,9	244,8
9	67,8	197,5	140,9	313,1
10	90,6	259,3	160,8	337,7
11	115,9	301	195,5	348,6
12	126,5	323,3	213,2	347,4
13	126,1	325,1	206,4	331,9
14	119,5	303,8	207,5	341,8
15	103,3	259,3	177	360,3
16	73,8	206	142,2	343,6
17	46,4	169,5	108,1	299,7
18	18,3	62,7	70,5	194,7
19	1,6	0	31,1	40,2
20			4,3	0

Period 5

kl	*May* Diffuse horizontal radiation mean (W/m2)	*May* Direct normal radiation mean (W/m2)	*June* Diffuse horizontal radiation mean (W/m2)	*June* Direct normal radiation mean (W/m2)
3	0,3		3,7	0
4	8,2		17,4	0
5	33,5	61,2	53,2	24,5
6	83	136,1	96,5	76,7
7	125,2	222,2	133,8	123,7
8	159,3	313,2	183,5	177,1
9	182,2	371,9	209,5	240,6
10	214,9	359,3	235,8	262
11	232	391,3	261,8	314,1
12	254,9	379,8	265,1	359,2
13	256,3	356,9	255,4	382,3
14	244,7	373,8	245,1	405,1
15	221,5	362,5	228,3	398
16	192,2	318,7	202,7	364,9
17	164,2	273,3	188	291,9
18	126,8	200,5	150,7	215,6
19	78,6	113,8	108	112,5
20	37,4	19,7	63,5	32,6
21	7,8		22,4	0
22	0,3		4,7	0

Period 5 continues

kl	*July* Diffuse horizontal radiation mean (W/m2)	*July* Direct normal radiation mean (W/m2)	*August* Diffuse horizontal radiation mean (W/m2)	*August* Direct normal radiation mean (W/m2)
3	0,9	0	0,3	0
4	10,2	0	7	0
5	37,5	10,3	35,3	0
6	85,5	39,6	85,1	13,3
7	137,6	88	141,7	46,7
8	183,1	186,5	185,4	128,5
9	212,1	273,2	211,9	208,8
10	227,6	337,7	228,8	265,8
11	249,8	373,1	241,4	317,3
12	264,5	382,1	237,7	326,2
13	268,5	367,4	236,8	316,5
14	267	384	223,9	310,5
15	245,3	380	197,3	272,1
16	217,6	337,1	154,2	199,8
17	196,4	273,4	102,9	146,8
18	154,2	192,7	46,8	68,3
19	108,4	79,9	11,8	15,7
20	54,7	16,2	0,8	0
21	16,1	0		
22	2,2	0		

Period 6 and 7

kl	*September*		*October*	
	Diffuse horizontal radiation mean (W/m2)	Direct normal radiation mean (W/m2)	Diffuse horizontal radiation mean (W/m2)	Direct normal radiation mean (W/m2)
6	4,3	0		
7	30,2	20,1	1,6	
8	76,8	108	19,8	28
9	123,9	166,2	56,5	119,2
10	156,5	200,1	81,1	195,4
11	175	237,6	99,8	259,4
12	177	257,3	109	272,6
13	175	238,6	105,9	246,8
14	166	245,5	95,3	210,2
15	148,3	211,1	69,5	147,2
16	115,2	154,8	36,9	49,7
17	73,3	85,2	8,6	0,1
18	29,8	15	0,2	
19	4,6	0		

Period 8 and 9

kl	*November* Diffuse horizontal radiation mean (W/m2)	Direct normal radiation mean (W/m2)	*December* Diffuse horizontal radiation mean (W/m2)	Direct normal radiation mean (W/m2)
9	5,6	1,3		
10	23,6	20,2	1,3	
11	40,2	79,1	15,7	5,8
12	51,5	84,5	25,2	46,5
13	48,2	85	24,6	40,6
14	36,4	76,4	14,3	1,4
15	16	13,2	0,3	
16	1,5			

Appendix C: Solar radiation data from PVGIS

Appendix C: Solar radiation data from PVGIS

C.1 Appendix comment

Solar radiation for different angles.

REF: http://re.jrc.ec.europa.eu/pvgis/apps4/pvest.php#

C.2 Solar radiation data from PVGIS

Month	H horizontal plane (Wh/m2/day)	H optimal angle (45°) (Wh/m2/day)	H(70°) (Wh/m2/day)	Inclination optimal (degrees)
Jan	173	603	721	82
Feb	769	1930	2180	75
Mar	1940	3270	3360	62
Apr	3420	4290	3960	44
May	4810	5140	4400	30
Jun	5310	5250	4350	24
Jul	4730	4780	4010	24
Aug	3420	3810	3370	35
Sep	1980	2730	2640	52
Oct	926	1730	1850	67
Nov	297	911	1070	79
Dec	81,8	341	416	84
Year	2330	2900	2690	45

Appendix D: Moore method, ground temperature estimation model

An article by Glenn Moore from 1986 is attached below. It describes the ground temperature estimation model used for the BASESIMP configuration. This article was obtained from Julia Purdy at National Resources Canada (Purdy, 2013).

HOT-2000 ENERGY ANALYSIS PROGRAM

Soil Temperature Estimation Model

Prepared for: R-2000 Homes Program
Energy, Mines and Resources, Canada

Prepared by : Glenn Moore
7 July 1986

1.0 Introduction

This soil temperature estimation model was developed to assist the HOT-2000 energy analysis computer program. HOT-2000 currently simulates the energy performance of air, water and ground source space heating heat pumps. To improve the accuracy of ground source heat pumps, it is necessary to know the temperature profile of the soil at a specified depth (dependant on heat pump placement).

To estimate soil temperatures for a given location, this model uses two weather parameters from the HOT-2000 weather files. These two parameters are the location's average monthy ambient dry air temperature and its annual heating degree days. From this information, the model can estimate the temperature of the soil for any given depth at any time of the year. The simplified weather requirements allow this model to be applied universally.

This paper outlines the methodology and derivation of the model and how it is able to estimate these soil temperatures at various depths. A statistical analysis of the estimated soil temperatures to the actual data is presented in the conclusion of the report.

2.0 Temperature Profile Function

The first step in developing the mathematical model was to decide on an appropriate time function to represent the temperatures of the soil during the year for any particular depth. It was found that a simple cosine function could be used to create this temperature profile. Test data acquired from Agricultural Canada Tech Bulletin 85 (1) confirmed that the temperature profile closely matched a cosine function.

A cosine curve needs only three variables to completely describe itself.

Referring to Fig.1, "A" represents the mean temperature. This is a temperature in which one half the cosine curve lies above and one half lies below. "B" is the amplitude of the curve, or a measure of how much the temperature oscillates. "P" is the phase shift angle, and measures the amount the curve is shifted to the right.

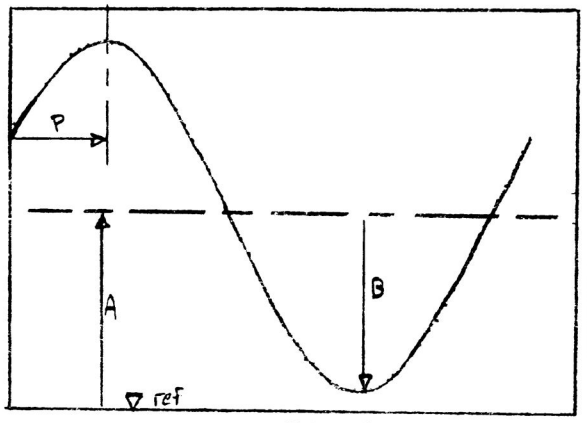

Fig.1

Thus the equation can be written as;

$$T = A - B * \cos(2 * Pi * n / 8766 - P) \quad (1)$$

where:

T = temperature of soil at given depth and time of year (C)
A = mean temperature of soil (C)
B = soil temperature amplitude at given depth (C)
Pi = 3.1415927
n = number of hours into year (8766 hours/year)
P = phase angle at given depth (degrees)

With knowledge of A, B & P at a specified depth, the soil temperature for any time during the year can be estimated.

2.1 Soil Temperature Modeling Proceedures

HOT-2000 weather files store the average monthly ambient dry air temperatures for each location. The heating degree days are also stored. With this information the following procedure was adopted:

1. The average monthy ambient dry air temperatures are fitted to a cosine curve using a least squares technique as developed in Kusuda & Achenbach (2). For a complete description of this technique, refer to Appendix A. Thus an Aa, Ba & Pa value is obtained.

2. It is an incorrect assumption to assume the temperature profile of the soil at the surface of the ground matches the ambient dry air temperature profile. A difference exists for such factors as direct sunshine heating the ground faster than air and snow in the winter insulating the ground against severe cold air. Using three correlations involving degree days, an As, Bs & Ps value is obtained for the soil at the surface. The development of these correlations is described in section 2.4. As, Bs & Ps represent the modified values of the Aa, Ba & Pa values extracted from the air in step 1.

3. With the temperature profile defined at the ground surface, the next step is to determine the corresponding temperature profile for any depth. As the depth of the ground increases, the mean soil temperature approaches a constant value. Between the surface and a 3 meter depth, the temperature amplitude decreases and the phase shift angle shifts more to the right (increases). The diffusivity of the soil will determine how much the amplitude decreases and how much the phase shift increases. The diffusivity is a measure of how well the soil conducts heat. This differs at each location, depending on soil composition and presence of moisture. Correlations, again involving degree days are used to find the diffusivity of the soil at any particular degree day location. The development of these correlations is discussed in section 2.3.4. With this information found, the following equation can now be applied;

$$T(x) = As - Bs*b * \cos(2 * Pi * n / 8766 - Ps - p) \quad (2)$$

where:

T(x) = temperature of soil at depth x (C)
As = mean temperature of soil at surface (C)
Bs = soil temperature amplitude at surface (C)
" b = decrease in amplitude for depth x
Pi = 3.1415927
n = number of hours into year (8766 hours/year)
Ps = phase angle at surface
" p = shift in phase angle for depth x

" - determined by diffusivity.

2.2 Test Data

Fourty-eight locations across Canada where selected from Bulletin 85. These locations were selected, as their monthly ambient dry air temperatures and degree day values were available from the HOT-2000 weather files. For each location, twelve monthly average soil temperatues for six different depths were obtained from Bulletin 85. The depths were 1cm, 10cm, 20cm, 50cm, 100cm and 150cm from the surface. A list of these locations with their corresponding degree days is presented in Appendix C.

2.3 Determining Location Soil Diffusivity

2.3.1 Calculated Diffusivity By Depth

For each of the 48 locations, a cosine curve was fitted to each of the six depths. Thus a value of A, B & P were obtained for each of the depth. From this information, the diffusivity of the soil at each location could next be calculated. This was calculated using the technique described in Kusuda & Achenbach (1). This method assumes homogeneous soil composition and

permeability. In reality, soil is rarely homogeneous, but the effects of this assumption do not severely distort the average monthy derived soil temperatures.

Using this technique the diffusivity was calculated in two ways. One was from the decrease in cyclic temperature amplitude and the other by the increase in the phase angle. Both methods compared the changes against a given depth increase.

The 1cm depth was chosen as a reference depth and the amplitude decreases and phase angle increases of the remaining five depths were used to calculate five sets of diffusivities. The 1cm depth was chosen as a reference simply because it is the closest to the ground surface, which is used as the model reference depth (as described in section 2.1). Thus;

$$D1 = (Pi/8766) * ((X/\ln(Bo/B))^2 \quad (3)$$

and

$$D2 = (Pi/8766) * ((X/(P-Po))^2 \quad (4)$$

where:

D1 = amplitude diffusivity at given depth (m^2/h)
D2 = phase diffusivity at given depth (m^2/h)
Pi = 3.1415927
X = (ground depth - .01) (m)
Bo = amplitude of temperature curve at 1cm depth (C)
Po = phase angle of temperature curve at 1cm depth
B = amplitude of temperature curve at given depth (C)
P = phase angle of temperature curve at given depth

2.3.2 Fitting Inconsistant Diffusivity Data

The two values, D1 & D2, should theoretically be identical, but seldom were. This was due possibly to the fact that a cosine curve is only an approximation to the actual curve. Also, the actual soil from which the data is taken from is assumed to be homogeneous; yet it reality, seldom was. Thus they were kept separate and were defined as 'amplitude diffusivity' and 'phase diffusivity'.

Also, the calculated amplitude diffusivity tended to increase with increased ground depth. Theoretically, it should have remained constant, but continued to vary proportionally with ground depth. There is no definite reason why this was so. A possible explanation could be an increase in soil density with deeper ground depth. Thus the least squares method was applied to obtain a linear equation relating amplitude diffusivity with ground depth. The phase diffusivity was not affected by ground depth and an average phase diffusivity was assumed.

Therefore each location produced three values relating to diffusivity (**A1, B1, PH**). Two values, A1 and B1 defined a line to represent the amplitude diffusivity. Thus;

$$D(amp) = A1 + B1*X \qquad (5)$$

where:

D(amp) = amplitude diffusivity at given depth (m^2/h)
B1 = slope of D1 line (calculated by Least Squares) (m/h)
X = (soil depth) (m)
A1 = intercept of D1 line (calculated by L.S.) (m^2/h)

The third value, PH is the average of the phase diffusivities found at each depth. Thus phase diffusivity is represented as;

$$D(phase) = PH \qquad (6)$$

where:

D(phase) = phase diffusivity at given depth (m^2/h)
PH = sum(D2 values)/5 (m^2/h)

2.3.3 Calculating Diffusivity Coefficients

With the values D(amp) and D(phase) to account for the irregularities of D1 & D2, the coefficients 'b' and 'p' can be found to fit into equation (2). Solving Equations (3) and (4) gives;

$$B/Bo = e^{(-X*\sqrt{(Pi/D(amp)/8766))}} \qquad (7)$$
$$P-Po = -X*\sqrt{(Pi/D(phase)/8766)} \qquad (8)$$

where:

B = temperature amplitude at given depth (C)
P = phase shift at given depth
Bo = temperature amplitude at 1cm depth (C)
Po = phase shift at 1cm depth
X = (ground depth - .01) (m)
Pi = 3.141529
D(amp) = calculated amplitude diffusivity at given depth (m^2/h)
D(phase) = calculated phase diffusivity (m^2/h)
8766 = number of hours in the year (h)

but let $b = B/Bo$ and $p = P-Po$

and therefore;

$$b = e^{(-X*\sqrt{(Pi/D(amp)/8766))}} \qquad (9)$$
$$p = -X*\sqrt{(Pi/D(phase)/8766)} \qquad (10)$$

thus;

$$T = Ao - b*Bo * \cos(2*Pi*n/8766 - Po - p) \qquad (11)$$

where:

T	=	temperature of the soil (C)
X	=	(ground depth -.01) (m)
Pi	=	3.141529
Ao	=	average soil temperature at 1cm depth (C)
Bo	=	temperature amplitude at 1cm depth (C)
Po	=	phase shift at 1cm depth
b	=	diffusivity amplitude coefficient
P	=	diffusivity phase coefficient

2.3.4 Correlation of Diffusivity with Degree Days

The values A1, B1 & PH, defined in section 2.3.2 were compared against the location's degree days and its deep soil temperature (3 metre depth). Both of these parameters are found in HOT-2000 weather files. The correlation of diffusivity to deep soil temperature was not as consistant as degree days. The model can only deal with averages, thus using the 48 locations as statistical representations Therfore an exact fit was not required. Some data was eliminated because it varied too far from the normal. Figures 2-4 represent the log of these values vs degree days.

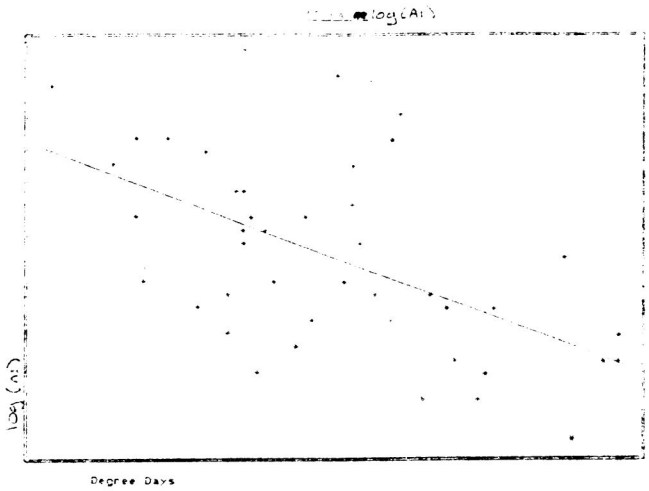

Figure 2
Degree Days vs log(A1)

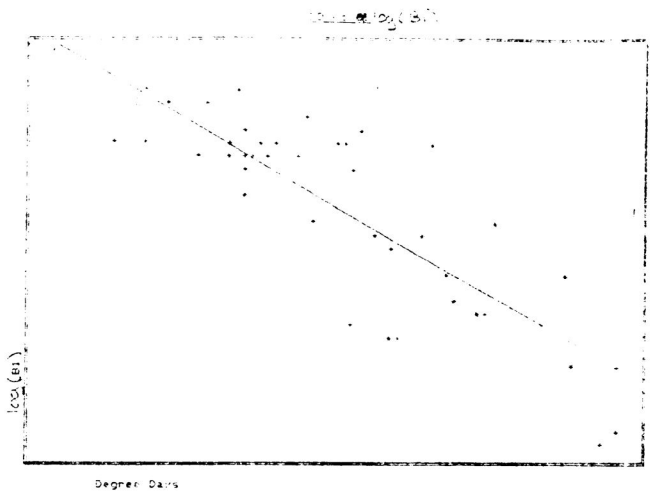

Figure 3
Degree Days vs log(B1)

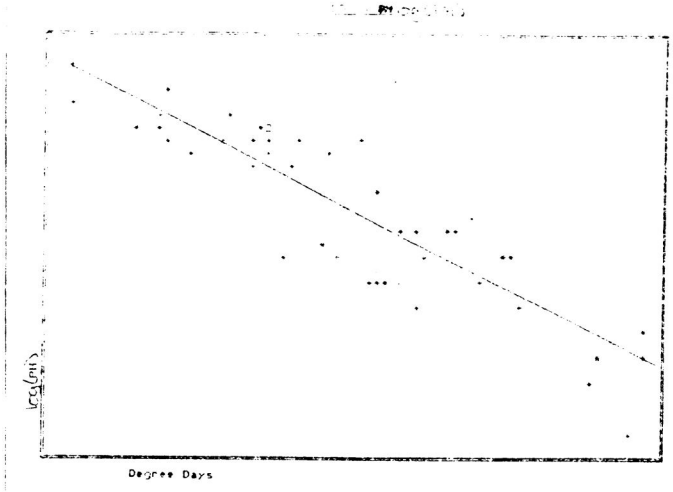

Figure 4
Degree Days vs log(PH)

The correlations found from figures 2-4 were as follows:

$$A1 = (10^{((-8.740e-5)*DD - 0.0271)})/1000 \quad (12)$$
$$B1 = (10^{((-1.678e-4)*DD - 0.7918)})/1000 \quad (13)$$
$$PH = (10^{((-9.371e-5)*DD - 0.5865)})/1000 \quad (14)$$

where:

A1 = intercept of D1 line) (for use in D(amp)) (m^2/h)
B1 = slope of D1 line (for use in D(amp)) (m/h)
PH = phase diffusivity (D(phase)) (m^2/h)
DD = degree days of location

2.4 Correlation of Top Soil Temperature to Ambient Air Temperature

Equations 15,16,17 will estimate the soil temperature for any depth given a temperature profile at 1cm depth. However, this information is not available considering that the only two parameters available are the monthly average ambient dry air temperature and the location's heating degree days. The logical reference depth is 0cm or the surface of the ground. It is an incorrect assumption however to assume that the temperature at the surface of the ground will match the ambient air temperature. Factors such as snow cover and direct sunshine in the summer will cause the two temperatures to differ. Thus a correlation is needed to relate the ambient air temperature profile to the ground surface profile.

Using the known temperature profile at 1cm for each location from Technical Bulletin 85 and the calculated diffusivity of the soil from degree day correlations, the temperature profile at depth 0cm was calculated. Using the least squares method as was used in section 2.3.2, this temperature profile was fitted to a cosine curve. The ambient air temperature profile was also fitted to a cosine curve and the difference between the A, B & P values of the two curves are plotted against degree days in Figs. 5-7.

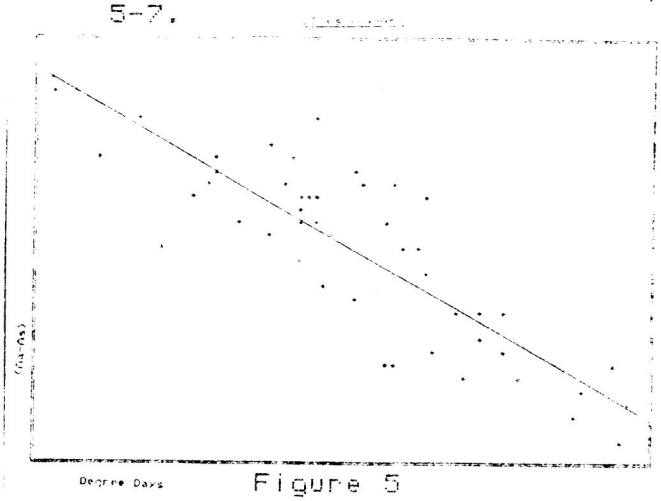

Figure 5
Degree Days vs Mean Air Temperature: Mean Soil Surface Temperature Difference

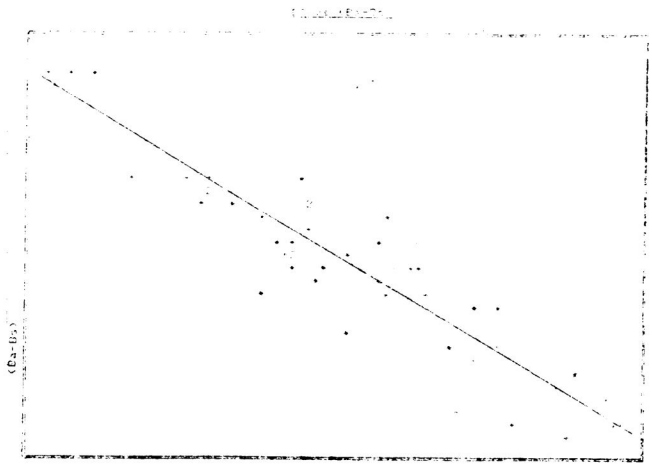

Figure 6
Degree Days vs Air Temperature Amplitude Soil Surface Temperature Amplitude Difference

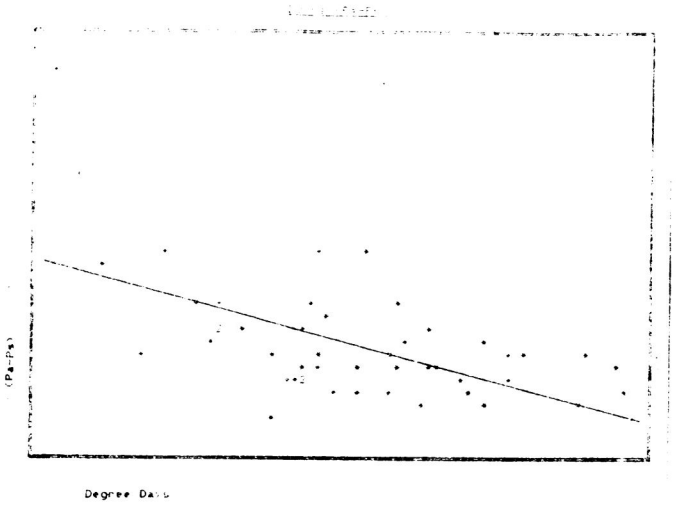

Figure 7
Degree Days Vs Air Temperature Phase Shift:Soil Surface Temperature Phase Shift Difference

A perfect correlation is not possible given the inexact correlation between mean air temperature and soil temperature for reasons outlined earlier. Linear equations were fitted to the plots in Figures 5-7. The resulting equations were:

$$As = (9.189e-4)*DD - 1.438 + Aa \quad (15)$$
$$Bs = (1.970e-3)*DD - 7.875 + Ba \quad (16)$$
$$Ps = (2.128e-5)*DD - 0.0756 + Pa \quad (17)$$

where:

As = mean temperature at soil surface (C)
Bs = temperature amplitude at soil surface (C)
Ps = temperature phase shift at soil surface
Aa = mean temperature of ambient air (C)
Ba = temperature amplitude of ambient air (C)
Pa = temperature phase shift of ambient air
DD = degree days of location

7.0 Summary

To estimate the temperature profile for any location, the only data required is the monthly average ambient dry air temperature and the annual heating degree days.

With this information, the model will proceed to fit the ambient air temperature profile to a cosine curve as described in section 2.4 Mean temperature, temperature amplitude and phase shift of the air temperature cosine curve result in the variables Aa, Ba & Pa respectively.

Next the model converts the air temperature profile, to the ground surface temperature profile. This is achieved by converting Aa, Ba & Pa to As, Bs &Ps. These variables represent the temperature profile of the ground surface. The conversion is done by the following correlations: (see section 2.4 for derivation)

$$As = (9.189e-4)*DD - 1.438 + Aa$$
$$Bs = (1.970e-3)*DD - 7.875 + Ba$$
$$Ps = (2.128e-5)*DD - 0.0756 + Pa$$

The ground diffusivity values A1, B1 & PH are determined for a location by the following correlations: (see section 2.3.4 for derivation)

$$A1 = (10^((-8.740e-5)*DD - 0.0271))/1000$$
$$B1 = (10^((-1.678e-4)*DD - 0.7918))/1000$$
$$PH = (10^((-9.371e-5)*DD - 0.5865))/1000$$

Next, the ground depth (m) from the surface (X) is used to calculate diffusivity values. (see section 2.3.2 for derivation)

$$D(amp) = A1 + B1*X$$
$$D(phase) = PH$$

With these values, the diffusivity 'b' and 'p' coefficients can now be found. Note that X is now from the ground surface rather than 0.01m below ground as was the case in section 2.3.3 when all calculations were done from 0.01m as a reference depth.

$$b = e^(-X*sqrt(Pi/D(amp)/8766))$$
$$p = -X*sqrt(Pi/D(phase)/8766)$$

And thus the final soil temperature equation is;

$$T = As - b*Bs * cos(2*Pi*n/8766 - Ps - p)$$

T(x) = temperature of soil at depth x (C)
As = mean temperature of soil at surface (C)
Bs = soil temperature amplitude at surface (C)
b = decrease in amplitude for depth x
Pi = 3.1415927
n = number of hours into year (8766 hours/year)
Ps = phase angle at surface
p = shift in phase angle for depth x

This equation assumes that the ground is of constant permeability. Also the average monthly ambient dry air temperature is assumed to occur at the middle of the month.

An error analysis was conducted on the model in Appendix B. Of 1,728 test points at 0.5 - 1.5m the maximum error between estimated and actual temperature points was 3.6(C). The mean difference between the two was 0.0203(C) with a standard

deviation of 1.0962. This is within acceptable limits of estimation, considering the model only requires heating degree days, ambient monthly dry air temperature and a user defined soil depth.

APPENDIX A

Fitting Temperature Data to a Cosine Curve

Method of fitting data to a cosine curve of the form:

$$T = A - B * \cos(2 * Pi * n / 8766 - P)$$

using techniques outlined in Kusuda & Achenbach.

1. 12 monthy average temperatures must be given.

e.g.

jan	feb	mar	apr	may	jun	jul	aug	sep	oct	nov	dec
1.2	0.4	0.6	3.9	10.3	15.6	19.0	19.2	16.7	12.0	6.8	3.0

therefore t(1) = 1.2, t(2) = 0.4 ...etc

2. To fit monthly data to a cosine curve, it is assumed the temperature given corresponds to the middle of the month.

3.

$$A = \frac{\sum_{k=1}^{12} t(k)}{12}$$

$$S1 = \sum_{k=1}^{12} t(k) * \sin(2 * Pi / 12 * (k-0.5))$$

$$C1 = \sum_{k=1}^{12} t(k) * \cos(2 * Pi / 12 * (k-0.5))$$

* - note (k-0.5) represents the middle of the month.

$$B = (-2/12) * \text{sqrt} (s1^2 + c1^2)$$

$$P = \arctan (s1/c1)$$

4. The variables A, B & P represent respectively the mean, amplitude and phase shift of the data.

APPENDIX B

Accuracy of Generated Soil Temperatures

The original 48 locations across Canada, used to generate the correlations, were compared against model estimated values for the depths of 0.5m , 1.0m and 1.5m. These depths were chosen, for the reason that most earth coupled heat pumps are placed in this depth regime. Thus 48 locations X 12 months X 3 depths gave a total of 1728 cases to analyse.

A statistical correlation comparing each measured temperature case to its corresponding estimated temperature was completed. The correlation, shown in Figure 8, yielded a slope of 0.96562 and an intercept of 0.2844. The coefficent of correlation was 0.9806. An ideal fit of measured temperature to predicted temperature would contain a slope of 1 and a correlation coefficent of 1.0.

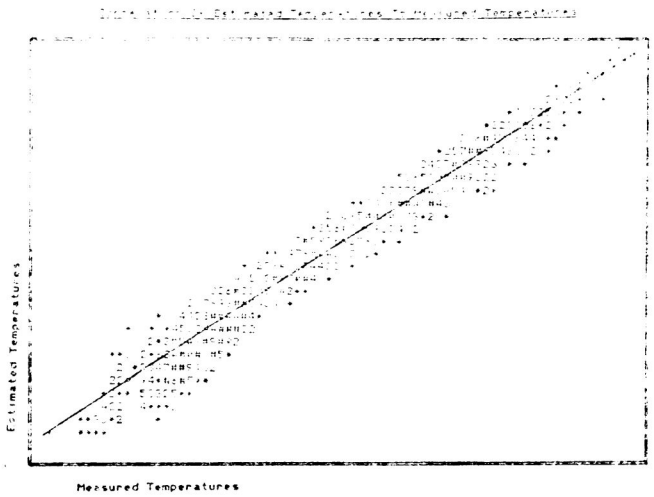

Figure 8

An analysis of the difference between each case gave a mean of -0.0203C with a standard deviation of 1.0962. The maximum difference was 3.61C.

APPENDIX C

Location	Degree Days
ABBOTSFORD	3150
BAGOTVILLE	5776
BRANDON	6037
CALGARY	5345
CHARLOTTETOWN	4623
CHATHAM	4884
EDMONTON	5589
ESTEVAN	5542
FORT MCMURRAY	6778
FREDERICTON	4699
GANDER	5039
GOOSE BAY	6522
GREENWOOD	4130
HALIFAX	4123
KAMLOOPS	3756
KINGSTON	4266
LETHBRIDGE	4718
LONDON	4068
MONCTON	4709
MONTREAL	4471
MUSKOKA	4837
NORTH BAY	5318
OTTAWA	4673
PRINCE ALBERT	6562
PRINCE GEORGE	5388
QUEBEC	5080
REGINA	5920
ROCKY MOUNTAIN HOUSE	5550
SASKATOON	6077
SHERBROOKE	5242
SIMCOE	3962
SMITHERS	5290
SAINT JOHN	4771
ST. JOHN'S	4804
STEPHENVILLE	4783
SUFFIELD	5102
SUMMERLAND	3318
SUMMERSIDE	4600
SWIFT CURRENT	5482
SYDNEY	4459
THE PAS	6852
THUNDER BAY	5746
TORONTO	4082
TRURO	4704
VAL D'OR	6146
VANCOUVER	3007
WINDSOR	3590
WINNIPEG	5889

Appendix E: Heat storage calculations

HEAT STORAGE CALCULATIONS				
	Method 1	diff. between the months	Method 2	diff. between the months
01-Jan	0		444	
31-Jan	-34,2	34,2	377	67
28-Feb	-18,3	-15,9	394	-17
31-Mar	44,7	-63	502	-108
30-Apr	130,4	-85,7	658	-156
31-May	91,9	38,5	630	28
30-Jun	84,6	7,3	623	7
31-Jul	87,7	-3,1	632	-9
31-Aug	91,8	-4,1	642	-10
30-Sep	162,9	-71,1	747	-105
31-Oct	171,9	-9	766	-19
30-Nov	135,7	36,2	703	63
31-Dec	73,7	62	592	111

Appendix F: Climate data from Östersund, Sweden

Figure 14.1 shows the ambient dry bulb temperature over a year in Östersund. The data is collected from the climate file in ESP-r. Direct- and diffuse solar radiation over a year in Östersund can be seen in Figure 14.2.

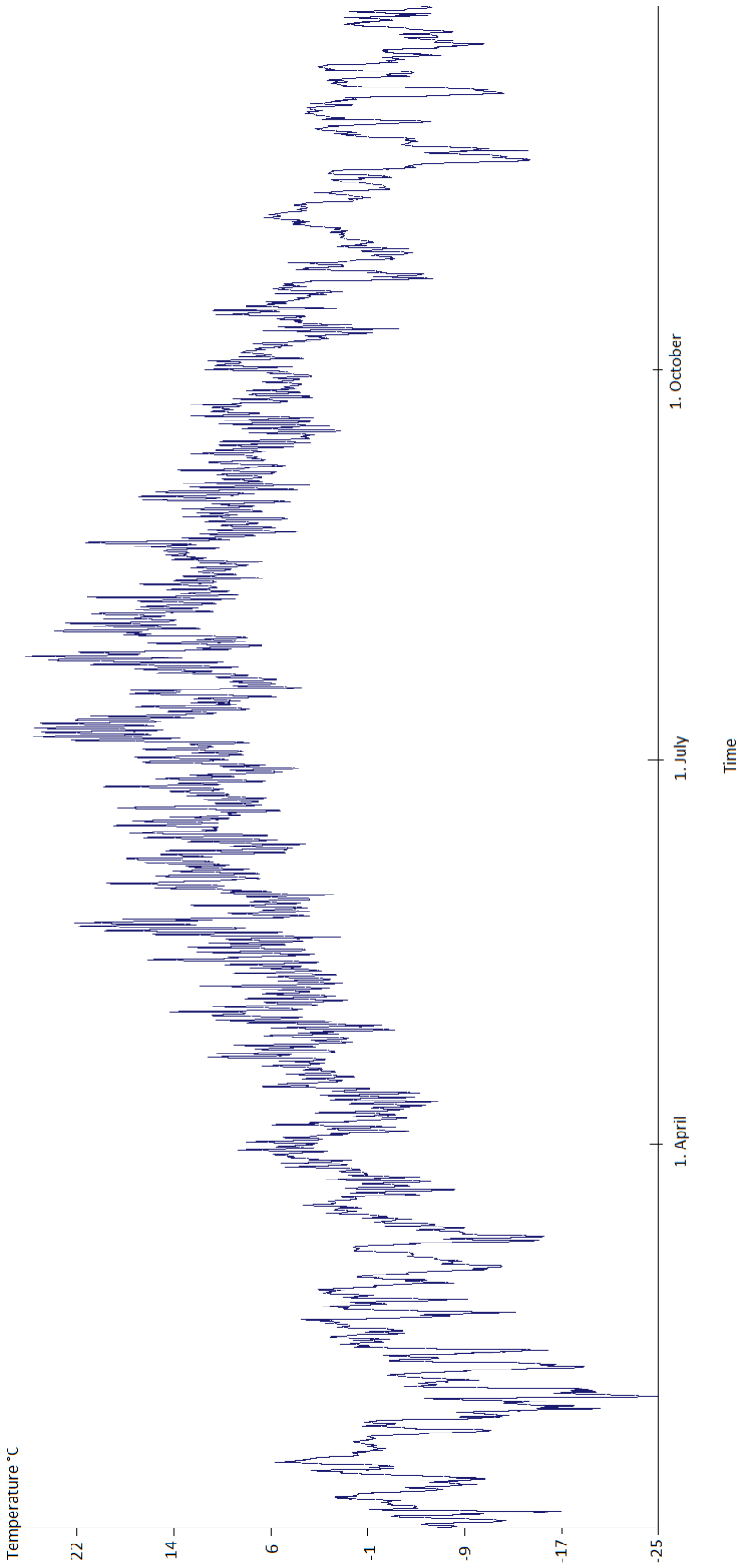

Figure 14.1: Ambient dry bulb temperature over a year in Östersund

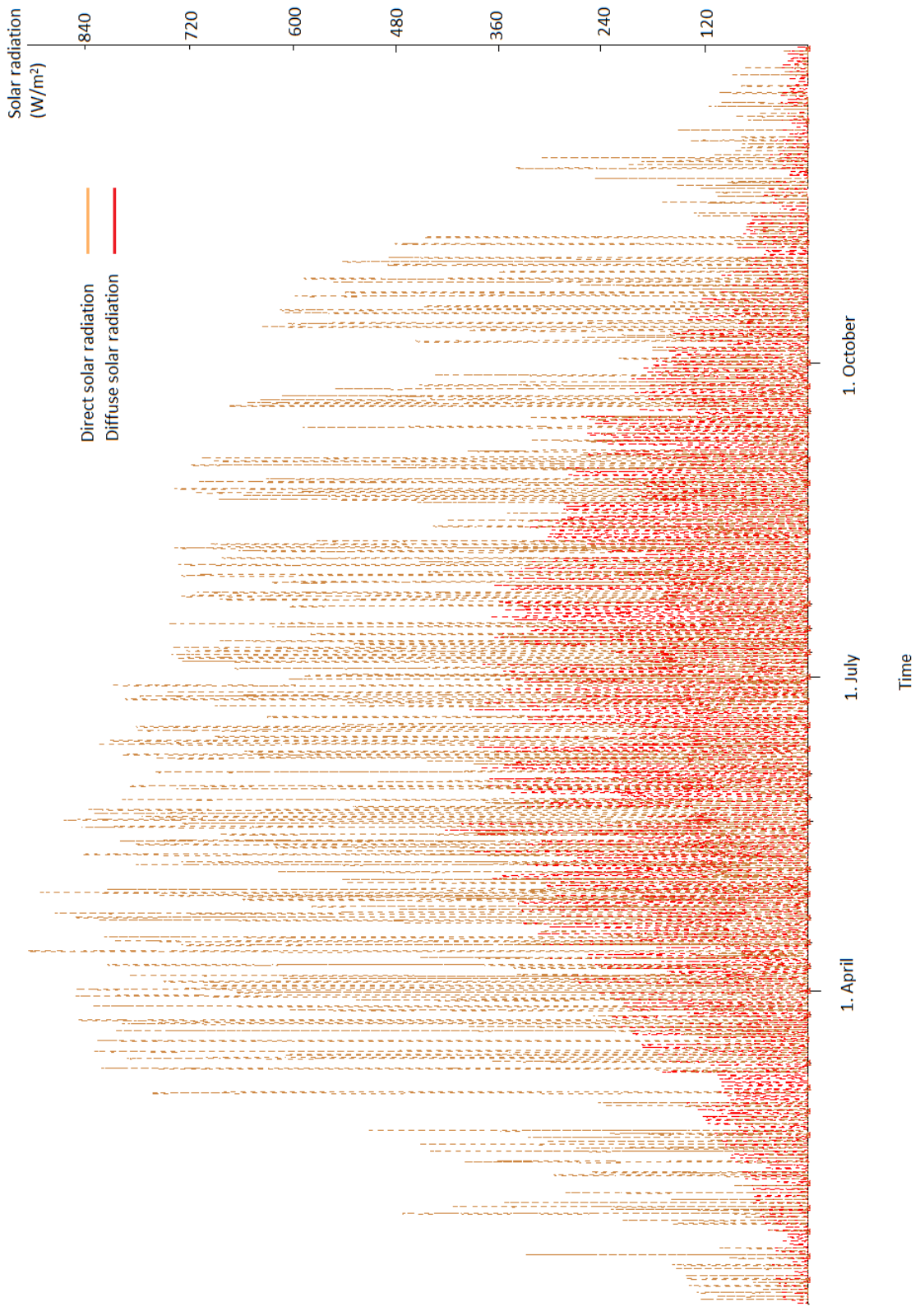

Figure 14.2: Direct- and diffuse solar radiation over a year in Östersund

Appendix G: Results from the project thesis

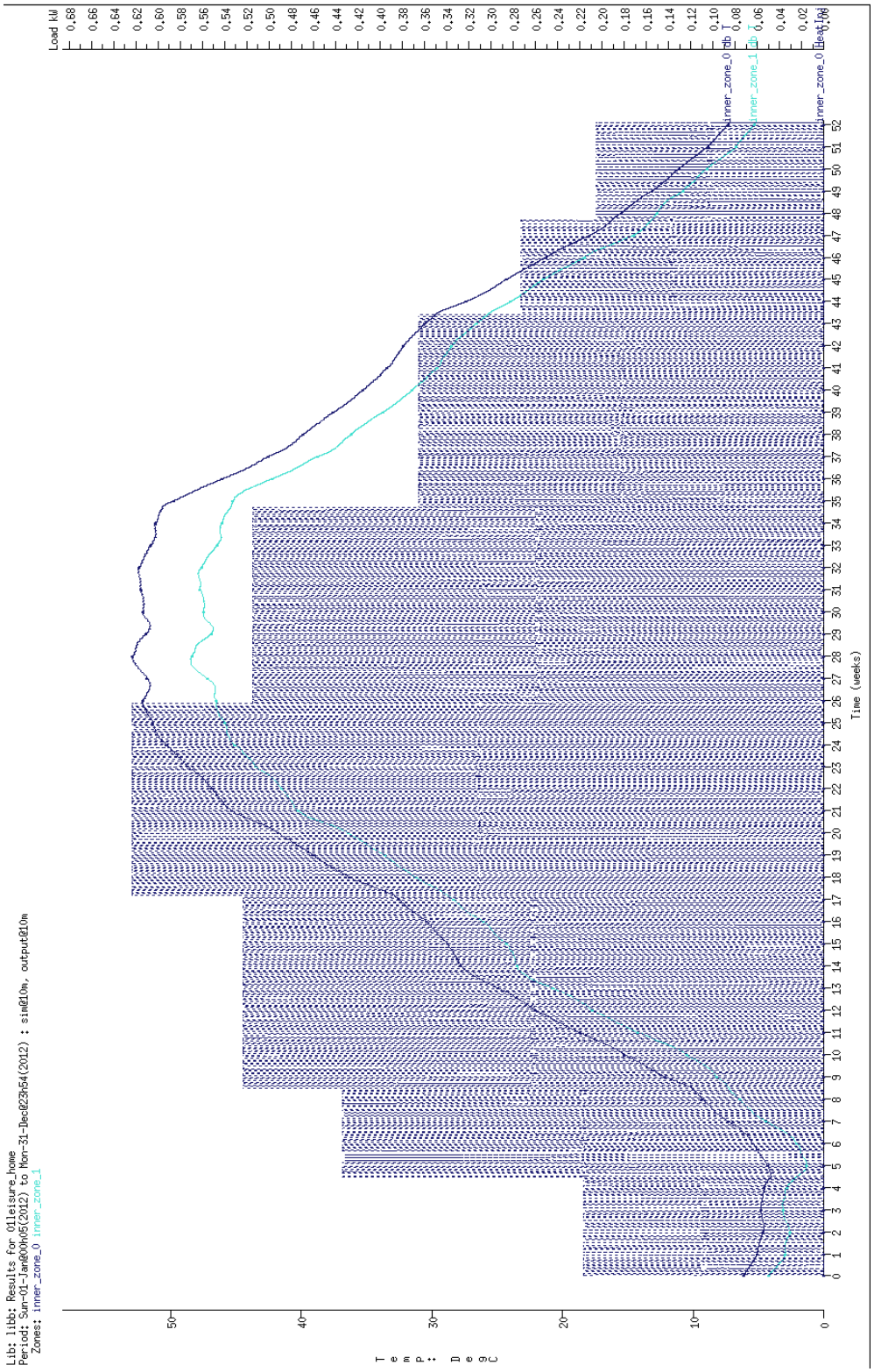

Figure 14.3: Temperature profiles for the inner zones with Case 1, PROJECT THESIS, old model

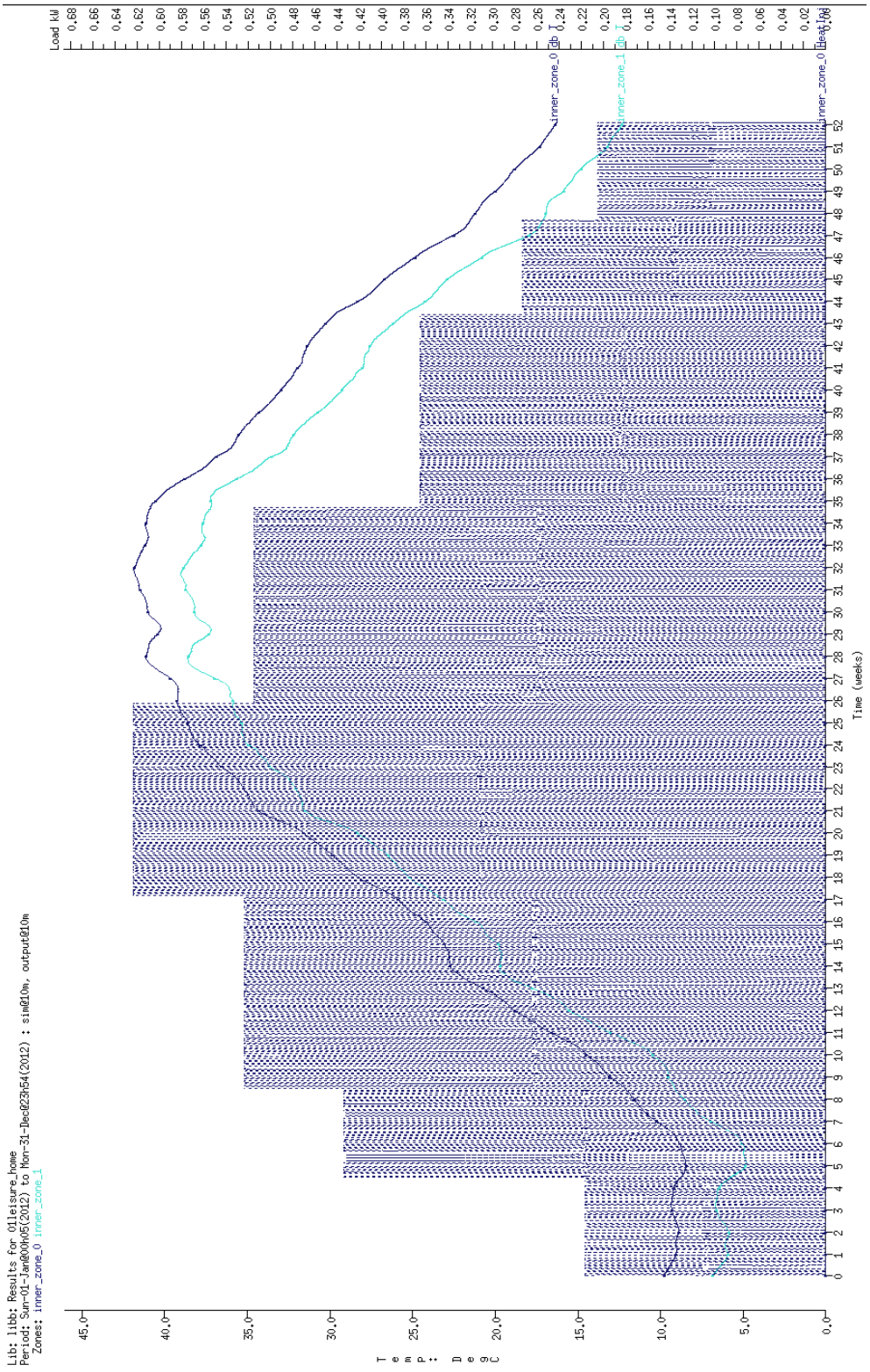

Figure 14.4: Temperature profiles for the inner zones with Case 4, PROJECT THESIS, old model

Appendix H: Results

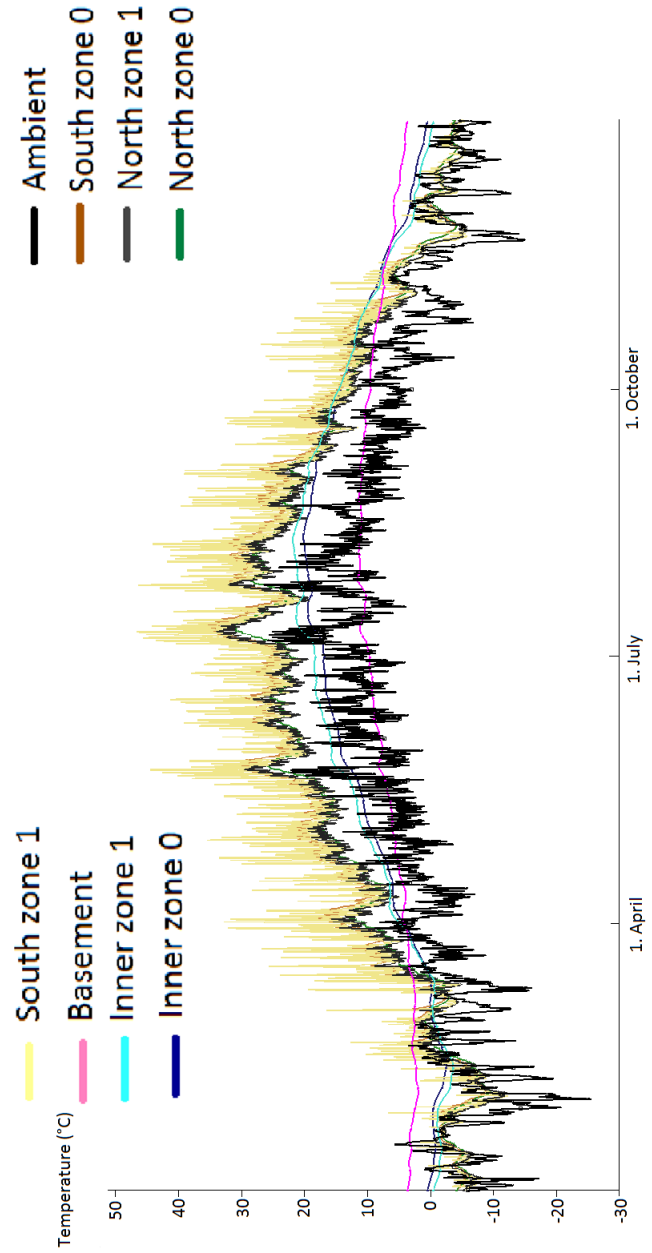

Figure 14.5: Temperature profiles for the new model for all zones with no heat injection

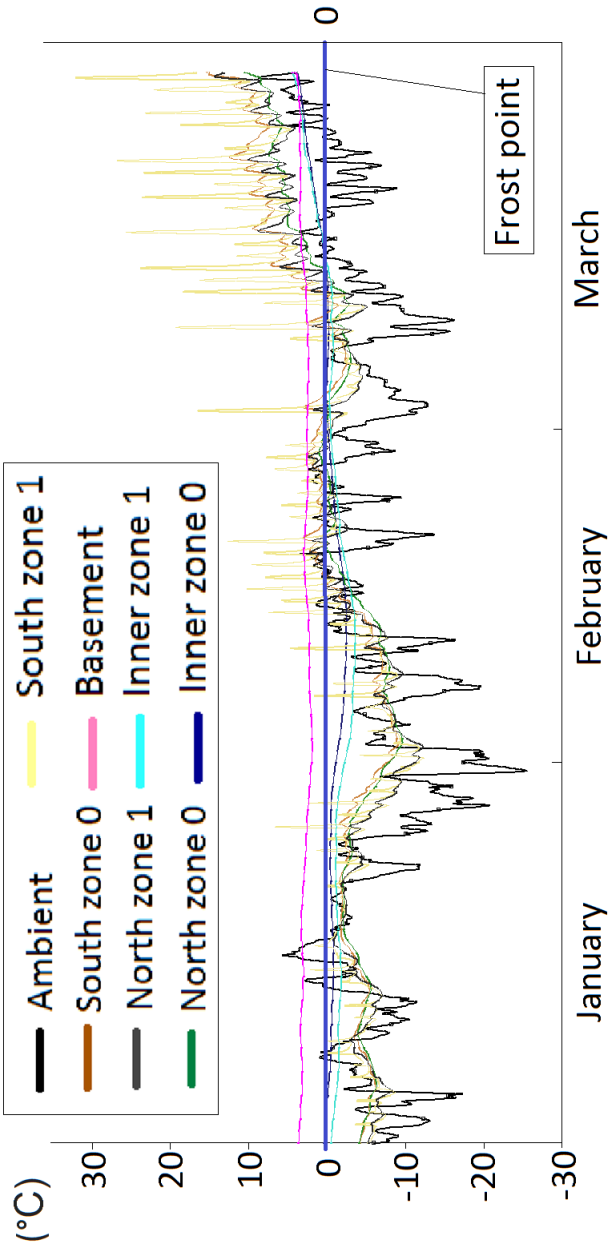

Figure 14.6: Temperature profiles for all the zones in the new model for the critical period January-March *without* any heat injection over the year

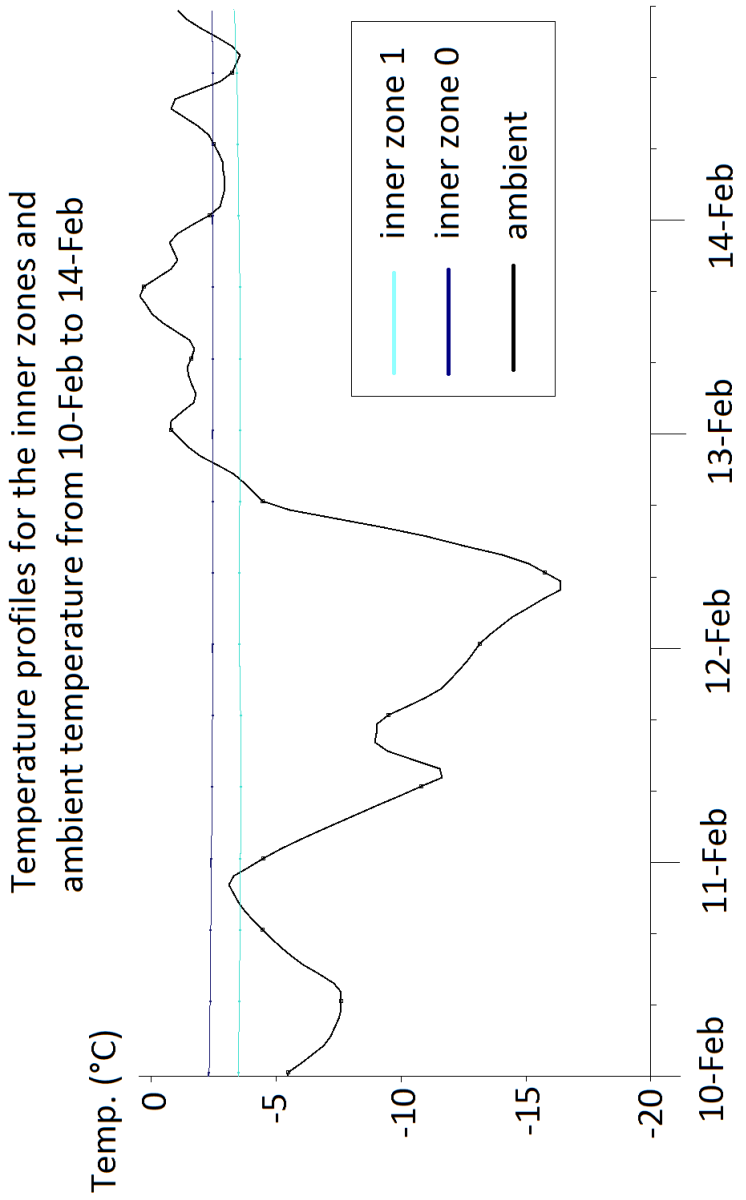

Figure 14.7: Temperature profiles for the inner zones in the new model for the period when the lowest temperatures in the inner zones occur - *without* any heat injection over the year